Quantifying the Impact of Wide Base Tires on Pavement Performance in Michigan

FINAL REPORT

Prepared by:

Zhanping You

Lei Yin

Jacob E. Hiller

Dongzhao Jin

DEPARTMENT OF CIVIL, ENVIRONMENTAL, AND GEOSPATIAL ENGINEERING

MICHIGAN TECHNOLOGICAL UNIVERSITY

1400 TOWNSEND DRIVE

HOUGHTON, MICHIGAN 49931

MTUengineering

Submitted to:

MICHIGAN DEPARTMENT OF TRANSPORTATION

8885 RICKS ROAD

LANSING, MI 48909

Report No. SPR-1720

December 2022

TECHNICAL REPORT DOCUMENTATION PAGE

1. Report No. SPR-1720	**2. Government Accession No.** N/A	**3. Recipient's Catalog No.** N/A
4. Title and Subtitle Quantifying the Impact of Wide Base Tires on Pavement Performance in Michigan		**5. Report Date** December 2022 **6. Performing Organization Code** N/A
7. Author(s) Zhanping You, Lei Yin, Jacob E. Hiller, Dongzhao Jin		**8. Performing Organization Report No.** N/A
9. Performing Organization Name and Address Michigan Technological University 1400 Townsend Drive, Houghton, MI 49931-1295		**10. Work Unit No.** N/A **11. Contract or Grant No.** Contract 2019-0311 Z2
12. Sponsoring Agency Name and Address Michigan Department of Transportation (MDOT) Research Administration 8885 Ricks Road P.O. Box 33049 Lansing, Michigan 48909		**13. Type of Report and Period Covered** Final Report, 3/15/2021 – 12/31/2022 **14. Sponsoring Agency Code** N/A

15. Supplementary Notes
Conducted in cooperation with the U.S. Department of Transportation, Federal Highway Administration. MDOT research reports are available at www.michigan.gov/mdotresearch.

16. Abstract
Since dual tires (DT) have been the trucking industry standard for many decades, existing modeling of the stresses imparted to the pavement through the tires is based on DTs. However, the freight industry has started to use wide base single tires (WBT) due to their economic benefits. This study aimed to investigate the use of WBTs in Michigan (MI) to quantify the effect of different percentages of WBT loads on flexible and rigid pavements. Surveys and field investigations were conducted to quantify WBT usage in MI. The JULEA (for flexible pavements) and Illislab (for rigid pavements) software programs were used to calculate the mechanical response between DT and WBT loads, while the Mechanical-Empirical (ME) pavement design process was utilized for damage accumulation and pavement distress analysis. Investigation results rationalized the assumption of WBT proportion for design purposes as 10% currently and up to 25% in the future for MI, with the majority of axle loads still employing DT assemblies. WBT loads were found to increase pavement distress mechanistically using this process, with fatigue cracking for flexible pavement and faulting for rigid pavement being the most critical. For flexible pavement, thicker hot mix asphalt (HMA) layers were beneficial in reducing WBT impact on fatigue cracking, while rutting was much less impacted by the thickness of the HMA under WBT. For rigid pavement, thicker concrete slabs helped reduce WBT impacts on both transverse cracking and faulting for jointed plain concrete pavement (JPCP). It was also found that WBT loads did not significantly affect the international roughness index (IRI) for both HMA and JPCP. Based on analysis results, the WBT impact on pavement structures with 5-12" HMA or 6-13" JPCP were quantified for up to 25% WBTs, with the respective adjusted Pavement ME design threshold, traffic parameter, and recommendation for implementation. Additionally, weigh-in-motion (WIM) technologies were reviewed to support possible WBT update strategies and improve the identification of tire types.

17. Key Words Wide base tire; dual tire; pavement design; mechanical-empirical design; AASHTO 93 design; flexible pavements; rigid pavements	**18. Distribution Statement** No restrictions. This document is also available to the public through the Michigan Department of Transportation.

19. Security Classif. (of this report) Unclassified	**20. Security Classif. (of this page)** Unclassified	**21. No. of Pages** 243	**22. Price** N/A

Form DOT F 1700.7 (8-72) Reproduction of completed page authorized

DISCLAIMER

ACKNOWLEDGEMENTS

The research work was sponsored by the Michigan Department of Transportation (MDOT) and Federal Highway Administration (FHWA). The authors appreciate the guidance and involvement of Justin Schenkel of MDOT as project manager, Andre Clover as a project engineer, Michael Eacker, Thomas Foltz, Teresa Logan, Scott Greene, Brandon Lambrix, Fawaz Kaseer, Kevin Kennedy, and Chris Hund in the Research Advisory Panel (RAP). The authors also appreciate Emily Kastamo as the English editor for this report. This project could not have been completed without the significant contribution from other research team members including Kwadwo Boateng, Josh King, Emily Bergstrom, and Kai Xin.

Table of Contents

List of Tables

List of Figures

1. CHAPTER 1: BACKGROUND AND RESEARCH STATEMENT

1.1. Background

With the large percentage of goods moved by commercial trucks in the freight industry, trucks consume natural resources such as fuel and contribute to gas emissions, significantly impacting the environment. There is a need for innovative technologies that can improve the efficiency of trucking operations while minimizing damage to the environment. Due to the significant savings in energy consumption and simple mechanical load assembly, wide-based tires (WBT), or super single tires, are becoming one example of this technology and are increasing in truck axle applications in many states [1-4].

The tire size code explanation is presented in Figure 1.1, with the first number indicating the width in mm; WBTs have a wider width than conventional dual tires (DT) used in trucks (e.g., 225 mm, 275 mm, 295 mm widths). The WBT was first introduced in North America in 1982. Early versions of WBTs, noted as super single tires (e.g., 385 mm, 425 mm widths), are rarely found anymore in load axles of trucks, as their limited contact area has been proven to cause tremendous deformations and distress development in pavements [5]. WBTs currently in use are primarily the new generation tires with a wider section width (e.g., 445 mm, 455 mm) to help spread these concentrated loads over a wider area [6, 7]. These new generations of wide-base tires were designed to inflict less pavement damage and provide other safety and cost-saving advantages, including fuel savings and less tire waste in comparison to DT assemblies [8, 9]. With the potential benefits to the trucking industry from the use of WBTs, it is anticipated that the market share of tire sales and usage will increase in the future.

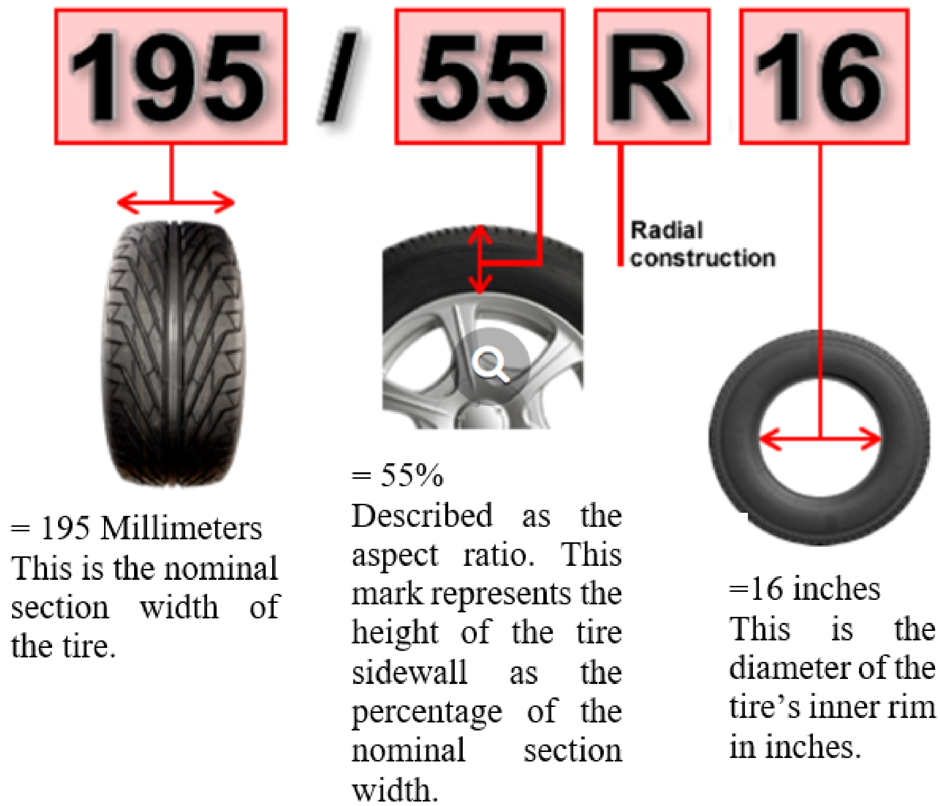

Figure 1.1. Tire size code explanation [10]

However, dual tires have been the trucking industry standard for many decades. Thus, existing prediction algorithms of stresses/strains inflicted on the pavement through external loads are based on dual tire setups, whether in the AASHTO Guide for Design of Pavement Structures (AASHTO 93) or the latest method, Mechanistic-Empirical Pavement Design, with its software, AASHTOWare Pavement ME Design. This project aims to quantify the effect WBTs have on pavement response and distress development for Michigan's climate and construction practices. The effect of WBTs on both flexible pavement (Hot Mix Asphalt - HMA) and rigid pavement (refer to Jointed Plain Concrete Pavement - JPCP in this study) will be analyzed with the typical design parameters in Michigan. Furthermore, this project will identify the impacts that WBTs have on the current MDOT flexible and rigid pavement design methods and provide recommendations to adjust the design process in AASHTO 93 and Pavement ME to incorporate the effects of WBT loads into the pavement design.

1.2. Research statement

The Michigan Department of Transportation (MDOT) initiated this study to identify the impact of WBTs on pavement performance in Michigan and to involve the WBT impact in the design process. Several Michigan State Police (MSP) weigh stations were made available to investigate WBT usage. Many existing studies have evaluated WBT loads' impact on pavement by simulation or field test; however, limited research has focused on quantifying the impact of different WBT proportions on various pavements (with different layer thicknesses). In addition, most states, including Michigan, have conducted a local Pavement Mechanistic-Empirical (ME) calibration. Therefore, an objective of this study is to involve the WBT impact in the Michigan design process by using local ME calibration factors. One of the limitations of this study is that the ME process is developing, and some local calibration work for the latest models (e.g., flexible top-down cracking model) in Michigan is undergoing, which cannot be adopted in this study due to the timing. Another limitation is that the AASHTO 93 pavement design method does not incorporate pavement mechanical response in its methodology but instead uses empirical relationships to estimate the pavement serviceability. Therefore, it is difficult to compare or correlate the WBT mechanistic impacts from the ME method to AASHTO 93.

1.3. Research tasks

The original research plan involved six tasks. However, combinations and modifications were made to the original tasks to address the critical issues in the proposal. According to the modified work plan, the research contents of each task are described below.

Task 1. Literature Review

- WBT usage in other states
- WBT accounting method
- Impact of WBT on pavement performance
- Differences between WBTs and dual tires

Task 2. Investigate WBT usage in Michigan

- Survey WBT (types, amounts, locations) usage in Michigan
- Develop test matrix for WBTs used in Michigan
- Estimate WBT types used in MI
- Predict specific types of WBT to be used on Michigan pavements in the future

Task 3. Determine impacts of WBT on pavement performance

- Identify routes and quantities of each WBT type being used in the state
- Perform mechanistic analysis, collect ME input data

- Compare results between WBTs and DTs

Task 4. Identification of advanced WIM and other technologies in detecting WBT usage

- Determine WBT percentage in FHWA truck classifications
- Make investigations and recommendations for advanced WIM technologies

Task 5 Final report and summary of the recommendations

- Final report
- MS presentation for MDOT
- Summarize recommendations

2. CHAPTER 2: LITERATURE REVIEW

2.1. Current research on WBTs' impact on pavement

The use of WBTs on our road systems has been prevalent for many years, and researchers have analyzed WBTs' impact on pavement via mathematic simulation (e.g., finite element) or field tests (using sensor gauges). This chapter will review current research on WBTs' impact on different distresses of pavement. As there is little research evaluating WBT and DT load differences for rigid pavements, this section will review only research on flexible pavements.

Fatigue cracking is one of the most concerning distresses of flexible pavement, and many studies have focused on WBTs' impact on flexible pavement's fatigue performance. Asphalt concrete (AC) bottom tensile strain is the critical response for calculating bottom-up fatigue distress in the current AASHTO Mechanistic-Empirical (ME) pavement design process [11]. Numerical simulation is the most widely adopted method in evaluating the impact of WBTs as to their high efficiency and accuracy in obtaining tensile strain response. Priest et al. used layered elastic analysis and calculated that with the same axle load weight, the horizontal strain under WBT load is 46% higher than under DT load for the parameters utilized in the study [12]. Greene et al. used the finite element (FE) method to argue that compared with DT load, the 445/50R22.5 WBT would produce slightly higher bottom-up cracking but less top-down cracking, while the slightly wider 455/55R22.5 WBT would not cause more fatigue cracking [13]. Wang et al. used the FE model and found that WBT loads caused greater fatigue damage, but a thicker base would lower the impact [14]. Said et al.'s FE simulation resulted in WBT loads creating approximately 17% larger AC bottom tensile strain than DT loads [15]. Molavi Nojumi et al.'s research showed that with 20% of WBT loads in the truck market, the fatigue damage would be 5.7-11.5% higher than in the DT assembly-only scenario, depending on the quality of pavement analyzed [16].

Some research has focused on distresses other than the fatigue of flexible pavement, such as rutting (AC and subgrade). Elseifi et al. used Abaqus to calculate the rutting of the 1.5" AC layer structure under DTs and WBTs. The result showed that at low speed, AC under a DT load would suffer up to 16% more load cycles than under WBT loads (445mm widths), while the subgrade would suffer up to 43% more in the same scenario [17]. Wang et al.'s simulation proved that the damage ratio of AC rutting caused by 455 WBTs with respect to DTs is about 1.75 and would be stable in different base thicknesses [14]. Gungor et al. established the equation of pavement response between under DT load and under WBT load, as presented in Table 2.1; the result shows that the vertical compressive strain (for rutting distress calculation in Pavement ME) in upper layers is more easily impacted by WBT loads by a 37% increase in the AC layer **[9]**. Fedujwar et al. adopted the 3D-Move Analysis Software to analyze the pavement response and found that the rutting life of pavement decreased by approximately 89% when super single tires (425mm widths) replaced all dual tires [18].

Table 2.1. Equations for pavement response under WBTs [9]

Pavement Response	Location	Linear Equation	R^2
Maximum tensile strain in traffic direction	AC surface	WBT=1.6×DTA-2.0509	0.9939
Maximum tensile strain in transverse direction	AC surface	WBT=1.4039×DTA-10.09	0.9657
Maximum tensile strain in traffic direction	Bottom of AC	WBT=1.2014×DTA+4.3014	0.9867
Maximum tensile strain in transverse direction	Bottom of AC	WBT=1.5861×DTA-4.92	0.9927
Maximum vertical compressive strain	Within AC	WBT=1.3689×DTA+0.4778	0.9909
Maximum vertical compressive strain	Within base	WBT=1.1655×DTA+1.2327	0.9944
Maximum vertical compressive strain	Within subgrade	WBT=1.1615×DTA-4.5571	0.9898
Maximum vertical shear strain	Within AC	WBT=1.3873×DTA-2.8506	0.9685
Maximum vertical shear strain	Within base	WBT=1.2077×DTA-3.297	0.9944
Maximum vertical shear strain	Within subgrade	WBT=1.1113×DTA-0.5281	0.9902

The research results noted above showed that the WBT load tended to cause more significant fatigue and rutting damage on flexible pavement than the standard DT loads. However, the proportion of WBTs in the total vehicle mix is a developing value rather than fixed. Rutting and fatigue cracking of flexible pavement are highly related to AC thickness and material quality [18-20]. Most research has failed to consider the range of WBT proportion and AC thickness impacts, which does not lend itself well to the practical pavement design process. Michigan and many other states have completed a local calibration for the ME pavement design method, which means some analyses based on global calibration do not fit well in local area pavement performance [21]. In addition, the top-down cracking is merged into the bottom-up cracking model according to the Michigan calibration process, and MDOT would consider the total rutting rather than AC rutting only in the design process, which is different from the global ME design process. Furthermore, although rigid pavement seems to be strong enough to suffer more extreme load conditions compared with flexible pavement, the WBT impact on rigid pavement needs to be similarly assessed. All in all, current research is not well connected with the Michigan local ME pavement design process. The impact on pavement distress from WBTs is not well quantified, as the existing Pavement ME analysis procedures cannot directly assess the impact of WBTs on pavement response and ultimate pavement performance predictions.

2.2. Contact pressure (area) difference between DT and WBT loads

The essential difference in various types of WBTs relates to the tire-pavement contact pressure (load weight/contact area) [22]. According to Greene et al.'s research, the average increase in contact pressure for 445/50R22.5 and 455/55R22.5 WBTs is 21.3% and 19.0%, respectively, compared with a standard dual-tire at similar internal tire pressures [23]. Hernandez et al. also measured the contact area of DTs and WBTs (445/50R22.5) and calculated that the contact pressure of a 445/50R22.5 WBT is approximately 30% larger than a DT [8]. Therefore, the load number difference in tires (2×2 for DT, 2×1 for WBT) and increased contact pressure (e.g., 20%) for WBTs can be used to quantify the differences between WBTs and DTs on pavement response.

According to a review of tire-road contact for wide-base tires and dual tires, it is expected that the actual contact pressure of tires on the pavement is not equal to the tire's inner pressure due to the deformation restriction. However, *"load divided by contact area"* equals *"contact pressure"* equals *"tire inner pressure"* is a basic assumption in the linear elastic software JULEA. So, before analyzing more profound pavement distress, calibration must be conducted to obtain the actual contact area and contact pressure of wide-base tires.

Greene et al. measured the contact area of WBTs and DTs under different inflated tire pressures and weights [13]. The actual contact pressure for different tire types can be computed according to their measured contact area, as shown in Table 2.2. Since WBTs always have a larger contact pressure than DT loads with the same inflation pressures and weights, the percent increase of WBT contact pressure compared with DT loads was computed in Table 2.3 to demonstrate the difference. According to Table 2.3, the research team concluded that the average increase in contact pressure for 445/50R22.5 and 455/55R22.5 WBT is 21.3% and 19.0%, respectively, compared with DTs.

Table 2.2. Computed contact pressure from Greene et al.'s research (From [13])

Tire type	Tire inflation pressure (psi)	Computed contact pressure under different wheel/tire loads (psi)			
		9 kip	12 kip	15 kip	18 kip
11R22.5 (Dual-tire)	80	72.6	80.0	86.7	103.4
	100	75.6	82.8	90.9	/
	125	87.4	90.2	98.7	/
425/65R22.5 (Super single)	80	92.8	100	108.7	
	115	120	116.5	129.3	
	125	116.9	125	125	
445/50R22.5	80	90	99.2	107.1	/
	100	89.1	96	108.7	/
	125	109.8	111.1	116.3	126.8
455/55R22.5	80	79.6	88.8	98.0	/
	100	93.7	105.3	107.1	/
	125	111.1	105.3	123.0	126.8

Table 2.3. Percent increase of WBT contact pressure compared with dual tires

WBT type	Tire inflation pressure (psi)	Contact pressure change under different wheel/tire loads (%)			
		9 kip	12 kip	15 kip	Average
425/65R22.5 (Super single)	80	+27.8	+25	+25.4	+29.5
	115	/	/	/	
	125	+33.8	+38.5	+26.6	
445/50R22.5	80	+23.9	+24	+23.6	+21.3
	100	+17.8	+16.0	+19.6	
	125	+25.6	+23.2	+17.8	
455/55R22.5	80	+9.7	+11	+13.1	+19.0
	100	+23.9	+27.2	+17.8	
	125	+27.1	+16.7	+24.6	

Hernandez and Al-Qadi et al. also measured the contact area of DTs and WBTs (445/50R22.5) and analyzed their relationship, as presented in Figure 2.1 [8]. The contact area of a dual tire assembly is typically 100-130% of a WBT, which also means the contact pressure of a 445/50R22.5 WBT is 0-30% larger than a dual tire.

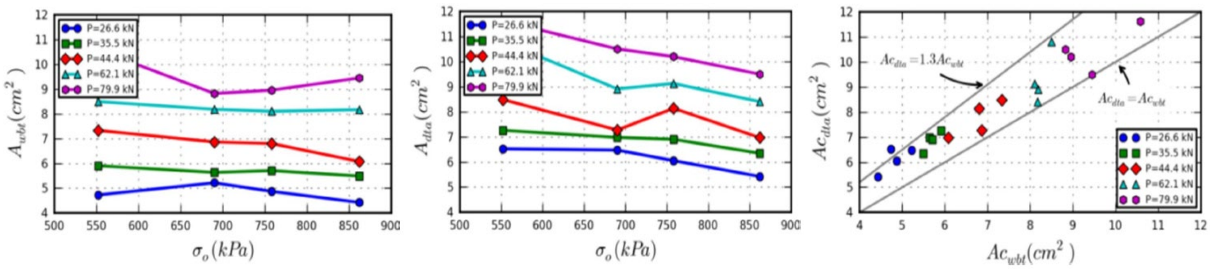

(a) WBT: 445/50R22.5 (b) DT (c) Relationship

Figure 2.1. Variation of contact area for WBTs and DTs and the relationship (From [8])

Based on current research of the actual contact area for WBTs and DTs as well as obtained survey results of WBT types used in Michigan, the research team decided to assume 10%, 20%, and 30% larger contact pressures for WBTs than DTs to evaluate the difference of pavement mechanical response. For pavement distress analysis, 20% larger contact pressure will be used since 455/55R22.5 and 445/50R22.5 are the most common WBT types used in Michigan.

3. CHAPTER 3: INVESTIGATION OF WIDE-BASE TIRE USAGE IN MICHIGAN

3.1. Introduction and background

According to the literature review in section 2, WBT loads seem to impact pavement distress negatively in most cases. The North American Council conducted a survey on 21 major carriers and found that the use of WBTs in tractors rose from 6% in 2003 to 51% in 2012 but then declined to 38% in 2018, which shows a huge variance of WBTs on pavement, even in several years [24]. WBT sale data from the US Tire Manufacturers Association (USTMA) in Figure 3.1 present the growing market of WBTs in the US (before the pandemic). Some companies based in Michigan, such as Meijer, have large fleets using WBTs in the state. Therefore, WBTs have become an inevitable issue to address with respect to Michigan's pavement infrastructure. As axle load is a critical parameter in the mechanical-related distresses of pavement, and as the percentage of WBT loads varies in different areas and even in different road sections, it is crucial to find out the actual WBT proportion in Michigan before conducting quantitative studies.

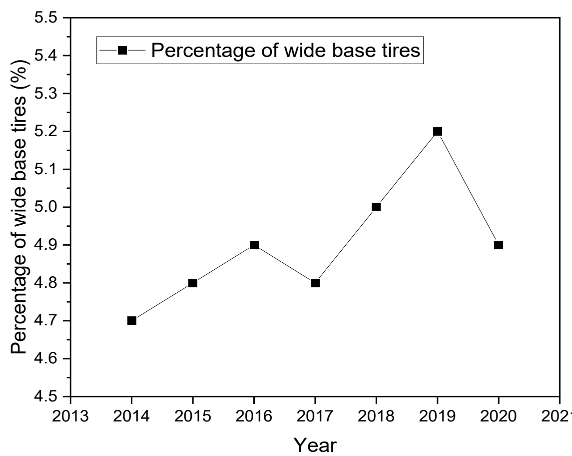

Figure 3.1. Percentage of WBTs among all truck tire sales according to USTMA

Before conducting the field investigation, the research team conducted user and manufacturer surveys, as presented in Appendix A in its entirety. As part of this effort, the team contacted more than 300 companies by email and phone. However, only ten responses from WBT users and one from a tire manufacturer have been obtained. About 60% of responded truck companies state that more than half of their trucks have some WBTs used (Figure A.1). The WBT types used in Michigan are primarily new generation (with a width of 445mm or 455mm) and can be in any axles (Figure A.2, A.4). Fuel economy is the primary reason that WBTs are adopted (Figure A.6), as economics (reduced load or increased payload) and environmental concerns have driven some companies' policies. The only manufacturer who responded to the survey is not optimistic about WBT sales in the future; however, the manufacturer's survey results support that 445mm width WBTs are the most popular (Figure A.9).

3.2. Comparison of WBT tire usage investigation methods

Based on the survey in section 3.1, some valuable information was obtained (e.g., type and market scale of WBTs in Michigan); however, a more accurate WBT proportion in Michigan remains unknown, so the research team conducted a field investigation to quantify this factor better. While measurements using in-service sensors (pressure mats on the surface) were discussed, the research team felt that this was not a cost-effective way to obtain this data within the scope of this project. The general plan for field investigation was to record the traffic in some areas of Michigan, using convolutional neural networks (CNN) to distinguish the axle and tire types and then calculate the WBT percentage of trucks and axles from the obtained data. Various techniques (camera, radar, laser, etc.) can be used to record videos. Before conducting the field investigation, the team compared these video recording techniques and developed a comparison table in Table 3.1.

Table 3.1. Comparison of typical video recording equipment

Types	GoPro	Infrared camera	Laser sensor	Professional Camera	Radar
Stability	B	C	B	A	A
Clarity	B	C	B	A	C
Low-cost	A	B	C	C	C
Usability for CNN	B	C	B	A	C
Portability	A	B	C	C	C
Endurance	A	B	C	C	B
Low impact on traffic	A	B	B	C	A
Availability in dark	C	A	B	B	A

*: " A " indicates excellent; " B " indicates good; " C " indicates poor

After considering the options, the research team took videos to investigate truck tire types (WBT; DT) with a GoPro camera during this task for the following reasons:

(1) Stability

As a professional sports brand, the most significant advantage of the GoPro camera is capturing stable images of moving objects, and it has been successfully applied to the pavement field for cracking inspection [25]. As this task required recording moving trucks on the road, the GoPro camera's anti-shake property was critical for recording.

(2) Clarity of images at a low cost

Although GoPro cannot provide in-depth information like laser sensors [26], moving truck images shot by GoPro are clear enough for further analysis. GoPro images' expense and process costs are relatively low, while complex algorithms need inputs for optimal radar images [27]. Furthermore, applying radar in axle identification is rarely seen in current research [28, 29]. The GoPro camera is cheap and easy to install and use, significantly satisfying axle-type identification requirements at a low cost.

(3) Usability for CNN

The team used convolutional neural networks (CNN) to distinguish the axle and tire types in the task. Deep learning was applied with a vast number of actual truck pictures in different classes. So, technically, the imported images ought to be in natural light rather than infrared or radar images [30, 31]. It would be nearly impossible to find enough infrared pictures of trucks in different classes as the database for deep learning and training of a CNN.

(4) Portability and endurance

In this task, the team investigated the usage of WBTs in eight different locations across Michigan, covering the Lower and Upper Peninsulas. A portable tool is essential for completing the investigation within the required time, and GoPro perfectly satisfies this requirement.

The recording time for the video survey could last 3 hours at most to obtain enough data. A GoPro can continuously record 2 hours of video without an external power source, and then the user can quickly and easily replace the batteries, an advantage not easily found in other tools for this task.

(5) Low impact on traffic

The recording location must be close to the trucks to get clear images of truck axles with tire-type information. Complex photographic equipment with a higher resolution ratio may distract drivers and compromise safety during data collection. The GoPro camera used in this survey was installed right by the roadside. Beneficial for its unobtrusive size, the camera was able to gather videos and pictures of axles without attracting attention from drivers.

3.3. WBT field investigation process

The research team took videos to investigate the volume and percentage of trucks (Classes 7 through 13) with WBTs or DTs at several slow-speed MSP weigh stations in the Lower Peninsula. Three pavement sections in the Upper Peninsula were selected for investigation since traffic in the

Upper Peninsula is relatively low and MSP weigh stations are not prevalent. The locations of these investigated areas are shown in Figure 3.2, with the longitude and latitude information in Table 3.2. Before taking these videos, the research group obtained the advance notice and approval of permitted activities files from MDOT, as shown in Appendix B.

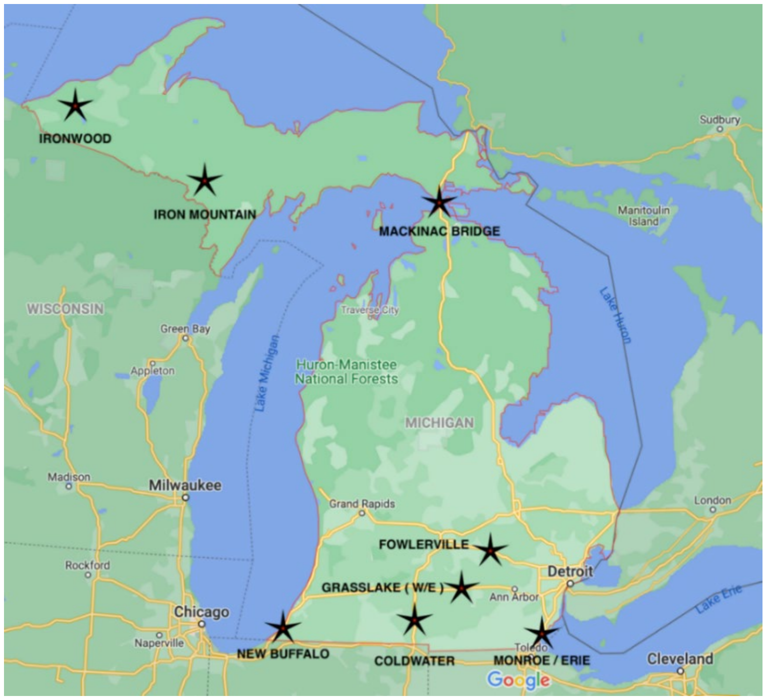

Figure 3.2. Location of weigh stations and pavement sections for investigation

Table 3.2. Latitude and Longitude of investigated areas

Location	Latitude	Longitude
I-96 Fowlerville weigh station	42.646032	-84.085092
I-94 Grass Lake(W/E) weigh station	42.284719	-84.283530
I-75 Monroe/Erie weigh station	41.816805	-83.442808
I-94 New Buffalo weigh station	41.768933	-86.738116
I-69 Coldwater weigh station	41.848744	-84.996319
I-75 Mackinac Bridge	45.850527	-84.722166
US 2 Ironwood (MN/WI Traffic)	46.463048	-90.195617
US 2 Iron Mountain (WI Traffic)	45.817074	-88.065522

As shown in Figure 3.2, five MSP weigh stations were selected for investigation in the Lower Peninsula. The weigh station access allowed for safe installation, monitoring, and recording of data of trucks moving slowly over the scales. For each weigh station, at least three hours of video was recorded between 10 am and 2 pm.

In addition to assessing trucks at MSP weigh stations, the research team also investigated some rest areas and truck stops in the Lower Peninsula to sample the percentage of trucks using

WBTs to assess WBTs installed on trucks utilizing the MDOT trunkline system. The locations are presented in Figures 3.3 and 3.4.

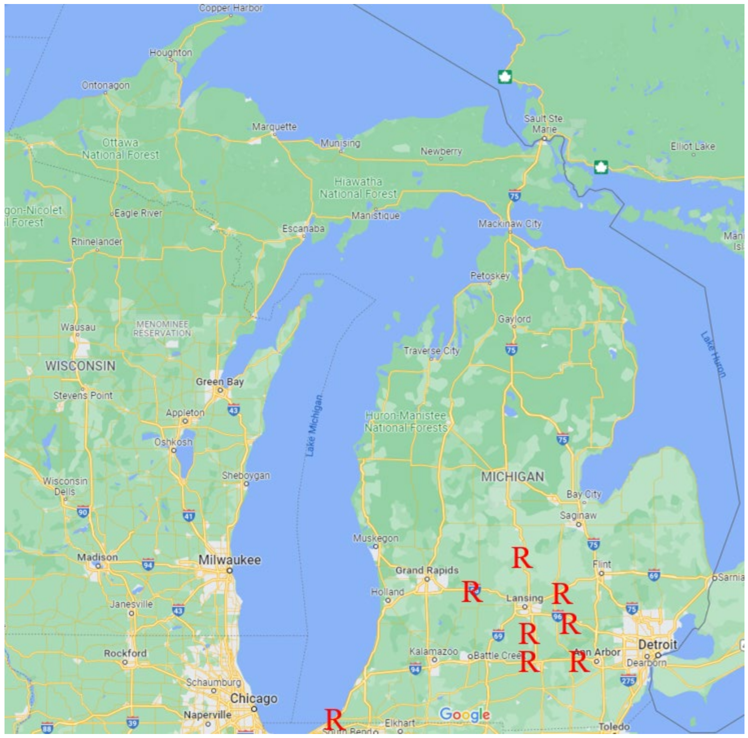

Figure 3.3. Location of rest areas for investigation

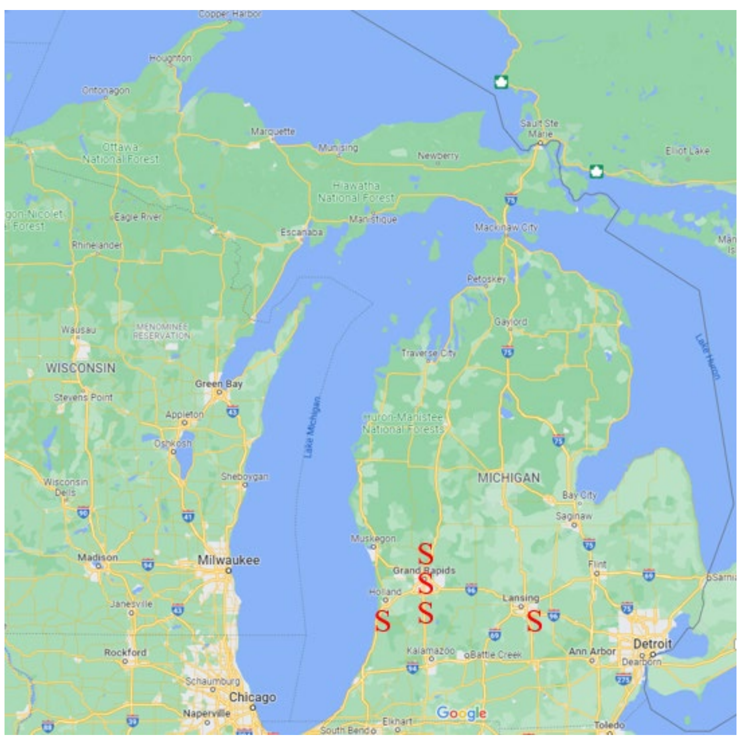

Figure 3.4. Location of truck stops for investigation

The research team developed a convolutional neural network (CNN) app to distinguish tire types and Federal Highway Administration (FHWA) vehicle classes from the recorded videos. The operation windows and code for the CNN app are presented in Appendix C. CNNs are deep learning algorithms that utilize images to assign importance (learnable weights and biases) to various aspects of an image and to be able to differentiate one from the other. This tool is handy in assessing minor differences in an image, as one would need to accomplish to distinguish tire types.

3.4. WBT field investigation results

3.4.1. Investigation results in the Lower Peninsula

The results of the total recorded number of trucks in different weigh stations in the Lower Peninsula are shown in Figure 3.5. The I-75 Monroe/Erie and I-94 New Buffalo weigh stations sampled a relatively high truck number, at 1,337 for New Buffalo and 1,250 for Monroe/Erie. In contrast, the I-69 Coldwater weigh station has the lowest recorded truck number at 163.

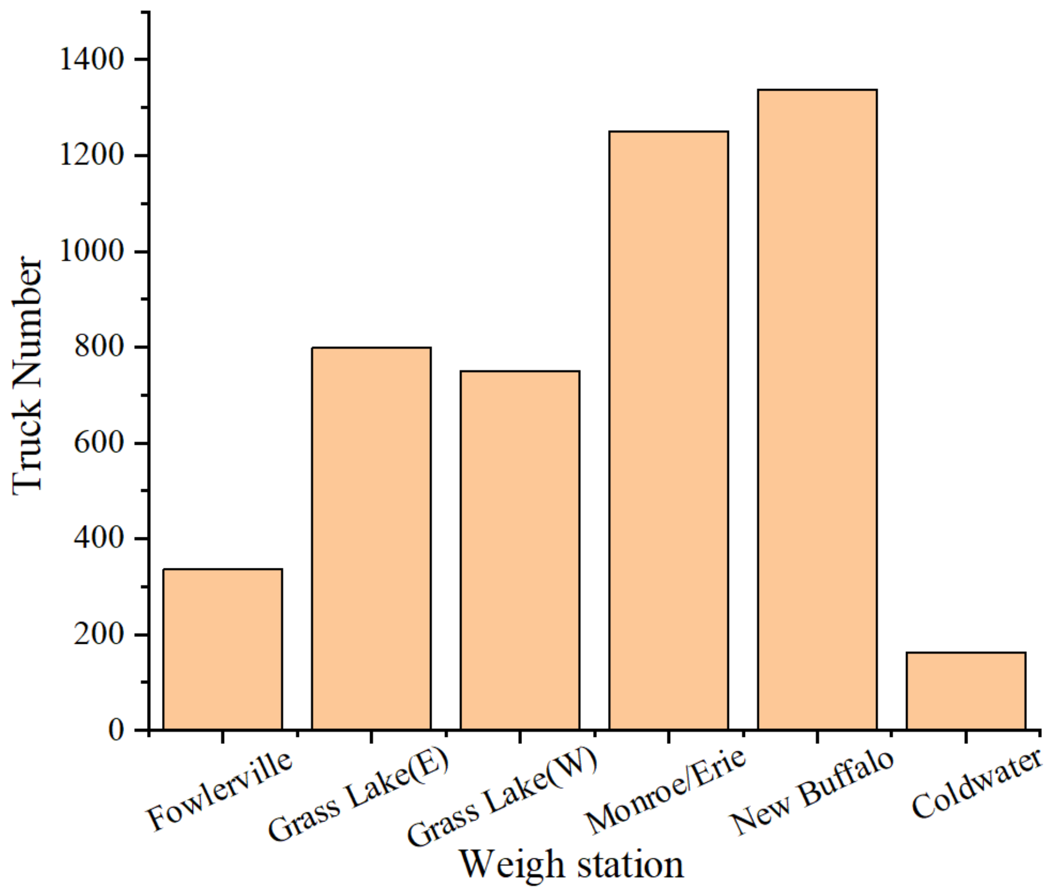

Figure 3.5. Total number of trucks recorded at Lower Peninsula MSP weigh stations

The percentage of trucks with any WBTs (either in drive axle, trailer axle, or both) in the above-recorded trucks was analyzed by the CNN model, as shown in Figure 3.6. The percentage of trucks with any WBTs at Lower Peninsula MSP weigh stations ranged from 9.1%-12.9%, with an average value of 11%. The I-94 Grass Lake(E) weigh station showed the highest percentage of trucks with any WBTs at 12.9%, while the I-94 New Buffalo weigh station demonstrated the lowest value at 9.1%.

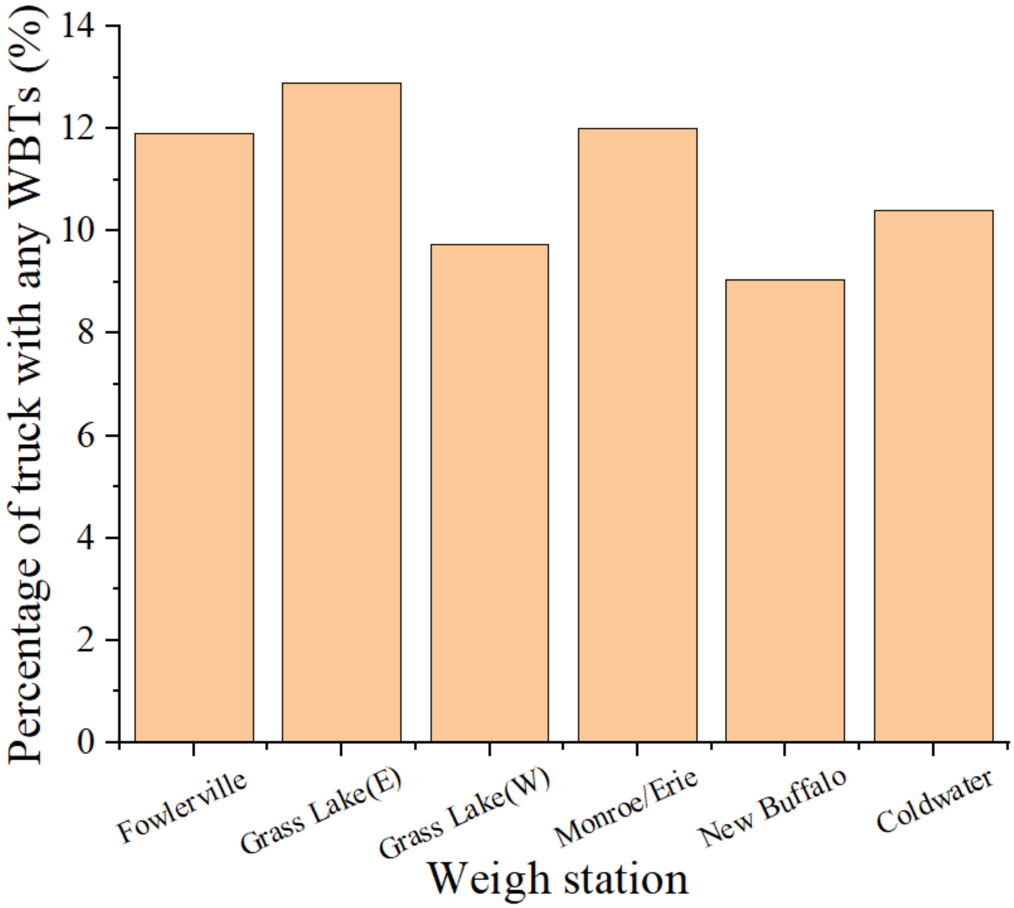

Figure 3.6. Percentage of trucks with any WBTs at Lower Peninsula MSP weigh stations

According to the investigation, the research team noticed that Class 9 is the primary type of truck with WBTs. The percentage and number of class 9 trucks in total investigated trucks with any WBTs at Lower Peninsula weigh stations are shown in Figure 3.7. Class 9 trucks occupied 87% (on average) of total trucks with any WBTs and are above 75% at every weigh station. The remaining trucks with any WBTs are in Class 10 or Class 13.

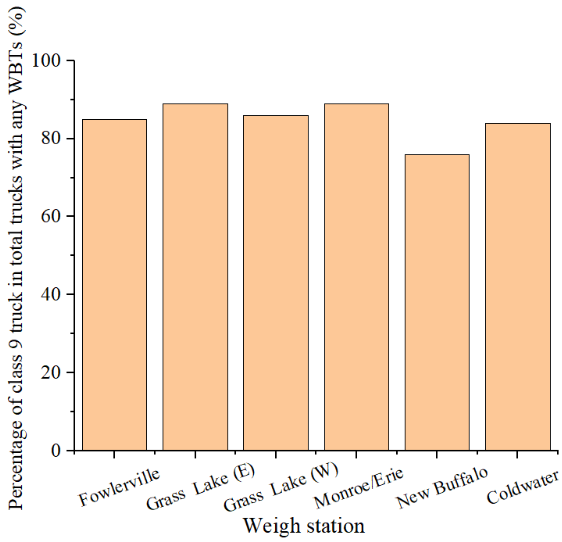

(a) Percentage of class 9

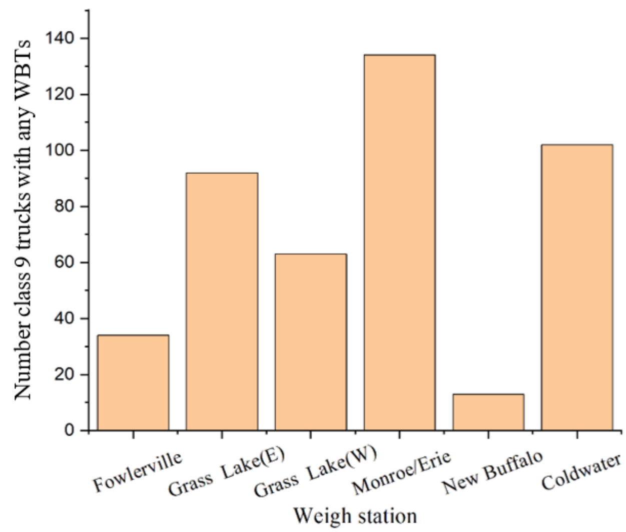

(b) Number of class 9

Figure 3.7. Percentage and number of class 9 trucks on total trucks with any WBTs at Lower Peninsula weigh stations

As introduced in section 3.3, the WBT usage at rest areas and truck stops was also investigated. The percentage of trucks with WBTs is shown in Figure 3.8 from the rest areas and Figure 3.9 from the truck stops.

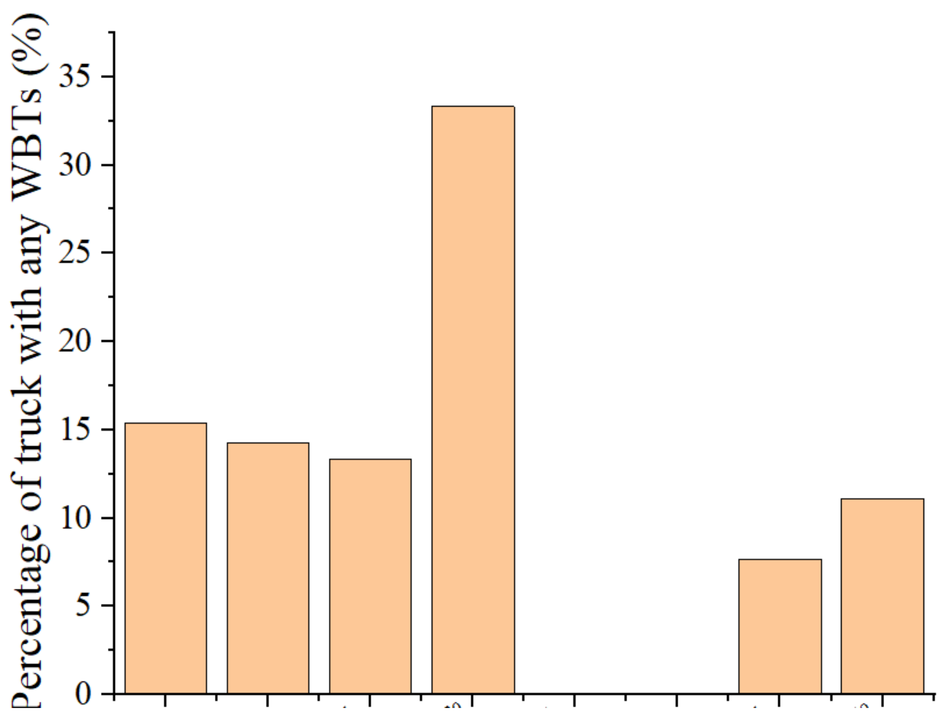

Figure 3.8. Percentage of trucks with any WBTs at Lower Peninsula rest areas

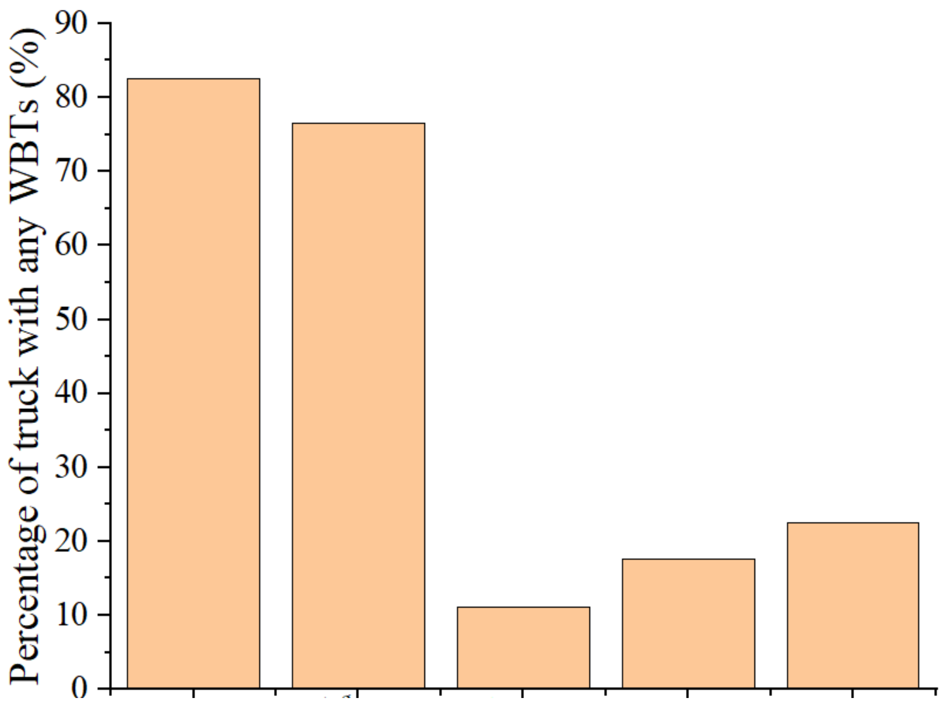

Figure 3.9. Percentage of trucks with any WBTs at Lower Peninsula truck stops

As shown in Figures 3.8-3.9, the results vary significantly between individual rest areas and truck stops, which wouldn't logically reflect the general WBT percentage in Michigan. The average percentage of trucks with any WBTs at rest areas is 13.5%. The average percentage of trucks with WBTs at truck stops is 46.9% based on this small sample, which was highly influenced by the oversampling of vehicles from particular companies who have higher than average volumes of WBTs in their fleets.

A relatively stable percentage of trucks using any WBTs is obtained at Lower Peninsula weigh stations (Figure 3.6); however, these WBTs are distributed in different axles. As the pavement mechanical-related distress is determined by axle load repetitions rather than the number of trucks with WBTs, it's essential to identify the percentage of WBT axles noted from the above data. In order to achieve that, the distribution of WBTs in different axles should be determined. Since Class 9 trucks are the primary contributor of WBTs in the investigation (see Figure 3.7 (a)), the research team used the axle distribution of WBTs in class 9 to represent the axle distribution of all trucks with any WBTs. Figure 3.10 shows the distribution of WBTs in different axles for Class 9 trucks at Lower Peninsula weigh stations.

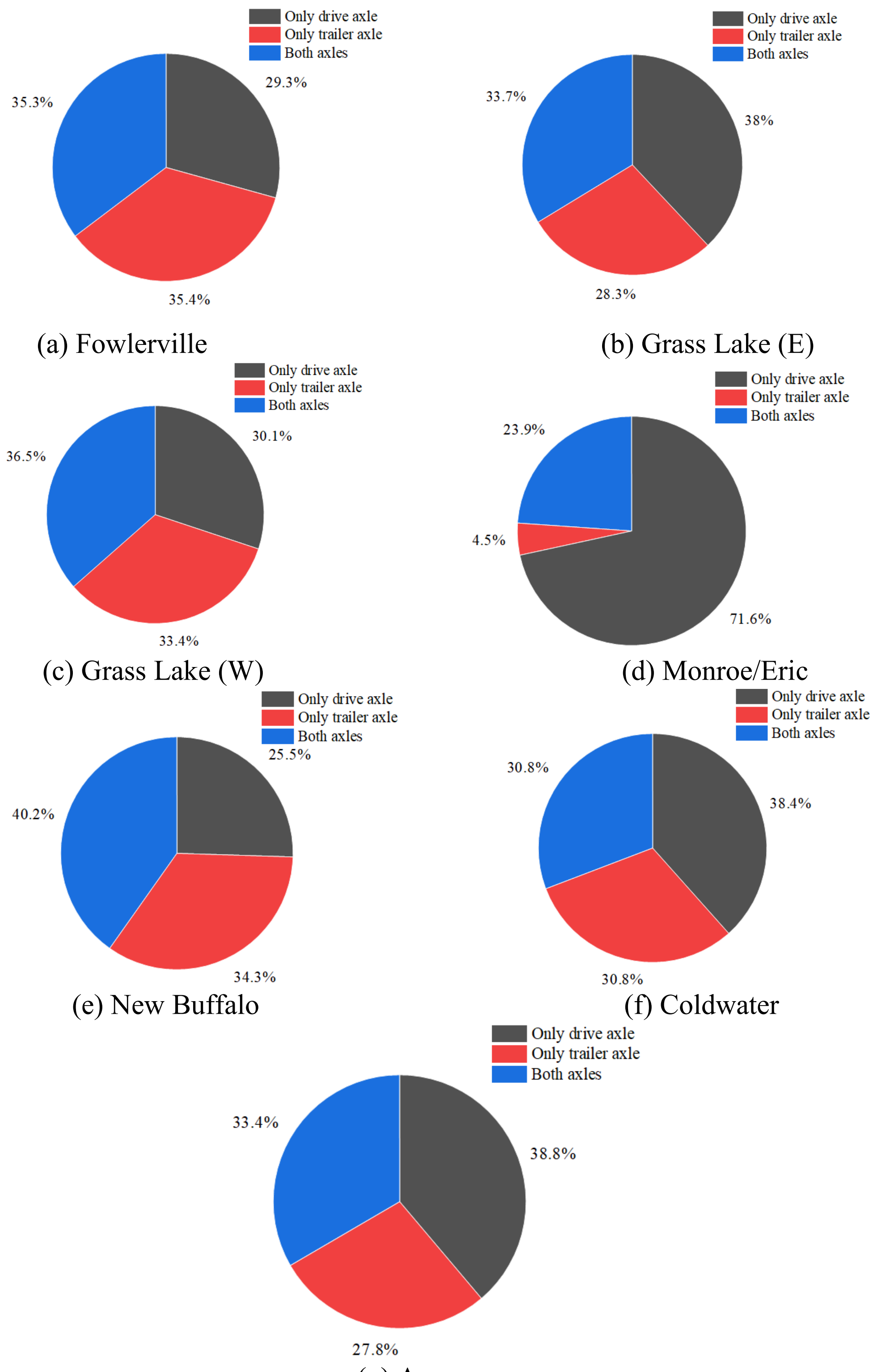

Figure 3.10. Distribution of WBTs in different axles for Class 9 trucks at Lower Peninsula weigh stations

According to Figure 3.10, the distribution of WBTs in drive axles, trailer axles, and both axles are 33.8%, 27.8%, and 33.4%, respectively, on average. Based on Figure 3.6 and Figure 3.10, the percentage of WBT loaded axles ($P_{\text{WBT load axle}}$) can be computed using equation (3.1); the results are shown in Table 3.3.

$$P_{WBT\ load\ axle} = P_{Truck\ with\ any\ WBT} \times (P_{In\ both\ drive\ and\ trailer\ axles} + 0.5 \times (1 - P_{In\ both\ drive\ and\ trailer\ axles}))/100 \quad (3.1)$$

Table 3.3. Percentage of WBT loaded axles at different weigh stations

Location	$P_{\text{Truck with any WBT}}$ (%)	$P_{\text{In both drive and trailer axles}}$ (%)	$P_{\text{WBT load axle}}$ (%)
Fowlerville	11.9	35.3	8.05
Grass Lake (E)	12.9	33.7	8.62
Grass Lake (W)	9.7	36.5	6.62
Monroe/Erie	12	23.9	7.43
New Buffalo	9.1	40.2	6.38
Coldwater	10.4	30.8	6.80
Average	**11**	**33.4**	**7.32**

According to Table 3.3, the percentage of WBT loaded axles is 7.32% using the distribution of WBTs in different axles for Class 9 trucks. This research did not investigate some classes of trucks included in AASHTO 93 pavement design (Class 5 - 6) or Pavement ME design (Class 4 - 6). However, the research team would assume Class 4 - 6 trucks would have similar WBT percentages as those investigated in MSP weigh stations. In addition, the pavement design life in Michigan is typically 20 years, so at least ten years of the WBT's growth may be added to the current WBT percentage for any design considering WBT to approximate an average value over the design life. Considering all these impacts, the research team would suggest rounding up to a conservative 10% as the current WBT percentage in the Lower Peninsula.

3.4.2. Investigation results in the Upper Peninsula

The investigation results from several pavement sections are presented in Table 3.4. The percentage of trucks with any WBTs in the Upper Peninsula was found to be consistently lower than that in the Lower Peninsula. The average percentage of trucks with any WBTs in the Upper Peninsula was 5.68%. If the distribution of axles utilizing WBTs for the Upper Peninsula is assumed to be similar to the Lower Peninsula (drive axle, trailer axle, or both), then the WBT percentage of loaded axles would be less than 5% in the Upper Peninsula.

Table 3.4 Percentage of trucks with any WBTs on Upper Peninsula pavement sections

Location	Number of Trucks	Percentage of trucks with any WBT (%)	Recording time
US-2 Ironwood (MN/WI to MI)	48	2.1	3h
US-2 Ironwood (MI to MN/WI)	45	4.4	3h
US-41 Iron Mountain (MI to WI)	43	6.9	3h
US-41 Iron Mountain (WI to MI)	86	5.8	3h
I-75 Mackinac Bridge (UP to Lower Peninsula)	85	7.5	2h 30 min
I-75 Mackinac Bridge (Lower Peninsula to UP)	80	5.9	2h 30 min
Average	**64.5**	**5.68**	**2h 50 min**

3.4.3. Future WBT usage estimation

Based on the statistical data from the US Tire Manufacturers Association (USTMA), the percentage of WBTs among all truck tires in recent years is shown in Figure 3.11 (a).

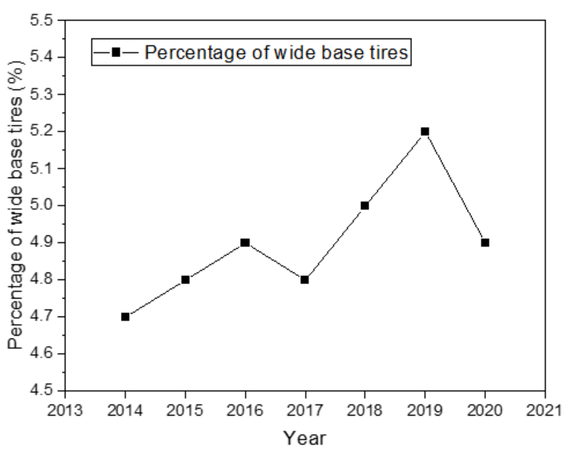

(a) Original data (2014-2020)

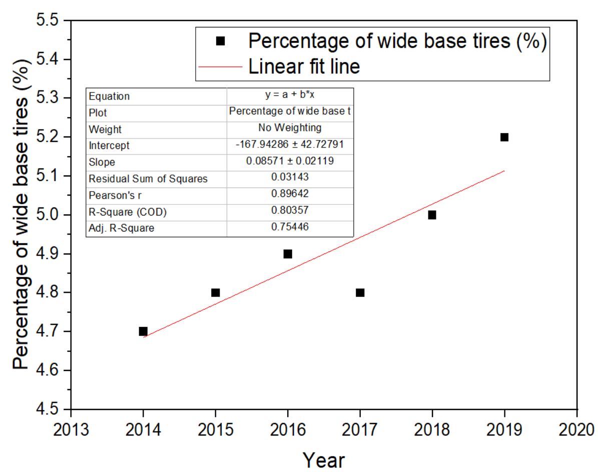

(b) Linear fit results (2014-2019)

Figure 3.11. Prediction of WBT sales among all truck tire sales based on USTMA data

It is worth pointing out that the percentage of WBTs among all truck tires in Figure 3.11 (a) is not equal to the proportion of WBT loads since tires would be assembled onto load axles with four tires required for dual tire assemblies and only two tires for WBT single axles. However, the increase of WBTs every year would be valuable for WBT load prediction. As shown in Figure 3.11 (a), the percentage of WBTs among all truck tires is slowly increasing (after a decrease in 2020 due to the COVID-19 pandemic).

Based on the WBT sales data from 2014 to 2019, the research team linear fitted the trend of the percentage of WBTs (Figure 3.11 (b)) and found that the WBT load proportion in Michigan would grow from 10% to 25% after approximately 80 years. However, there could be a huge variance of WBT proportion in different years from others' research, as shown in section 3.1, and linear prediction presents how WBT loads would develop only if under this limited assumption, which does not mean the WBT usage has to follow this trend in the future.

3.5. Chapter summary

Based on the investigation of WBT usage in Michigan from this chapter, the following conclusions can be drawn:

(1) The percentage of trucks with any WBT was relatively consistent in the Lower Peninsula, with an average of 11% of trucks using any WBTs (roughly 1 in 9 trucks). 87% of trucks with WBTs are Class 9 trucks. The remaining 13% of WBT trucks are Class 10 and 13. The percentage of trucks using any WBTs in the Upper Peninsula was lower than in the Lower Peninsula, with an average of 5.68% of the traffic sampled.

(2) The percentage of axle loads with WBTs is 7.32% in the Lower Peninsula and less than 5% in the Upper Peninsula when accounting for the fact that not all axles utilized WBTs on these trucks.

(3) A higher percentage of WBTs are in the drive axles. The distribution of WBTs in drive axles (only), trailer axles (only), and both drive and trailer axles are 33.8%, 27.8%, and 33.4%, respectively.

(4) The percentage of trucks with WBTs at truck stops and rest areas varied significantly due to less representative sampling.

(5) Sales of WBT from USTMA suggest a roughly yearly 0.1% increase in WBT percentage based on data from 2014 to 2019. This would suggest a roughly 1% increase in WBT usage for every decade of a pavement service life (7.32% to 8.32% in 10 years). Based on field investigation and this assumption of sales growth, 10% would be recommended as the current WBT design proportion of axles in the quantitative impact analysis for the Lower Peninsula, with 5% recommended for the Upper Peninsula. This accounts for some small level of conservatism and potential growth in the near term. The quantitative analysis presented in Chapters 4 and 5 allows for WBT axle use up to 25% (more than 100 years is needed to increase from 10% to 25%

according to current WBT growth) to account for potential future WBT proportions, considering possible WBT usage growth.

4. CHAPTER 4: QUANTIFICATION OF WBT IMPACT ON FLEXIBLE PAVEMENT AND DESIGN IMPROVEMENT

4.1. Preparation for flexible pavement distress analysis

The research team adopted the linear elastic analysis software "JULEA," which is also used in Pavement ME software, to obtain the critical response under dual-tire (DT) and wide base tire (WBT) loads. Then, the impact of different proportions of WBT loads on the distress of flexible pavement was computed with the critical response results from JULEA. The flowchart of the process is presented in Figure 4.1.

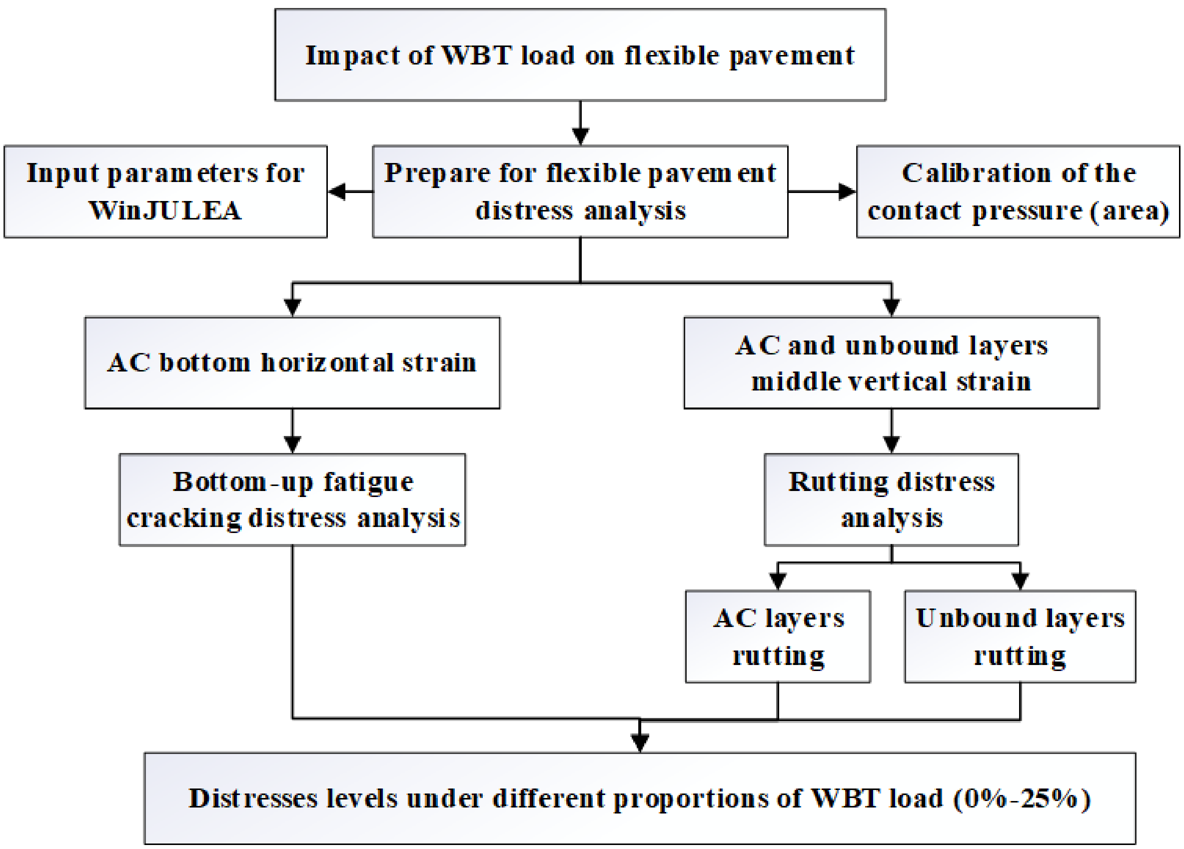

Figure 4.1. Flow chart of this chapter

Four flexible pavement structures with various asphalt concrete (AC) thicknesses (5"-11.5") were selected for analysis in this project, as presented in Table 4.1. The different AC thickness structures are suitable for roads with CADT (commercial annual daily traffic) from about 500 (5" AC) to about 9000 (11.5" AC), which cover the traffic on most roads of the Michigan trunkline system. According to the current MDOT flexible pavement manual, the minimum AC thickness adopted in Michigan is 6.5". However, MDOT is trying to assess the feasibility of the 5" AC structure under lower-traffic scenarios (CADT around 500), so the 5" AC structure is included in this project.

Table 4.1. Flexible pavement structures for analysis

Structure type		5" AC structure	6.5" AC structure	9.5" AC structure	11.5" AC structure
AC courses	Top course (Layer 1)	2.0" HMA 4E3	1.5" HMA 5E3	2.0" HMA 5E10	2.0" HMA GGSP
	Leveling course (Layer 2)	3.0" HMA 3E3	2.0" HMA 4E3	2.5" HMA 4E10	2.5" HMA 4E30
	Base course (Layer 3)	/	3" HMA 3E3	5.0" HMA 2E10	7.0" HMA 3E30
Base		6" Unbound aggregate, M_r = 33,000 psi			
Subbase		18" Unbound sand, M_r = 20,000 psi			
Subgrade		Sandy clay subgrade, M_r = 5,000 psi			

The axle load information of DT and WBT loads used in JULEA is shown in Table 4.2. For DT and WBT loads, the same weight was assumed to be applied on the axle. Based on previous research on typical truck tire pressures, tire pressures of 80, 100, 110, 120, and 125 psi for both loads were analyzed.

Table 4.2. Axle load information of DTs and WBTs

Load type	Load weight of half axle (lbs)	Tire spacing (inch)	Tire pressures (psi)
DT load	9000	12	80, 100, 110, 120, 125
WBT load	9000	N/A	80, 100, 110, 120, 125

The analysis positions for different mechanical responses in the JULEA software are presented in Table 4.3 and Figure 4.2.

Table 4.3. Pavement mechanical response analysis positions

Distress type	Response type and position
Fatigue cracking (Bottom-up)	Tensile strain at the bottom of AC layer
Fatigue cracking (Top-down)	
AC rutting	Vertical strain at the middle of each AC sublayer
Total rutting (AC + Unbound layers + Subgrade)	AC+ Vertical strain at the middle of each unbound layer (Subgrade: 6" below top)

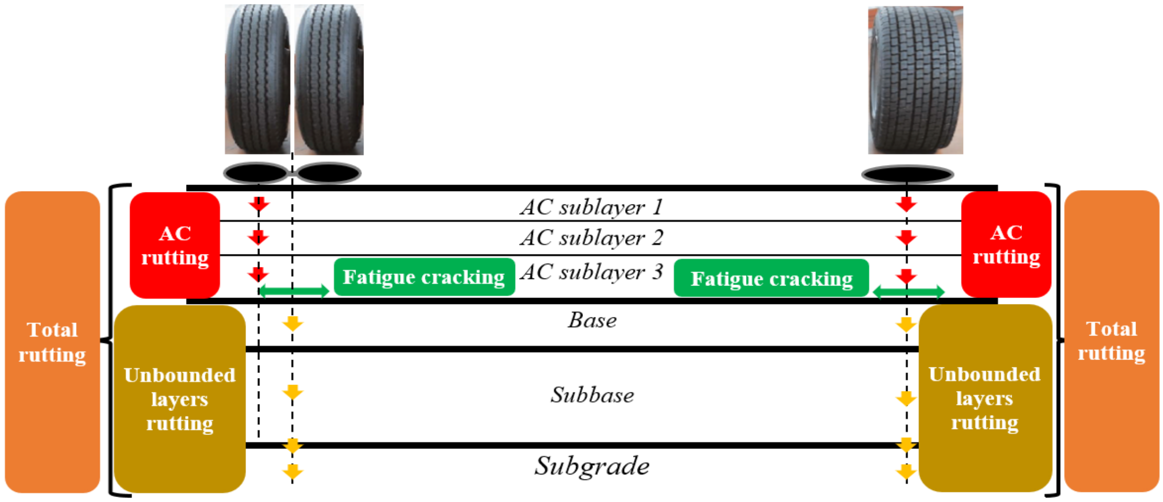

Figure 4.2. Pavement mechanical response analysis positions

The research team used the measured dynamic modulus of AC materials mentioned in Table 4.1 from previous research in this project. However, the elastic modulus rather than dynamic modulus should be input into JULEA software for mechanical response calculation. To transform current dynamic modulus data to elastic modulus, the research team multiplied the dynamic modulus (at 70 °F, 10Hz) by the dynamic modulus reduction factor (RF_{DM}) of 0.5, 0.4, and 0.3. The obtained modulus shown in Table 4.4 is within the typical elastic modulus range recommended in MDOT MEPDG.

Table 4.4. Dynamic modulus and elastic modulus of AC

Structure type	AC type	Dynamic modulus (E*) at 70 °F, 10Hz (psi)	Elastic modulus (E) in different reduction factors (psi)		
			×0.5	×0.4	×0.3
5” and 6.5” AC structure	5E3	272,062	136,031	108,825	81,619
	4E3	311,309	155,655	124,524	93,393
	3E3	571,086	285,543	228,434	171,326
9.5” AC structure	5E10	713,565	356,783	285,426	214,070
	4E10	857,698	428,849	343,079	257,309
	2E10	1,008,063	504,032	403,225	302,419
11.5” AC structure	GGSP	609,288	304,644	243,715	182,786
	4E30	820,258	410,129	328,103	246,077
	3E30	1,379,247	689,624	551,699	413,774

In order to evaluate the impact of elastic modulus on the pavement critical response and determine the most reasonable RF_{DM}, the tensile strain at the bottom of AC for the 9.5” AC structure with different RF_{DM} was computed for demonstration. Part of the JULEA output examples is presented in Figure 4.3.

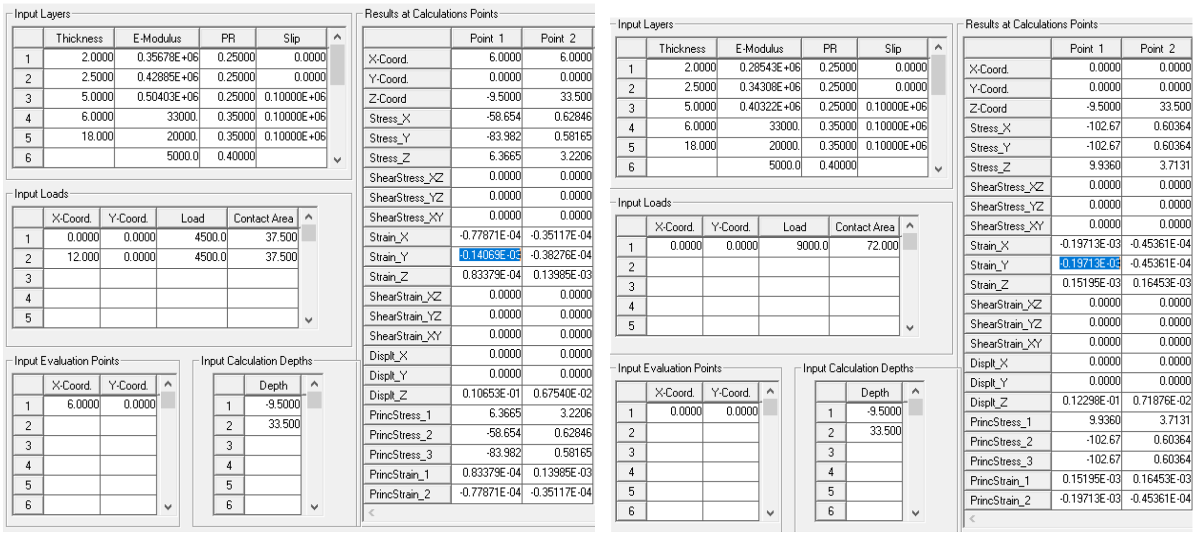

(a) under DT load **(b) under WBT load**

Figure 4.3. JULEA output examples

The horizontal tensile strain at the AC bottom of the 9.5" AC structure under WBT and DT loads with different RF_{DM} is shown in Table 4.5. Compared with the strain value under DT load, the percent increase of strain under WBT load with different RF_{DM} was calculated and presented in Figure 4.4.

Table 4.5. Horizontal tensile strain at the bottom of the AC layer

Tire pressure (psi)	Horizontal tensile strain with different reduction factors (με)					
	E=0.5E*		E=0.4E*		E=0.3E*	
	DT	WBT	DT	WBT	DT	WBT
80	136.7	149.3	162.1	177.7	201.1	221.4
100	139.1	157.6	165.0	187.9	204.9	234.8
110	140.0	160.9	166.1	192.0	206.4	240.1
120	140.7	163.8	167.0	195.6	207.5	244.8
125	141.0	165.1	167.4	197.2	208.1	246.9

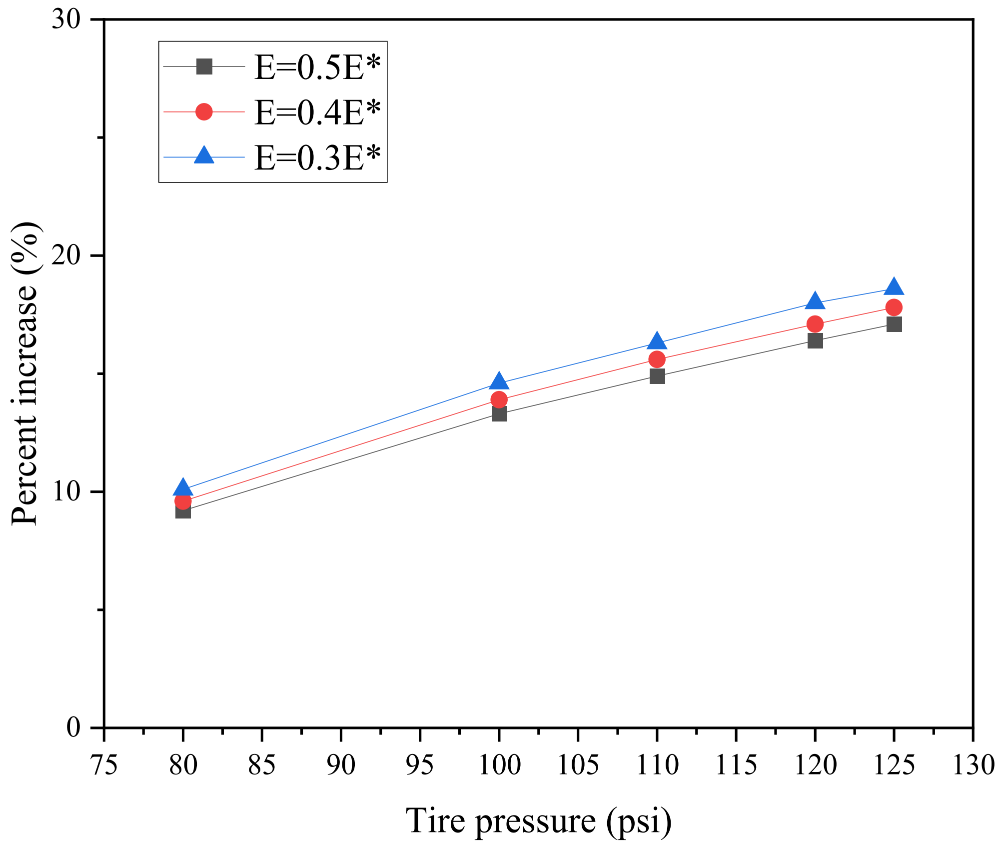

Figure 4.4. Change rate of tensile strain

Table 4.5 shows that for both DT and WBT loads, the horizontal tensile strain increases significantly with tire pressures under all RF_{DM}. However, Figure 4.4 proves that the percent increase of tensile strain from under DT load to under WBT load has a limited correlation with the RF_{DM}. This phenomenon means that the value of RF_{DM} would have little influence on evaluating the impact of WBT load on pavement distress. So, in the following analysis, the research team will choose 0.5 as the RF_{DM} value for the HMA elastic modulus for all AC thickness structures.

4.2. Pavement ME analysis for flexible structures

4.2.1. Input for Pavement ME

This section contains several Pavement ME analysis (version 2.6.1.0) examples in seven different WIM stations in Michigan and compares the difference in pavement distresses before and after considering the WBT loads. The location of the seven WIM stations is shown in Figure 4.5.

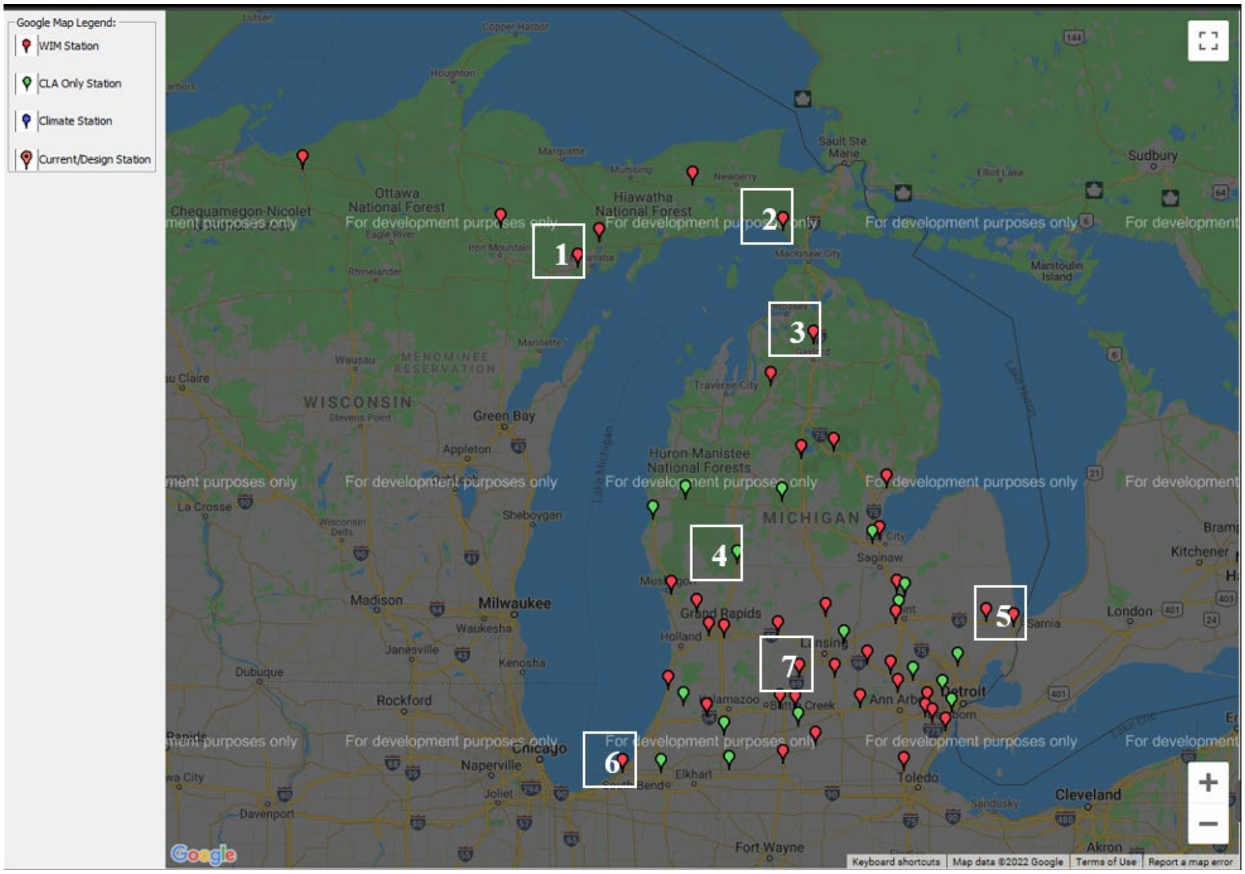

Figure 4.5. Location of 7 WIM stations

Based on the WIM stations' locations, the lane and CADT information in 2019 (Pre-Pandemic) was investigated, as shown in Table 4.6 and Figure 4.6. The AC thickness was determined based on the CADT value and corresponding traffic levels.

Table 4.6. Pavement section information

WIM station	Lanes in one direction	Two-way CADT in 2019*	Determined AC thickness (inch)	Climate NO.
US-41 (211459)	1	589 (Low)	5	150486
US-2 (492029)	1	496 (Low)	5	151065
I-75 (694049)	2	1330 (Low)	6.5	149914
US-131 (595249)	2	1965 (Medium)	9.5	148184
I-94 (776469)	2	3230 (Medium)	9.5	147613
I94 (117189)	3	12088 (Heavy)	11.5	146454
I69 (238869)	2	6203 (Heavy)	11.5	147033

***Source:**https://lrs-mdot.hub.arcgis.com/

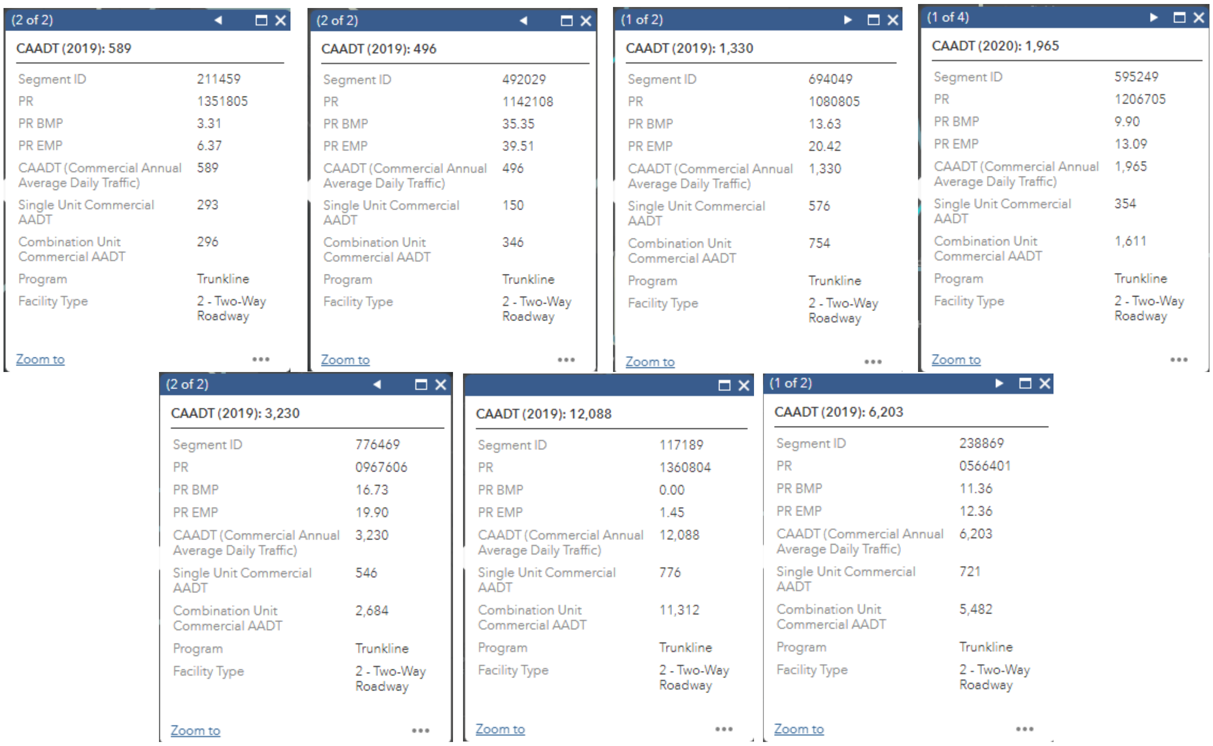

Figure 4.6. 2019 CADT information for WIM stations

The research team then used the Prep ME software to obtain the traffic and load distribution for each WIM station, as shown in Figure 4.7; combined with the above 2019 CADT, the traffic input files for the Pavement ME software were formed. The climate input files were selected at or near each WIM station.

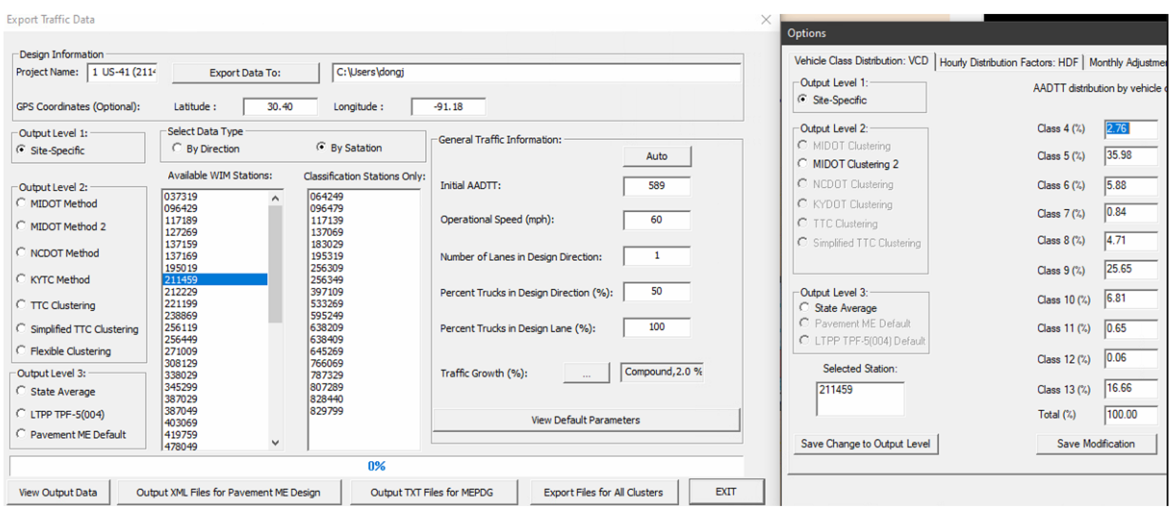

Figure 4.7. Prep ME operation window

4.2.2. Pavement ME analysis

The research team conducted the Pavement ME analysis (version 2.6.1.0) in this section.

Two different input levels were used for the input level of the asphalt binder and AC material (Level 3: Defaulted value; and Level 1: Laboratory value). The pavement distress calibration was divided in two (Global calibration and Michigan calibration).

It is worth noting that the top-down cracking distress model and function were revised after Version 2.6.1 Pavement ME software, but the MDOT pavement design manual (March 2021) did not adopt the latest top-down cracking model yet [21]. The top-down cracking distress in the Michigan ME design process is now involved in the bottom-up cracking. So, when adopting Michigan calibration, the top-down cracking should not be used; the AC rutting distress threshold should also not be used in Michigan calibration. The Pavement ME analysis results are presented in Tables 4.7-4.10, with details shown in Appendix D.

Table 4.7. Analysis results under level 3 and Global calibration

NO.	WIM station	Traffic	Distress value				
			Bottom-up (%)	Top-down (%)	AC rutting (inch)	Total rutting (inch)	IRI
Threshold			20	20	0.25	0.75	172.00
1	US-41 (211459)	Low	1.86	9.57	0.09	0.58	166.73
2	US-2 (492029)	Low	1.86	10.13	0.10	0.58	167.76
3	I-75 (694049)	Low	1.89	17.08	0.19	0.67	174.65
4	US-131 (595249)	Medium	1.86	16.25	0.09	0.51	166.56
5	I-94 (776469)	Medium	1.89	16.33	0.11	0.56	168.22
6	I94 (117189)	Heavy	1.93	16.41	0.09	0.44	161.33
7	I69 (238869)	Heavy	1.89	16.42	0.10	0.47	164.87

Table 4.8. Analysis results under level 3 and Michigan calibration

NO.	WIM station	Traffic	Distress value				
			Bottom-up (%)	Top-down* (%)	AC rutting* (inch)	Total rutting (inch)	IRI
Threshold			20	20	0.50	0.50	172.00
1	US-41 (211459)	Low	28.55	9.57	0.31	0.36	138.84
2	US-2 (492029)	Low	28.80	10.13	0.34	0.39	141.09
3	I-75 (694049)	Low	29.19	17.08	0.64	0.69	160.40
4	US-131 (595249)	Medium	18.90	16.25	0.35	0.39	142.42
5	I-94 (776469)	Medium	21.87	16.33	0.39	0.43	140.44
6	I94 (117189)	Heavy	19.95	16.41	0.36	0.39	137.01
7	I69 (238869)	Heavy	18.93	16.42	0.37	0.40	138.85

Table 4.9. Analysis results under level 1 and Global calibration

NO.	WIM station	Traffic	Distress value				
			Bottom-up (%)	Top-down (%)	AC rutting (inch)	Total rutting (inch)	IRI
Threshold			20	20	0.25	0.75	172.00
1	US-41 (211459)	Low	1.86	11.32	0.09	0.57	166.92
2	US-2 (492029)	Low	1.86	13.27	0.10	0.57	168.52
3	I-75 (694049)	Low	1.88	19.82	0.27	0.73	178.14
4	US-131 (595249)	Medium	1.86	15.50	0.08	0.49	187.98
5	I-94 (776469)	Medium	1.87	15.88	0.09	0.53	189.50
6	I94 (117189)	Heavy	1.87	16.38	0.11	0.44	161.14
7	I69 (238869)	Heavy	1.86	16.41	0.12	0.47	180.92

Table 4.10. Analysis results under level 1 and Michigan calibration

NO.	WIM station	Traffic	Distress value				
			Bottom-up (%)	Top-down* (%)	AC rutting* (inch)	Total rutting (inch)	IRI
Threshold			20	20	0.50	0.50	172.00
1	US-41 (211459)	Low	26.27	11.32	0.31	0.36	137.36
2	US-2 (492029)	Low	26.44	13.27	0.35	0.40	140.10
3	I-75 (694049)	Low	28.09	19.82	0.86	0.91	172.96
4	US-131 (595249)	Medium	17.47	15.50	0.30	0.34	147.70
5	I-94 (776469)	Medium	20.07	15.88	0.33	0.38	136.15
6	I94 (117189)	Heavy	18.16	16.38	0.40	0.43	138.95
7	I69 (238869)	Heavy	17.27	16.41	0.43	0.46	141.79

*: The criteria are not used in the MDOT pavement design manual.

4.3. Fatigue cracking distress analysis

4.3.1. Mechanical response calculation

The research team computed the horizontal tensile strain at the bottom of the AC layer with the JULEA software, as shown in Table 4.11 and Figure 4.8. Examples of the JULEA analysis process are presented in Figure 4.9. The horizontal tensile strain is a critical parameter for bottom-up fatigue cracking analysis. For the DT load, the contact pressure was assumed to be equal to the tire pressure. With respect to the WBT load, the contact pressure was calculated under four different conditions: (1) the theoretical pressure, which equals the tire pressure; (2) ~ (4) the assumed actual pressures, which are 10%, 20%, 30% larger than the tire pressure.

Table 4.11. Horizontal tensile strain at the bottom of the AC layer

Structure type	Tire pressure (psi)	Horizontal tensile strain at the bottom of the AC layer (με)				
		Under DT load	Under WBT load at different contact pressures			
			0% larger	10% larger	20% larger	30% larger
5" AC structure	80	426.1	483.3	508.6	532.1	553.8
	100	437.6	543.1	569.1	593.1	615.1
	110	441.7	569.1	595.3	619.4	641.5
	120	445.1	593.1	619.4	643.4	665.4
	125	445.6	604.3	630.6	654.6	676.6
6.5" AC structure	80	342.3	387.0	403.7	419.0	432.8
	100	351.0	426.1	442.5	457.3	470.8
	110	354.2	442.5	458.8	473.4	486.5
	120	356.8	457.3	473.4	487.7	500.6
	125	358.0	464.2	480.1	494.3	507.0
9.5" AC structure	80	136.7	149.3	153.0	156.2	159.0
	100	139.1	157.6	160.9	163.8	166.3
	110	139.9	160.9	164.1	166.8	169.3
	120	140.7	163.8	166.8	169.5	171.8
	125	141.0	165.1	168.2	170.7	172.9
11.5" AC structure	80	86.6	93.2	95.1	96.5	97.8
	100	87.8	97.2	98.7	100.0	101.1
	110	88.3	98.7	100.1	101.3	102.4
	120	88.7	100.0	101.3	102.5	103.5
	125	88.9	100.6	101.9	103.0	104.0

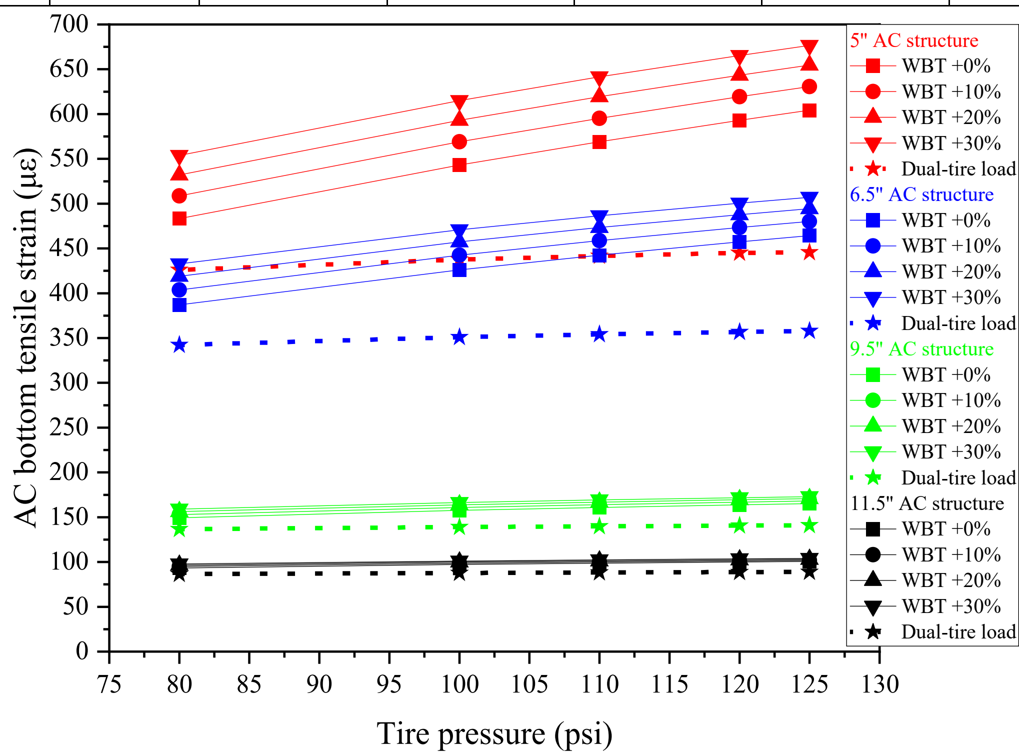

(a) General result

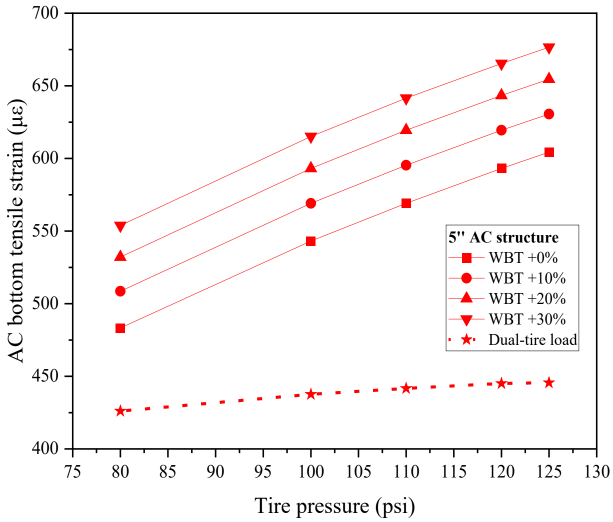

(b) 5" AC structure

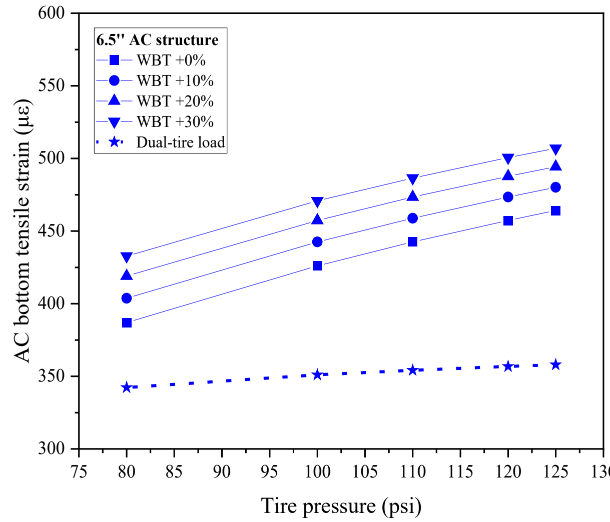

(c) 6.5" AC structure

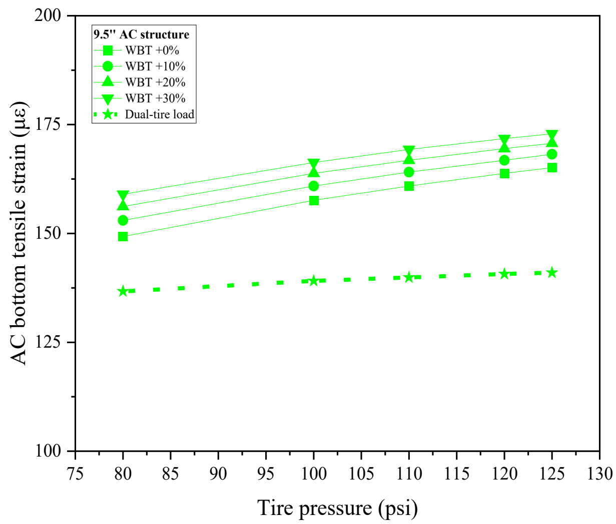

(d) 9.5" AC structure

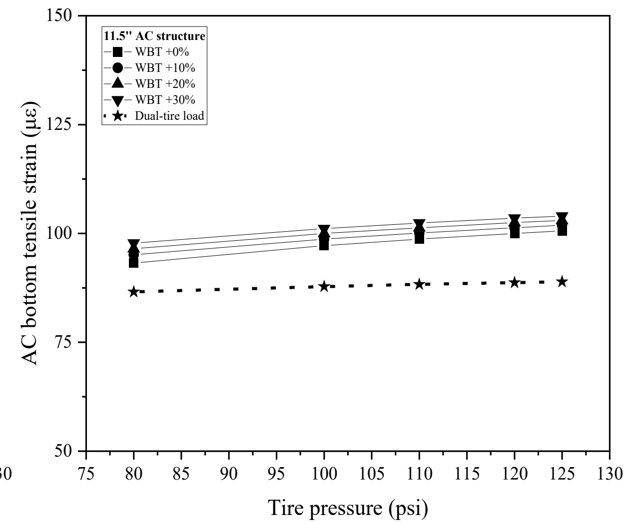

(e) 11.5" AC structure

Figure 4.8. Horizontal tensile strain at the bottom of the AC layer

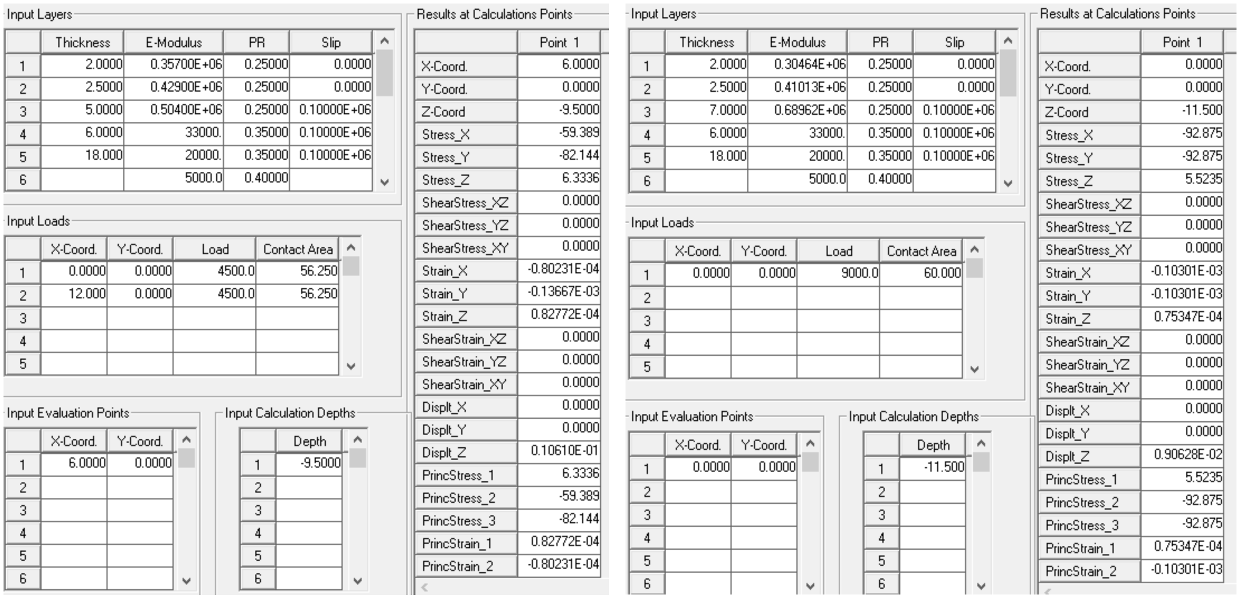

(a) Under DT load **(b) Under WBT load**

Figure 4.9. JULEA examples for AC bottom horizontal tensile strain

4.3.2. Fatigue life and damage index calculation

According to the MDOT User Guide for MEPD [21], the fatigue life of AC can be computed based on equation (4.1) with the obtained asphalt bottom horizontal tensile strain (ε_t) in Table 4.11 and some other parameters. The calibration factors in the equation are currently used by MDOT.

$$N_f = 0.00432 \times 10^{4.84\left(\frac{V_b}{V_a+V_b}-0.69\right)} \times k_1\beta_1\left(\frac{1}{\varepsilon_t}\right)^{k_2\beta_2}\left(\frac{1}{E}\right)^{k_3\beta_3} \tag{4.1}$$

where:

V_a = Percent air voids in the asphalt mixture, assume 7% in this project;

V_b = Effective asphalt content by volume, assume 11.6% in this project;

ε_t = Horizontal tensile strain at the bottom of the AC layer;

E = Resilient modulus of asphalt mixture;

k_1=0.007566; k_2=3.9492; k_3=1.281; $\beta_1 = \beta_2 = \beta_3$=1.

Since the objective of the research is to evaluate the difference in predicted distress levels between WBT and DT loads, the specific values of fatigue life are unnecessary, and only the percent difference is required. The research team assumes the fatigue life under DT load, and 120 psi tire pressure (as the default condition for analysis in Pavement ME) as 1, and relative fatigue life under other conditions can be computed based on the relationship in equation (4.1). The results are presented in Table 4.12.

Table 4.12. Relative fatigue life for different structures

Structure type	Tire pressure (psi)	Relative fatigue life				
		Under DT load	Under WBT load at different contact pressures			
			+0%	+10%	+20%	+30%
5" AC structure	80	1.19	0.72	0.59	0.49	0.42
	100	1.07	0.46	0.38	0.32	0.28
	110	1.03	0.38	0.32	0.27	0.24
	120	1.00	0.32	0.27	0.23	0.20
	125	1.00	0.30	0.25	0.22	0.19
6.5" AC structure	80	1.18	0.73	0.61	0.53	0.47
	100	1.07	0.50	0.43	0.38	0.33
	110	1.03	0.43	0.37	0.33	0.29
	120	1.00	0.38	0.33	0.29	0.26
	125	0.99	0.35	0.31	0.28	0.25
9.5" AC structure	80	1.12	0.79	0.72	0.66	0.62
	100	1.05	0.64	0.59	0.55	0.52
	110	1.02	0.59	0.54	0.51	0.48
	120	1.00	0.55	0.51	0.48	0.45
	125	0.99	0.53	0.49	0.47	0.44
11.5" AC structure	80	1.10	0.82	0.76	0.72	0.68
	100	1.04	0.70	0.66	0.62	0.60
	110	1.02	0.66	0.62	0.59	0.57
	120	1.00	0.62	0.59	0.56	0.54
	125	0.99	0.61	0.58	0.55	0.53

The damage index of fatigue can be calculated with equation (4.2).

$$D = \sum_{i=1}^{T} \frac{n_i}{N_i} \tag{4.2}$$

where:

D = Damage index;

T = Total number of periods;

n_i = Actual traffic for period i;

N_i = Traffic allowed under conditions prevailing in i.

The Pavement ME software would calculate the damage index of fatigue based on actual axle load weight and times. This process would contain tremendous computations, which are impossible to simulate manually due to the tremendous change in material parameters, load levels, etc., that are programmed into the software. To demonstrate the difference in damage index between DT and WBT loads, the research team used the reciprocal of relative fatigue life in Table

4.12 to represent the predicted damage index. The results are shown in Table 4.13.

Table 4.13. Relative damage index for different structures

Structure type	Tire pressure (psi)	Relative damage index				
		Under DT load	Under WBT load at different contact pressures			
			+0%	+10%	+20%	+30%
5" AC structure	80	0.84	1.38	1.69	2.02	2.37
	100	0.94	2.19	2.64	3.11	3.59
	110	0.97	2.64	3.15	3.69	4.24
	120	1.00	3.11	3.69	4.29	4.89
	125	1.00	3.35	3.96	4.59	5.23
6.5" AC structure	80	0.85	1.38	1.63	1.89	2.14
	100	0.94	2.02	2.34	2.66	2.99
	110	0.97	2.34	2.70	3.05	3.40
	120	1.00	2.66	3.05	3.44	3.81
	125	1.01	2.83	3.23	3.62	4.00
9.5" AC structure	80	0.89	1.27	1.39	1.52	1.61
	100	0.95	1.56	1.69	1.82	1.92
	110	0.98	1.69	1.85	1.96	2.08
	120	1.00	1.82	1.96	2.08	2.22
	125	1.01	1.89	2.04	2.13	2.27
11.5" AC structure	80	0.91	1.22	1.32	1.39	1.47
	100	0.96	1.43	1.52	1.61	1.67
	110	0.98	1.52	1.61	1.69	1.75
	120	1.00	1.61	1.69	1.79	1.85
	125	1.01	1.64	1.72	1.82	1.89

According to previous survey results, the proportion of WBT loads in Michigan is around 10%. So, the research team chose the proportions of WBT loads ranging from 0%-25% to calculate the relative damage index, considering possible future increases in WBT loads. The contact pressure increase for WBT load was selected as 20%, which corresponds with the primary types of WBTs used in Michigan. The calculated results of the relative damage index with different proportions of WBTs for different AC thickness structures are presented in Table 4.14.

Table 4.14. Relative damage index with different proportions of WBTs

Structure type	Tire pressure (psi)	Relative damage index with different proportions of WBT								
		0%	4%	6%	8%	10%	12%	14%	20%	25%
5" AC structure	80	0.84	0.89	0.91	0.93	0.96	0.98	1.01	1.08	1.14
	100	0.94	1.03	1.07	1.11	1.16	1.20	1.24	1.37	1.48
	110	0.97	1.08	1.13	1.19	1.24	1.30	1.35	1.51	1.65
	120	1.00	1.13	1.20	1.26	1.33	1.39	1.46	1.66	1.82
	125	1.00	1.14	1.22	1.29	1.36	1.43	1.50	1.72	1.90
6.5" AC structure	80	0.85	0.89	0.91	0.93	0.95	0.97	1.00	1.06	1.11
	100	0.94	1.01	1.04	1.08	1.11	1.15	1.18	1.28	1.37
	110	0.97	1.05	1.09	1.14	1.18	1.22	1.26	1.39	1.49
	120	1.00	1.10	1.15	1.20	1.24	1.29	1.34	1.49	1.61
	125	1.01	1.11	1.17	1.22	1.27	1.32	1.38	1.53	1.66
9.5" AC structure	80	0.89	0.92	0.93	0.94	0.95	0.97	0.98	1.02	1.05
	100	0.95	0.98	1.00	1.02	1.04	1.05	1.07	1.12	1.17
	110	0.98	1.02	1.04	1.06	1.08	1.10	1.12	1.18	1.23
	120	1.00	1.04	1.06	1.09	1.11	1.13	1.15	1.22	1.27
	125	1.01	1.05	1.08	1.10	1.12	1.14	1.17	1.23	1.29
11.5" AC structure	80	0.91	0.93	0.94	0.95	0.96	0.97	0.98	1.01	1.03
	100	0.96	0.99	1.00	1.01	1.03	1.04	1.05	1.09	1.12
	110	0.98	1.01	1.02	1.04	1.05	1.07	1.08	1.12	1.16
	120	1.00	1.03	1.05	1.06	1.08	1.09	1.11	1.16	1.20
	125	1.01	1.04	1.06	1.07	1.09	1.11	1.12	1.17	1.21

4.3.3. Fatigue cracking calculation

According to the MDOT User Guide for MEPD [21], bottom-up fatigue cracking and top-down fatigue cracking are both involved in the bottom-up cracking model, which can be calculated with equation (4.3); MDOT currently adopts the calibration factors in the equation.

$$FC_{Bottom-up} = \frac{6000}{1+e^{(C_1 \times C_1' + C_2 \times C_2' \times log_{10}(100D))}} \times \frac{1}{60} \quad (4.3)$$

where:

D = Damage index calculated from equation (4.2);

C_1=0.5; C_2=0.56; $C_2' = -2.40874 - 39.748 \times (1 + h_{AC})^{-2.856}$; $C_1' = -2C_2'$.

The bottom-up fatigue cracking ($FC_{Bottom-up}$) in equation (4.3) could be calculated using the above relative damage index. However, due to the sigmoidal damage function employed in Pavement ME software, the obtained cracking would be unrealistically high if directly substituted into the equation. The WBT loads' impact on fatigue distress is worth attention only when the calculated $FC_{Bottom-up}$ is near the distress threshold, as the WBT load is critical in determining whether the structure will fail or not. So, before substituting the relative damage index in Table

4.14 into equation (4.3), a damage reduction factor (R_F) should be introduced and multiplied by Table 4.14 so that the calculated bottom-up fatigue cracking would be around the design threshold in Michigan. The relationship between bottom-up fatigue cracking and damage index (D) is shown in Figure 4.10.

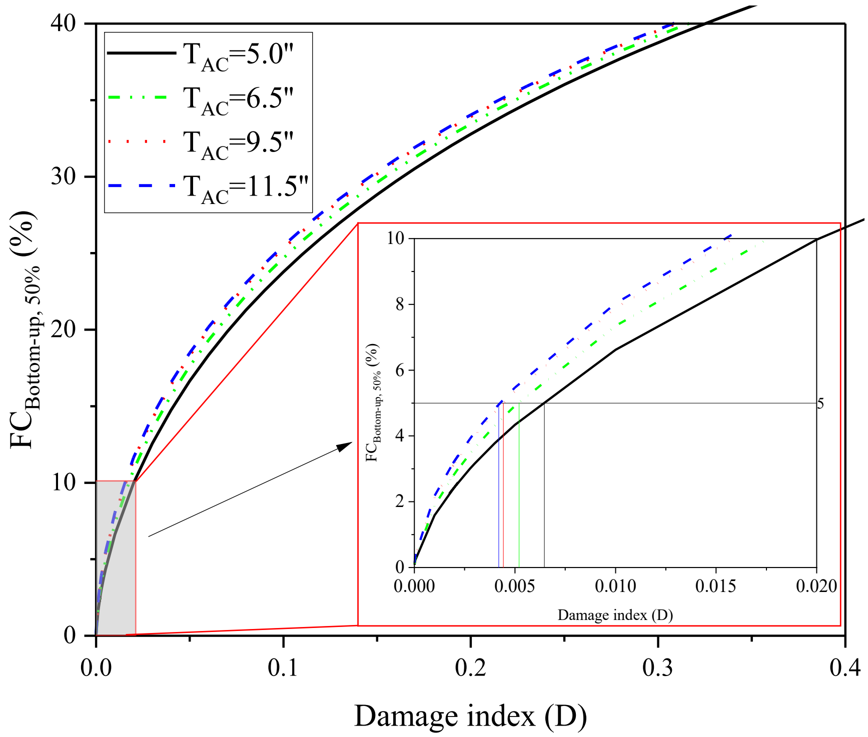

Figure 4.10. Relationship between bottom-up fatigue cracking and damage index

The failure threshold for fatigue cracking in Michigan is 20% (at 95% reliability). The analysis of the damage index in this paper and equation (4.3) are based on average values (at 50% reliability). Therefore, equation (4.4) can transform bottom-up cracking under 50% reliability ($FC_{Bottom\text{-}up,\ 50\%}$) into bottom-up cracking under 95% reliability ($FC_{Bottom\text{-}up,\ 95\%}$) by using the average cracking, standard error of the prediction (S_e), and Z-value for 95% confidence level one-tailed test. According to the back calculation of equation (4.4), the $FC_{Bottom\text{-}up,\ 95\%}$ would be close to the Michigan threshold of 20% if the mean fatigue cracking parameter $FC_{Bottom\text{-}up,\ 50\%}$ is near 5%.

$$FC_{Bottom-up,95\%} = FC_{Bottom-up,50\%} + S_e \times Z_{95} \tag{4.4}$$

where:

S_e is the standard error, and $S_e = 0.7874 + \frac{17.817}{1+e^{0.0699-0.4559\times log_{10}(D\times 100)}}$; Z_{95} is the Z-value for the 95%-confidence level one-tailed test, which equals 1.65.

According to Figure 4.10, the damage index for the four selected AC thickness structures would be approximately 0.005 if the $FC_{Bottom\text{-}up,\,50\%}$ is near 5%. Based on this analysis, a damage index reduction factor (R_F) of 0.005 would be multiplied by values noted in Table 4.14; then, the $FC_{Bottom\text{-}up,\,50\%}$ would be obtained (near the 5% threshold at 50% reliability). Finally, using equation (4.4) again, the $FC_{Bottom\text{-}up,\,95\%}$ would be obtained (near the 20% threshold at 95% reliability), as shown in Table 4.15.

Table 4.15. Impact of WBTs on bottom-up fatigue cracking under 95% reliability

Structure type	Tire pressure (psi)	Cracking percentage at different WBT proportions (%)								
		0%	4%	6%	8%	10%	12%	14%	20%	25%
5" AC structure	80	18.13	18.35	18.44	18.53	18.65	18.74	18.86	19.14	19.37
	100	18.57	18.94	19.10	19.26	19.45	19.60	19.74	20.20	20.56
	110	18.70	19.14	19.34	19.56	19.74	19.96	20.13	20.66	21.10
	120	18.82	19.34	19.60	19.82	20.06	20.27	20.50	21.13	21.60
	125	18.82	19.37	19.67	19.92	20.16	20.40	20.63	21.31	21.83
6.5" AC structure	80	18.72	18.91	19.00	19.09	19.18	19.27	19.40	19.65	19.86
	100	19.13	19.44	19.57	19.74	19.86	20.02	20.14	20.52	20.84
	110	19.27	19.61	19.78	19.98	20.14	20.29	20.44	20.92	21.26
	120	19.40	19.82	20.02	20.21	20.37	20.55	20.74	21.26	21.66
	125	19.44	19.86	20.10	20.29	20.48	20.66	20.88	21.39	21.82
9.5" AC structure	80	19.33	19.47	19.52	19.57	19.61	19.71	19.75	19.93	20.06
	100	19.61	19.75	19.84	19.93	20.02	20.06	20.15	20.36	20.56
	110	19.75	19.93	20.02	20.10	20.19	20.28	20.36	20.60	20.80
	120	19.84	20.02	20.10	20.23	20.32	20.40	20.48	20.76	20.96
	125	19.89	20.06	20.19	20.28	20.36	20.44	20.56	20.80	21.04
11.5" AC structure	80	19.54	19.63	19.68	19.73	19.77	19.82	19.86	20.00	20.09
	100	19.77	19.91	19.95	20.00	20.09	20.13	20.18	20.35	20.48
	110	19.86	20.00	20.04	20.13	20.18	20.26	20.31	20.48	20.64
	120	19.95	20.09	20.18	20.22	20.31	20.35	20.43	20.64	20.80
	125	20.00	20.13	20.22	20.26	20.35	20.43	20.48	20.68	20.84

It is worth noting that the specific cracking value in Table 4.15 is not that important, as this analysis aims to determine the impact of WBT loads on fatigue cracking for a range of WBT traffic proportions and AC thicknesses. Therefore, more attention has been given to the difference in cracking between 0% WBT (all DT loads as is standard in Pavement ME analyses) and a range of 4-25% WBT loads that may be typical for current and future traffic in the state of Michigan.

Comparing the predicted fatigue cracking percentage from all DT loads (0% WBT) with a range of 4-25% WBT loads in Table 4.15, the WBT loads' impact on thinner AC structures is more severe than on thicker AC structures. For example, the predicted cracking percentage increases from 18.82% (with 0% WBT loads) to 20.06% (with 10% WBT loads) for the 5" AC structure under 120 psi, while this same increase for 11.5" AC structures is quite mild at 19.95% to 20.31%. For a given WBT traffic proportion, higher tire pressure leads to a higher cracking increase. Based on these research results, if the WBT traffic proportion in Michigan increases to higher levels than the typical 10%, the impact of WBTs on flexible pavement bottom-up fatigue cracking would increase significantly.

The bottom-up fatigue cracking under 4-25% WBT loads and 0% WBT loads at the same tire pressure is compared to obtain the relative cracking increase for each WBT load proportion. The results of cracking increases are shown in Table 4.16.

Table 4.16. Bottom-up fatigue cracking increase for different structures

Structure type	Tire pressure (psi)	Cracking percentage increase at different WBT proportions (%)								
		0%	4%	6%	8%	10%	12%	14%	20%	25%
5" AC structure	80	0.00	1.24	1.72	2.20	2.91	3.37	4.05	5.60	6.87
	100	0.00	2.01	2.87	3.71	4.74	5.54	6.32	8.77	10.74
	110	0.00	2.38	3.42	4.63	5.60	6.74	7.67	10.51	12.85
	120	0.00	2.73	4.13	5.29	**6.59**	7.68	8.92	12.26	**14.77**
	125	0.00	2.94	4.52	5.85	7.14	8.39	9.61	13.22	15.97
6.5" AC structure	80	0.00	1.01	1.50	1.99	2.47	2.94	3.64	5.00	6.10
	100	0.00	1.61	2.27	3.15	3.79	4.62	5.24	7.23	8.94
	110	0.00	1.78	2.64	3.69	4.51	5.31	6.10	8.55	10.34
	120	0.00	2.16	3.20	4.21	**4.99**	5.96	6.90	9.60	**11.64**
	125	0.00	2.14	3.37	4.37	5.34	6.29	7.40	10.04	12.21
9.5" AC structure	80	0.00	0.74	0.98	1.22	1.46	1.94	2.17	3.10	3.78
	100	0.00	0.70	1.16	1.61	2.06	2.28	2.72	3.80	4.84
	110	0.00	0.91	1.35	1.79	2.22	2.65	3.08	4.32	5.33
	120	0.00	0.89	1.33	1.97	**2.40**	2.82	3.23	4.65	**5.63**
	125	0.00	0.88	1.53	1.96	2.38	2.79	3.41	4.61	5.78
11.5" AC structure	80	0.00	0.49	0.73	0.97	1.20	1.44	1.67	2.37	2.82
	100	0.00	0.70	0.92	1.15	1.60	1.82	2.05	2.92	3.56
	110	0.00	0.68	0.91	1.35	1.57	2.01	2.23	3.08	3.92
	120	0.00	0.67	1.11	1.33	**1.76**	1.98	2.40	3.45	**4.26**
	125	0.00	0.67	1.10	1.32	1.75	2.17	2.38	3.42	4.23

Based on Table 4.16, the bottom-up fatigue cracking percent increase with different WBT loads' proportions and tire pressures under 95% reliability are plotted, as presented in Figure 4.11.

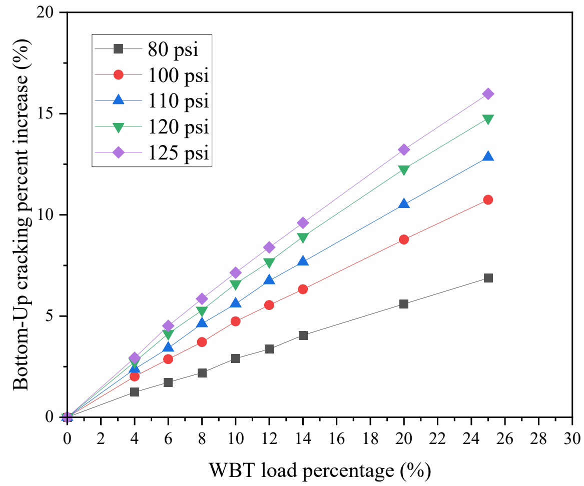

(a) 5" AC structure

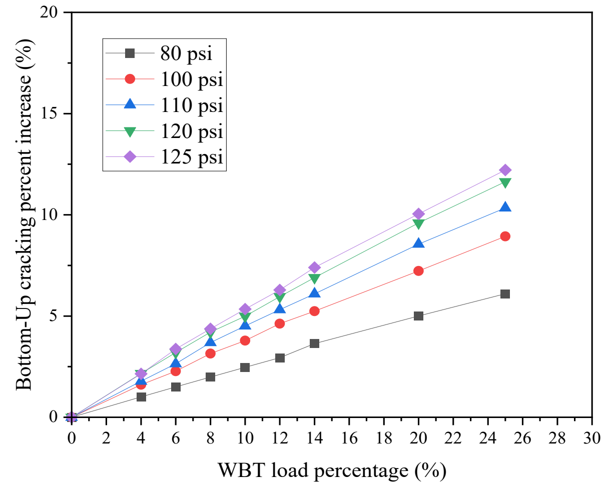

(b) 6.5" AC structure

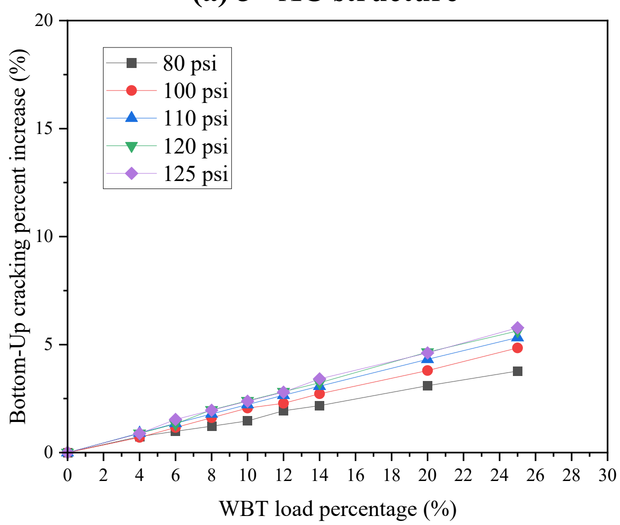

(c) 9.5" AC structure

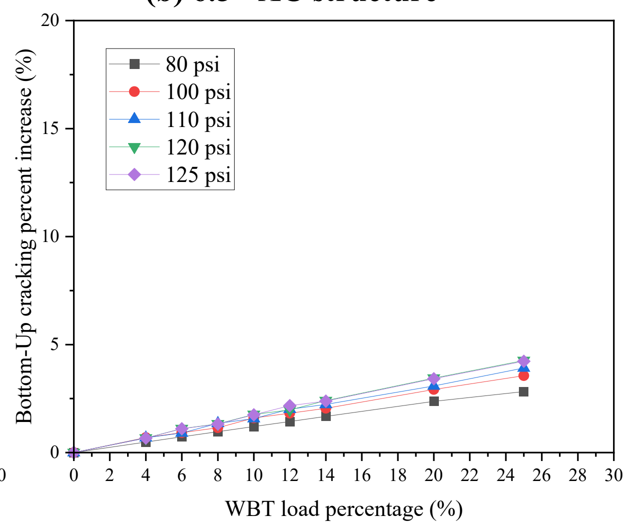

(d) 11.5" AC structure

Figure 4.11. Bottom-up fatigue cracking increase

According to Table 4.16, under 120 psi tire pressure, the bottom-up fatigue cracking with 10% WBT loads is 6.59% (For 5" AC structure) and 1.76% (For 11.5" AC structure) larger than that with only DT loads (0% WBT). The bottom-up fatigue cracking distress for thinner pavements is more sensitive to WBT loads than thicker pavements. Based on these results, the research team predicts that if the proportion of WBT loads in Michigan increased to 25% in the future, the bottom-up fatigue cracking would be 14.77% (For 5" AC structure) and 4.26% (For 11.5" AC structure) larger than that with no WBT loads considered.

4.4. Rutting distress analysis

4.4.1. AC layers rutting analysis

According to the MDOT User Guide for MEPD, the AC rutting depth (RD) calculation equations are presented in (4.5) and (4.6) [21]. The calibration factors in the equation are currently adopted by MDOT.

$$\varepsilon_p^i = \varepsilon_r^i \times (C_1 + C_2 D) \times 0.328196^D \beta_{r1} 10^{k_1} T^{k_2\beta_{r2}} N^{k_3\beta_{r3}} \tag{4.5}$$

$$RD = \sum_{i=1}^{n\,sublayers} \varepsilon_p^i h_{AC}^i \tag{4.6}$$

where:

$\varepsilon_p{}^i$	=	Plastic axial strain in the AC sublayer i;
$\varepsilon_r{}^i$	=	Resilient axial strain in the middle of AC sublayer i;
D	=	Depth of the sublayer i, inch;
$h_{AC}{}^i$	=	Thickness of the AC sublayer i, inch;
T	=	Mix or pavement temperature, °F;
N	=	Number of load repetitions;
C_1	=	$-0.1039(h_{AC})^2+2.4868h_{AC}-17.342$;
C_2	=	$0.0172(h_{AC})^2-1.7331h_{AC}+27.428$;

k_1=-3.35412; k_2=1.56; k_3=0.4791; β_{r1}=0.9453; β_{r2}=1.3; β_{r3}=0.7.

As this project proposes to find out the impact of WBT loads on pavement distress, the specific AC layers' strain value is not necessary for the research. As equation (4.5) presents, *T, N, and* h_{AC}, would be the same for both DT and WBT loads in each AC sublayer for a specific AC thickness structure. So, the ratio of AC rutting between under WBT and under DT loads ($RD_{WBT/DT}$) for each AC sublayer structure is critical in determining how the WBT load would impact the distress compared with the DT load. The ratio of AC rutting could be expressed as below:

$$RD_{WBT/DT}^i = \varepsilon_{r\,WBT}^{\;i} / \varepsilon_{r\,DT}^{\;i} \tag{4.7}$$

where:

$RD_{WBT/DT}^i$	=	the ratio of AC rutting between WBT and DT loads in sublayer i;
$\varepsilon_{r\,WBT}^{\;i}$	=	Resilient axial strain under WBT load in the middle of sublayer i;
$\varepsilon_{r\,DT}^{\;i}$	=	Resilient axial strain under DT load in the middle of sublayer i;

Then, the distribution of rutting proportion in each AC sublayer should be determined. A sublayer rutting factor, represented as F_{sub}^{i} (i means the number of the AC sublayer), was used in this project to represent the proportion of AC rutting in different sublayers. Analyzed from equation (4.5) and (4.6), F_{sub}^{i} is represented as equation (4.8).

$$F_{sub}^{i} = (C_1 + C_2 D_i) \times 0.328196^{D_i} \times h_{AC}^{i} \tag{4.8}$$

where:

F_{sub}^{i} is the sublayer rutting factor; other parameters have the same meaning as equation (4.5) and (4.6).

Combined with equation (4.7) and equation (4.8), the ratio of total AC rutting between under WBT and DT loads for a three AC layer structure could be expressed as below:

$$RD_{WBT/DT}^{Sum-AC} = \frac{F_{sub}^{i=1}\times(\varepsilon_{r\,WBT}^{\,i=1}/\,\varepsilon_{r\,DT}^{\,i=1})+F_{sub}^{i=2}\times(\varepsilon_{r\,WBT}^{\,i=2}/\,\varepsilon_{r\,DT}^{\,i=2})+F_{sub}^{i=3}\times(\varepsilon_{r\,WBT}^{\,i=3}/\,\varepsilon_{r\,DT}^{\,i=3})}{F_{sub}^{i=1}+F_{sub}^{i=2}+F_{sub}^{i=3}} \tag{4.9}$$

The research team then calculated the resilient axial strain ($\varepsilon_r^{\,i}$) in the middle of each AC sublayer for different AC thickness structures, as shown in Figure 4.12.

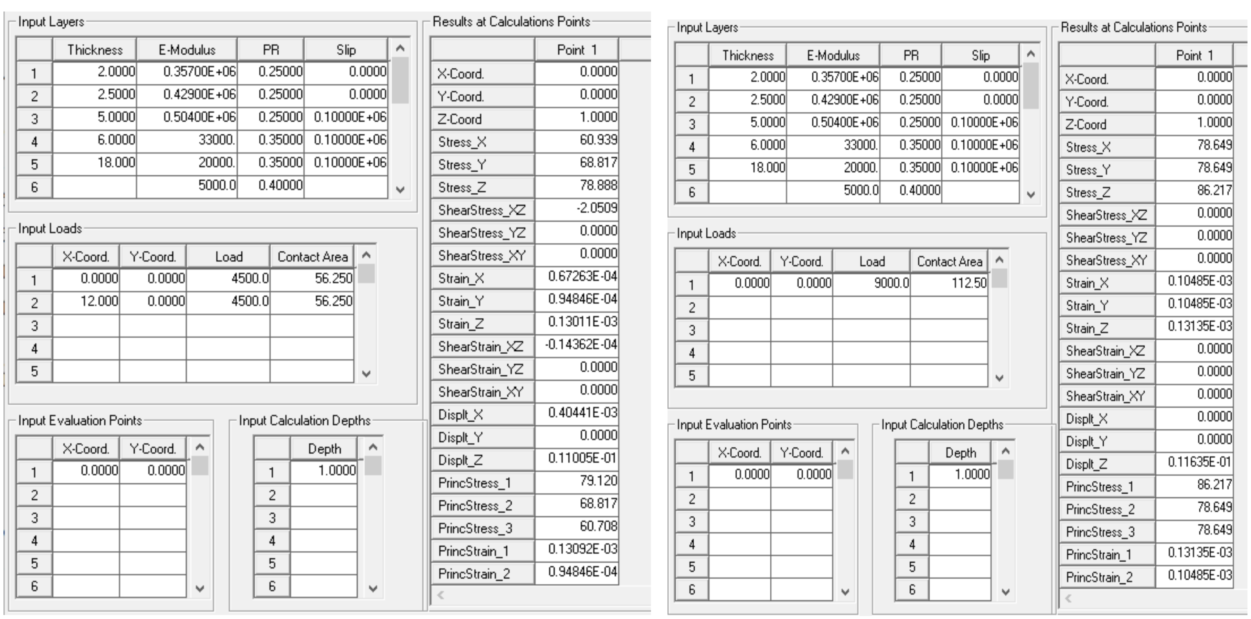

(a) Under DT load **(b) Under WBT load**

Figure 4.12. JULEA examples for AC middle axial strain

The research team noticed that the JULEA software has a near-surface computation error, leading to some unreasonable vertical strain results in the layer near the surface. So, before conducting the full analysis for all thicknesses, the research team first conducted a trial analysis on the 9.5" and 11.5" AC structures to check the quality of the vertical strain obtained from JULEA.

In the trial analysis, the critical vertical strain of each AC layer for these two structures under DT and WBT loads was calculated without considering the actual contact pressure increase of the WBT load. The results are presented in Tables 4.17 and Figure 4.13.

Table 4.17. Vertical strain at the middle of AC sublayers

AC layer	Structure type	Tire pressure (psi)	Vertical strain at the middle of asphalt layer (με)	
			Under DT load	Under WBT load
Top course (Layer 1)	9.5" AC structure	80	130.11	131.35
		100	175.61	172.80
		110	198.56	193.79
		120	221.67	197.66
		125	233.24	208.67
	11.5" AC structure	80	174.16	160.96
		100	228.62	208.78
		110	256.03	232.95
		120	283.61	266.27
		125	297.41	279.57
Leveling course (Layer 2)	9.5" AC structure	80	110.92	110.93
		100	136.92	143.87
		110	148.73	159.84
		120	159.87	175.35
		125	165.19	183.00
	11.5" AC structure	80	123.54	125.72
		100	152.56	162.72
		110	165.73	180.62
		120	178.15	197.99
		125	184.09	206.57
Base course (Layer 3)	9.5" AC structure	80	62.60	80.98
		100	66.60	89.53
		110	68.10	93.18
		120	69.42	96.50
		125	70.02	98.05
	11.5" AC structure	80	38.18	50.76
		100	40.40	56.29
		110	41.28	58.62
		120	42.05	60.70
		125	42.40	61.67

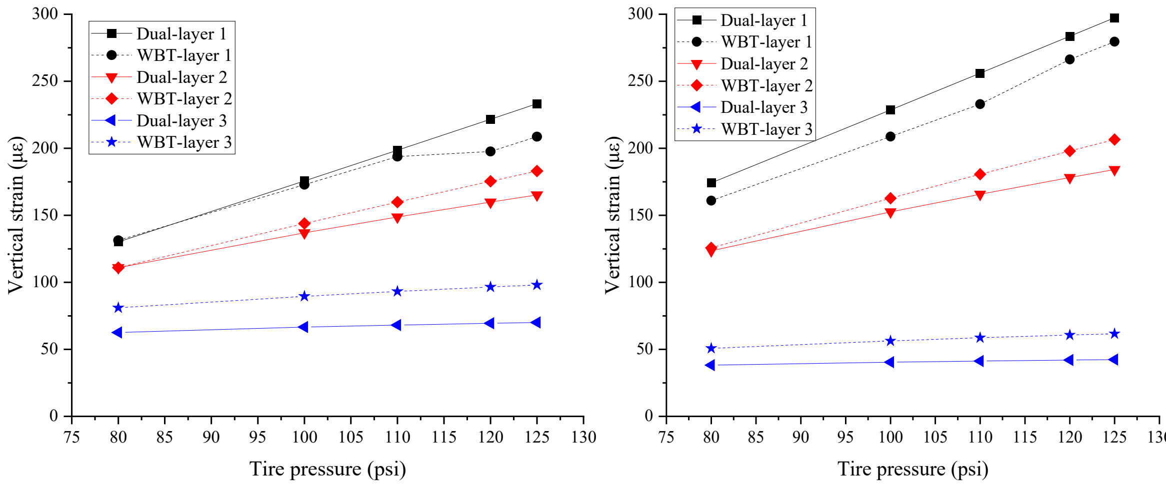

(a) 9.5" AC structure **(b)** 11.5" AC structure

Figure 4.13. AC middle axial strain results

As shown in Figure 4.13, the critical strain variance with tire pressures of layer 1 under WBT load is non-linear. This uncommon phenomenon is caused by a limitation of the JULEA software, the near face region, which does not exceed 20% of the tire contact area radius, leading to these unreasonable results. The solution is to interpolate linearly between the surface and at a depth corresponding to 20% of the tire contact area radius. Tire contact area radius under different tire pressures is computed in Table 4.18.

Table 4.18. Tire contact area radius under different tire pressures

Tire pressure (psi)	Under DT load		Under WBT load	
	Contact area (inch^2)	20% Radius (0.2 R) (inch)	Contact area (inch^2)	20% Radius (0.2 R) (inch)
80	56.250	0.846	112.500	1.197
100	45.000	0.757	90.000	1.070
110	40.909	0.722	81.818	1.021
120	37.500	0.691	75.000	0.977
125	36.000	0.677	72.000	0.957

The research team compared the initial JULEA results with another linear elastic software BISAR, as shown in Table 4.19. The input in BISAR software is presented in Figure 4.14. Based on the calculated contact area radius and 20% radius (0.2R) shown in Table 4.18, the linear interpolation results of AC vertical strain from JULEA are shown in Table 4.20.

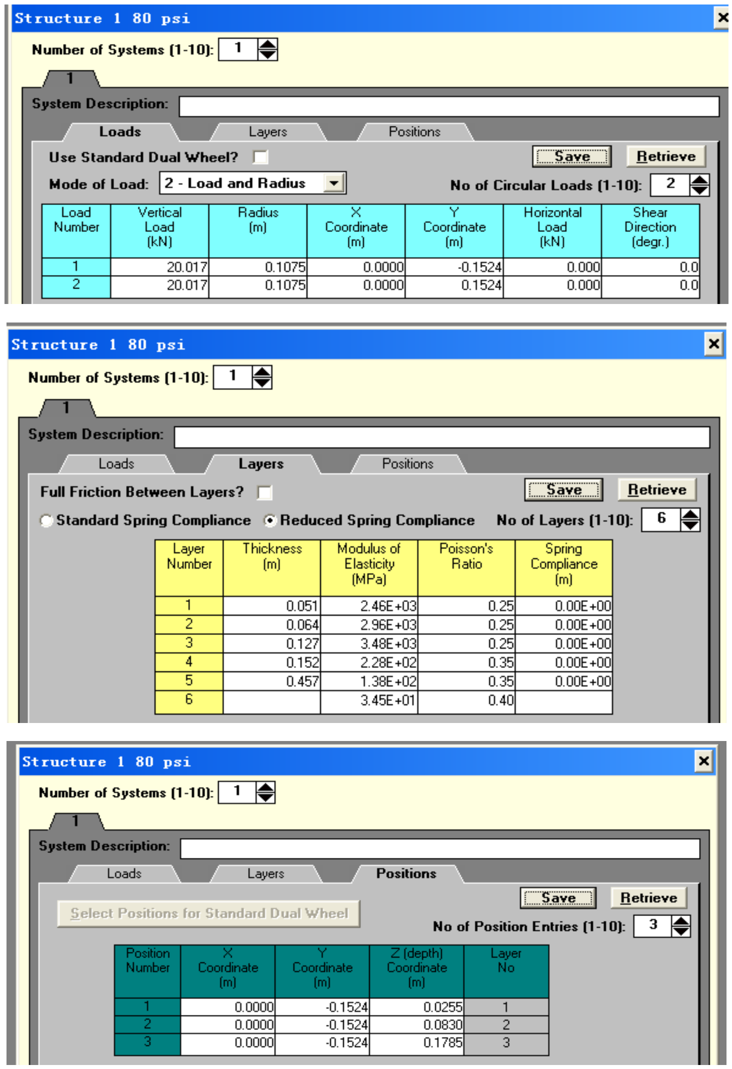

Figure 4.14. BISAR software calculation demonstration

Table 4.19. Vertical strain at the middle of AC layer 1

Structure type	Tire pressure (psi)	Critical strain under DT load (με)		Critical strain under WBT load (με)	
		JULEA	BISAR	JULEA	BISAR
9.5" AC structure	80	130.11	129.3	131.35	112.7
	100	175.61	175.1	172.80	155.6
	110	198.56	197.8	193.79	177.3
	120	221.67	220.8	197.66	199.2
	125	233.24	232.6	208.67	210.2
11.5" AC structure	80	174.16	172.2	160.96	160.4
	100	228.62	227.0	208.78	212.8
	110	256.03	254.0	232.95	239.0
	120	283.61	281.5	266.27	265.5
	125	297.41	295.5	279.57	278.7

Table 4.20. Vertical strain at the middle of AC layer 1 after linear interpolation

Structure type	Tire pressure (psi)	Critical strain under WBT load (με)			Interpolated result
		Strain at Z=0	Location of 0.2R	Strain at Z=0.2R	
9.5" AC structure	80	78.386	1.197	116.47	110.21
	100	113.63	1.071	156.26	153.47
	110	131.36	1.021	176.49	175.56
	120	/	0.977 (>1)	/	/
	125	/	0.958 (>1)	/	/
11.5" AC structure	80	136.89	1.197	165.02	160.39
	100	181.89	1.071	215.16	212.95
	110	204.27	1.021	240.35	239.61
	120	/	0.977 (>1)	/	/
	125	/	0.958 (>1)	/	/

The research team compared the initial JULEA, BISAR, and interpolated JULEA results of AC layer 1 middle vertical strain from Tables 4.19 and 4.20, as shown in Figure 4.15.

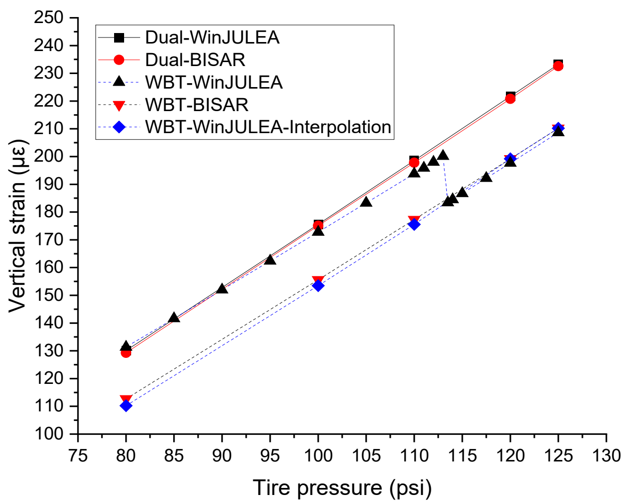

(a) 9.5" AC structure

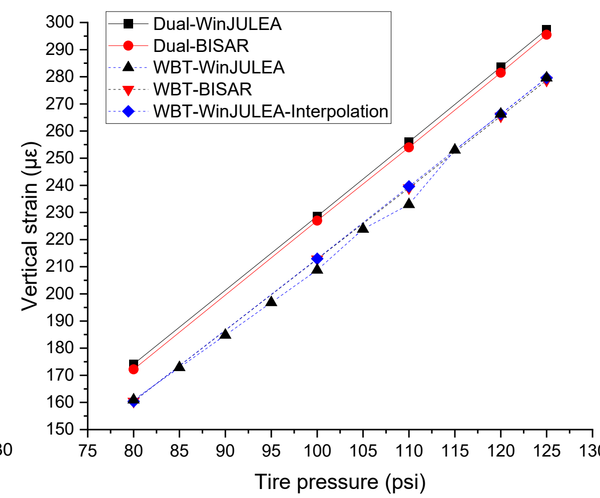

(b) 11.5" AC structure

Figure 4.15. AC Layer 1 middle vertical strain difference between JULEA and BISAR

Based on the above analysis, the research team believes that the linear interpolation method must be used for AC layer 1 under WBT load to obtain good results. Same as for AC bottom horizontal strain, the research team then considers the actual contact pressure increase of WBTs to calculate the actual vertical strain at the middle of the AC layers and expand the analysis to include the 5" and 6.5" AC structures.

As for the DT load, the contact pressure was assumed to be equal to the tire pressure. As for the WBT load, the contact pressure was calculated under four different conditions: (1) the theoretical pressure, which equals the tire pressure; (2) ~ (4) the assumed actual pressures, which are 10%, 20%, and 30% larger than the tire pressure. The vertical strain results of AC layers are presented in Tables 4.21 - 4.23.

Table 4.21. Vertical strain at the middle of AC layer 1

Structure type	Tire pressure (psi)	Vertical strain at the middle of AC layer (με)				
		Under DT load	Under WBT load at different contact pressures			
			0% larger	10% larger	20% larger	30% larger
5" AC structure	80	135.4	10.9	34.4	59.7	86.3
	100	218.7	72.8	107.3	142.4	177.8
	110	262.5	107.3	145.9	185.0	225.8
	120	307.5	142.4	185.0	229.7	276.0
	125	330.3	159.9	205.2	252.6	301.7
6.5" AC structure	80	186.2	74.5	107.9	138.6	172.2
	100	284.3	155.4	198.0	241.7	286.6
	110	333.6	198.0	246.3	295.8	345.9
	120	383.4	241.7	295.8	350.9	407.0
	125	408.5	264.0	320.9	379.1	438.0
9.5" AC structure	80	130.1	110.2	127.3	144.7	162.3
	100	175.6	153.5	175.6	197.7	219.7
	110	198.6	175.6	199.9	224.1	248.6
	120	221.7	197.7	224.1	250.9	277.8
	125	233.2	208.7	236.5	264.3	292.4
11.5" AC structure	80	174.2	160.4	181.3	202.4	223.6
	100	228.6	212.9	239.6	266.3	292.9
	110	256.0	239.6	268.9	298.2	327.7
	120	283.6	266.3	298.2	330.4	362.7
	125	297.4	279.6	312.9	346.6	380.3

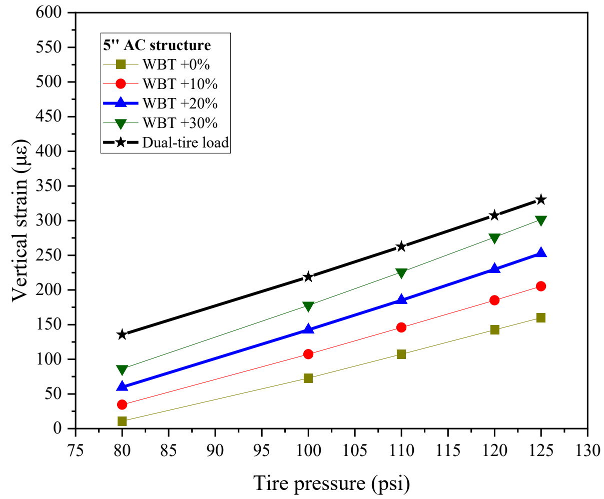

(a) 5" AC structure

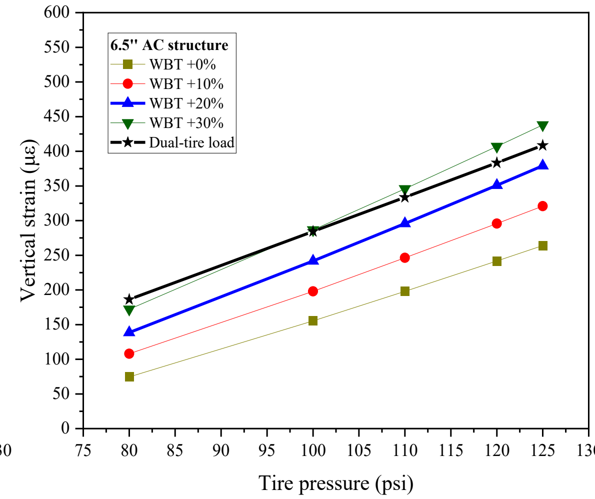

(b) 6.5" AC structure

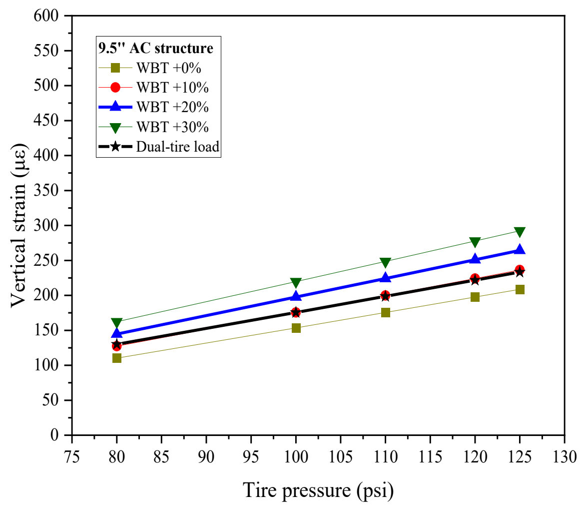

(a) 9.5" AC structure

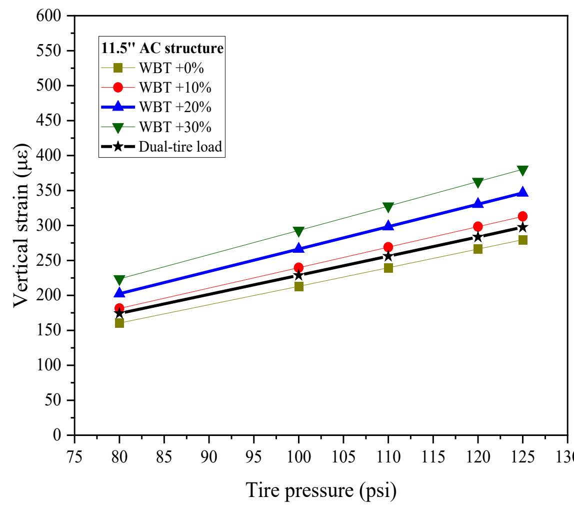

(b) 11.5" AC structure

Figure 4.16. AC Layer 1 middle vertical strain difference

Table 4.22. Vertical strain at the middle of AC layer 2

Structure type	Tire pressure (psi)	Vertical strain at the middle of AC layer (με)				
		Under DT load	Under WBT load at different contact pressures			
			0% larger	10% larger	20% larger	30% larger
5" AC structure	80	227.3	281.5	298.8	315.4	331.3
	100	257.6	323.5	343.1	362.1	380.4
	110	271.5	343.1	364.0	384.0	403.3
	120	284.7	362.1	384.0	405.1	425.3
	125	291.0	371.3	393.8	415.3	435.9
6.5" AC structure	80	262.4	199.2	231.4	264.4	297.9
	100	347.6	281.0	323.5	366.6	410.0
	110	389.0	323.5	370.9	418.7	466.5
	120	429.3	366.6	418.7	470.9	523.2
	125	449.0	388.2	442.6	497.2	551.3
9.5" AC structure	80	110.9	110.9	124.3	137.4	150.3
	100	136.9	143.9	159.8	175.4	190.6
	110	148.7	159.8	176.9	193.6	209.7
	120	159.9	175.4	193.6	211.2	228.2
	125	165.2	183.0	201.7	219.7	237.1
11.5" AC structure	80	123.5	125.7	140.7	155.4	169.9
	100	152.6	162.7	180.6	198.0	215.0
	110	165.7	180.6	199.8	218.4	236.4
	120	178.2	198.0	218.4	238.1	257.1
	125	184.1	206.6	227.5	247.7	267.1

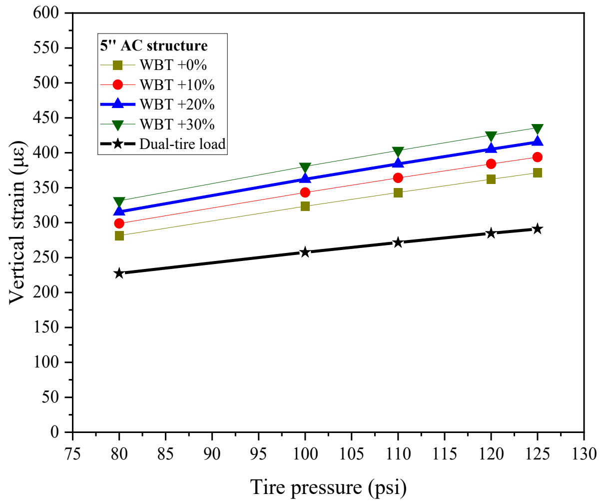

(a) 5" AC structure

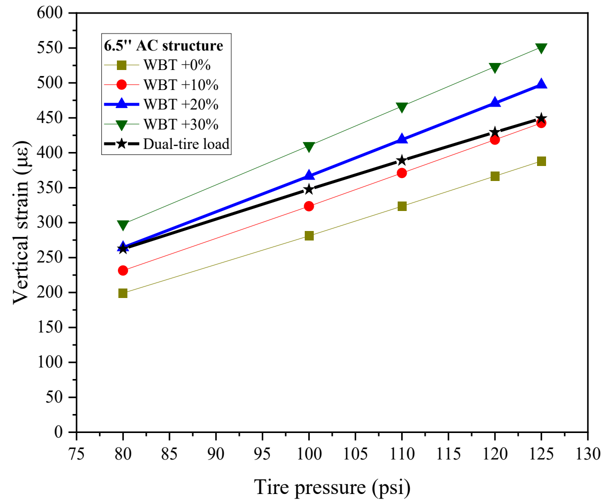

(b) 6.5" AC structure

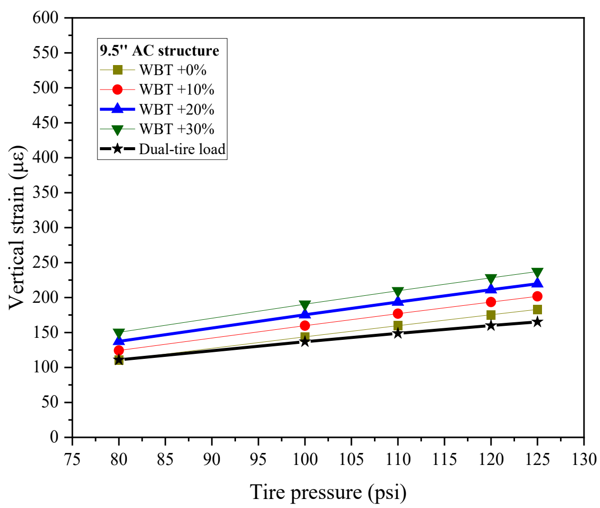

(a) 9.5" AC structure

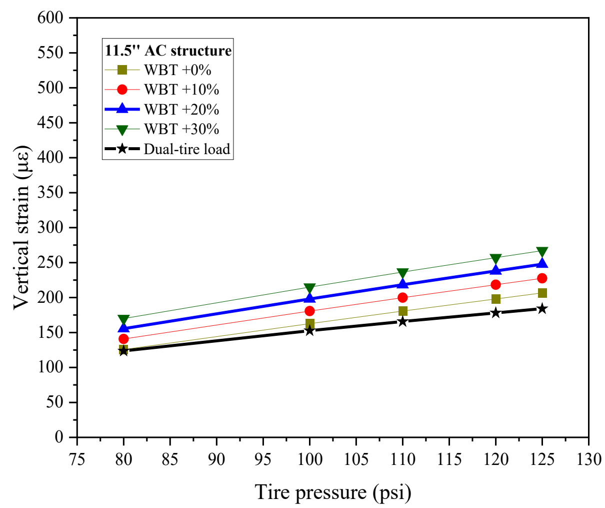

(b) 11.5" AC structure

Figure 4.17. AC Layer 2 middle vertical strain difference

Table 4.23. Vertical strain at the middle of AC layer 3

Structure type	Tire pressure (psi)	Vertical strain at the middle of AC layer (με)				
		Under DT load	Under WBT load at different contact pressures			
			0% larger	10% larger	20% larger	30% larger
6.5" AC structure	80	204.6	266.2	279.8	292.6	304.6
	100	222.8	298.7	313.2	326.8	339.5
	110	230.5	313.2	328.1	341.9	354.8
	120	237.4	326.8	341.9	356.0	369.0
	125	240.7	333.3	348.5	362.6	375.7
9.5" AC structure	80	62.6	81.0	84.6	88.0	91.0
	100	66.6	89.5	93.2	96.5	99.5
	110	68.1	93.2	96.8	100.1	103.1
	120	69.4	96.5	100.1	103.3	106.3
	125	70.0	98.1	101.6	104.8	107.7
11.5" AC structure	80	38.2	50.8	53.1	55.3	57.3
	100	40.4	56.3	58.6	60.7	62.6
	110	41.3	58.6	60.9	62.9	64.8
	120	42.1	60.7	62.9	64.9	66.7
	125	42.4	61.7	63.9	65.8	67.6

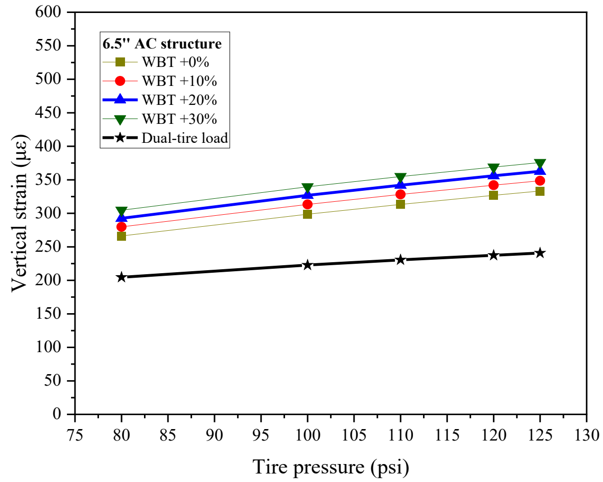

(a) 6.5" AC structure

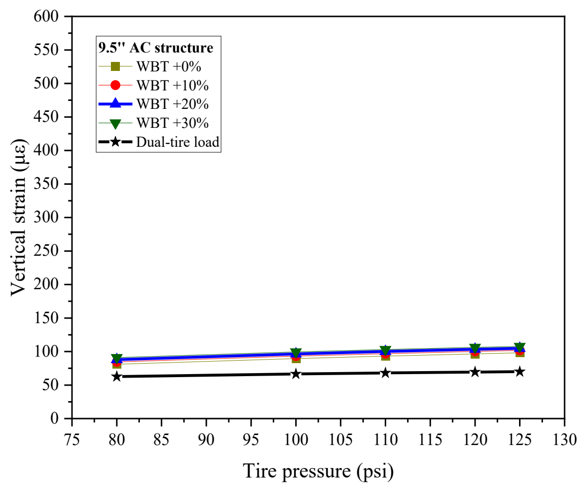

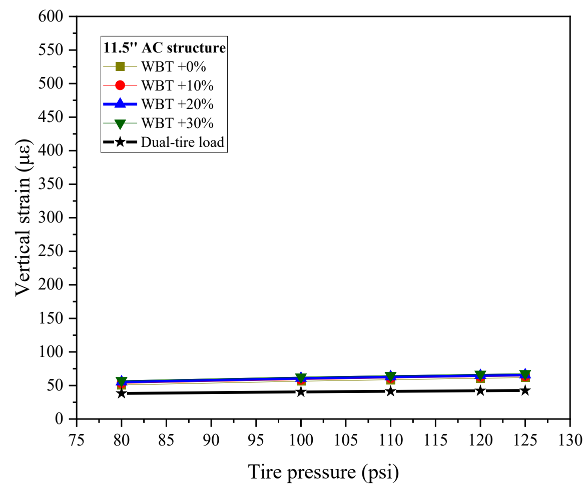

(a) 9.5" AC structure **(b) 11.5" AC structure**

Figure 4.18. AC Layer 3 middle vertical strain

The AC layer's middle vertical strain results from JULEA show that if considering a 20% of WBT contact pressure increase, WBT load would cause more vertical strain in each AC sublayer except for in two scenarios: AC Layer 1 with 5" and 6.5" AC thickness (Figure 4.16 (a) and (b)).

It is worth noting that the linear interpolation method was used for AC layer 1 in the project due to the computation limitations of JULEA at near-surface locations. The interpolation may lead to unreasonable values when the total AC thickness is very thin (5" and 6.5" AC). However, Figure 4.15 shows that the BISAR results of AC vertical strain are very consistent with the strain obtained from JULEA after interpolation, and the strain result from BISAR is directly obtained without manual interpolation. In order to avoid possible mistakes caused by JULEA interpolation, the research team then used BISAR software to calculate the AC layers' vertical strain to analyze this phenomenon further.

The vertical strain at the middle of the AC layer under DT load and WBT load (+20% tire pressure) is calculated with BISAR. The ratio of vertical strain under WBT load and DT load for each tire pressure can then be obtained and presented. A similar WBT/DT ratio calculated with JULEA (Tables 4.21 - 4.23) can also be calculated. The results are presented in Tables 4.24 - 4.26.

Table 4.24. Vertical strain (BISAR) at the middle of AC layer 1

Structure type	Tire pressure (psi)	Vertical strain at the middle of AC layer (με)		Ratio (WBT/DT)	
		Under DT load	Under WBT load (+20%)	BISAR	JULEA
5" AC structure	80	145.0	100.0	0.69	0.44
	100	230.7	183.1	0.79	0.65
	110	274.6	227.9	0.83	0.70
	120	320.1	273.9	0.86	0.75
	125	343.6	297.8	0.87	0.76
6.5" AC structure	80	200.8	183.2	0.91	0.74
	100	297.7	287.9	0.97	0.85
	110	346.2	342.2	0.99	0.89
	120	396.1	396.9	1.00	0.92
	125	421.7	424.9	1.01	0.93

Table 4.25. Vertical strain (BISAR) at the middle of AC layer 2

Structure type	Tire pressure (psi)	Vertical strain at the middle of AC layer (με)		Ratio (WBT/DT)	
		Under DT load	Under WBT load (+20%)	BISAR	JULEA
5" AC structure	80	166.3	230.7	1.39	1.39
	100	196.9	276.3	1.40	1.41
	110	210.7	297.9	1.41	1.41
	120	223.9	318.5	1.42	1.42
	125	230.3	328.7	1.43	1.43
6.5" AC structure	80	254.4	266.4	1.05	1.01
	100	341.5	371.6	1.09	1.05
	110	382.6	424.9	1.11	1.08
	120	423.1	477.7	1.13	1.10
	125	443.3	504.4	1.14	1.11

Table 4.26. Vertical strain (BISAR) at the middle of AC layer 3

Structure type	Tire pressure (psi)	Vertical strain at the middle of AC layer (με)		Ratio (WBT/DT)	
		Under DT load	Under WBT load (+20%)	BISAR	JULEA
6.5" AC structure	80	154.0	224.9	1.46	1.43
	100	172.1	258.6	1.50	1.47
	110	179.7	273.6	1.52	1.48
	120	186.7	287.4	1.54	1.50
	125	190.0	294.0	1.55	1.51

According to Tables 4.25 - 4.26 (AC layers 2 and 3), the strain ratio (WBT/DT) between BISAR and JULEA is quite similar. However, as for AC layer 1, the ratio from JULEA in Table 4.24 is much larger than that from BISAR, especially for the 5" AC structure. JULEA interpolation would lead to a significant strain difference between DT and WBT loads, while BISAR software does not have similar issues. Therefore, the following distress analysis would be based on the BISAR output for layer 1 of 5" and 6.5" AC structures.

Following the equation (4.7), considering the 20% larger contact pressure of WBT load, the value of $RD^{\mathrm{i}}_{\mathrm{WBT/DT}}$ for each AC thickness structure could be calculated, as shown in Tables 4.27-4.29.

Table 4.27. Rutting depth ratio in AC sublayer 1 ($RD^{\mathrm{i=1}}_{\mathrm{WBT/DT}}$)

Structure type	Tire pressure (psi)	Under DT load	Under WBT (20% larger contact pressure)	$RD^{i=1}_{\mathrm{WBT/DT}}$
5" AC structure	80	145.0	100.0	0.69
	100	230.7	183.1	0.79
	110	274.6	227.9	0.83
	120	320.1	273.9	0.86
	125	343.6	297.8	0.87
6.5" AC structure	80	200.8	183.2	0.91
	100	297.7	287.9	0.97
	110	346.2	342.2	0.99
	120	396.1	396.9	1.00
	125	421.7	424.9	1.01
9.5" AC structure	80	130.11	144.65	1.11
	100	175.61	197.66	1.13
	110	198.56	224.13	1.13
	120	221.67	250.85	1.13
	125	233.24	264.28	1.13
11.5" AC structure	80	174.16	202.39	1.16
	100	228.62	266.27	1.16
	110	256.03	298.23	1.16
	120	283.61	330.41	1.17
	125	297.41	346.55	1.17

Table 4.28. Rutting depth ratio in AC sublayer 2 ($RD^{i=2}_{WBT/DT}$)

Structure type	Tire pressure (psi)	Under DT load	Under WBT (20% larger contact pressure)	$RD^{i=2}_{WBT/DT}$
5" AC structure	80	227.3	315.4	1.39
	100	257.6	362.1	1.41
	110	271.5	384.0	1.41
	120	284.7	405.1	1.42
	125	291.0	415.3	1.43
6.5" AC structure	80	262.4	264.4	1.01
	100	347.6	366.6	1.05
	110	389.0	418.7	1.08
	120	429.3	470.9	1.10
	125	449.0	497.2	1.11
9.5" AC structure	80	110.92	137.38	1.24
	100	136.92	175.35	1.28
	110	148.73	193.55	1.30
	120	159.87	211.15	1.32
	125	165.19	219.72	1.33
11.5" AC structure	80	123.54	155.44	1.26
	100	152.56	197.99	1.30
	110	165.73	218.37	1.32
	120	178.15	238.06	1.34
	125	184.09	247.65	1.35

Table 4.29. Rutting depth ratio in AC sublayer 3 ($RD^{i=3}_{WBT/DT}$)

Structure type	Tire pressure (psi)	Under DT load	Under WBT (20% larger contact pressure)	$RD^{i=3}_{WBT/DT}$
6.5" AC structure	80	204.6	292.6	1.43
	100	222.8	326.8	1.47
	110	230.5	341.9	1.48
	120	237.4	356.0	1.50
	125	240.7	362.6	1.51
9.5" AC structure	80	62.60	87.96	1.41
	100	66.60	96.50	1.45
	110	68.10	100.10	1.47
	120	69.42	103.33	1.49
	125	70.02	104.82	1.50
11.5" AC structure	80	38.18	55.29	1.45
	100	40.40	60.70	1.50
	110	41.28	62.94	1.52
	120	42.05	64.93	1.54
	125	42.40	65.84	1.55

Next, following equation (4.8), the sublayer rutting factor (F^{i}_{sub}) for each AC thickness structure could be computed, as shown in Table 4.30.

Table 4.30. Sublayer rutting factor (F_{sub}^{i}) for each AC thickness structure

Structure type	i-value	C_1	C_2	D^i(inch)	F_{sub}^{i}
5" AC structure	1	-7.5055	19.1925	1	7.6713
	2	-7.5055	19.1925	3.5	3.6252
6.5" AC structure	1	-5.5676	16.8896	0.75	4.6177
	2	-5.5676	16.8896	2.5	4.5239
	3	-5.5676	16.8896	5	0.9011
9.5" AC structure	1	-3.0944	12.5159	1	6.1842
	2	-3.0944	12.5159	3.25	2.5139
	3	-3.0944	12.5159	7	0.1733
11.5" AC structure	1	-2.4846	9.7721	1	4.7834
	2	-2.4846	9.7721	3.25	1.9582
	3	-2.4846	9.7721	8	0.0713

* i is the layer number of AC; C_1 and C_2 are calibration factors; D_i is the depth in the middle of i-th AC layer; F_{sub}^{i} is the i-th sublayer rutting factor as presented in equation (4.8).

Then, based on equation (4.9), the rutting depth ratio results from Tables 4.27 - 4.29, and the sublayer rutting factor in Table 4.30, the sum of the rutting factor ratio of AC layers under 95% reliability can be calculated, as shown in Table 4.31.

Table 4.31. Sum of rutting ratio for each AC thickness structure

Structure type	Tire pressure (psi)	$RD_{\mathrm{WBT/DT}}^{Sum-AC}$
5" AC structure	80	0.9146
	100	0.9890
	110	1.0161
	120	1.0397
	125	1.0497
6.5" AC structure	80	1.0017
	100	1.0509
	110	1.0745
	120	1.0899
	125	1.0999
9.5" AC structure	80	1.1527
	100	1.1788
	110	1.1848
	120	1.1909
	125	1.1939
11.5" AC structure	80	1.1918
	100	1.2038
	110	1.2098
	120	1.2227
	125	1.2257

Before assessing the rutting increase caused by different proportions of WBT loads, the reliability issue in Michigan pavement design should be discussed. The failure threshold for AC rutting in Michigan is 0.5” (at 95% reliability), which, although not used in the final design, is still important in total rutting calculation.

Equation (4.10) can transform AC rutting under 50% reliability ($Rutting_{AC,\ 50\%}$) into AC rutting under 95% reliability ($Rutting_{AC,\ 95\%}$) by using the average rutting, standard error of the prediction (S_e), and Z-value for the 95% confidence level one-tailed test. According to the back calculation of equation (4.10), the $Rutting_{AC,\ 95\%}$ would be close to the Michigan threshold of 0.5” if the mean fatigue cracking parameter $Rutting_{AC,\ 50\%}$ is near 0.35”.

$$Rutting_{AC,95\%} = Rutting_{AC,50\%} + S_e \times Z_{95} \tag{4.10}$$

where:

S_e is the standard error, and $S_e = 0.1126 \times \mathrm{Rutting}_{\mathrm{AC,50\%}}{}^{0.2352}$; Z_{95} is the Z-value for the 95%-confidence level one-tailed test, which equals 1.65.

The AC rutting increase caused by a WBT load in 95% reliability would be approximately 0.35”/0.5”=0.7 times the AC rutting increase caused by a WBT load in 50% reliability.

Considering 95% reliability, and according to Table 4.31, the rutting increases under 4-25% WBT loads and 0% WBT loads at the same tire pressure are compared to obtain the rutting increase for each WBT load proportion. The results are shown in Tables 4.32 - 4.35.

Table 4.32. AC rutting increase at 95% reliability (5" AC)

Tire pressure (psi)	Rutting increase at different WBT proportions (%)								
	0%	4%	6%	8%	10%	12%	14%	20%	25%
80	0.00	-0.24	-0.36	-0.48	-0.60	-0.72	-0.84	-1.20	-1.49
100	0.00	-0.03	-0.05	-0.06	-0.08	-0.09	-0.11	-0.15	-0.19
110	0.00	0.05	0.07	0.09	0.11	0.14	0.16	0.23	0.28
120	0.00	0.11	0.17	0.22	**0.28**	0.33	0.39	0.56	**0.69**
125	0.00	0.14	0.21	0.28	0.35	0.42	0.49	0.70	0.87

Table 4.33. AC rutting increase at 95% reliability (6.5" AC)

Tire pressure (psi)	Rutting increase at different WBT proportions (%)								
	0%	4%	6%	8%	10%	12%	14%	20%	25%
80	0.00	0.00	0.01	0.01	0.01	0.01	0.02	0.02	0.03
100	0.00	0.14	0.21	0.29	0.36	0.43	0.50	0.71	0.89
110	0.00	0.21	0.31	0.42	0.52	0.63	0.73	1.04	1.30
120	0.00	0.25	0.38	0.50	**0.63**	0.76	0.88	1.26	**1.57**
125	0.00	0.28	0.42	0.56	0.70	0.84	0.98	1.40	1.75

Table 4.34. AC rutting increase at 95% reliability (9.5" AC)

Tire pressure (psi)	Rutting increase at different WBT proportions (%)								
	0%	**4%**	**6%**	**8%**	**10%**	**12%**	**14%**	**20%**	**25%**
80	0.00	0.43	0.64	0.86	1.07	1.28	1.50	2.14	2.67
100	0.00	0.50	0.75	1.00	1.25	1.50	1.75	2.50	3.13
110	0.00	0.52	0.78	1.03	1.29	1.55	1.81	2.59	3.23
120	0.00	0.53	0.80	1.07	**1.34**	1.60	1.87	2.67	**3.34**
125	0.00	0.54	0.81	1.09	1.36	1.63	1.90	2.71	3.39

Table 4.35. AC rutting increase at 95% reliability (11.5" AC)

Tire pressure (psi)	Rutting increase at different WBT proportions (%)								
	0%	**4%**	**6%**	**8%**	**10%**	**12%**	**14%**	**20%**	**25%**
80	0.00	0.54	0.81	1.07	1.34	1.61	1.88	2.68	3.36
100	0.00	0.57	0.86	1.14	1.43	1.71	2.00	2.85	3.57
110	0.00	0.59	0.88	1.17	1.47	1.76	2.06	2.94	3.67
120	0.00	0.62	0.94	1.25	**1.56**	1.87	2.18	3.12	**3.90**
125	0.00	0.63	0.95	1.26	1.58	1.90	2.21	3.16	3.95

Based on Tables 4.32 - 4.35, the rutting increase with different WBT load proportions is plotted, as presented in Figure 4.19.

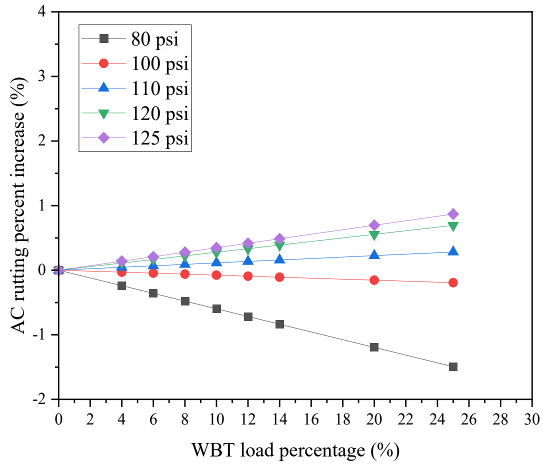

(a) 5" AC structure

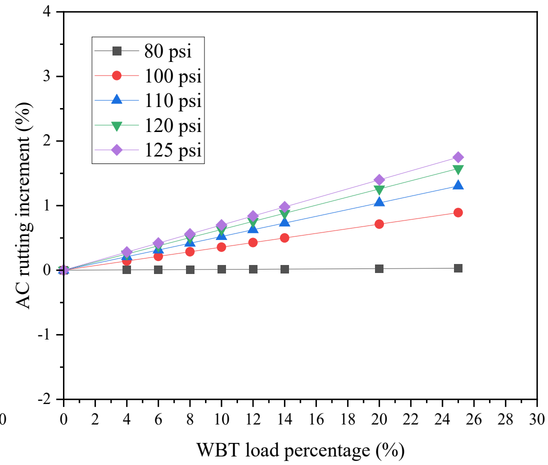

(b) 6.5" AC structure

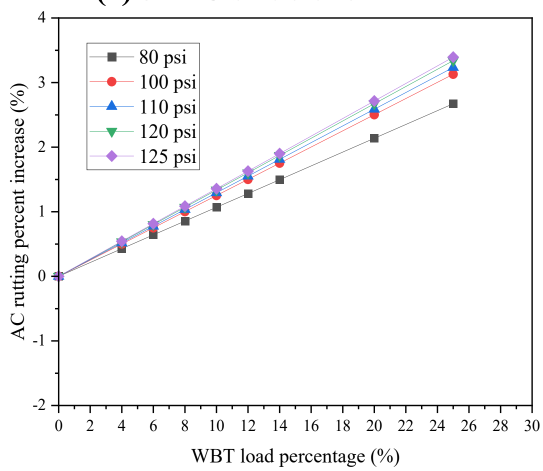

(c) 9.5" AC structure

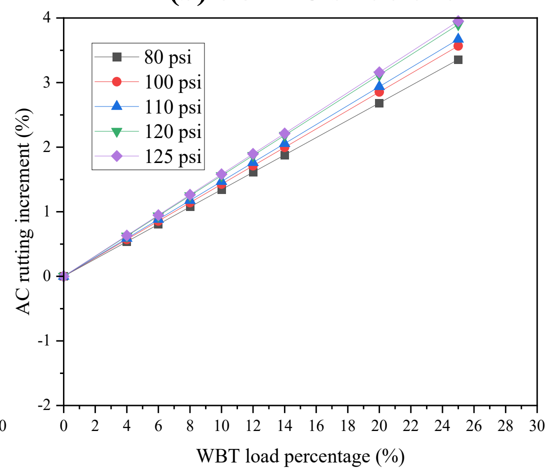

(d) 11.5" AC structure

Figure 4.19. AC rutting increase at 95% reliability

According to the AC rutting increase values under 120 psi tire pressure in Tables 4.32 - 4.35, the AC rutting increase under 10% WBT loads is 0.28% (for 5" AC structure) and 1.56% (for 11.5" AC structure) larger than that without WBT loads. Due to the 5" AC structure's limited thickness, the rutting increase value is miniscule since the energy from loads is mainly undertaken by the underlying layers, which weaken the tire shape impact. The research team can predict that if the proportion of WBT loads in Michigan increases to 25% in the future, the AC rutting depth would be 0.69% (for 5" AC structure) and 3.90% (for 11.5" AC structure) larger than that without WBT loads.

The impact of WBT loads on AC rutting is much smaller than that on fatigue cracking. For a given percentage of WBT loads, higher tire pressure leads to higher AC rutting increases, but the growth is quite limited.

4.4.2. Unbound layers rutting analysis

As for unbound layers, the layers' rutting depth (permanent deformation) can be calculated via equation (4.11) according to MDOT User Guide for MEPD [21].

$$RD = \beta_{s1} k_{s1} \varepsilon_v h (\frac{\varepsilon_0}{\varepsilon_r}) e^{-(\frac{\rho}{N})^{\beta}} \tag{4.11}$$

where:

ε_v	=	Average vertical resilient strain in the unbound layers;
ε_r	=	Resilient strain imposed in the laboratory to obtain ε_0, β, and ρ;
ε_0, β, ρ	=	Parameters related with material properties;
N	=	Number of load repetitions;

β_{s1}, k_{s1} are constants that differ for base, subbase, and subgrade.

The research team calculated the ε_v in base, subbase, and subgrade under DT and WBT loads with JULEA. As for the DT load, the contact pressure was assumed to be equal to the tire pressure. As for the WBT load, the contact pressure was calculated under four different conditions: (1) the theoretical pressure, which equals the tire pressure; (2) ~ (4) the assumed actual pressures, which are 10%, 20%, and 30% larger than the tire pressure. Vertical strain at the middle of the base and subbase are presented in Table 4.36 and Table 4.37. Vertical strain at the top and 6" below the top of the subgrade are presented in Table 4.38 and Table 4.39.

Table 4.36. Vertical strain at the middle of the base layer

Structur e type	Tire pressure (psi)	Vertical strain at the middle of the base layer (με)				
		Under DT load	Under WBT load at different contact pressures			
			0% larger	10% larger	20% larger	30% larger
5" AC structure	80	519.5	715.0	737.8	758.3	776.8
	100	539.1	767.8	789.5	808.9	829.8
	110	547.0	789.5	814.9	832.9	849.1
	120	553.8	808.9	832.9	850.5	866.2
	125	556.9	817.8	841.2	858.5	874.0
6.5" AC structure	80	390.5	532.1	545.3	557.2	567.8
	100	401.8	562.6	575.1	586.1	595.9
	110	406.2	575.1	587.1	597.7	607.1
	120	410.0	586.1	597.7	607.9	617.0
	125	411.5	591.1	602.6	612.6	621.4
9.5" AC structure	80	162.9	195.4	198.1	200.4	202.4
	100	163.6	201.4	203.8	205.9	207.7
	110	163.9	203.8	206.0	208.0	209.7
	120	164.0	205.9	208.0	209.8	211.4
	125	164.2	206.8	208.9	210.6	212.2
11.5" AC structure	80	112.3	128.3	129.6	130.6	131.6
	100	112.9	131.1	132.3	133.2	134.0
	110	113.1	132.3	133.3	134.2	135.0
	120	113.3	133.2	134.2	135.0	135.8
	125	113.3	133.7	134.6	135.4	136.1

Table 4.37. Vertical strain at the middle of the subbase layer

Structure type	Tire pressure (psi)	Vertical strain at the middle of the subbase layer (με)				
		Under DT load	Under WBT load at different contact pressures			
			0% larger	10% larger	20% larger	30% larger
5" AC structure	80	473.5	561.2	567.4	572.6	577.1
	100	477.6	574.9	580.1	584.5	588.2
	110	479.1	580.1	584.9	588.9	592.3
	120	480.3	584.5	588.9	592.6	595.8
	125	480.9	586.4	590.6	594.2	597.3
6.5" AC structure	80	382.2	442.4	446.6	450.1	453.2
	100	385.1	451.7	455.2	458.1	460.7
	110	386.2	455.2	458.4	461.1	463.4
	120	387.1	458.1	461.1	463.6	465.8
	125	387.5	459.5	462.3	464.8	466.8
9.5" AC structure	80	172.8	189.7	190.8	191.7	192.5
	100	173.7	192.1	193.1	193.8	194.5
	110	174.0	193.1	193.9	194.6	195.2
	120	174.3	193.8	194.6	195.3	195.8
	125	174.4	194.2	194.9	195.5	196.1
11.5" AC structure	80	119.9	129.7	130.3	130.8	131.2
	100	120.4	131.0	131.5	131.9	132.3
	110	120.5	131.5	132.0	132.4	132.7
	120	120.7	131.9	132.4	132.7	133.1
	125	120.7	132.1	132.5	132.9	133.2

Table 4.38. Vertical strain at the subgrade top

Structure type	Tire pressure (psi)	Vertical strain at the subgrade top (με)				
		Under DT load	Under WBT load at different contact pressures			
			0% larger	10% larger	20% larger	30% larger
5" AC structure	80	306.2	336.8	338.7	340.4	341.8
	100	307.9	341.1	342.7	344.0	345.2
	110	308.6	342.7	344.2	345.4	346.5
	120	309.1	344.0	345.4	346.5	347.5
	125	309.3	344.7	346.0	347.0	348.0
6.5" AC structure	80	261.3	284.2	285.6	286.9	287.9
	100	262.7	287.4	288.6	289.5	290.4
	110	263.1	288.6	289.6	290.5	291.3
	120	263.5	289.5	290.5	291.4	292.1
	125	263.6	290.0	291.0	291.7	292.4
9.5" AC structure	80	139.1	147.1	147.6	148.0	149.3
	100	139.6	148.1	148.6	148.9	149.1
	110	139.7	148.6	148.9	149.1	149.5
	120	139.8	148.9	149.2	149.5	149.7
	125	139.9	149.0	149.3	149.6	149.8
11.5" AC structure	80	102.0	107.2	107.5	107.7	107.9
	100	102.3	107.8	108.0	108.2	108.4
	110	102.4	108.0	108.2	108.4	108.5
	120	102.4	108.2	108.4	108.5	108.7
	125	102.5	108.3	108.5	108.7	108.8

Table 4.39. Vertical strain at 6" below the subgrade top

Structure type	Tire pressure (psi)	Vertical strain at 6" below the subgrade top (με)				
		Under DT load	Under WBT load at different contact pressures			
			0% larger	10% larger	20% larger	30% larger
5" AC structure	80	225.8	242.3	243.4	244.2	244.9
	100	226.8	244.6	245.5	246.1	246.7
	110	227.1	245.5	246.2	246.8	247.3
	120	227.4	246.1	246.8	247.4	247.9
	125	227.5	246.4	247.1	247.6	248.1
6.5" AC structure	80	198.9	211.8	212.6	213.2	213.8
	100	199.6	213.5	214.1	214.7	215.1
	110	199.9	214.1	214.7	215.2	215.6
	120	200.1	214.7	215.2	215.6	216.0
	125	200.2	214.9	215.4	215.8	216.2
9.5" AC structure	80	116.2	121.5	121.8	122.0	122.2
	100	116.5	122.1	122.4	122.6	122.7
	110	116.6	122.4	122.6	122.8	122.9
	120	116.7	122.6	122.8	122.9	123.0
	125	116.7	122.6	122.8	123.0	123.1
11.5" AC structure	80	88.2	91.8	91.9	92.1	92.2
	100	88.2	92.1	92.3	92.4	92.5
	110	88.4	92.3	92.5	92.6	92.6
	120	88.4	92.4	92.6	92.6	92.7
	125	88.4	92.5	92.6	92.7	92.8

Parameters of β_{s1}, k_{s1}, h, ε_r, ε_0, β, ρ, and N in equation (4.11) are related to unbound layers' types, material properties, or traffic, which are not affected by the load difference between DTs and WBTs. The vertical strain (ε_v) is valuable in evaluating the impact of WBT loads on unbound layers' rutting. So, the research team calculated the vertical strain (ε_v) increase of unbound layers under WBT load compared with the condition under DT load, considering ε_v at 20% larger contact pressure under WBT load. For subgrade, the average of ε_v on the top and 6" below the top was used for calculation. The results are presented in Table 4.40.

Table 4.40. Increase of ε_v from DT load to WBT load

Structure type	Tire pressure (psi)	Increase in ε_v for different layers (%)		
		Base	Subbase	Subgrade
5" AC structure	80	45.97	20.93	9.89
	100	50.05	22.38	10.36
	110	52.27	22.92	10.55
	120	53.58	23.38	10.70
	125	54.16	23.56	10.77
6.5" AC structure	80	42.69	17.77	8.67
	100	45.87	18.96	9.06
	110	47.14	19.39	9.22
	120	48.27	19.76	9.36
	125	48.87	19.95	9.42
9.5" AC structure	80	22.98	10.95	5.76
	100	25.83	11.59	6.01
	110	26.91	11.85	6.10
	120	27.90	12.03	6.20
	125	28.32	12.12	6.23
11.5" AC structure	80	16.35	9.07	5.02
	100	18.04	9.60	5.27
	110	18.68	9.82	5.34
	120	19.23	9.97	5.40
	125	19.49	10.04	5.45

The increase of ε_v in Table 4.40 is equal to the increase of pavement unbound layers' rutting from DT load to WBT loads. Considering the proportion of WBT loads, the rutting increase of the base layer for different AC thickness structures are presented in Tables 4.41 - 4.44.

Table 4.41. Base layer rutting increase (5" AC)

Tire pressure (psi)	Rutting increase under different WBT proportions (%)								
	0%	4%	6%	8%	10%	12%	14%	20%	25%
80	0.00	1.84	2.76	3.68	4.60	5.52	6.44	9.19	11.49
100	0.00	2.00	3.00	4.00	5.01	6.01	7.01	10.01	12.51
110	0.00	2.09	3.14	4.18	5.23	6.27	7.32	10.45	13.07
120	0.00	2.14	3.21	4.29	5.36	6.43	7.50	10.72	13.40
125	0.00	2.17	3.25	4.33	5.42	6.50	7.58	10.83	13.54

Table 4.42. Base layer rutting increase (6.5" AC)

Tire pressure (psi)	Rutting increase under different WBT proportions (%)								
	0%	4%	6%	8%	10%	12%	14%	20%	25%
80	0.00	1.71	2.56	3.42	4.27	5.12	5.98	8.54	10.67
100	0.00	1.83	2.75	3.67	4.59	5.50	6.42	9.17	11.47
110	0.00	1.89	2.83	3.77	4.71	5.66	6.60	9.43	11.79
120	0.00	1.93	2.90	3.86	4.83	5.79	6.76	9.65	12.07
125	0.00	1.95	2.93	3.91	4.89	5.86	6.84	9.77	12.22

Table 4.43. Base layer rutting increase (9.5" AC)

Tire pressure (psi)	Rutting increase under different WBT proportions (%)								
	0%	4%	6%	8%	10%	12%	14%	20%	25%
80	0.00	0.92	1.38	1.84	2.30	2.76	3.22	4.60	5.75
100	0.00	1.03	1.55	2.07	2.58	3.10	3.62	5.17	6.46
110	0.00	1.08	1.61	2.15	2.69	3.23	3.77	5.38	6.73
120	0.00	1.12	1.67	2.23	2.79	3.35	3.91	5.58	6.98
125	0.00	1.13	1.70	2.27	2.83	3.40	3.96	5.66	7.08

Table 4.44. Base layer rutting increase (11.5" AC)

Tire pressure (psi)	Rutting increase under different WBT proportions (%)								
	0%	4%	6%	8%	10%	12%	14%	20%	25%
80	0.00	0.65	0.98	1.31	1.64	1.96	2.29	3.27	4.09
100	0.00	0.72	1.08	1.44	1.80	2.16	2.53	3.61	4.51
110	0.00	0.75	1.12	1.49	1.87	2.24	2.62	3.74	4.67
120	0.00	0.77	1.15	1.54	1.92	2.31	2.69	3.85	4.81
125	0.00	0.78	1.17	1.56	1.95	2.34	2.73	3.90	4.87

The rutting increase of the subbase layer for different AC thickness structures are presented in Tables 4.45 - 4.48.

Table 4.45. Subbase layer rutting increase (5" AC)

Tire pressure (psi)	Rutting increase under different WBT proportions (%)								
	0%	4%	6%	8%	10%	12%	14%	20%	25%
80	0.00	0.84	1.26	1.67	2.09	2.51	2.93	4.19	5.23
100	0.00	0.90	1.34	1.79	2.24	2.69	3.13	4.48	5.60
110	0.00	0.92	1.38	1.83	2.29	2.75	3.21	4.58	5.73
120	0.00	0.94	1.40	1.87	2.34	2.81	3.27	4.68	5.85
125	0.00	0.94	1.41	1.88	2.36	2.83	3.30	4.71	5.89

Table 4.46. Subbase layer rutting increase (6.5" AC)

Tire pressure (psi)	Rutting increase under different WBT proportions (%)								
	0%	4%	6%	8%	10%	12%	14%	20%	25%
80	0.00	0.71	1.07	1.42	1.78	2.13	2.49	3.55	4.44
100	0.00	0.76	1.14	1.52	1.90	2.28	2.65	3.79	4.74
110	0.00	0.78	1.16	1.55	1.94	2.33	2.71	3.88	4.85
120	0.00	0.79	1.19	1.58	1.98	2.37	2.77	3.95	4.94
125	0.00	0.80	1.20	1.60	2.00	2.39	2.79	3.99	4.99

Table 4.47. Subbase layer rutting increase (9.5” AC)

Tire pressure (psi)	Rutting increase under different WBT proportions (%)								
	0%	4%	6%	8%	10%	12%	14%	20%	25%
80	0.00	0.44	0.66	0.88	1.10	1.31	1.53	2.19	2.74
100	0.00	0.46	0.70	0.93	1.16	1.39	1.62	2.32	2.90
110	0.00	0.47	0.71	0.95	1.19	1.42	1.66	2.37	2.96
120	0.00	0.48	0.72	0.96	1.20	1.44	1.68	2.41	3.01
125	0.00	0.48	0.73	0.97	1.21	1.45	1.70	2.42	3.03

Table 4.48. Subbase layer rutting increase (11.5” AC)

Tire pressure (psi)	Rutting increase under different WBT proportions (%)								
	0%	4%	6%	8%	10%	12%	14%	20%	25%
80	0.00	0.36	0.54	0.73	0.91	1.09	1.27	1.81	2.27
100	0.00	0.38	0.58	0.77	0.96	1.15	1.34	1.92	2.40
110	0.00	0.39	0.59	0.79	0.98	1.18	1.37	1.96	2.46
120	0.00	0.40	0.60	0.80	1.00	1.20	1.40	1.99	2.49
125	0.00	0.40	0.60	0.80	1.00	1.20	1.41	2.01	2.51

The rutting increase of the subgrade layer for different AC thickness structures are presented in Tables 4.49 - 4.52.

Table 4.49. Subgrade rutting increase (5" AC)

Tire pressure (psi)	Rutting increase under different WBT proportions (%)								
	0%	4%	6%	8%	10%	12%	14%	20%	25%
80	0.00	0.40	0.59	0.79	0.99	1.19	1.38	1.98	2.47
100	0.00	0.41	0.62	0.83	1.04	1.24	1.45	2.07	2.59
110	0.00	0.42	0.63	0.84	1.06	1.27	1.48	2.11	2.64
120	0.00	0.43	0.64	0.86	1.07	1.28	1.50	2.14	2.68
125	0.00	0.43	0.65	0.86	1.08	1.29	1.51	2.15	2.69

Table 4.50. Subgrade rutting increase (6.5" AC)

Tire pressure (psi)	Rutting increase under different WBT proportions (%)								
	0%	4%	6%	8%	10%	12%	14%	20%	25%
80	0.00	0.35	0.52	0.69	0.87	1.04	1.21	1.73	2.17
100	0.00	0.36	0.54	0.72	0.91	1.09	1.27	1.81	2.27
110	0.00	0.37	0.55	0.74	0.92	1.11	1.29	1.84	2.31
120	0.00	0.37	0.56	0.75	0.94	1.12	1.31	1.87	2.34
125	0.00	0.38	0.57	0.75	0.94	1.13	1.32	1.88	2.36

Table 4.51. Subgrade rutting increase (9.5" AC)

Tire pressure (psi)	Rutting increase under different WBT proportions (%)								
	0%	4%	6%	8%	10%	12%	14%	20%	25%
80	0.00	0.23	0.35	0.46	0.58	0.69	0.81	1.15	1.44
100	0.00	0.24	0.36	0.48	0.60	0.72	0.84	1.20	1.50
110	0.00	0.24	0.37	0.49	0.61	0.73	0.85	1.22	1.53
120	0.00	0.25	0.37	0.50	0.62	0.74	0.87	1.24	1.55
125	0.00	0.25	0.37	0.50	0.62	0.75	0.87	1.25	1.56

Table 4.52. Subgrade rutting increase (11.5" AC)

Tire pressure (psi)	Rutting increase under different WBT proportions (%)								
	0%	4%	6%	8%	10%	12%	14%	20%	25%
80	0.00	0.20	0.30	0.40	0.50	0.60	0.70	1.00	1.26
100	0.00	0.21	0.32	0.42	0.53	0.63	0.74	1.05	1.32
110	0.00	0.21	0.32	0.43	0.53	0.64	0.75	1.07	1.34
120	0.00	0.22	0.32	0.43	0.54	0.65	0.76	1.08	1.35
125	0.00	0.22	0.33	0.44	0.55	0.65	0.76	1.09	1.36

According to Tables 4.41- 4.52, the order of WBT impact on unbound layers' rutting is Base > Subbase > Subgrade; this is because the deeper area in the pavement is less sensitive to loads. Then, the proportion of rutting in base, subbase, and subgrade should be determined. β_{s1}, k_{s1}, and the multiple values of β_{s1}, k_{s1}, h in equation (4.11) for the base, subbase, and subgrade are shown in Table 4.53.

Table 4.53. Parameters of β_{s1} and k_{s1} for the base, subbase, and subgrade

Unbound layers	β_{s1}	k_{s1}	$\beta_{s1}\times k_{s1}\times h$
Base	0.0985	2.03	1.1997
Subbase	0.0985	2.03	3.5992
Subgrade	0.0367	1.35	0.2973

Load repetitions N is the same for all unbound layers. According to AASHTO MEPDG 3 [11], β can be computed with the water content of unbound layer material, and ρ can be calculated with β. The research assumes the same water content for all unbound layers in this project, meaning the same β and ρ for all unbound layers.

Next, the research team assumed $\frac{\varepsilon_0}{\varepsilon_r}$ is inversely proportional to the resilient modulus, which is not a precise assumption; however, it corresponds with the fundamental property that weaker unbound material deforms more (ε_0) in laboratory tests under the same resilient strain (ε_r) imposed. So, the proportion of $\frac{\varepsilon_0}{\varepsilon_r}$ for the base, subbase, and subgrade is $\frac{1}{33000}: \frac{1}{20000}: \frac{1}{5000} = 1: 1.65: 6.6$. Combined with the value of $\beta_{s1}\times k_{s1}\times h$ in Table 4.53, the proportion of rutting for base, subbase, and subgrade is 1.1997×1: 3.5992×1.65: 0.2973×6.6 = 1.1997: 5.9387: 1.9622 = 13%: 65%: 22%. So, the proportion of rutting for the base, subbase, and subgrade is about 13%, 65%, and 22%.

The reliability in Michigan pavement design for unbound layers should be discussed. As for the granular base or subbase layer, equation (4.12) could be used to transform rutting under 50% reliability into rutting under 95% reliability by using the average rutting, standard error of the prediction (S_e), and Z-value for the 95% confidence level one-tailed test.

$$Rutting_{Base\ OR\ Subbase,95\%} = Rutting_{Base\ OR\ Subbase,50\%} + S_e \times Z_{95} \tag{4.12}$$

where:

S_e is the standard error, and $S_e = 0.1145 \times \text{Rutting}_{\text{Base OR Subbase,50\%}}{}^{0.3907}$; Z_{95} is the Z-value for the 95%-confidence level one-tailed test, which equals 1.65.

As for the fine subgrade layer, equation (4.13) could be used to transform rutting under 50% reliability into rutting under 95% reliability.

$$Rutting_{Subgrade,95\%} = Rutting_{Subgrade,50\%} + S_e \times Z_{95} \tag{4.13}$$

where:

S_e is the standard error, and $S_e = 3.6118 \times \text{Rutting}_{\text{Subgrade,50\%}}{}^{1.0951}$; Z_{95} is the Z-value for the 95%-confidence level one-tailed test, which equals 1.65.

The unbound layers' rutting is not an individual threshold used in pavement design, so the relationship between unbound layers' rutting in 50% reliability and that in 95% reliability varies with different structures with specific unbound layers' rutting values. However, according to the Pavement ME analysis examples in section 4.2, the rutting of unbound layers based on Michigan calibration is insignificant (less than 0.05").

The unbound layers' rutting proportion is 78% (13% + 65%) from base + subbase and 22% from subgrade. Assuming the total unbound layers' rutting is 0.05" in a pavement design at 95%

reliability, there would be approximately 0.04” from $Rutting_{Base\ OR\ Subbase,95\%}$ and 0.01” from $Rutting_{Subgrade,95\%}$. Back-calculation of equations (4.12) and (4.13) shows that at this time, the $Rutting_{\text{Base OR Subbase},50\%}$ would be around 0.01”, while the $Rutting_{\text{Subgrade},50\%}$ would be around 0.0025”.

So, the rutting increase in base + subbase layers caused by WBT load in 95% reliability would be approximately 0.01”/0.04”=0.25 times the rutting increase caused by WBT load in 50% reliability. As for the subgrade layer, the value would be 0.0025/0.01”=0.25 times the rutting increase caused by WBT load in 50% reliability.

Based on this rutting proportion and 95% reliability, the research team calculated the rutting increase for total unbound layers (Base + Subbase + Subgrade), as shown in Table 4.54 - 4.57 and Figure 4.20.

Table 4.54. Total unbound layers’ rutting increase in 95% reliability (5" AC)

Tire pressure (psi)	Rutting increase at different WBT proportions (%)								
	0%	**4%**	**6%**	**8%**	**10%**	**12%**	**14%**	**20%**	**25%**
80	0.00	0.22	0.33	0.44	0.54	0.65	0.76	1.09	1.36
100	0.00	0.24	0.35	0.47	0.59	0.70	0.82	1.17	1.46
110	0.00	0.24	0.36	0.48	0.60	0.72	0.84	1.20	1.50
120	0.00	0.25	0.37	0.49	**0.61**	0.74	0.86	1.23	**1.53**
125	0.00	0.25	0.37	0.49	0.62	0.74	0.87	1.24	1.55

Table 4.55. Total unbound layers’ rutting increase in 95% reliability (6.5" AC)

Tire pressure (psi)	Rutting increase at different WBT proportions (%)								
	0%	**4%**	**6%**	**8%**	**10%**	**12%**	**14%**	**20%**	**25%**
80	0.00	0.19	0.29	0.38	0.48	0.57	0.67	0.95	1.19
100	0.00	0.20	0.31	0.41	0.51	0.61	0.71	1.01	1.27
110	0.00	0.21	0.31	0.42	0.52	0.62	0.73	1.04	1.30
120	0.00	0.21	0.32	0.42	**0.53**	0.64	0.74	1.06	**1.32**
125	0.00	0.22	0.32	0.43	0.54	0.64	0.75	1.07	1.34

Table 4.56. Total unbound layers’ rutting increase in 95% reliability (9.5” AC)

Tire pressure (psi)	Rutting increase at different WBT proportions (%)								
	0%	**4%**	**6%**	**8%**	**10%**	**12%**	**14%**	**20%**	**25%**
80	0.00	0.12	0.17	0.23	0.29	0.34	0.40	0.57	0.71
100	0.00	0.12	0.19	0.25	0.31	0.37	0.43	0.61	0.76
110	0.00	0.13	0.19	0.25	0.32	0.38	0.44	0.63	0.79
120	0.00	0.13	0.19	0.26	**0.32**	0.38	0.45	0.64	**0.80**
125	0.00	0.13	0.20	0.26	0.32	0.39	0.45	0.65	0.81

Table 4.57. Total unbound layers' rutting increase in 95% reliability (11.5" AC)

Tire pressure (psi)	Rutting increase at different WBT proportions (%)								
	0%	4%	6%	8%	10%	12%	14%	20%	25%
80	0.00	0.09	0.14	0.18	0.23	0.28	0.32	0.46	0.57
100	0.00	0.10	0.15	0.20	0.24	0.29	0.34	0.49	0.61
110	0.00	0.10	0.15	0.20	0.25	0.30	0.35	0.50	0.63
120	0.00	0.10	0.15	0.20	**0.26**	0.31	0.36	0.51	**0.64**
125	0.00	0.10	0.15	0.21	0.26	0.31	0.36	0.51	0.64

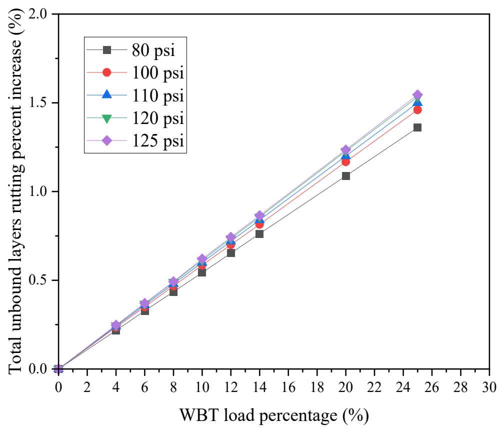

(a) 5" AC structure

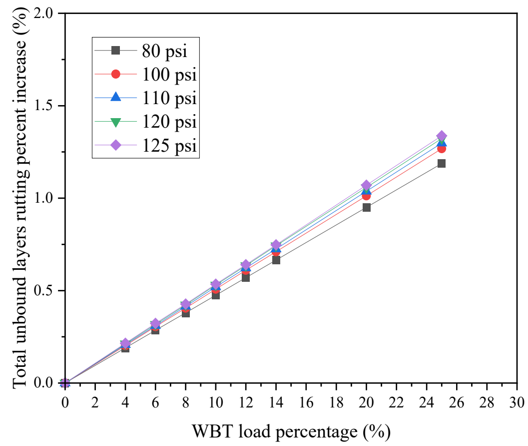

(b) 6.5" AC structure

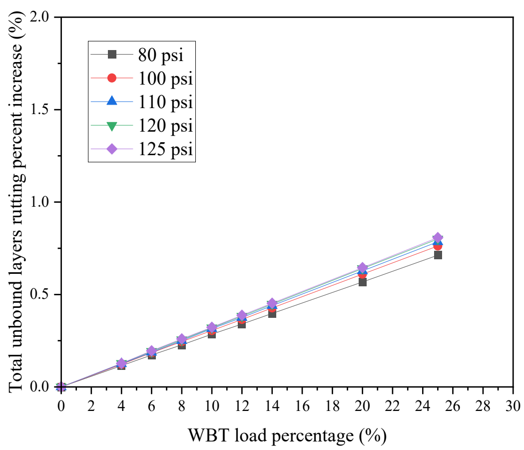

(a) 9.5" AC structure

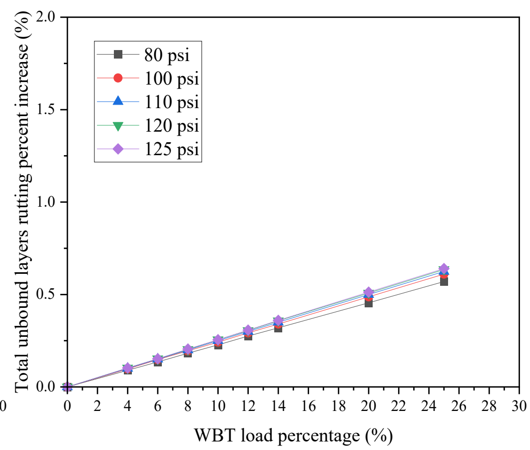

(b) 11.5" AC structure

Figure 4.20. Total unbound layers' rutting increase

According to Figure 4.20, the impact of WBT load on unbound layers' rutting is much less than that on AC rutting because unbound layers are deeper than AC layers. The mechanical strain of unbound layers is less sensitive to load types and contact pressure.

When the tire pressure is 120 psi, the unbound layers' rutting with 10% WBT loads is 0.61% (for 5" AC structure) and 0.26% (for 11.5" AC structure) larger than that with 0% WBT loads. The WBT loads have less impact on the thicker AC structures, which is reasonable because the unbound layers for the thicker AC structures (9.5" and 11.5") are deeper while loaded less. Based on research results, the research team predicts that if the proportion of WBT loads in Michigan increases to 25% in the future, the unbound layers' rutting depth would be 1.53% (for 5" AC structure) and 0.64% (for 11.5" AC structure) larger than that with 0% WBT loads.

4.4.3. Total rutting analysis

At this point, the research team has determined the impact of WBT load on AC rutting and unbound layers' rutting separately. Since total rutting of pavement is combined with AC rutting and unbound layers' rutting, if the proportion of rutting for AC layers and unbound layers is determined, the impact of WBT load on total rutting can be computed. The research team conducted test scenarios using Pavement ME, and according to the output result, the AC rutting occupies approximately 85% to 95% of total rutting for different AC thickness structures. The research team assume that total rutting contains 90% of AC rutting and 10% of unbound layers' rutting for the total rutting analysis. Based on the AC rutting increase in section 4.4.1 and total unbound layers' rutting increase in section 4.4.2, the total rutting increase under different WBT loads is computed, as presented in Table 4.58 and Figure 4.21.

Table 4.58. Total rutting increase for different structures

Structure type	Tire pressure (psi)	Rutting increase at different WBT proportions (%)								
		0%	**4%**	**6%**	**8%**	**10%**	**12%**	**14%**	**20%**	**25%**
5" AC structure	80	0.00	-0.19	-0.29	-0.39	-0.49	-0.58	-0.68	-0.97	-1.21
	100	0.00	0.00	-0.01	-0.01	-0.01	-0.01	-0.02	-0.02	-0.03
	110	0.00	0.07	0.10	0.13	0.16	0.20	0.23	0.33	0.40
	120	0.00	0.12	0.19	0.25	**0.31**	0.37	0.44	0.63	**0.77**
	125	0.00	0.15	0.23	0.30	0.38	0.45	0.53	0.75	0.94
6.5" AC structure	80	0.00	0.02	0.04	0.05	0.06	0.07	0.09	0.11	0.15
	100	0.00	0.15	0.22	0.30	0.38	0.45	0.52	0.74	0.93
	110	0.00	0.21	0.31	0.42	0.52	0.63	0.73	1.04	1.30
	120	0.00	0.25	0.37	0.49	**0.62**	0.75	0.87	1.24	**1.55**
	125	0.00	0.27	0.41	0.55	0.68	0.82	0.96	1.37	1.71
9.5" AC structure	80	0.00	0.40	0.59	0.80	0.99	1.19	1.39	1.98	2.47
	100	0.00	0.46	0.69	0.93	1.16	1.39	1.62	2.31	2.89
	110	0.00	0.48	0.72	0.95	1.19	1.43	1.67	2.39	2.99
	120	0.00	0.49	0.74	0.99	**1.24**	1.48	1.73	2.47	**3.09**
	125	0.00	0.50	0.75	1.01	1.26	1.51	1.76	2.50	3.13
11.5" AC structure	80	0.00	0.50	0.74	0.98	1.23	1.48	1.72	2.46	3.08
	100	0.00	0.52	0.79	1.05	1.31	1.57	1.83	2.61	3.27
	110	0.00	0.54	0.81	1.07	1.35	1.61	1.89	2.70	3.37
	120	0.00	0.57	0.86	1.15	**1.43**	1.71	2.00	2.86	**3.57**
	125	0.00	0.58	0.87	1.16	1.45	1.74	2.03	2.90	3.62

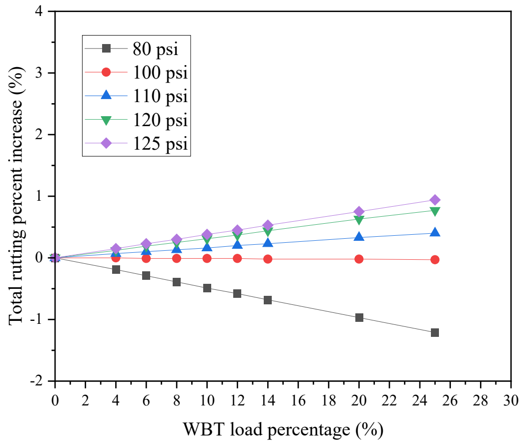

(a) 5" AC structure

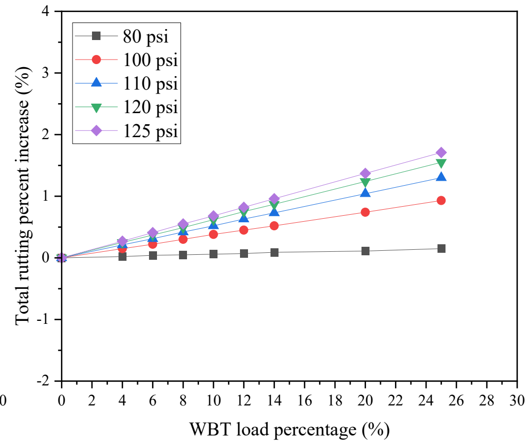

(b) 6.5" AC structure

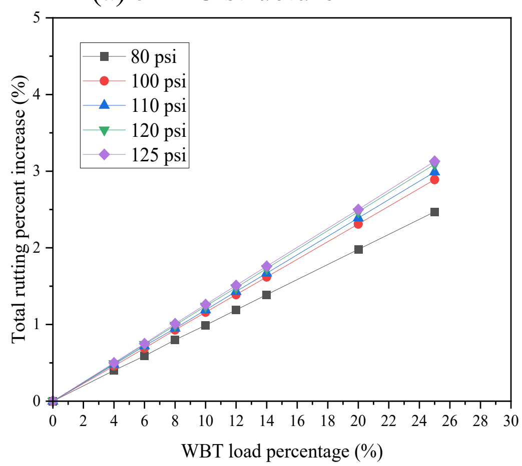

(c) 9.5” AC structure

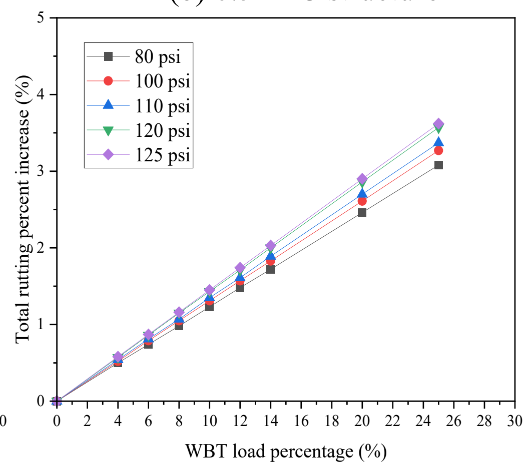

(d) 11.5” AC structure

Figure 4.21. Total rutting increase

According to Tables 4.58, under 120 psi tire pressure, total rutting with 10% WBT loads is 0.31% (for 5” AC structure) and 1.43% (for 11.5” AC structure) larger than that with 0% WBT loads. The impact of WBT loads on total rutting distress for those two structures is similar.

Figure 4.21 shows that the thinner AC structures (5” AC; 6.5”AC) are more sensitive to tire pressure than the thicker AC structures (9.5” AC; 11.5”AC) in total rutting distress due to the total thickness difference. Based on research results, the research team can predict that if the proportion of WBT loads in Michigan increased to 25% in the future, the total rutting depth would be 0.77% (for 5” AC structure) and 3.57% (for 11.5” AC structure) larger than that with 0% WBT loads.

4.5. IRI impact analysis

4.5.1. IRI analysis method introduction

International Roughness Index (IRI) is another criterion in the ME pavement design process. Using the process developed for the Pavement ME software, the IRI value for flexible pavement structures could be predicted with equation (4.14).

$$IRI = IRI_0 + C_1(RD) + C_1(FC_{Total}) + C_3(TC) + C_4(SF) \qquad (4.14)$$

where:

IRI = Predicted IRI, MDOT recommended failure value is 172, in/mile

SF = Site factor

IRI_0 = Initial IRI after construction; defaulted 67 for MDOT, in/mile

FC_{Total} = Fatigue cracking area, %

TC = Length of transverse cracking, ft/mile

RD = Average rut depth, inch

C_1=50.372; C_2= 0.4102; C_3=0.0066; C_4=0.0068

Thermal cracking is related to AC properties and climate conditions; SF is related to pavement age, precipitation, and subgrade soil properties.

As the value of IRI is a combination of other pavement distress, it would be difficult to theoretically calculate the WBT impact, considering the reliability issue. However, the relationship between IRI and other distress could be analyzed from Pavement ME outputs. According to the Pavement ME results under Michigan calibration and level 1 input (section 4.2), the Pavement ME distress comparison is shown in Table 4.59.

Table 4.59. Pavement ME distress comparison

NO.	WIM station	Traffic	Distress value			
			Bottom-up cracking (%)	Thermal cracking (feet)	Total rutting (inch)	IRI
Threshold			20	2000	0.50	172
1	US-41 (211459)	Low	26.27	346.55	0.36	137.36
2	US-2 (492029)	Low	26.44	346.55	0.4	140.1
3	I-75 (694049)	Low	28.09	346.61	0.91	172.96
4	US-131 (595249)	Medium	17.47	2625.96	0.34	147.7
5	I-94 (776469)	Medium	20.07	372.3	0.38	136.15
6	I94 (117189)	Heavy	18.16	346.55	0.43	138.95
7	I69 (238869)	Heavy	17.27	346.57	0.46	141.79

As shown in Table 4.59, Nos. 1, 2, 3, 6, and 7 have almost the same thermal cracking values. Also, since all projects have the same soil condition and age assumption in Michigan, the site factors for those projects would be similar. So, fatigue cracking and rutting would be two critical parameters for IRI impact analysis considered in this project. The research then uses fatigue cracking, rutting, and IRI values in these scenarios (Nos. 1, 2, 3, 6, 7 in Table 4.59) to establish the IRI prediction equation (95% reliability) with the format of $IRI = a{\cdot}x + b{\cdot}y + c$ (x is cracking, y is rutting). The result is shown in Figure 4.22.

Multiple Regression (8/29/2022 16:10:38)

Notes

Input Data

Masked Data - Values Excluded from Computations

Bad Data (missing values) -- Values that are invalid and thus not used in computations

Parameters

		Value	Standard Error	t-Value	Prob>|t|
C	Intercept	107.02897	1.38794	77.11379	1.68123E-4
	A	0.28094	0.06353	4.42245	0.04752
	B	63.81327	1.43885	44.3503	5.08014E-4

Standard Error was scaled with square root of reduced Chi-Sqr.

Statistics

	C
Number of Points	5
Degrees of Freedom	2
Residual Sum of Squares	0.70848
R-Square (COD)	0.99922
Adj. R-Square	0.99843

Summary

	Intercept		A		B		Statistics
	Value	Standard Error	Value	Standard Error	Value	Standard Error	Adj. R-Square
C	107.02897	1.38794	0.28094	0.06353	63.81327	1.43885	0.99843

ANOVA

		DF	Sum of Squares	Mean Square	F Value	Prob>F
C	Model	2	902.7502	451.3751	1274.21398	7.84182E-4
	Error	2	0.70848	0.35424		
	Total	4	903.45868			

At the 0.05 level, the fitting function is significantly better than the function y=constant.

Figure 4.22. IRI multiple regression result

According to Figure 4.22, Equation (4.15) could be obtained.

$$IRI = 107.03 + 0.28x + 63.81y \tag{4.15}$$

where:

x is fatigue cracking value, %; y is rutting depth, inch; IRI value is in 95% reliability.

The following equations could be obtained by applying different IRI (IRI_a, IRI_b), cracking (x_a, x_b), and faulting (y_a,y_b) values to equation (4.15).

$$IRI_a = 107.03 + 0.28x_a + 63.81y_a \tag{4.16}$$

$$IRI_b = 107.03 + 0.28x_b + 63.81y_b \quad (4.17)$$

$$\frac{IRI_b - IRI_a}{IRI_a} = \frac{0.28(x_b - x_a)}{IRI_a} + \frac{63.81(y_b - y_a)}{IRI_a} \quad (4.18)$$

Then, the equation with the dependent variable of IRI percent change ($P_{IRI}=\frac{IRI_b - IRI_a}{IRI_a}$) in value and independent variables of percentage change of cracking and rutting in value ($P_{Cracking}=\frac{x_b - x_a}{x_a}$); $P_{Rutting}=\frac{y_b - y_a}{y_a}$) could be established, as shown in equation (4.19).

$$P_{IRI} = 0.28\frac{x_a}{IRI_a}P_{Cracking} + 63.81\frac{y_a}{IRI_a}P_{Rutting} \quad (4.19)$$

Assume that $m = 0.28\frac{x_a}{IRI_a}$; $n = 63.81\frac{y_a}{IRI_a}$; and m and n values could be calculated, as shown in Table 4.60.

Table 4.60. Factors of IRI percent change equation

NO.	Percent fatigue cracking (x_a)	Rutting in inches (y_a)	IRI_a (inch/mile)	m	n
1	26.27	0.36	137.67	0.054	0.167
2	26.44	0.4	140.27	0.053	0.182
3	28.09	0.91	173.27	0.046	0.335
6	18.16	0.43	139.86	0.036	0.196
7	17.27	0.46	141.53	0.034	0.207
Average				**0.045**	**0.218**

Using average values for both m and n, the equation to calculate the IRI percent change could be finally obtained, as presented in equation (4.20)

$$P_{IRI} = 0.045\ P_{Cracking} + 0.218\ P_{Rutting} \quad (4.20)$$

4.5.2. Analysis results of WBT impact on IRI of flexible pavement

According to the percent increase of fatigue cracking (Table 4.16) and rutting (Table 4.58) at different WBT proportions, the $P_{Cracking}$ and $P_{Rutting}$ in equation (4.20) can be obtained. The P_{IRI} (which equals the IRI growth rate) at different WBT proportions can be calculated, as shown in Table 4.61 and Figure 4.23.

Table 4.61. IRI percent increase at different WBT proportions

Structure type	Tire pressure (psi)	IRI increase at different WBT proportions (%)								
		0%	**4%**	**6%**	**8%**	**10%**	**12%**	**14%**	**20%**	**25%**
5" AC structure	80	0.00	0.01	0.01	0.01	0.02	0.03	0.03	0.04	0.05
	100	0.00	0.09	0.13	0.16	0.21	0.25	0.28	0.39	0.48
	110	0.00	0.12	0.18	0.24	0.29	0.35	0.40	0.54	0.67
	120	0.00	0.15	0.23	0.29	**0.36**	0.43	0.50	0.69	**0.83**
	125	0.00	0.17	0.25	0.33	0.40	0.48	0.55	0.76	0.92
6.5" AC structure	80	0.00	0.05	0.08	0.10	0.12	0.15	0.18	0.25	0.31
	100	0.00	0.11	0.15	0.21	0.25	0.31	0.35	0.49	0.61
	110	0.00	0.13	0.19	0.26	0.32	0.38	0.43	0.61	0.75
	120	0.00	0.15	0.22	0.30	**0.36**	0.43	0.50	0.70	**0.86**
	125	0.00	0.16	0.24	0.32	0.39	0.46	0.54	0.75	0.92
9.5" AC structure	80	0.00	0.12	0.17	0.23	0.28	0.35	0.40	0.57	0.71
	100	0.00	0.13	0.20	0.28	0.35	0.41	0.48	0.67	0.85
	110	0.00	0.15	0.22	0.29	0.36	0.43	0.50	0.72	0.89
	120	0.00	0.15	0.22	0.30	**0.38**	0.45	0.52	0.75	**0.93**
	125	0.00	0.15	0.23	0.31	0.38	0.45	0.54	0.75	0.94
11.5" AC structure	80	0.00	0.13	0.19	0.26	0.32	0.39	0.45	0.64	0.80
	100	0.00	0.14	0.21	0.28	0.36	0.42	0.49	0.70	0.87
	110	0.00	0.15	0.22	0.29	0.36	0.44	0.51	0.73	0.91
	120	0.00	0.15	0.24	0.31	**0.39**	0.46	0.54	0.78	**0.97**
	125	0.00	0.16	0.24	0.31	0.39	0.48	0.55	0.79	0.98

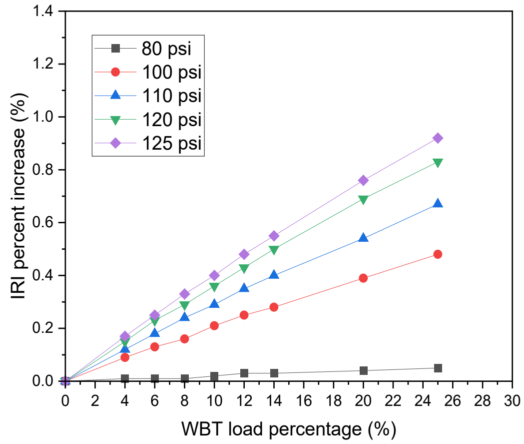

(a) 5" AC structure

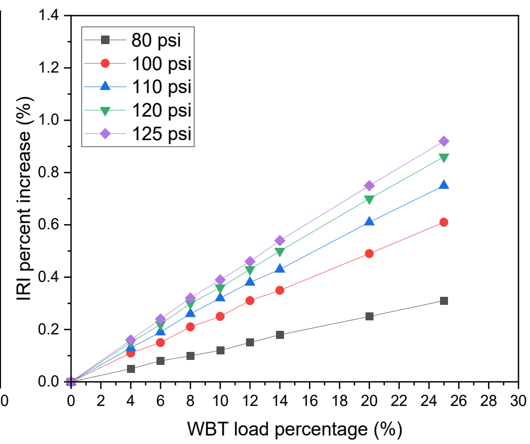

(b) 6.5" AC structure

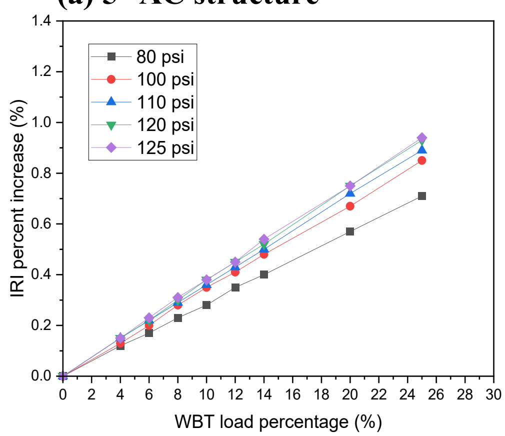

(c) 9.5” AC structure

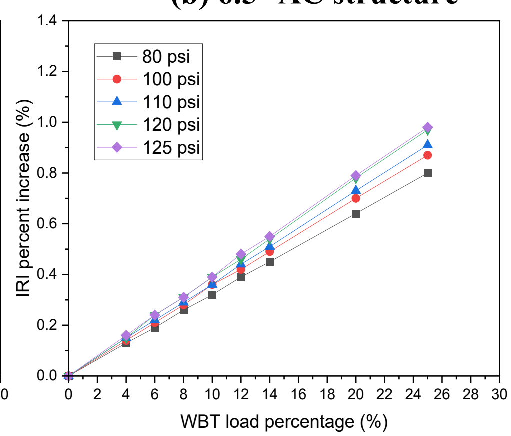

(d) 11.5” AC structure

Figure 4.23. Impact of WBT on flexible pavement IRI in different AC thicknesses

According to Table 4.61, the percent increase of IRI with 10% WBT loads ranges from 0.36% (5" AC thickness) to 0.39% (11.5" AC thickness) under the standard 120 psi tire pressure. The research team predicts that if the proportion of WBT loads in Michigan increased to 25% in the future, the IRI percent increase caused by WBT load would be in the range of 0.83% (5" AC thickness) to 0.97% (11.5" AC thickness).

The impact of WBT loads on the IRI of thinner AC thickness structures is more sensitive to tire pressures compared with the thicker AC structures, as the lines in Figure 4.23 (a) and (b) are farther apart than those in Figure 4.23 (c) and (d). The impact of WBT loads on flexible pavements’ IRI is negatively related to the AC thickness, while positively related to the WBT proportion. Thicker AC thickness would slightly decrease the pavement failure risk caused by increasing WBT loads.

4.6. Prediction function establishment of WBT loads' impact on flexible pavement

4.6.1. Prediction with simple linear regression

The research team has found the impact of WBT loads on flexible pavement distress with different AC thicknesses (5", 6.5", 9.5", 11.5") and WBT proportions. According to the flexible pavement distress increase data under four thicknesses, the increase in fatigue cracking values correlates with AC thickness positively. In contrast, rutting increase has a negative correlation with AC thickness. So, the research team tried to fit the data with linear regression functions. The WBT proportion is fixed at 10%, the independent is set as AC thickness, and the four flexible pavements' distress is the dependent. The regression results are shown in Figure 4.24.

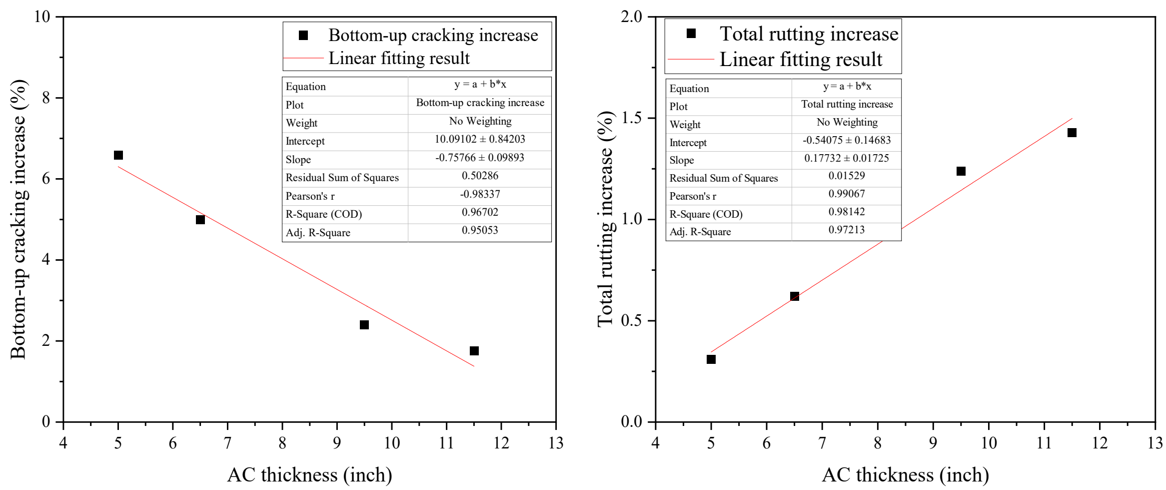

(a) Bottom-up cracking (b) Total rutting

Figure 4.24. Simple linear regression results

According to the regression results in Figure 4.24, two prediction functions for the different distresses can be established, as presented in equations (4.21) - (4.22).

$$f_1=10.09102-0.75766\times T_{AC} \quad (4.21)$$

$$f_2=-0.54075+0.17732\times T_{AC} \quad (4.22)$$

where:

f_1 : Bottom-up fatigue cracking increase by linear regression (%);

f_2 : Total rutting increase by linear regression (%);

T_{AC} : AC thickness (inch).

The above two linear prediction functions can quickly estimate the impact of WBT loads on the distress of flexible pavement in different thicknesses. The WBT load's proportion in those functions is fixed at 10%, corresponding with the WBT load survey results. Those functions' R^2

(coefficient of determination) are all greater than 0.96, showing good regression accuracy.

4.6.2. Prediction with multiple regression

Although linear regression in section 4.6.1 would make it easy to estimate WBT loads' impact on the distress of flexible pavements with different thicknesses, this approach does not involve different WBT proportion scenarios. So, the research team then conducted multiple regression analyses. The distress increase scatters with the WBT proportion are presented in Figure 4.25.

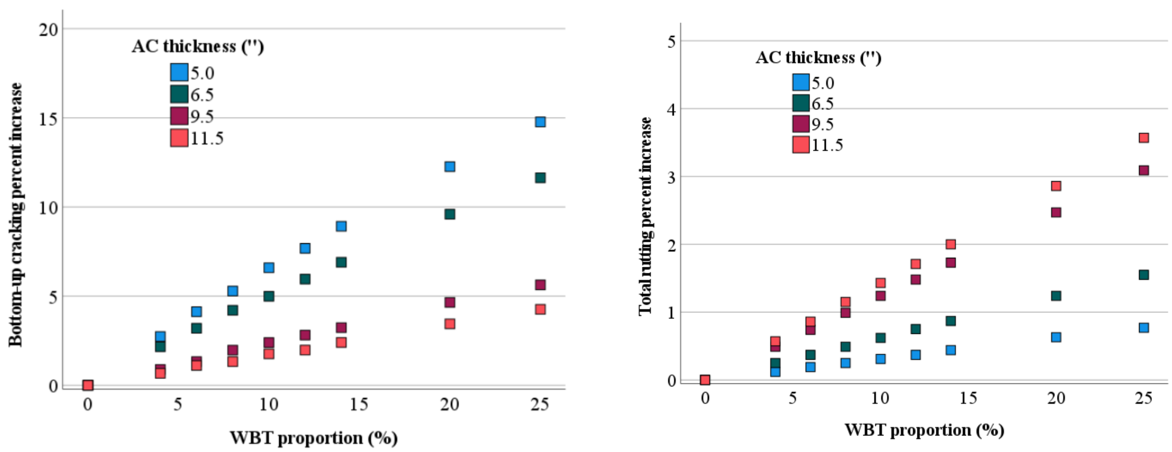

(a) Bottom-up cracking (b) Total rutting

Figure 4.25. Distress increase with the WBT proportion

As for another dimension, the scatters of distress percent increase with the AC thickness are presented in Figure 4.26.

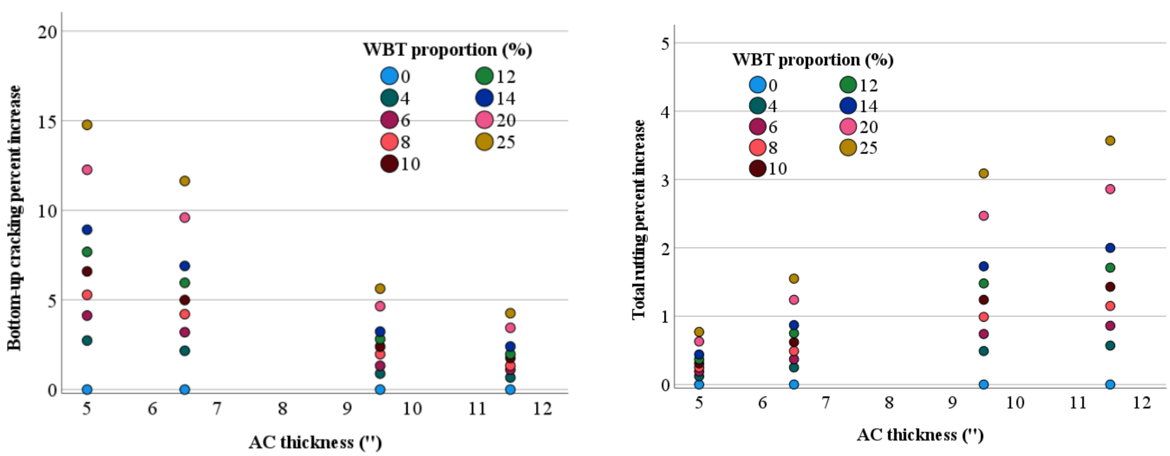

(a) Bottom-up cracking (b) Total rutting

Figure 4.26. Distress increase with the AC thickness

Figures 4.25 – 4.26 show that the flexible pavement's distress increase strongly correlates with the WBT proportion and the AC thickness. The Poly 2D surface fitting model, as shown in (4.23), should accurately fit the distress with these two independents. The two variables (x and y) are quadratically regressed to improve accuracy, and the relationship between x and y is considered with a coefficient of f.

$$z = z0 + ax + by + cx^2 + dy^2 + fxy \tag{4.23}$$

Using the Poly 2D surface fitting model, the multiple regression results of the bottom-up cracking distress, top-down cracking distress, AC rutting distress, and total rutting distress can be obtained, as shown in Figures 4.27 – 4.28.

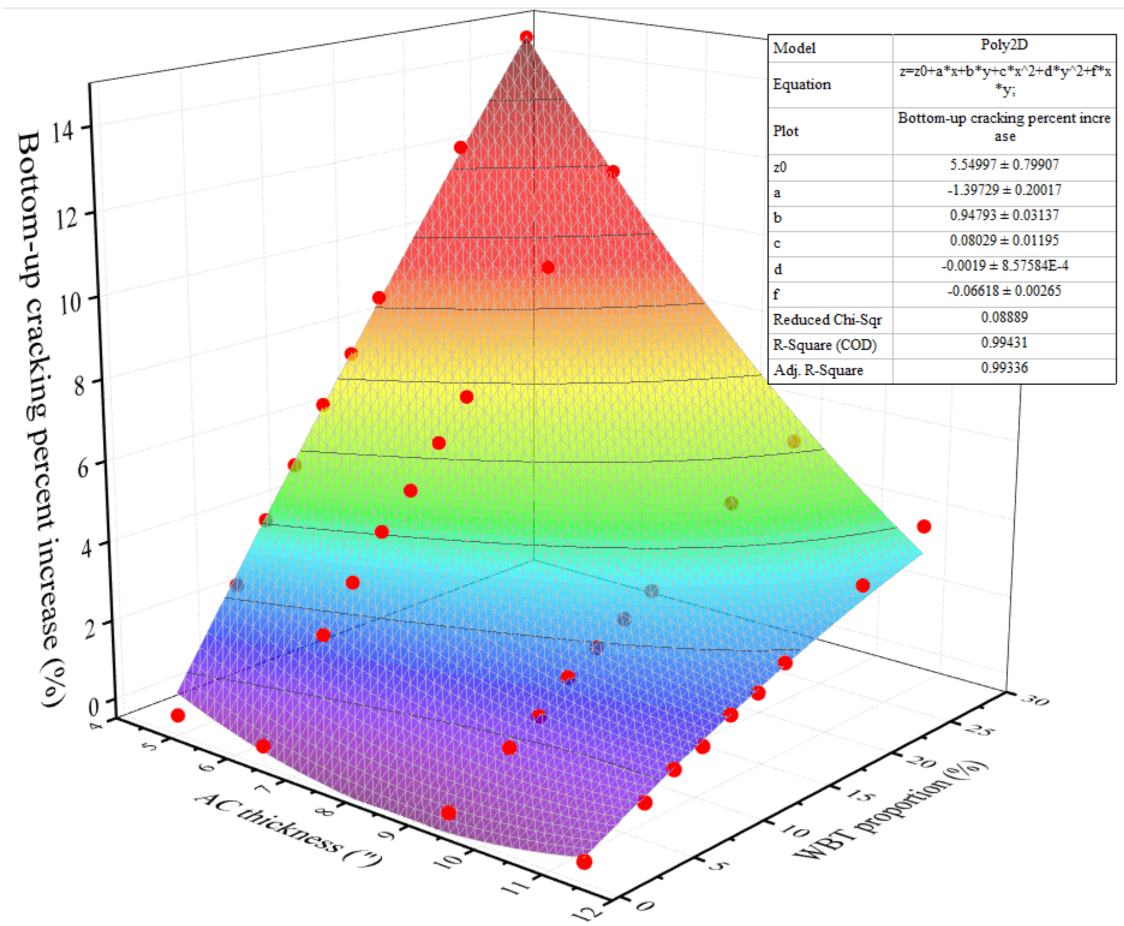

Figure 4.27. Multiple regression of the bottom-up cracking distress

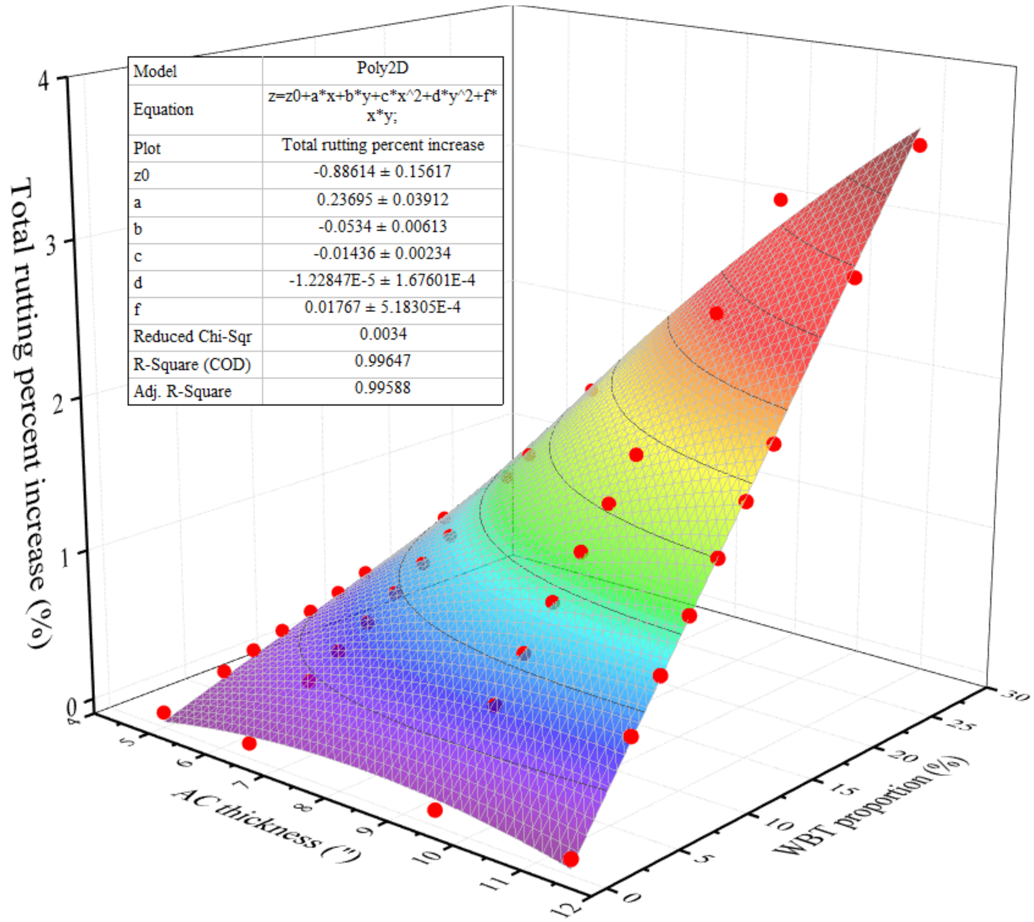

Figure 4.28. Multiple regression of total rutting distress

The multiple regression with the Poly 2D surface fitting model shows excellent accuracy. The functions' R^2 (Coefficient of determination) is 0.994 for bottom-up cracking and 0.996 for total rutting. Quadratic regression is better than linear regression for this data set. Since the WBT proportion impact is computed linearly, the final regression shows a very good R^2. It is worth mentioning that the quadratic regression would achieve peak values at specific points, and the trend will be reversed after the peak. In order to avoid these issues, for all the multiple regression functions above, the range of AC thickness should be within 5-12 inches, and the range of WBT proportion should be within 0-25%.

According to the multiple regression results in Figures 4.27 - 4.28, predictive equations for the bottom-up fatigue cracking and total rutting can be established, as noted in equations (4.24) and (4.25). With these equations, the impact of WBT loads on fatigue cracking and total rutting under WBT traffic proportions in the range of 0-25% and any AC thicknesses in 5"-12" can be calculated. It is worth noting that the quadratic regression would achieve peak values at specific points, and the trend would be opposite after the peak. Therefore, predictions outside the 5-12" AC thickness range or 0-25% WBT traffic proportion are unreliable.

Bottom-up fatigue cracking distress increase:

$$F_1 = 5.54997 - 1.39729T_{AC} + 0.94793P_{WBT} + 0.08029{T_{AC}}^2 - 0.0019{P_{WBT}}^2 - 0.06618T_{AC} \times P_{WBT} \quad (4.24)$$

Total rutting distress increase:

$$F_2 = -0.88614 + 0.23695T_{AC} - 0.0534P_{WBT} - 0.01436{T_{AC}}^2 + 0.0000123{P_{WBT}}^2 + 0.01767T_{AC} \times P_{WBT} \quad (4.25)$$

where:

F_1	:	Bottom-up fatigue cracking increase (%);
F_2	:	Total rutting increase (%);
T_{AC}	:	AC thickness (inch);
P_{WBT}	:	WBT load proportion (%).

4.7. Adjustment of flexible pavement design considering WBT loads

4.7.1. Based on Pavement ME - adjusted distress threshold

With the two multiple regression functions in section 4.6.2, the flexible pavement distress increases at any AC thickness between 5-12 inches and at any WBT proportion between 0-25% can be computed. Table 4.26 presents distress increase prediction results at AC thickness and WBT proportion combinations in the range of the regression equations developed.

Different colors are used to represent different impact extents. Green represents impact below 2.5%; yellow represents impact above 2.5% but below 5.0%; red represents impact above 5%. As for green scenarios, no action is suggested to be taken, as the WBT loads' impact is insignificant. Yellow scenarios mean the revised design method is recommended. Red scenarios mean the revised design process is highly recommended to involve the significant WBT impact on pavement.

Table 4.62. Prediction of flexible pavement distress percent increase

Distress type	Variables		Distress percent increase (%) AC thickness (inch) 5	6	7	8	9	10	11	12
Bottom-up cracking	WBT proportion (%)	5	3.61	2.76	2.08	1.56	1.19	0.99	0.95	1.07
		10	6.55	5.38	4.36	3.51	2.81	2.28	1.90	1.69
		15	9.40	7.89	6.55	5.36	4.34	3.47	2.77	2.22
		20	12.15	10.31	8.64	7.12	5.76	4.57	3.53	2.66
		25	14.81	12.64	10.63	8.78	7.10	5.57	4.21	3.00
Total rutting		5	0.11	0.28	0.42	0.53	0.61	0.66	0.69	0.68
		10	0.29	0.55	0.77	0.97	1.14	1.28	1.39	1.48
		15	0.47	0.81	1.13	1.41	1.67	1.90	2.10	2.27
		20	0.64	1.08	1.48	1.85	2.20	2.52	2.81	3.07
		25	0.82	1.34	1.83	2.30	2.73	3.14	3.51	3.86

* Green: Low impact, distress percent increase ≤ 2.5%; **no action recommended**.

Yellow: Moderate impact, 2.5% ≤ distress percent increase ≤ 5%; revised design **recommended**.

Red: High impact, 5% ≤ distress percent increase; revised design **highly recommended**.

The research team then modified the distress threshold in Pavement ME to include the impact of WBT loads on the pavement design. The general process is presented in Figure 4.29. The method to compute the adjusted distress threshold is shown in equation (4.26).

Figure 4.29. The process of modifying the design considering WBT impact

Adjusted distress threshold = Initial threshold /(1+Increase in percentage) (4.26)

The adjusted flexible pavement distress thresholds are shown in Table 4.63.

Table 4.63. Adjusted flexible pavement distress threshold

Distress type	Variables		Adjusted design threshold (% or inch) AC thickness (inch)							
			5	**6**	**7**	**8**	**9**	**10**	**11**	**12**
Bottom-up cracking (%) (Standard: 20%)	WBT proportion (%)	5	19.30	19.46	19.59	19.69	19.76	19.80	19.81	19.79
		10	18.77	18.98	19.16	19.32	19.45	19.55	19.63	19.67
		15	18.28	18.54	18.77	18.98	19.17	19.33	19.46	19.57
		20	17.83	18.13	18.41	18.67	18.91	19.13	19.32	19.48
		25	17.42	17.76	18.08	18.38	18.67	18.94	19.19	19.42
Total rutting (inch) (Standard: 0.5”)		5	0.4994	0.4986	0.4979	0.4974	0.4970	0.4967	0.4966	0.4966
		10	0.4986	0.4973	0.4962	0.4952	0.4944	0.4937	0.4931	0.4927
		15	0.4977	0.4960	0.4944	0.4930	0.4918	0.4907	0.4897	0.4889
		20	0.4968	0.4947	0.4927	0.4909	0.4892	0.4877	0.4863	0.4851
		25	0.4959	0.4934	0.4910	0.4888	0.4867	0.4848	0.4830	0.4814

* Green: Low impact, distress percent increase ≤ 2.5%; **no action recommended**.

Yellow: Moderate impact, 2.5% ≤ distress percent increase ≤ 5%; revised design **recommended**.

Red: High impact, 5% ≤ distress percent increase; revised design **highly recommended**.

With Table 4.63, the impact of WBT load on flexible pavement distress can be easily considered in the Pavement ME software by adjusting the distress threshold based on AC thickness and assumed proportion of WBT loads.

To demonstrate the WBT impact, the research team then calculated the specific WBT proportion that would lead to failure for Michigan calibration scenarios based on equations (4.24) - (4.25), shown in section 4.6.2. The results are shown in Tables 4.64 - 4.65.

Table 4.64. Calculated WBT proportion that leads to failure (Level 3)

NO.	WIM station	Traffic	Calculated WBT proportion for each distress (%)		
			Bottom-up cracking	**AC rutting**	**Total rutting**
1	US-41 (211459)	Low	0	>25	>25
2	US-2 (492029)	Low	0	>25	>25
3	I-75 (694049)	Low	0	0	0
4	US-131 (595249)	Medium	23	>25	>25
5	I-94 (776469)	Medium	0	>25	>25
6	I94 (117189)	Heavy	1	>25	>25
7	I69 (238869)	Heavy	>25	>25	>25

Table 4.65. Calculated WBT proportion that leads to failure (Level 1)

NO.	WIM station	Traffic	Calculated WBT proportion for each distress (%)		
			Bottom-up cracking	AC rutting	Total rutting
1	US-41 (211459)	Low	0	>25	>25
2	US-2 (492029)	Low	0	>25	>25
3	I-75 (694049)	Low	0	0	0
4	US-131 (595249)	Medium	>25	>25	>25
5	I-94 (776469)	Medium	0	>25	>25
6	I94 (117189)	Heavy	>25	>25	>25
7	I69 (238869)	Heavy	>25	>25	>25

* : 0 means that the structure failed before considering the WBT load

4.7.2. Based on Pavement ME – adjusted CADT

Although adjusting distress thresholds could take the impact of WBT load on all pavement distresses into consideration, it still needs multiple steps which could not accommodate the design directly. In this section, the research team will try to involve WBT loads' impact on flexible ME design by adjusting a more specific parameter – commercial annual daily traffic (CADT) or AADTT (the input parameter in Pavement ME).

According to the results in section 4.7.1, the critical distress for flexible pavement is fatigue cracking when considering WBTs' impact, so the relative damage index for fatigue in Table 4.13 would be used to adjust the CADT (under tire pressure of 120psi and +20% contact pressure).

By multiplying the CADT value by the CADT adjustment factor (F_{CADT}) when conducting the ME flexible pavement design process, the extra damage caused by the WBT load would be involved. The first step is determining the CADT adjustment factor ($F_{CADT-100}$) when loads were 100% WBT loads. Since the impact of WBT loads on the damage index of different AC thicknesses is different, the $F_{CADT-100}$ is assumed to be a piecewise function with the following control points.

- The relative damage index in the 5" AC structure is 4.29, assuming $F_{CADT-100} = 4.29$ corresponds to CADT < 500;
- The relative damage index in the 6.5" AC structure is 3.44, assuming $F_{CADT-100} = 3.44$ corresponds to CADT = 1000;
- The relative damage index in the 9.5" AC structure is 2.08, assuming $F_{CADT-100} = 2.08$ corresponds to CADT = 5000;
- The relative damage index in the 11.5" AC structure is 1.79, assuming $F_{CADT-100} = 1.79$ corresponds to CADT ≥ 9000;

- Then, the linear interpolation method would be used to determine $F_{CADT-100}$ in the CADT range of 500 - 1000, 1000 - 5000, and 5000 - 9000.

The piecewise function for the CADT adjustment factor ($F_{CADT-100}$) when loads were 100% WBT loads are shown in Figure 4.30 and equation (4.27) below.

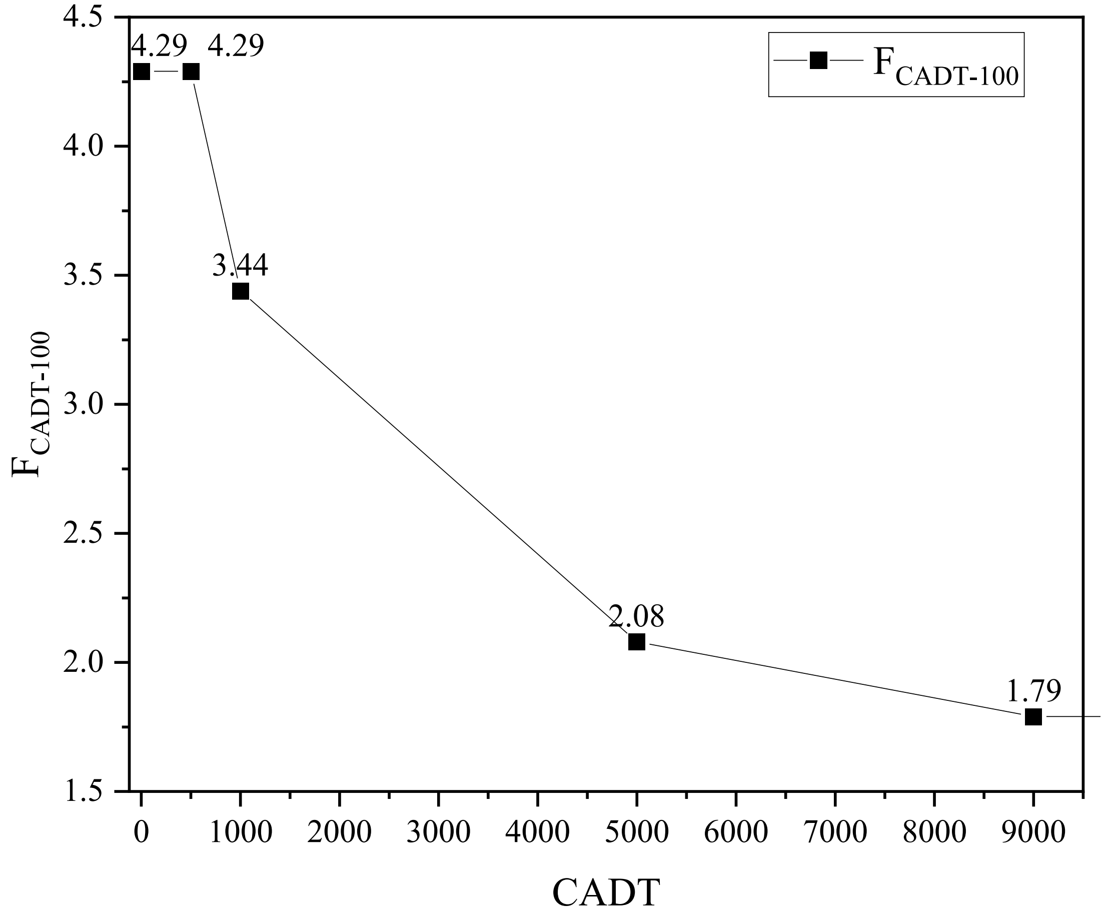

Figure 4.30. The adjustment factor for flexible pavement under different CADTs

$$F_{CADT-100} = \begin{cases} 4.29 & \text{when CADT} < 500 \\ -0.0017 \times CADT + 5.14 & \text{When } 500 \leq CADT < 1000 \\ -0.00034 \times CADT + 3.78 & \text{When } 1000 \leq CADT < 5000 \\ -0.0000725 \times CADT + 2.4425 & \text{When } 5000 \leq CADT < 9000 \\ 1.79 & \text{When } CADT \geq 9000 \end{cases} \quad (4.27)$$

Since the load type in Michigan is not 100% WBT according to field investigation in section 3, the second step is determining the CADT adjustment factor (F_{CADT-P}) with the WBT percentage of P. The relative damage index for fatigue is assumed as 1 under DT load so that the F_{CADT-P} could be calculated with the equation below.

$$F_{CADT\text{-}P} = F_{CADT\text{-}100} \times P/100 + 1\times(100\text{-}P)/100 \tag{4.28}$$

The CADT adjustment factor ($F_{CADT\text{-}P}$) with the WBT percentage of P can be computed using the equation (4.28). Below are the examples of $F_{CADT\text{-}P}$ with P in 5%, 10%, and 25%.

(1) When *P = 5%,* the $F_{CADT\text{-}5}$ is shown in equation (4.29).

$$F_{CADT\text{-}5} = \begin{cases} 1.1645 & \text{When CADT} < 500 \\ -0.000085\times CADT + 1.207 & \text{When } 500 \le \text{CADT} < 1000 \\ -0.000017\times CADT + 1.139 & \text{When } 1000 \le \text{CADT} < 5000 \\ -0.000003625\times CADT + 1.072125 & \text{When } 5000 \le \text{CADT} < 9000 \\ 1.0395 & \text{When CADT} \ge 9000 \end{cases} \tag{4.29}$$

(2) When *P = 10%,* the $F_{CADT\text{-}10}$ is shown in equation (4.30).

$$F_{CADT\text{-}10} = \begin{cases} 1.329 & \text{When CADT} < 500 \\ -0.00017\times CADT + 1.414 & \text{When } 500 \le \text{CADT} < 1000 \\ -0.000034\times CADT + 1.278 & \text{When } 1000 \le \text{CADT} < 5000 \\ -0.00000725\times CADT + 1.14425 & \text{When } 5000 \le \text{CADT} < 9000 \\ 1.079 & \text{When CADT} \ge 9000 \end{cases} \tag{4.30}$$

(3) When *P = 25%,* the $F_{CADT\text{-}25}$ is shown in equation (4.31).

$$F_{CADT\text{-}25} = \begin{cases} 1.8225 & \text{When CADT} < 500 \\ -0.000425\times CADT + 2.035 & \text{When } 500 \le \text{CADT} < 1000 \\ -0.000085\times CADT + 1.695 & \text{When } 1000 \le \text{CADT} < 5000 \\ -0.000018125\times CADT + 1.360625 & \text{When } 5000 \le \text{CADT} < 9000 \\ 1.1975 & \text{When CADT} \ge 9000 \end{cases} \tag{4.31}$$

4.7.3. Based on AASHTO 93 – adjusted structure number (SN)

The AASHTO 93 and the ME pavement design methods have different design processes and thresholds. Structural number (SN) is the critical parameter used in AASHTO 93 for flexible pavement design to describe the thickness and stiffness required to withstand the traffic and reliability level for support conditions on a given site. The design SN is related to traffic, subgrade resilient modulus, change in serviceability, reliability, etc., as presented in equation (4.32). The calculated SN is related to the properties of the pavement structure to be used. The design SN must $\geqslant$ calculated SN.

$$\log(W_{18}) = Z_R \bullet S_0 + 9.36 \bullet \log(SN+1) - 0.20 + \frac{\log \frac{\Delta PSI}{4.2-1.5}}{0.4 + \frac{1094}{(SN+1)^{5.19}}} + 2.32 \bullet \log(M_R) - 8.07 \tag{4.32}$$

where:

W_{18}	=	Equivalent single axle loads (ESALs);
Z_R	=	Z-value for the 95% (MDOT) confidence level one-tailed test;
S_0	=	Standard deviation, typically 0.49 for MDOT;
ΔPSI	=	Change in present serviceability index, typically 2.0 for MDOT;
M_R	=	Resilient modulus of subgrade, psi, typically 3000-5000 for MDOT.

PSI is different from the above pavement distresses (Cracking, rutting, IRI) analyzed for ME design; however, PSI has some relationship with the cracking and smoothness. The research team would use the most significantly impacted distress, *fatigue cracking,* as the basis to adjust the AASHTO 93 design method; the WBT impact on pavement serviceability (AASHTO 93 process) is assumed to be the same as the impact on fatigue cracking (ME process).

As the WBT loads lead to more distress, the pavement's ΔPSI should be lower than the default design value for MDOT (which = 4.5-2.5 = 2). Through this process, the designed pavement structure would be stronger to offset the impact of WBT loads. Artificially increasing the terminal PSI is a feasible way to lower the ΔPSI and account for the distress and reduction in serviceability that WBTs may contribute to the pavement over its design life. For example, if the WBT loads caused 10% more distress, the ΔPSI should be 10% less, meaning the terminal PSI would be 2.7 (or 2.5+2*10%). The result of adjusted terminal PSI considering WBT impact is presented in Table 4.66.

The relationship between fatigue cracking percent increase and the terminal PSI is shown in equation (4.33).

$$Terminal_{PSI} = 2.5 + 0.02 \times P_{cracking} \tag{4.33}$$

where:

$Terminal_{PSI}$	=	Adjusted terminal PSI considering WBT impact;
$P_{cracking}$	=	Percent change in fatigue cracking caused by WBT loads, %;

Table 4.66. Adjusted terminal PSI considering WBT impact (2.5 originally)

AC thickness (inch)	Adjusted terminal PSI considering WBT impact								
	0%	4%	6%	8%	10%	12%	14%	20%	25%
5	2.50	2.55	2.58	2.61	**2.63**	2.65	2.68	2.75	**2.80**
6.5	2.50	2.54	2.56	2.58	**2.60**	2.62	2.64	2.69	**2.73**
9.5	2.50	2.52	2.53	2.54	**2.55**	2.56	2.56	2.59	**2.61**
11.5	2.50	2.51	2.52	2.53	**2.54**	2.54	2.55	2.57	**2.59**

The process of adjusting AASHTO 93 flexible pavement design considering WBT impact would be as follows:

(1) Calculate the design SN (structure number) of flexibility as usual;

(2) Using the design SN from process (1) to design the pavement structure, get the AC thickness;

(3) Use the AC thickness from process (2) and Table 4.66 with linear interpolation to get the proper adjusted terminal PSI and reconduct steps (1) and (2);

The research team also conducted a sensitivity check of different terminal PSI numbers on SN, with the input parameters shown in Figure 4.31. Sensitivity analysis results are shown in Figures 4.32 - 4.33.

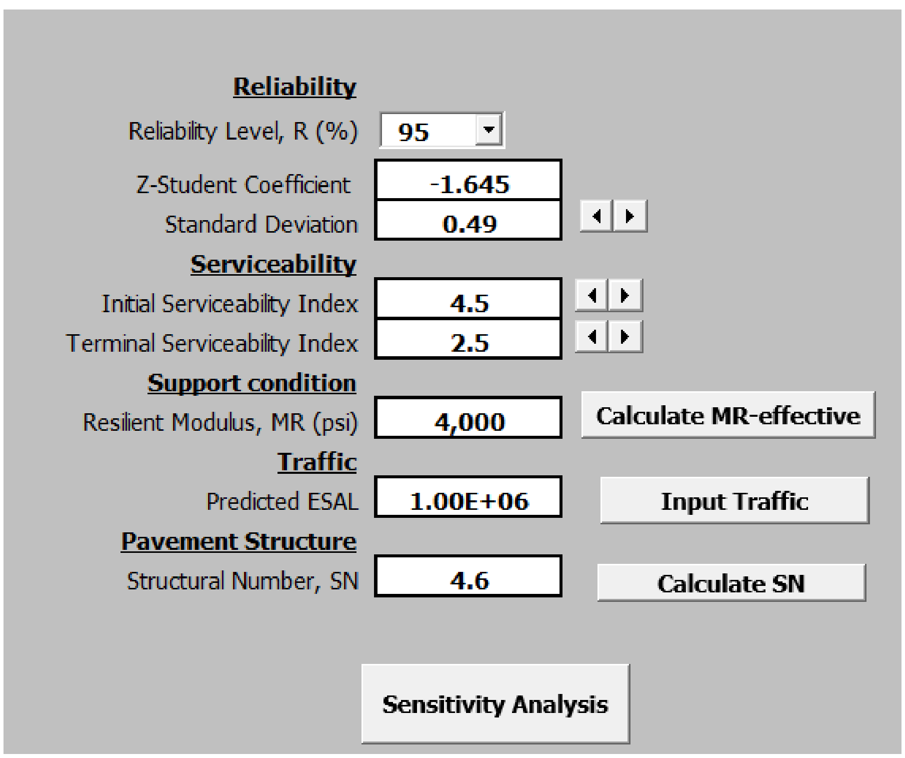

Figure 4.31. The AASHTO 93 analysis process for flexible pavement

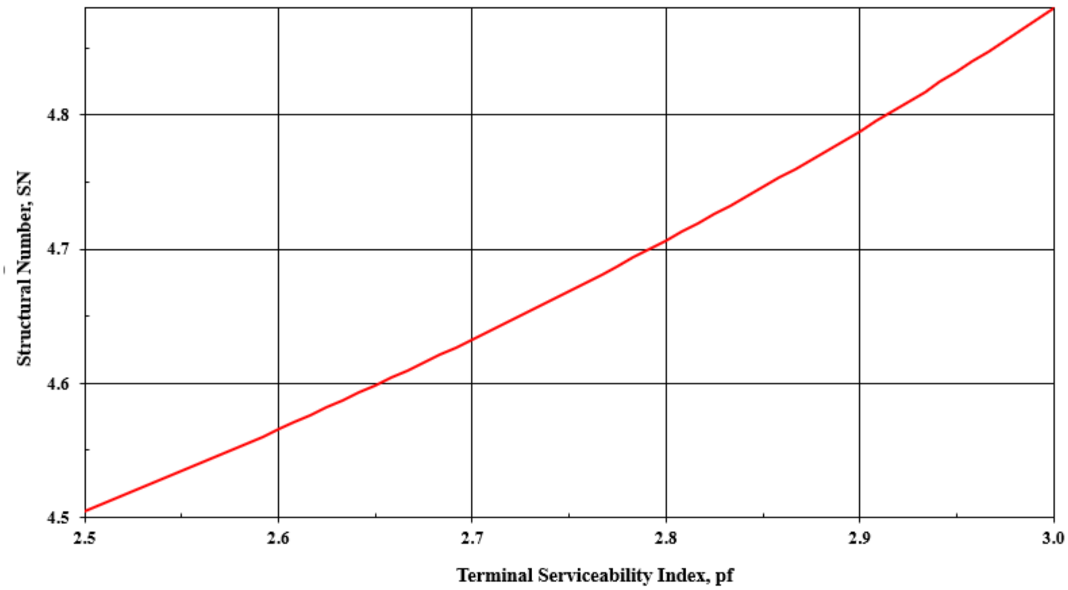

Figure 4.32. Sensitivity analysis of terminal PSI (ESALs: 1E6)

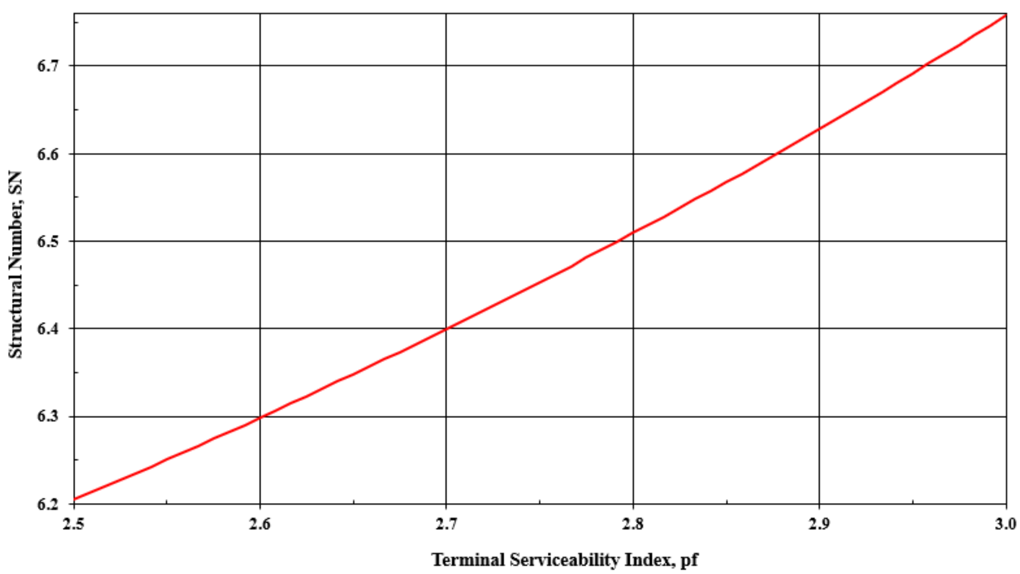

Figure 4.33. Sensitivity analysis of terminal PSI (ESALs: 1E7)

4.7.4. Based on AASHTO 93 – adjusted ESAL

In this section, the similar adjustment process in section 4.7.2 will be adopted to adjust traffic parameters in the AASHTO 93 pavement design process. Unlike the CADT (or AADTT) parameter used in the ME design, ESAL is the traffic parameter input in the AASHTO 93 design. Since ESAL is computed with load axle number and weight distribution, it does not have a strict relationship with CADT. In this research, the team used the Michigan freeway average vehicle class distribution, freeway axle load spectrum (average of 12 month) [32], and other traffic parameters shown in Table 4.67 to convert the CADT values used in section 4.7.2 to the calculate the ESAL. The obtained ESAL used were round to integer for calculation simplify, as shown in Table 4.68.

Table 4.67. Traffic parameters used for ESAL calculation

Design life (year)	Traffic growth rate (%)	Lane factor under different CADT value			
		500	1000	5000	9000
20	0.5	0.92 (2 lanes)	0.86 (2 lanes)	0.60 (3 lanes)	0.55 (3 lanes)

Table 4.68. CADT to ESAL transformation for flexible pavement

CADT	**Estimated ESAL**
500	1.2×10^6
1000	2.2×10^6
5000	7.5×10^6
9000	12.5×10^6

Similar to the adjustment of CADT in section 4.7.2, the first step is determining the ESAL adjustment factor ($F_{ESAL-100}$) if all loads were WBT loads with the following control points.

- The relative damage index in the 5" AC structure is 4.29, assuming $F_{ESAL-100} = 4.29$ corresponds to ESAL < 1.2×10^6;
- the relative damage index in the 6.5" AC structure is 3.44, assuming $F_{ESAL-100} = 3.44$ corresponds to ESAL = 2.2×10^6;
- the relative damage index in the 9.5" AC structure is 2.08, assuming $F_{ESAL-100} = 2.08$ corresponds to ESAL = 7.5×10^6;
- The relative damage index in the 11.5" AC structure is 1.79, assuming $F_{ESAL-100} = 1.79$ corresponds to ESAL ≥ 12.5×10^6;
- Using linear interpolation method to determine $F_{ESAL-100}$ in the ESAL range of 1.2×10^6-2.2×10^6, 2.2×10^6- 7.5×10^6, and 7.5×10^6- 12.5×10^6.

The piecewise function for the ESAL adjustment factor ($F_{ESAL-100}$) when loads were 100% WBT loads is shown in Figure 4.34 and equation (4.34) below.

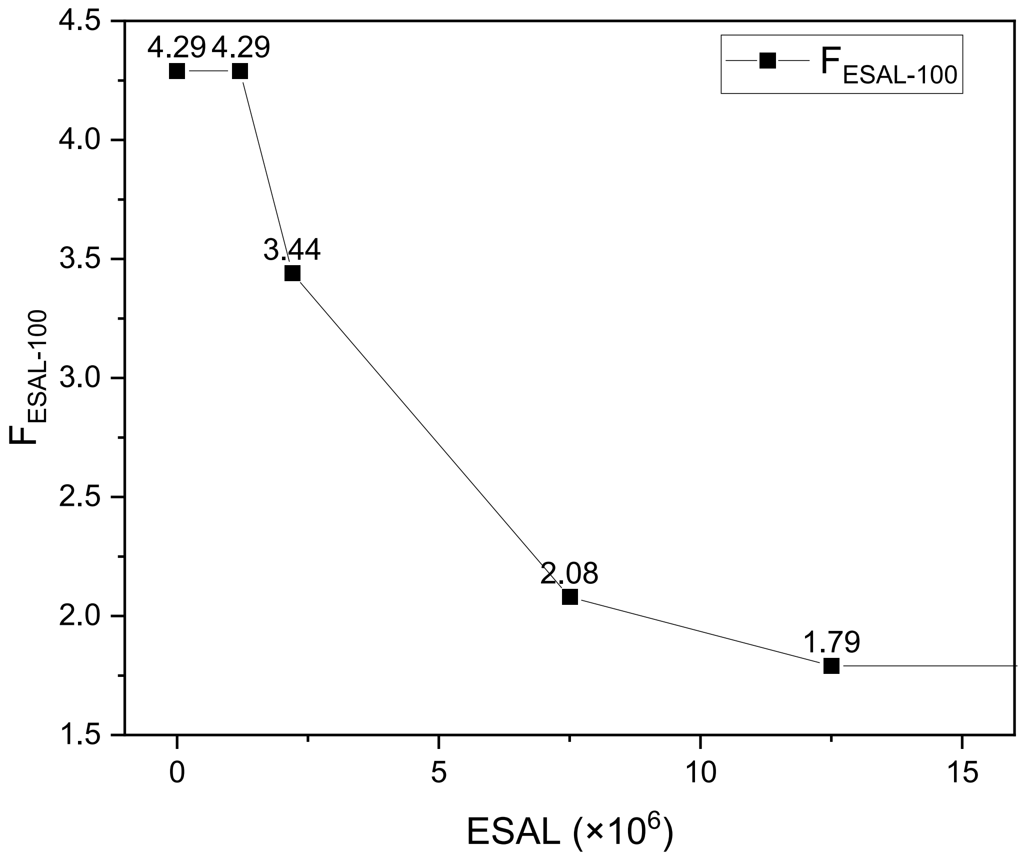

Figure 4.34. Adjust factor for flexible pavement under different ESALs

$$F_{ESAL-100} = \begin{cases} 4.29 & \text{when ESAL} < 1.2\times10^6 \\ -0.850\times10^{-6}\times ESAL + 5.310 & \text{When } 1.2\times10^6 \le ESAL < 2.2\times10^6 \\ -0.257\times10^{-6}\times ESAL + 4.005 & \text{When } 2.2\times10^6 \le ESAL < 7.5\times10^6 \\ -0.058\times10^{-6}\times ESAL + 2.515 & \text{When } 7.5\times10^6 \le ESAL < 12.5\times10^6 \\ 1.79 & \text{When ESAL} \ge 12.5\times10^6 \end{cases} \quad (4.34)$$

The second step is determining the CADT adjustment factor (F_{CADT-P}) with the WBT percentage of P. As for DT load, the relative damage index for fatigue is assumed as 1, so the F_{ESAL-P} could be calculated with the equation below.

$$F_{ESAL-P} = F_{ESAL-100} \times P/100 + 1\times(100-P)/100 \quad (4.35)$$

The ESAL adjustment factor (F_{ESAL-P}) with the WBT percentage of P can be computed using the equation (4.35). Below are the examples of F_{ESAL-P} with P in 5%, 10%, and 25%.

(1) When *P = 5%,* the F_{ESAL-5} is shown in equation (4.36).

$$F_{ESAL\text{-}5} = \begin{cases} 1.1645 & \text{When ESAL} < 1.2\times10^6 \\ -0.0425\times10^{-6}\times ESAL + 1.2155 & \text{When } 1.2\times10^6 \le \text{ESAL} < 2.2\times10^6 \\ -0.01285\times10^{-6}\times ESAL + 1.15025 & \text{When } 2.2\times10^6 \le \text{ESAL} < 7.5\times10^6 \\ -0.0029\times10^{-6}\times ESAL + 1.07575 & \text{When } 7.5\times10^6 \le \text{ESAL} < 12.5\times10^6 \\ 1.0395 & \text{When ESAL} \ge 12.5\times10^6 \end{cases} \tag{4.36}$$

(2) When $P = 10\%$, the $F_{ESAL\text{-}10}$ is shown in equation (4.37).

$$F_{ESAL\text{-}10} = \begin{cases} 1.329 & \text{When ESAL} < 1.2\times10^6 \\ -0.085\times10^{-6}\times ESAL + 1.431 & \text{When } 1.2\times10^6 \le \text{ESAL} < 2.2\times10^6 \\ -0.0257\times10^{-6}\times ESAL + 1.3005 & \text{When } 2.2\times10^6 \le \text{ESAL} < 7.5\times10^6 \\ -0.0058\times10^{-6}\times ESAL + 1.1515 & \text{When } 7.5\times10^6 \le \text{ESAL} < 12.5\times10^6 \\ 1.079 & \text{When ESAL} \ge 12.5\times10^6 \end{cases} \tag{4.37}$$

(3) When $P = 25\%$, the $F_{ESAL\text{-}25}$ is shown in equation (4.38).

$$F_{ESAL\text{-}25} = \begin{cases} 1.8225 & \text{When ESAL} < 1.2\times10^6 \\ -0.2125\times10^{-6}\times ESAL + 2.0775 & \text{When } 1.2\times10^6 \le \text{ESAL} < 2.2\times10^6 \\ -0.06425\times10^{-6}\times ESAL + 1.75125 & \text{When } 2.2\times10^6 \le \text{ESAL} < 7.5\times10^6 \\ -0.0145\times10^{-6}\times ESAL + 1.37875 & \text{When } 7.5\times10^6 \le \text{ESAL} < 12.5\times10^6 \\ 1.1975 & \text{When ESAL} \ge 12.5\times10^6 \end{cases} \tag{4.38}$$

4.8. Chapter summary

Based on the above flexible pavement distress analysis results, the research team summarized the WBT loads' impact on the distress of different AC thickness structures under tire pressures of 120 psi. According to field WBT load survey results in section 3, Michigan's current WBT load proportion was found to be 7.32% from a limited assessment at MSP weigh stations. Therefore, a recommended level for a somewhat conservative design would be approximately 10% WBTs. The distresses' percent increases under 10% WBT loads were plotted, corresponding with Michigan's current WBT load proportion, and the results are presented in Figure 4.35.

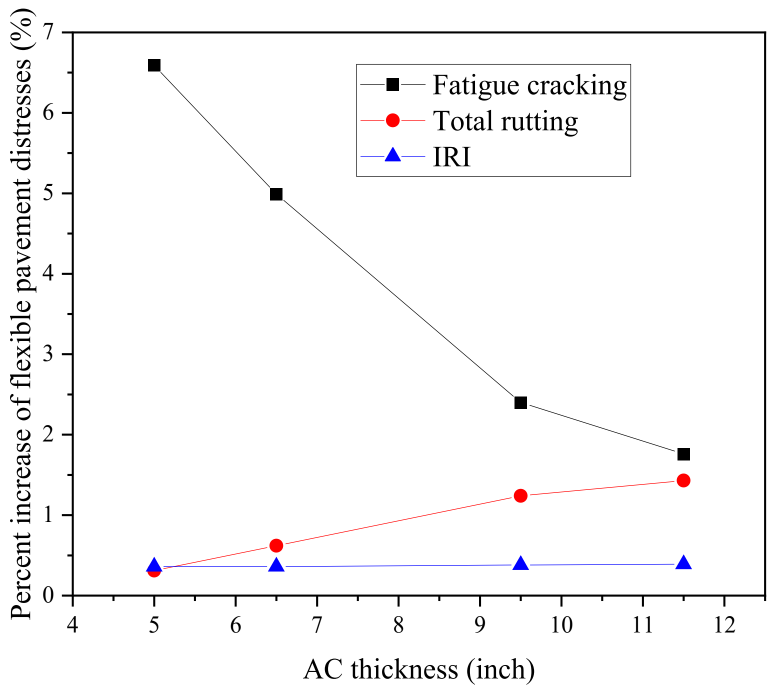

Figure 4.35. Distress increase under 10% WBT load for different AC thickness structures

Considering WBT loads' increase in the future, the research team compared the increase of distress under 25% WBT loads, as shown in Figure 4.36.

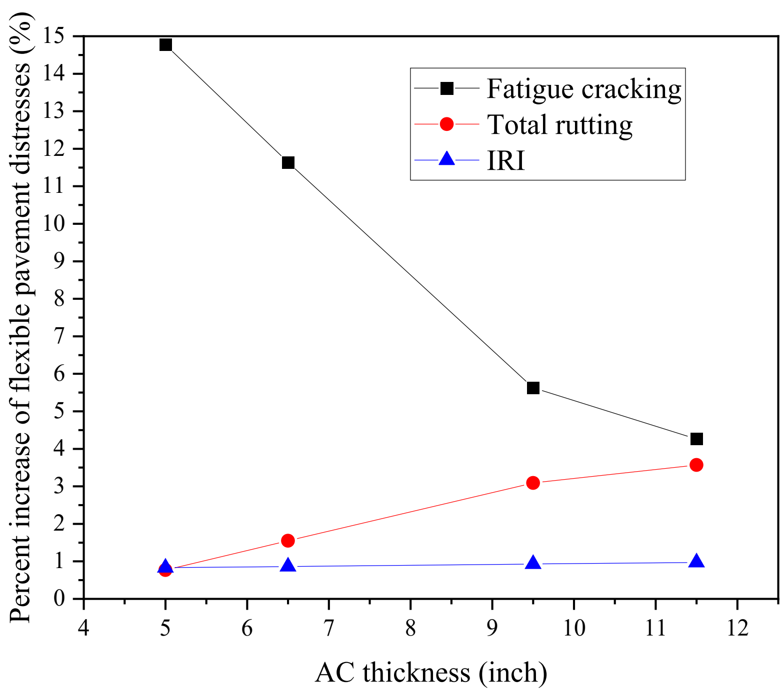

Figure 4.36. Distress increase under 25% WBT load for different AC thickness structures

All in all, flexible pavement fatigue cracking is more affected by the use of WBTs than are rutting and IRI. As for the different AC thickness structures, the thinner AC structures are more impacted by WBT loads in fatigue cracking distress. However, the thicker AC structure in this study still experiences higher relative rutting increases due to thicker AC layer thickness. The WBT loads' impact on IRI does not significantly relate to the AC thickness.

Under the roughly 10% WBT load proportion as suggested from several Michigan truckline locations from this study, all flexible pavement relative distress increases are relatively minor, although fatigue cracking was found to be a larger issue from the impact of WBT usage in comparison with rutting for AC thickness structures. If the WBT load proportion in Michigan were to increase to 25% in the future, this impact would likely be more significant, with bottom-up fatigue cracking impacted the most.

5. CHAPTER 5: QUANTIFICATION OF WBT IMPACT ON RIGID PAVEMENT (JPCP) AND DESIGN IMPROVEMENT

5.1. Preparation for rigid pavement distress analysis

In an effort to mimic the approach taken to assess WBT impacts on flexible pavement design using Pavement ME principles, the research team adopted the Illislab software, which is also used to train artificial neural networks for the stress prediction algorithm in Pavement ME software, to obtain the critical response under dual tire (DT) and wide base tire (WBT) loads of rigid pavement. Since CRCP pavements are not standard for MDOT, these performance criteria will not be analyzed in this project. As for JPCP pavement, transverse cracking (bottom-up; top-down) and mean joint faulting are the primary distresses considered in the design. The critical load and response for each JPCP distress are presented in Figure 5.1.

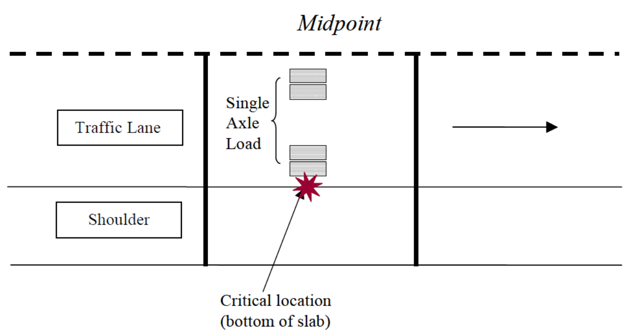

(a) For JPCP bottom-up transverse cracking

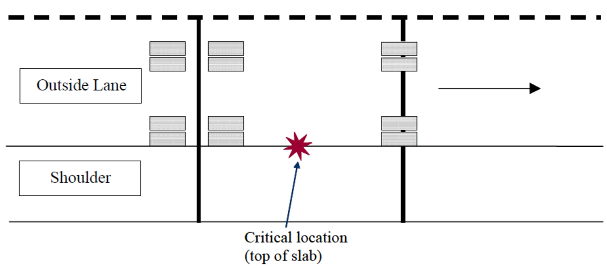

(b) For JPCP top-down transverse cracking

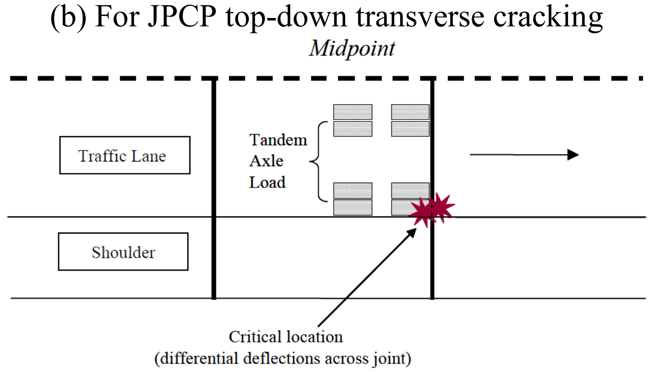

(c) For JPCP joint faulting

Figure 5.1. Critical load and response for each JPCP distress [33]

Based on Figure 5.1, the load location is vital in identifying the distress level. The fixed input parameters for JPCP distress analysis used in Illislab software are presented in Table 5.1. The variables used in Illislab are shown in Table 5.2. The LTE-x value is from tie bars in longitudinal joints, which is assumed to be constant at 50%, while the LTE-y value is due to load transfer from dowel bars at the transverse joints. LTE-y is set as 70% for cracking distress to simulate undesirable working conditions, but mid-slab stresses are not sensitive to this input parameter. As for the faulting distress analysis, LTE-y is set as 50%, 70 %, and 90% since faulting is extremely sensitive to transverse load transfer capacity. The ΔT in Table 5.2 indicates the temperature gradient which would cause slab curling and impact stress development. The ΔT is positive for bottom-up cracking and negative for top-down cracking.

Table 5.1. Fixed parameters used in Illislab

Parameter	Value
Mesh dimension (inch)	3
Number of slabs	3×3
LTE-x (%) *	50
Dimension of the slab (')	12×14
Subgrade reaction (k-value)	Winkler (150psi)
PCC thickness (inch)	10
PCC Elastic modulus (psi)	4,200,000
PCC Poisson's ration	0.20
PCC unit weight (lbs/ft^3)	145
Single axle weight (lbs)	18,000
Coefficient of thermal expansion	4.4×10^{-6}

* LTE—load transfer efficiency

Table 5.2. Variables used in Illislab

JPCP distress	ΔT (°F)	Tire pressure (psi)	Distance from shoulder joint	LTE-y (%)
Bottom-up cracking	0; +10; +20	80; 100; 120	18”; 10”; 0”	70
Top-down cracking	0; -10; -20	80; 100; 120	18”; 10”; 0”	70
Faulting	0	80; 100; 120	18”; 10”; 0”	50; 70; 90

5.2. Pavement ME analysis for JPCP structures

5.2.1. Pavement ME input parameters

This chapter will contain the Pavement ME analysis (version 2.6.1.0) for JPCPs in seven different locations across Michigan. The research team selected seven WIM stations adopted in flexible pavement analysis to assure a broad representation of typical sites in the MDOT trunkline network. The locations of the WIM stations are shown in Figure 5.2.

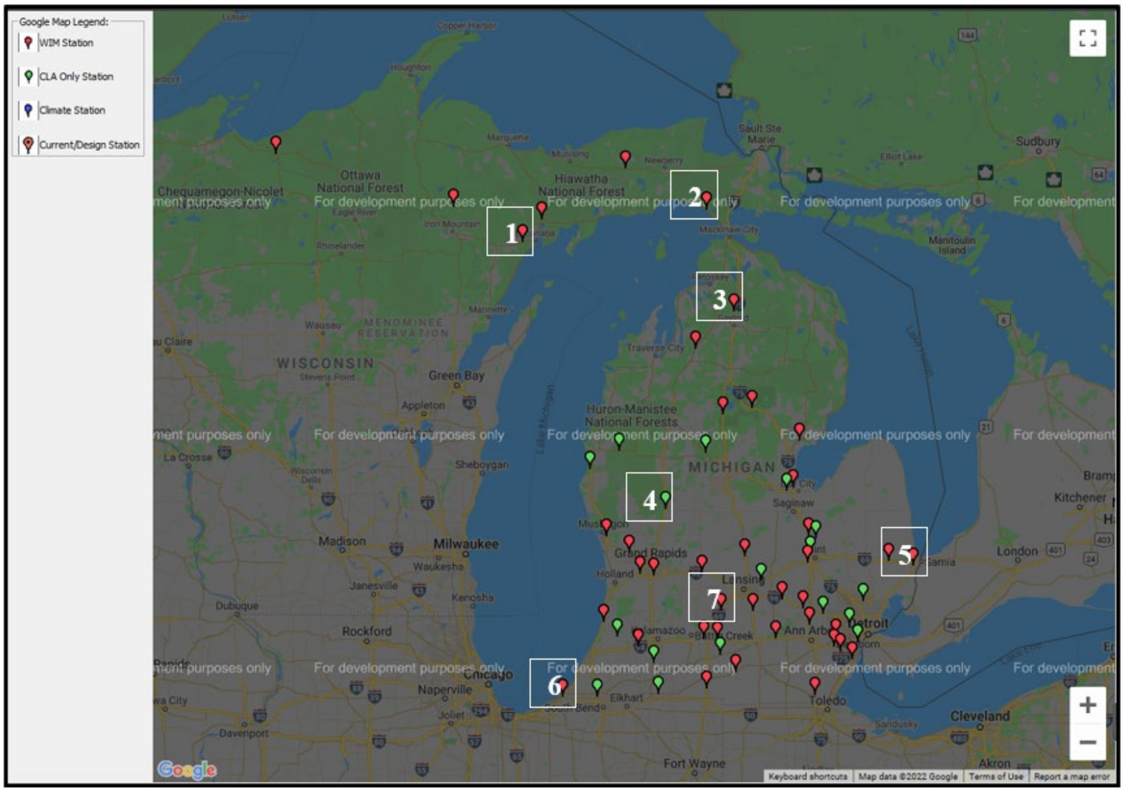

Figure 5.2. Location of 7 WIM stations

The number of lanes and CADT information in 2019 (pre-pandemic) for each area were investigated, as shown in Table 5.3. The parameters used for JPCP structures in Pavement ME are presented in Table 5.4. Prep ME software was used to obtain each WIM station's traffic and load distribution data, and combined with the above CADT information, the traffic input files for the Pavement ME software were formed. The climate input files were selected at or near each WIM station. The climate stations' numbers are presented in Table 5.3, and their specific locations are shown in Figure 5.3.

Table 5.3. Pavement section information

WIM station	Lanes in one direction	Two-way CADT in 2019	Climate number
US-41 (211459)	1	589	94893
US-2 (492029)	1	496	14841
I-75 (694049)	2	1330	04854
US-131 (595249)	2	1965	94860
I-94 (776469)	2	3230	14822
I94 (117189)	3	12088	94871
I69 (238869)	2	6203	14836

Table 5.4. JPCP parameters used in Pavement ME

Category	Parameter	Value
JPCP design properties	PCC surface shortwave absorptivity	0.85
	Doweled joints (inch)	Spacing 12; Diameter 1~1.5
	Fairly erodible	Fairly erodible (4)
	PCC-base contact friction	Full friction with friction loss at (60) months
	PCC joint spacing (')	12~16
	Permanent curl/warp effective temperature difference (°F)	-10
	Sealant type	Other
	Tired shoulders	Tied with long term load transfer efficiency of 50
	Widened slab	Not widened
PCC properties	Poisson's ratio	0.2
	Thickness (inch)	Minimal to pass the criteria (6~13)
	Unit weight (pcf)	145
	PCC coefficient of thermal expansion (in/in/°F) × 10^{-6}	4.4
	PCC heat capacity (BTU/lb-°F)	0.28
	PCC thermal conductivity (BTU/(h · ft · °F))	1.25
	28-day compressive strength (psi)	5600
Base	Gradation	Open graded; Dense graded
	Resilient modulus (psi)	33000
	Thickness (inch)	6
Subbase	Gradation	A-1-b (Sand subbase)
	Resilient modulus (psi)	20000
	Thickness (inch)	10
Subgrade	Gradation	A-2-7
	Modulus (psi)	5000

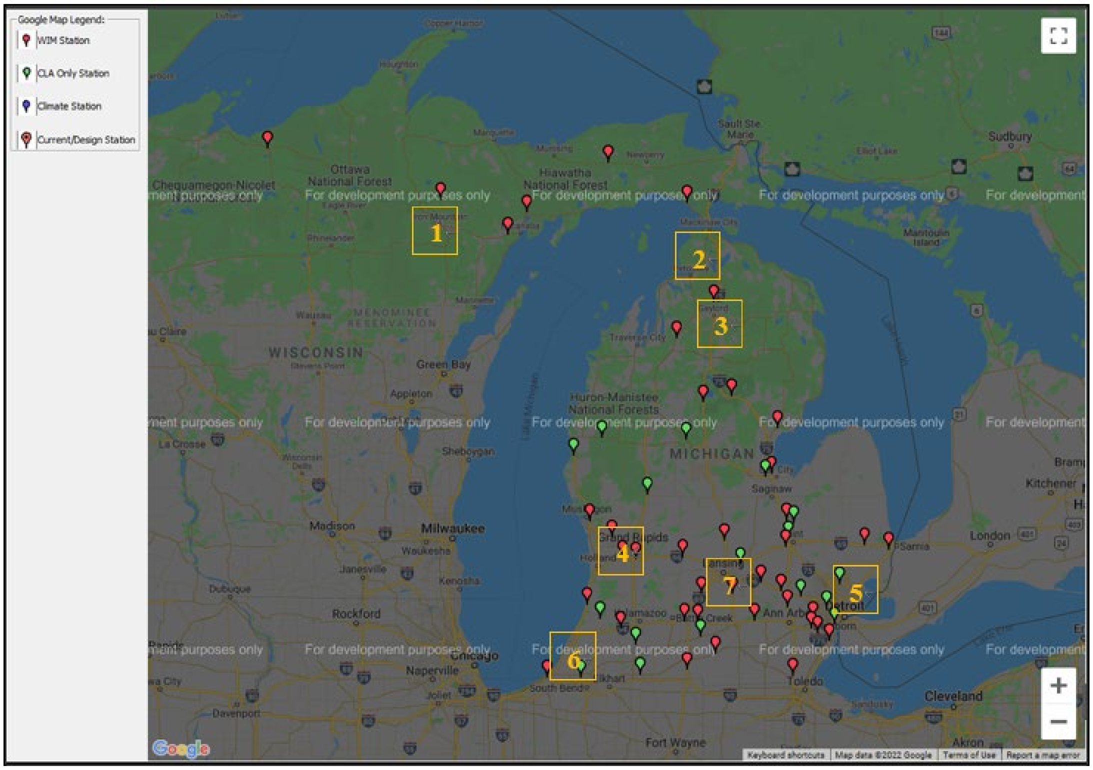

Figure 5.3. Location of 7 climate stations

5.2.2. Pavement ME analysis results

The research team conducted the Pavement ME analysis (version 2.6.1.0) with the previously noted traffic, climate, and material information. The pavement distress calibration was set in global calibration, as MDOT calibration was not finalized at the time of the analysis. Open-graded and dense-graded bases were analyzed, and the results are presented in Tables 5.5 (Open-graded base) and 5.6 (Dense-graded base), with details shown in Appendix E.

Table 5.5. JPCP Pavement ME analysis result (Open-graded base)

<table>
<tr><th rowspan="2">NO.</th><th rowspan="2">WIM station</th><th rowspan="2">Slab thickness (inch)</th><th rowspan="2">Dowel Diameter (inch)</th><th rowspan="2">Joint spacing (inch)</th><th colspan="3">Distress value</th></tr>
<tr><th>Transverse cracking (%)</th><th>Mean faulting (inch)</th><th>IRI</th></tr>
<tr><td colspan="5">Threshold</td><td>15</td><td>0.125</td><td>172</td></tr>
<tr><td rowspan="3">1</td><td rowspan="3">US-41 (211459)</td><td>6</td><td>1</td><td>12</td><td>33.96</td><td>0.04</td><td>166.47</td></tr>
<tr><td>6.5</td><td>1</td><td>12</td><td>12.83</td><td>0.04</td><td>150.30</td></tr>
<tr><td>7</td><td>1</td><td>12</td><td>6.13</td><td>0.05</td><td>148.09</td></tr>
<tr><td rowspan="3">2</td><td rowspan="3">US-2 (492029)</td><td>6</td><td>1</td><td>12</td><td>8.71</td><td>0.05</td><td>143.24</td></tr>
<tr><td>6.5</td><td>1</td><td>12</td><td>4.44</td><td>0.05</td><td>143.24</td></tr>
<tr><td>7</td><td>1</td><td>12</td><td>2.79</td><td>0.05</td><td>143.85</td></tr>
<tr><td rowspan="3">3</td><td rowspan="3">I-75 (694049)</td><td>7.5</td><td>1</td><td>12</td><td>1.23</td><td>0.10</td><td>179.72</td></tr>
<tr><td>8</td><td>1.25</td><td>12</td><td>1.23</td><td>0.05</td><td>143.59</td></tr>
<tr><td>8.5</td><td>1.25</td><td>12</td><td>1.23</td><td>0.05</td><td>142.25</td></tr>
<tr><td rowspan="3">4</td><td rowspan="3">US-131 (595249)</td><td>7.5</td><td>1</td><td>12</td><td>2.46</td><td>0.16</td><td>223.90</td></tr>
<tr><td>8</td><td>1.25</td><td>12</td><td>1.23</td><td>0.07</td><td>156.57</td></tr>
<tr><td>8.5</td><td>1.25</td><td>12</td><td>1.23</td><td>0.07</td><td>154.64</td></tr>
<tr><td rowspan="4">5</td><td rowspan="4">I-94 (776469)</td><td>8</td><td>1.25</td><td>12</td><td>1.23</td><td>0.10</td><td>172.75</td></tr>
<tr><td>8</td><td>1.5</td><td>12</td><td>1.23</td><td>0.07</td><td>154.22</td></tr>
<tr><td>8.5</td><td>1.25</td><td>12</td><td>1.23</td><td>0.09</td><td>170.42</td></tr>
<tr><td>9</td><td>1.25</td><td>14</td><td>1.23</td><td>0.11</td><td>175.19</td></tr>
<tr><td rowspan="4">6</td><td rowspan="4">I94 (117189)</td><td>12</td><td>1.5</td><td>16</td><td>1.23</td><td>0.13</td><td>176.24</td></tr>
<tr><td>12</td><td>1.5</td><td>14</td><td>1.23</td><td>0.10</td><td>169.07</td></tr>
<tr><td>12.5</td><td>1.5</td><td>16</td><td>1.23</td><td>0.12</td><td>173.53</td></tr>
<tr><td>13</td><td>1.5</td><td>16</td><td>1.23</td><td>0.12</td><td>172.65</td></tr>
<tr><td rowspan="3">7</td><td rowspan="3">I69 (238869)</td><td>10</td><td>1.25</td><td>14</td><td>1.23</td><td>0.14</td><td>197.57</td></tr>
<tr><td>10.5</td><td>1.5</td><td>14</td><td>1.23</td><td>0.09</td><td>164.00</td></tr>
<tr><td>11</td><td>1.5</td><td>14</td><td>1.23</td><td>0.09</td><td>161.85</td></tr>
</table>

Table 5.6. JPCP Pavement ME analysis result (Dense graded base)

NO.	WIM station	Slab thickness (inch)	Dowel Diameter (inch)	Joint spacing (')	Distress value		
					Transverse cracking (%)	Mean faulting (inch)	IRI
Threshold					**15**	**0.125**	**172**
1	US-41 (211459)	6	1	12	**35.33**	0.05	**173.03**
		6.5	1	12	13.24	0.05	156.60
		7	1	12	6.26	0.06	154.38
2	US-2 (492029)	6	1	12	9.08	0.05	146.77
		6.5	1	12	4.52	0.06	146.80
		7	1	12	2.79	0.06	147.26
3	I-75 (694049)	7.5	1	12	1.23	0.11	**188.94**
		8	1.25	12	1.23	0.05	146.69
		8.5	1.25	12	1.23	0.05	145.04
4	US-131 (595249)	7.5	1	12	2.46	**0.17**	**233.61**
		8	1.25	12	1.23	0.08	161.21
		8.5	1.25	12	1.23	0.08	158.68
5	I-94 (776469)	8	1.25	12	1.23	0.10	**178.73**
		8	*1.5*	*12*	*1.23*	*0.08*	*158.47*
		8.5	1.25	12	1.23	0.10	**176.04**
		9	1.25	14	1.23	0.10	**180.38**
6	I94 (117189)	12	1.5	16	1.23	**0.13**	**178.71**
		12	*1.5*	*14*	*1.23*	*0.11*	*171.46*
		12.5	1.5	16	1.23	**0.13**	**175.72**
		13	1.5	16	1.23	0.12	**172.79**
7	I69 (238869)	10	1.25	14	1.23	**0.16**	**204.75**
		10.5	1.5	14	1.23	0.10	168.58
		11	1.5	14	1.23	0.10	164.99

5.2.3. Temperature gradient analysis

Based on the Enhanced Integrated Climatic Model embedded in the Pavement ME output files, the PCC thermal data for different depths can be obtained, with which the temperature gradient for a particular site can be calculated. Since the temperature gradient is mainly determined by climate location and slab thickness, the slab thickness was set from 6" to 13" for each of the seven climate locations. The temperature gradient distribution was then calculated, shown in Table 5.7. The permanent curl/warp temperature gradient of -10°F was considered as utilized for MDOT design.

Table 5.7. Percentage of temperature gradient distribution

Climate station number	Slab thickness (inch)	Percentage of temperature gradient (%)						
		-30°F (-35~-25)	-20°F (-25~-15)	-10°F (-15~-5)	0°F (-5~5)	10°F (5~15)	20°F (15~25)	30°F (25~35)
1	6	0.72	34.16	39.03	19.48	6.31	0.30	0.00
	8	2.50	35.54	34.53	18.51	7.78	1.12	0.01
	10	4.60	34.88	32.43	17.54	8.43	2.01	0.06
	12	5.96	34.05	31.54	16.81	8.79	2.56	0.16
	13	6.40	33.52	31.40	16.57	8.92	2.76	0.20
2	6	0.12	30.07	46.53	17.49	5.66	0.13	0.00
	8	0.76	33.38	41.16	16.67	7.34	0.69	0.00
	10	2.05	34.29	38.22	15.94	8.03	1.45	0.03
	12	3.21	34.10	36.74	15.57	8.24	2.05	0.07
	13	3.60	33.96	36.30	15.45	8.30	2.28	0.09
3	6	0.19	31.72	43.72	18.41	5.79	0.17	0.00
	8	1.13	34.26	38.78	17.60	7.42	0.80	0.00
	10	2.76	34.50	36.18	16.80	8.17	1.55	0.03
	12	4.11	34.07	34.75	16.33	8.49	2.15	0.08
	13	4.59	33.77	34.35	16.21	8.58	2.36	0.12
4	6	0.29	33.26	40.57	19.02	6.63	0.23	0.00
	8	1.65	35.29	35.74	18.06	8.30	0.96	0.00
	10	3.53	34.97	33.45	17.19	8.95	1.89	0.03
	12	4.87	34.20	32.39	16.68	9.19	2.56	0.09
	13	5.39	33.81	32.11	16.51	9.24	2.80	0.12
5	6	0.31	32.06	42.14	19.37	5.88	0.24	0.00
	8	1.53	34.30	37.18	18.63	7.35	1.00	0.01
	10	3.13	34.35	34.68	17.86	8.15	1.80	0.03
	12	4.36	33.73	33.57	17.33	8.58	2.30	0.11
	13	4.85	33.35	33.33	17.13	8.69	2.48	0.15
6	6	0.22	32.69	40.46	19.46	6.90	0.26	0.00
	8	1.44	34.79	35.63	18.48	8.61	1.04	0.00
	10	3.36	34.47	33.17	17.76	9.19	1.99	0.05
	12	5.39	34.16	31.42	16.88	9.35	2.66	0.13
	13	5.89	33.66	31.20	16.76	9.40	2.89	0.16
7	6	0.38	33.46	40.08	19.53	6.29	0.25	0.00
	8	1.77	35.25	35.42	18.64	7.84	1.08	0.01
	10	3.76	34.75	33.19	17.69	8.66	1.91	0.04
	12	5.15	33.89	32.20	17.12	9.03	2.49	0.11
	13	5.71	33.43	31.92	16.95	9.12	2.69	0.14

According to the data in Table 5.7, the temperature gradient distribution at different locations is plotted, as shown in Figures 5.4 – 5.8.

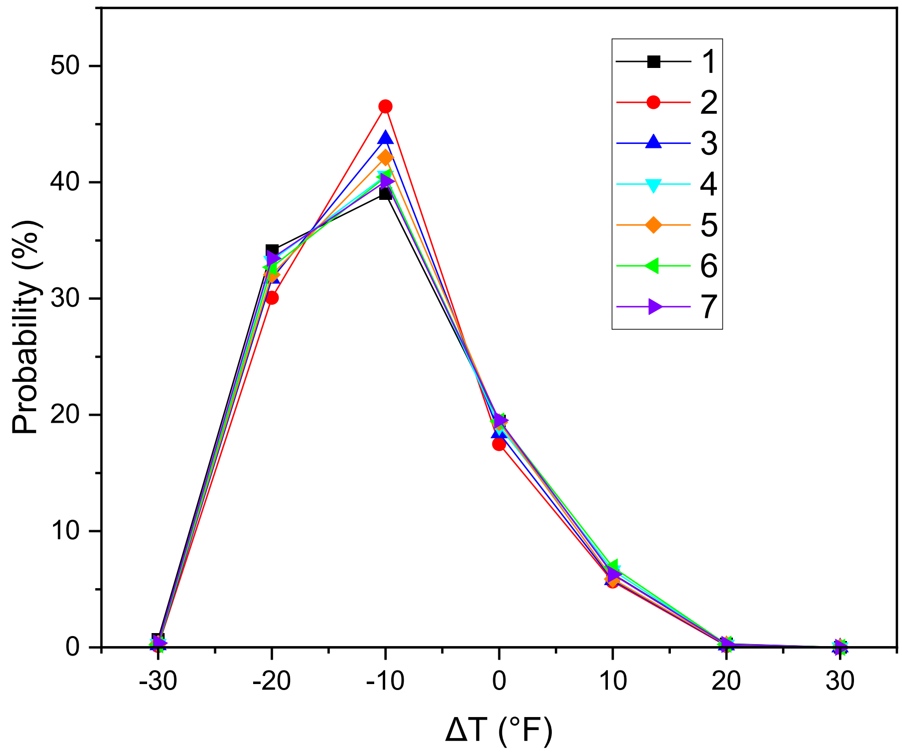

Figure 5.4. Temperature gradient distribution (6" slab thickness)

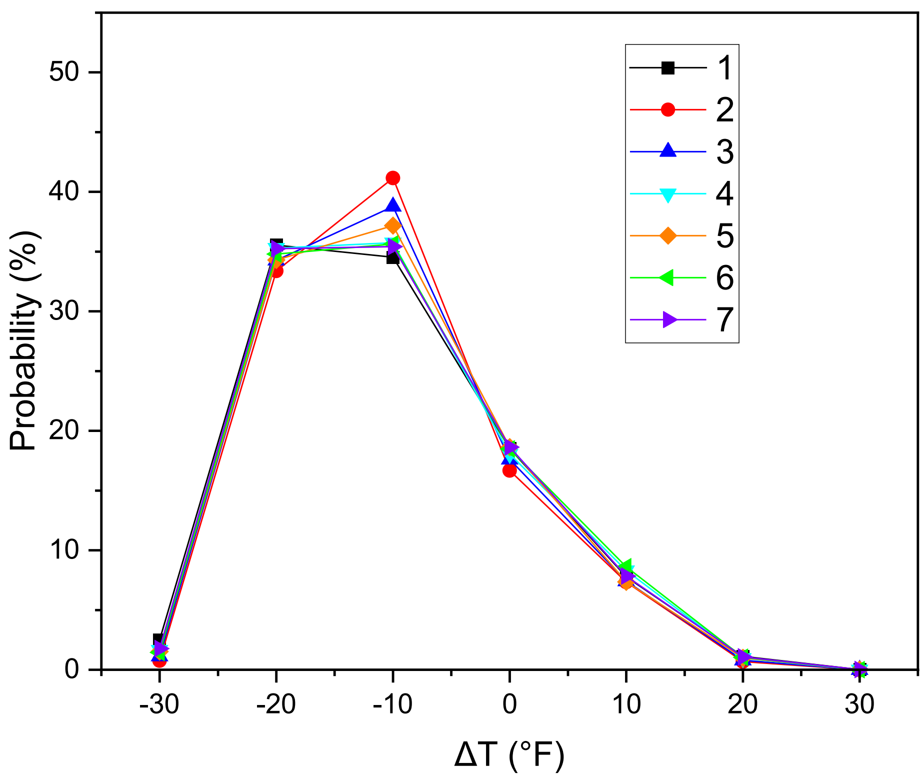

Figure 5.5. Temperature gradient distribution (8" slab thickness)

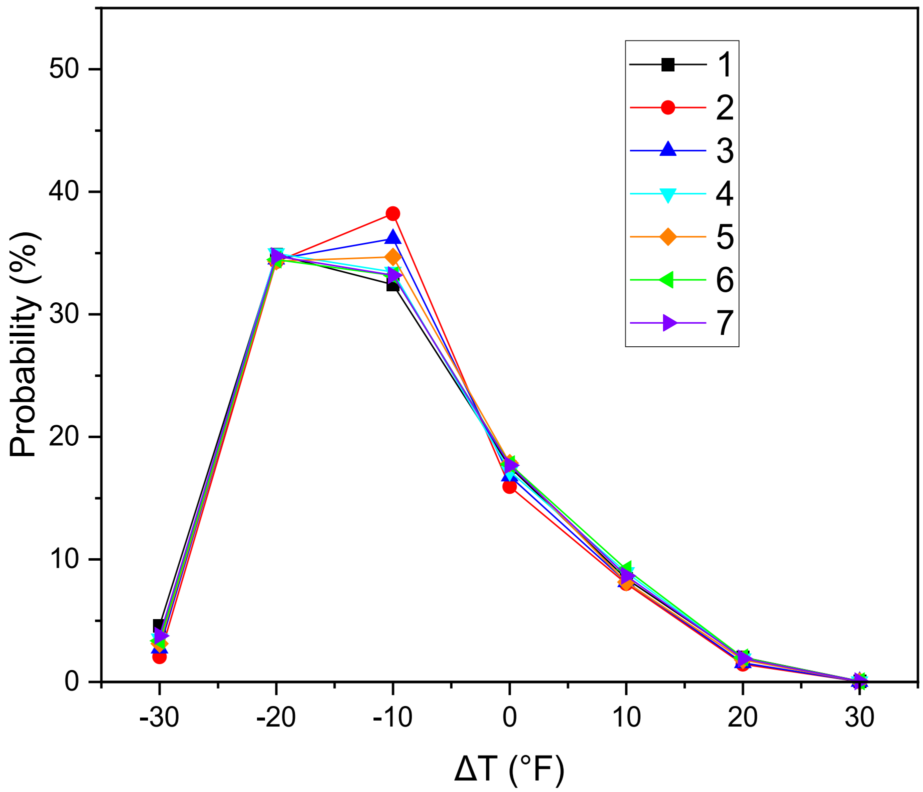

Figure 5.6. Temperature gradient distribution (10" slab thickness)

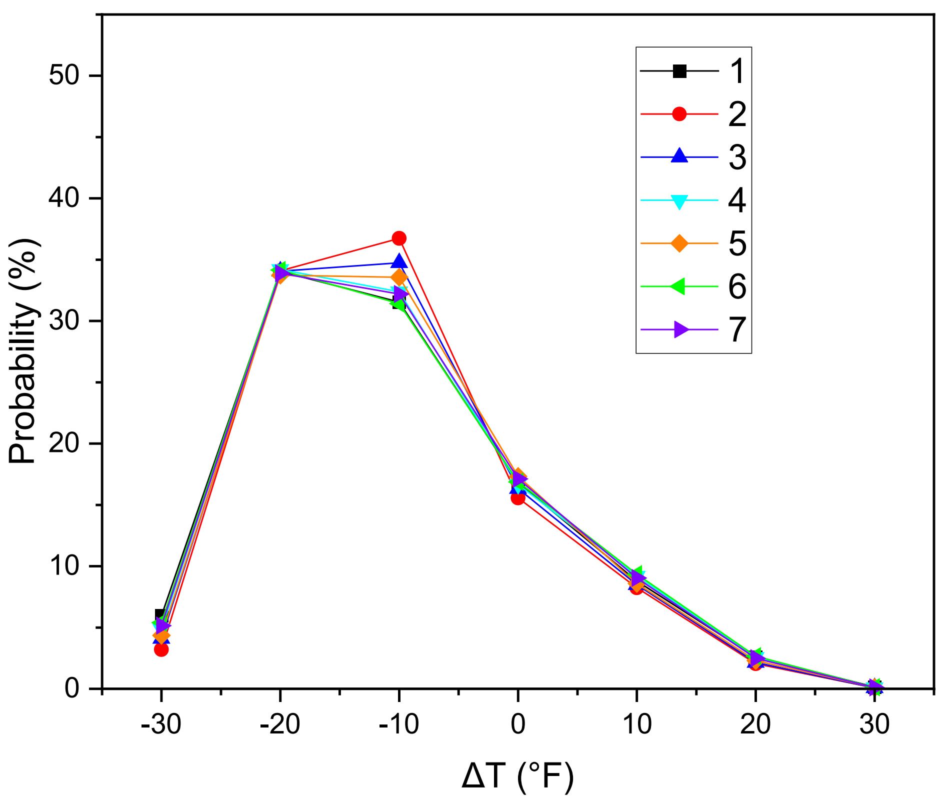

Figure 5.7. Temperature gradient distribution (12" slab thickness)

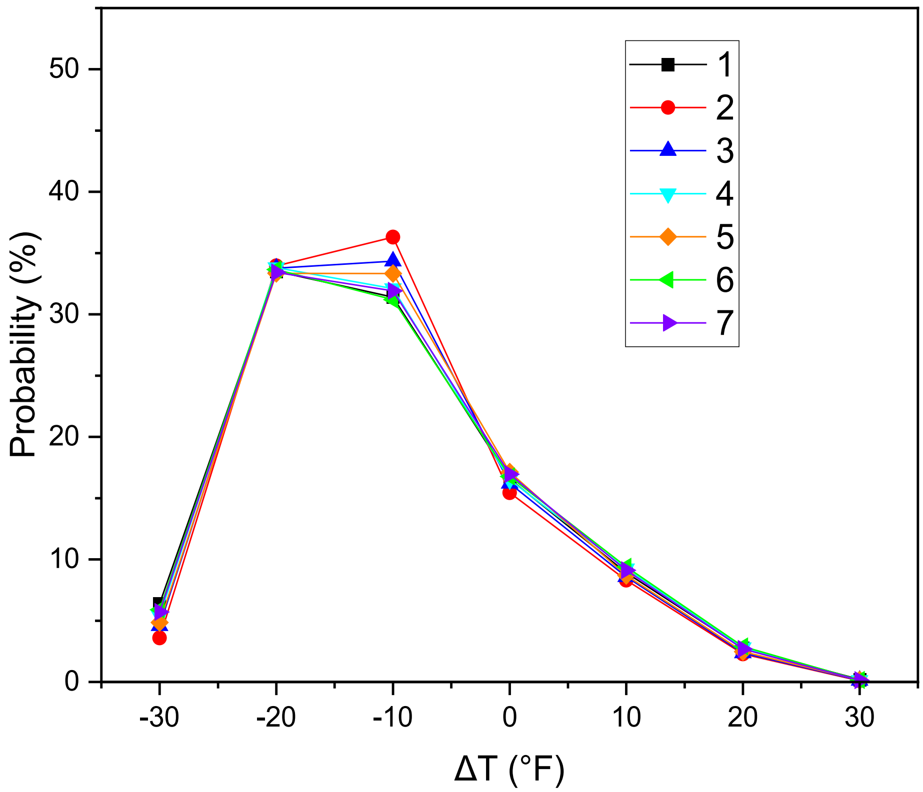

Figure 5.8. Temperature gradient distribution (13" slab thickness)

The distribution regularity shown in Figures 5.4 – 5.8 proves that while some differences exist, the temperature gradient distributions for different slab thicknesses across Michigan climate stations are quite similar. Therefore, the research team then determined the average temperature gradient distribution percentage, as shown in Table 5.8, which would be used in the WBT impact analysis. These determined distributions are approximate values but reasonable to mimic Michigan's practice.

Table 5.8. Determined temperature gradient distribution

Intervals (°F)	**-30 (-35~-25)**	**-20 (-25~-15)**	**-10 (-15~-5)**	**0 (-5~5)**	**10 (5~15)**	**20 (15~25)**	**30 (25~35)**
Percentage (%)	5	35	35	15	8	2	0

5.3. Transverse cracking distress analysis

5.3.1. Slab bottom stress analysis with Illislab

As described previously, transverse cracking is divided into bottom-up and top-down cracking. When the load is placed on the middle of the slab and the slab curves downward (positive temperature gradient), the bottom of the slab tends to suffer the most extensive stress, leading to bottom-up cracking.

The research team adopted Illislab software to compare the slab bottom stress difference under DT and WBT loads. The variables utilized in Illislab are presented in Table 5.9. Slab thicknesses range from 6" to 13", with the dowel diameter and joint spacing corresponding with slab thickness in Figure 5.9, as dictated by MDOT design practice.

The temperature gradient ranges from -30°F to 30°F. The load edge from slab edge ranges from 0 to 18". The tire pressure for loads is set as 80, 100, and 120 psi.

Table 5.9. Variables used in Illislab for cracking analysis

Variables	Values				
Slab thickness (inch)	6	8	10	12	13
Distance from shoulder (inch)	0; 10; 18				
Temperature gradient (°F)	-30; -20; -10; 0; 10; 20; 30				
Joint spacing (')	12	12	14	16	16
Tire pressure (psi)	80; 100; 120				

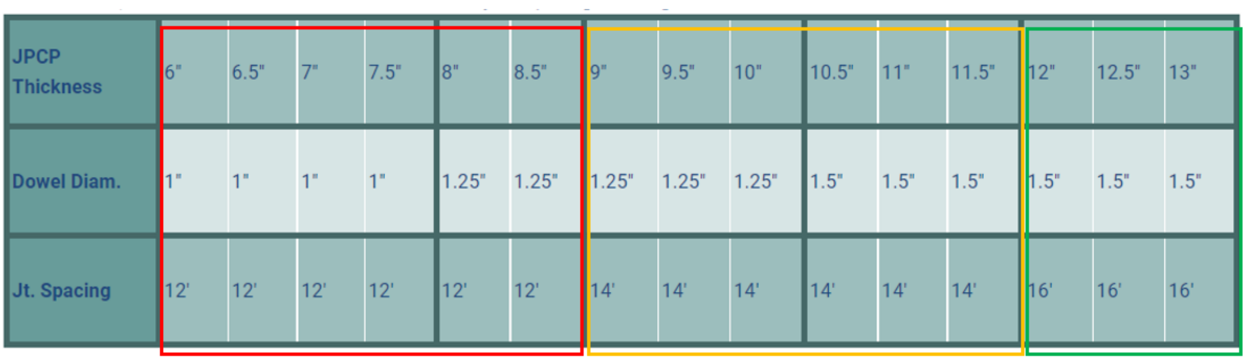

JPCP Thickness	6"	6.5"	7"	7.5"	8"	8.5"	9"	9.5"	10"	10.5"	11"	11.5"	12"	12.5"	13"
Dowel Diam.	1"	1"	1"	1"	1.25"	1.25"	1.25"	1.25"	1.25"	1.5"	1.5"	1.5"	1.5"	1.5"	1.5"
Jt. Spacing	12'	12'	12'	12'	12'	12'	14'	14'	14'	14'	14'	14'	16'	16'	16'

Figure 5.9. JPCP dowel diameter and joint spacing

Stress at the bottom of the slab for different slab thicknesses and load distances obtained from Illislab are shown in Appendix F. With the stress data in Appendix F, the stress at the bottom of the slab for different thicknesses under the dual tire design standard of 120 psi is plotted, as shown in Figures 5.10 – 5.12. The upper surface of plotted squares in Figures 5.10 – 5.12 represents the stress under dual-tire (DT) load, while the bottom surface indicates the increased stress under more concentrated WBT loads.

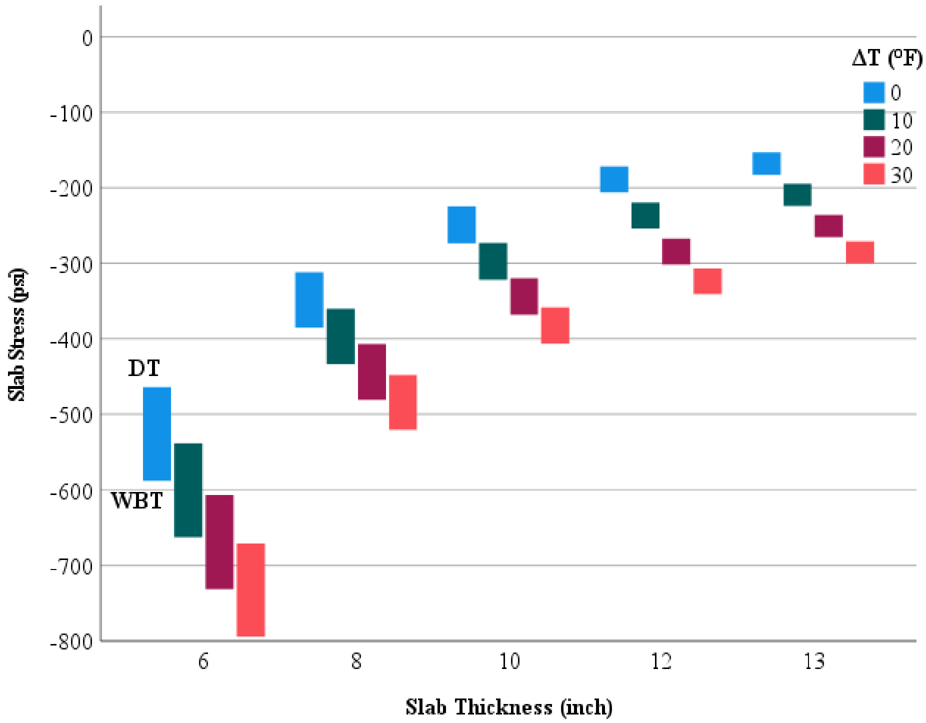

Figure 5.10. Stress at the bottom of the slab in different thicknesses (0" from shoulder joint)

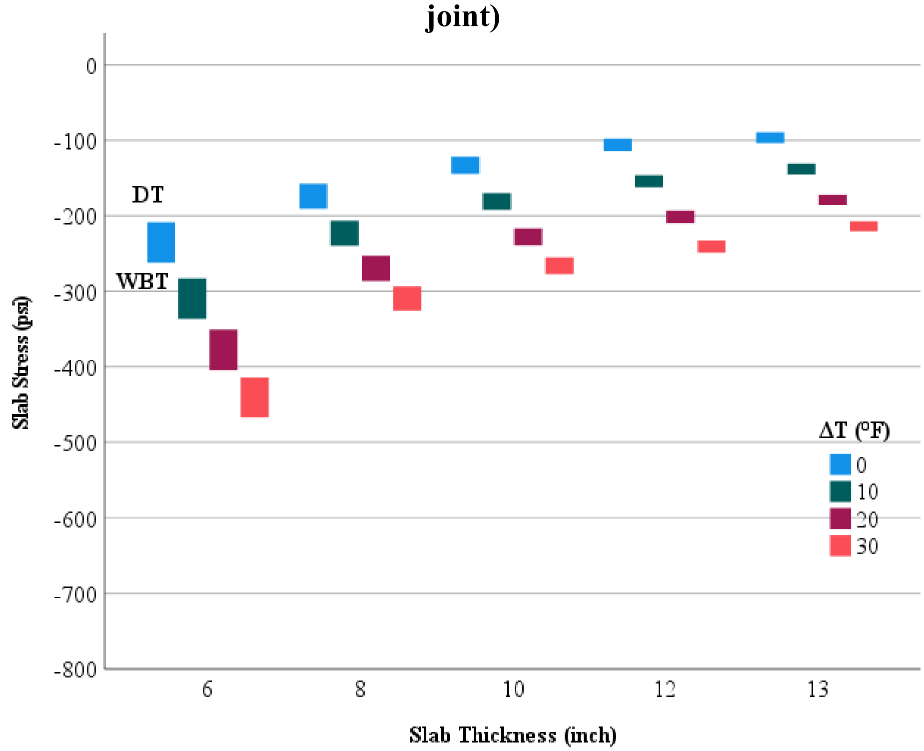

Figure 5.11. Stress at the bottom of the slab in different thicknesses (10" from shoulder joint)

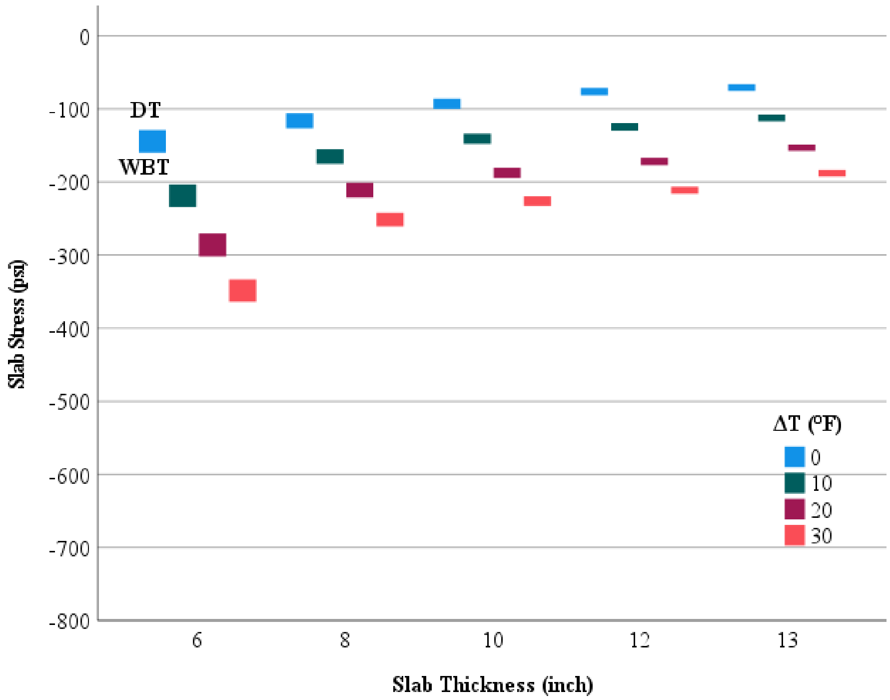

Figure 5.12. Stress at the bottom of the slab in different thicknesses (18" from shoulder joint)

As shown in Figures 5.10 – 5.12, the difference in stress between DT and WBT loads decreases with the slab thickness for all load locations, which proves JPCP structure with a thinner slab thickness is more sensitive to WBT load impact. When the positive temperature gradient increases, slab bottom stress under both DT and WBT loads increases significantly. However, there is little apparent difference between DT and WBT loads with the temperature gradient. The distance of the loads' exterior edge from the shoulder joint also has a significant influence on WBT impact, especially for thinner slab thicknesses, as the squares' height in Figure 5.10 (0" from shoulder joint) is much higher than that in Figure 5.12 (18" from shoulder joint).

5.3.2. Slab top stress analysis with Illislab

When the loads are placed on the slab's edges and the slab curves upward (negative temperature gradient), the top of the slab tends to suffer the most extensive stress, leading to top-down cracking. The variables in Illislab are presented in Table 5.9. Stress at the top of the slab for different slab thicknesses and load distances obtained from Illislab are shown in Appendix G.

With the stress data in Appendix G, the stress at the top of the slab for different thicknesses under the dual tire design standard of 120 psi can also be plotted, as shown in Figures 5.13 – 5.15. The upper surface of squares in Figures 5.13 – 5.15 represents stress under dual-tire (DT) load, while the bottom surface again indicates the increased stress under corresponding WBT loads.

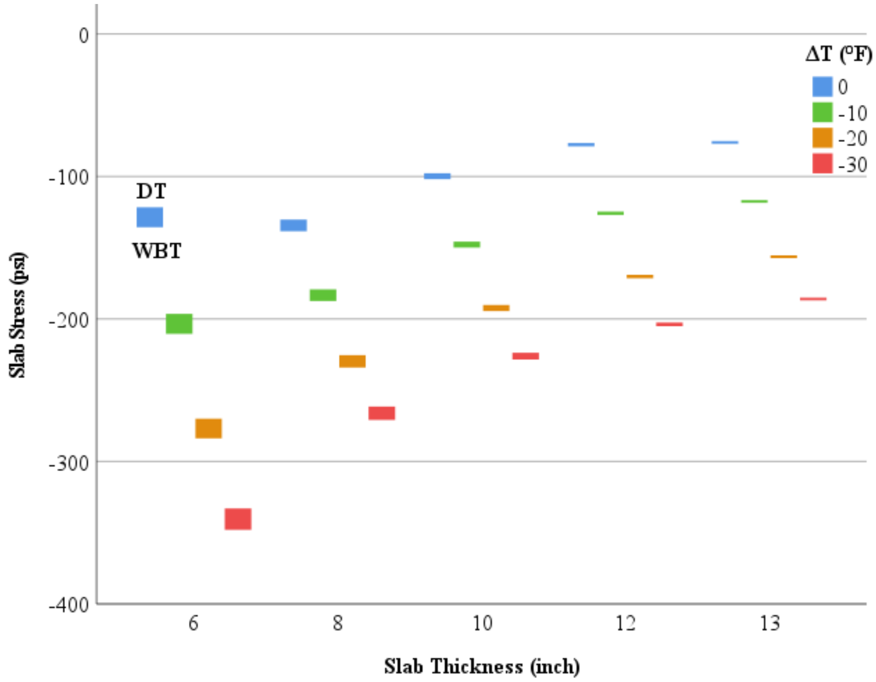

Figure 5.13. Stress at the top of the slab at different thicknesses (0" from shoulder joint)

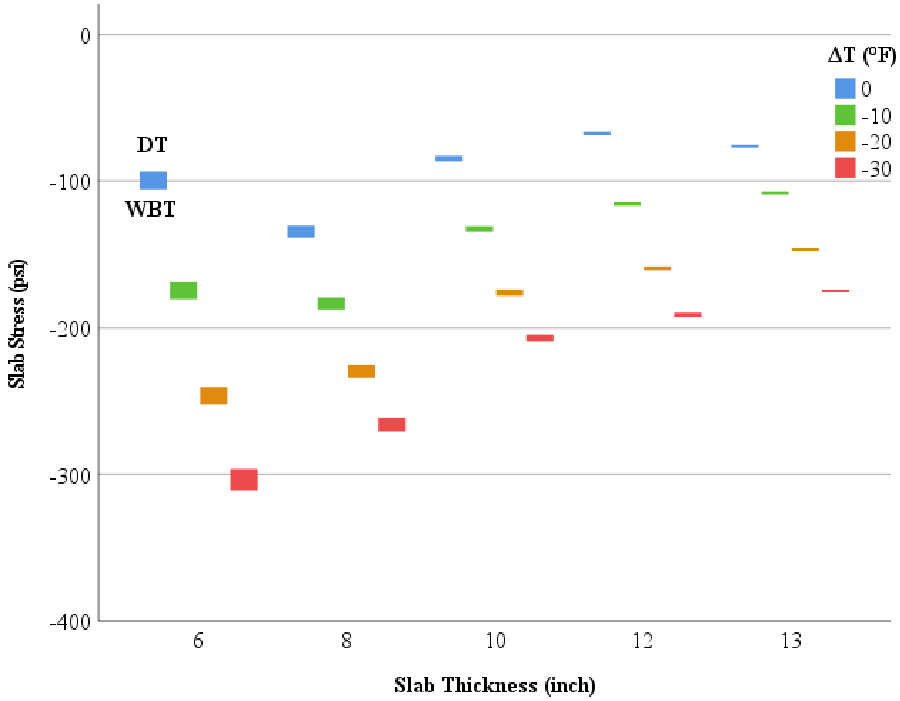

Figure 5.14. Stress at the top of the slab at different thicknesses (10" from shoulder joint)

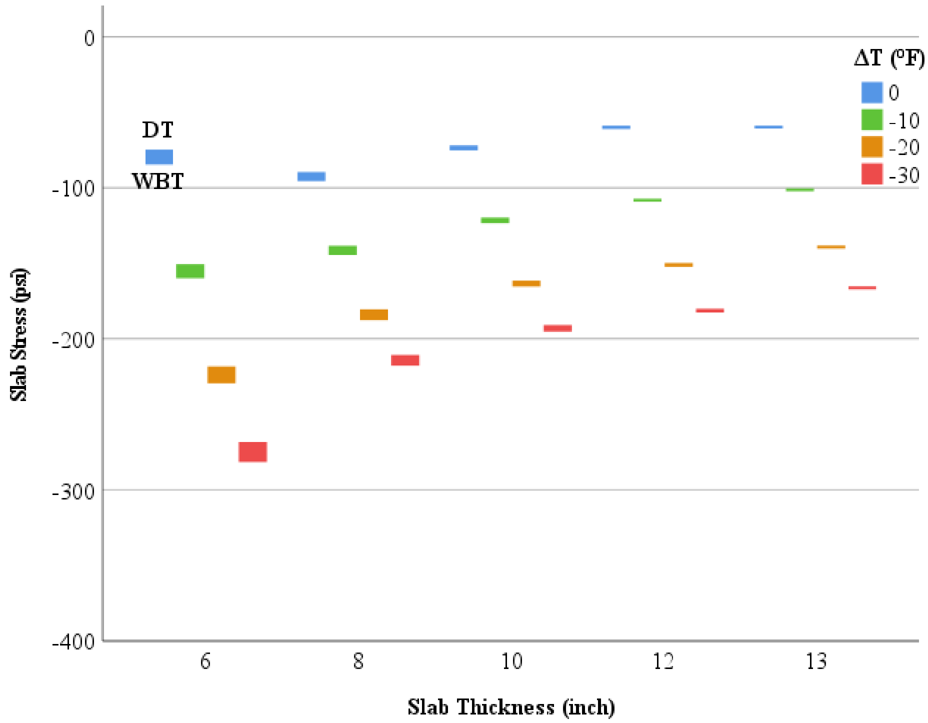

Figure 5.15. Stress at the top of the slab at different thicknesses (18" from shoulder joint)

As shown in Figures 5.13 - 5.15, the development of squares' height with slab thickness is similar to that for slab bottom stress figures (Figures 5.10 - 5.12). JPCP structures with a thinner slab thickness are more sensitive to WBT load impact. However, the stress difference between DT and WBT loads is much lower compared with slab bottom stress scenarios, especially for thinner slab structures. The distance of load from the edge of the shoulder joint does not significantly influence the WBT impact, as the squares' height does not change too much with the distance. It is worth mentioning that the slab stress does not show a decreasing trend from 6" to 8" slab thickness when the temperature gradient is equal to 0 or -10°F (at or near fully supported slab conditions).

5.3.3. Analysis of WBT impact on transverse cracking

With the slab bottom and top stresses obtained from the Illislab analysis, the research team started the JPCP transverse cracking analysis using the method described in AASHTO MEPDG 3 [11]. The allowable number of load applications is calculated based on equation (5.1).

$$\log N_{i,j,k \dots} = C_1 \times \left(\frac{MR_i}{\sigma_{i,j,k,l,m,n}}\right)^{C_2} \quad (5.1)$$

where:

$N_{i,j,k,\dots}$ = Allowable number of load applications at condition i, j, k, l, m, n

MR_i = PCC modulus of rupture at age i, psi

$\sigma_{i,j,k,\ldots}$ = Applied stress at condition i, j, k, l, m, n

$C_{1,2}$ = Calibration coefficients; $C_1 = 2.0$; $C_2 = 1.22$

The total fatigue damage index DI_F can be obtained with allowable load N applications and applied load applications *n* from equation (5.2) below.

$$DI_F = \sum \frac{n_{i,j,k,l,m,n,o}}{N_{i,j,k,l,m,n,o}} \tag{5.2}$$

Where:

DI_F = Total fatigue damage index (top-down or bottom-up)

$n_{i,j,k,\ldots}$ = Applied number of load applications at condition i, j, k, l, m, n

The applied load applications *n* are assumed to be the same for DT and WBT loads, so the inverse of N was assumed as DI_F in this project.

The distribution of wheel edge distance from the shoulder joint is based on a mean distance of 18 inches and a standard deviation of 10 inches, with resulting probabilities presented in Figure 5.16 and Table 5.10, while the temperature gradient distribution is shown in Table 5.8 in section 5.2.3. The combined distribution of wheel edge distance and temperature gradient is then obtained, as shown in Table 5.11.

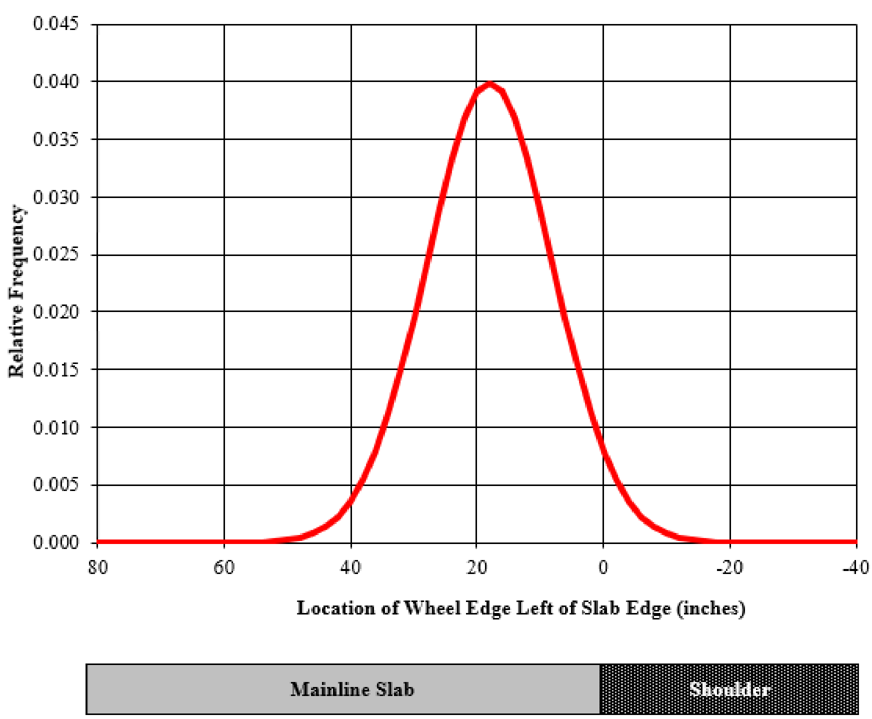

Figure 5.16. Distribution of wheel edge distance from shoulder joint

Table 5.10. Distribution of wheel edge distance from shoulder joint

Distance from shoulder joint (inch)	Location (inch)	Probabilities
5 to -100	0	0.106
14 to 5	10	0.258
>14	18	0.636

Table 5.11. Combined distribution of wheel edge distance and temperature gradient

		Temperature gradient						
		-30°F (-35~-25)	**-20°F (-25~-15)**	**-10°F (-15~-5)**	**0°F (-5~5)**	**10°F (5~15)**	**20°F (15~25)**	**30°F (25~35)**
Distance	0	0.0053	0.0371	0.0371	0.0159	0.0085	0.0021	0.0000
	10	0.0129	0.0903	0.0903	0.0387	0.0206	0.0052	0.0000
	18	0.0318	0.2226	0.2226	0.0954	0.0509	0.0127	0.0000

The predicted amount of bottom-up or top-down cracking can be calculated with the damage index DI_F, as shown in equation (5.3). The relation between DI_F and CRK is plotted in Figure 5.17.

$$CRK = \frac{100}{1+C_4 {DI_F}^{C_5}} \tag{5.3}$$

where:

CRK = Predicted amount of bottom-up or top-down cracking (fraction);

DI_F = Fatigue damage index calculated;

$C_{4,5}$ = Calibration coefficients; $C_4 = 0.52$; $C_5 = -2.17$.

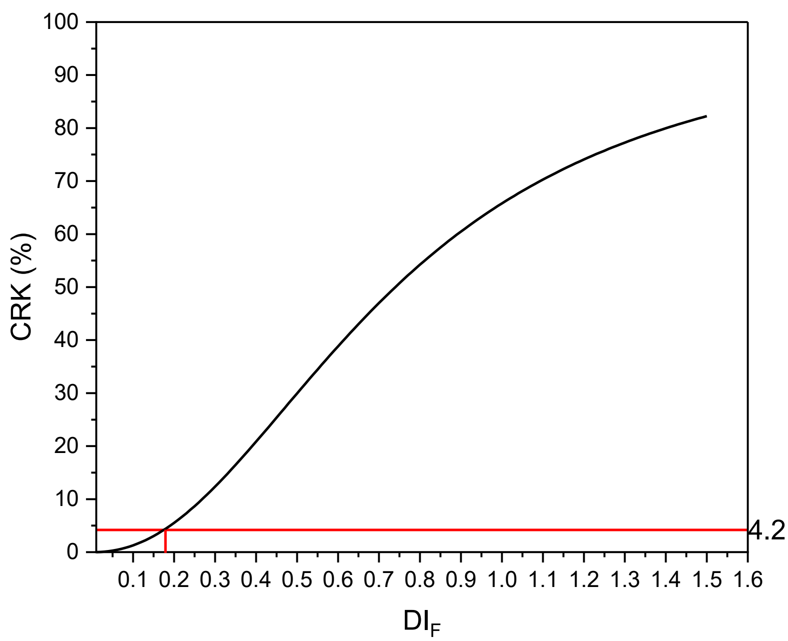

Figure 5.17. Relationship between DI_F and CRK

The threshold of JPCP transverse cracking in Michigan is 15% (95% reliability). When calculating the average value (50% reliability), 4.2% cracking would arrive at the threshold. According to Figure 5.17, when the CRK is 4.2%, the DI_F is about 0.175. The damage index under different slab thicknesses was multiplied with various DI_F reduced factors presented in Table 5.12. The CRK calculated with DI_F and DI_F reduced factor will be around the 4.2% cracking threshold under 50% reliability and 15% under 95% reliability.

Table 5.12. DI_F reduced factor for bottom-up and top-down cracking

Slab thickness (inch)	6	8	10	12	13
Reduced factor (Bottom-up)	0.0958	0.0687	0.0527	0.0427	0.0388
Reduced factor (Top-down)	0.0810	0.0678	0.0573	0.0496	0.0451

With the combined distribution in Table 5.11 and the reduced factor in Table 5.12, the combined damage index for bottom-up and top-down cracking is calculated. The percent increase percentage from DT load to WBT load is also obtained. The results are shown in Tables 5.13 - 5.14.

Table 5.13. Combined damage index for bottom-up cracking

Slab thickness (inch)	Tire pressure (psi)	Damage index		Percent increase (%)
		Under DT load	Under WBT tire load	
6	80	0.1575	0.2111	34.03
	100	0.1645	0.2221	35.02
	120	0.1699	0.2305	35.67
8	80	0.1554	0.2022	30.12
	100	0.1617	0.2119	31.05
	120	0.1665	0.2194	31.77
10	80	0.1599	0.2001	25.14
	100	0.1654	0.2086	26.12
	120	0.1696	0.2151	26.83
12	80	0.1625	0.1971	21.29
	100	0.1673	0.2046	22.30
	120	0.1710	0.2103	22.98
13	80	0.1567	0.1895	20.93
	100	0.1612	0.1966	21.96
	120	0.1648	0.2021	22.63

Table 5.14. Combined damage index for top-down cracking

Slab thickness (inch)	Tire pressure (psi)	Damage index		Percent increase (%)
		Under DT load	Under WBT tire load	
6	80	0.1620	0.1798	10.99
	100	0.1635	0.1817	11.13
	120	0.1647	0.1831	11.17
8	80	0.1621	0.1752	8.08
	100	0.1653	0.1794	8.53
	120	0.1677	0.1825	8.83
10	80	0.1610	0.1692	5.09
	100	0.1634	0.1723	5.45
	120	0.1653	0.1746	5.63
12	80	0.1667	0.1718	3.06
	100	0.1686	0.1742	3.32
	120	0.1700	0.1759	3.47
13	80	0.1683	0.1714	1.84
	100	0.1704	0.1739	2.05
	120	0.1720	0.1758	2.21

With the damage index for DT and WBT loads, the relative damage index at different WBT proportions for bottom-up and top-down cracking can be calculated considering WBT proportions from 0 to 25%. The relative damage index at different WBT proportions (bottom-up; top-down) is presented in Tables 5.15 - 5.16.

Table 5.15. Relative damage index at different WBT proportions (Bottom-up)

Slab thickness (inch)	Tire pressure (psi)	Relative damage index at different WBT proportions								
		0%	4%	6%	8%	10%	12%	14%	20%	25%
6	80	0.1575	0.1596	0.1607	0.1618	0.1629	0.1639	0.1650	0.1682	0.1709
	100	0.1645	0.1668	0.1680	0.1691	0.1703	0.1714	0.1726	0.1760	0.1789
	120	0.1699	0.1723	0.1735	0.1747	0.1760	0.1772	0.1784	0.1820	0.1851
8	80	0.1554	0.1573	0.1582	0.1591	0.1601	0.1610	0.1620	0.1648	0.1671
	100	0.1617	0.1637	0.1647	0.1657	0.1667	0.1677	0.1687	0.1717	0.1743
	120	0.1665	0.1686	0.1697	0.1707	0.1718	0.1728	0.1739	0.1771	0.1797
10	80	0.1599	0.1615	0.1623	0.1631	0.1639	0.1647	0.1655	0.1679	0.1700
	100	0.1654	0.1671	0.1680	0.1689	0.1697	0.1706	0.1714	0.1740	0.1762
	120	0.1696	0.1714	0.1723	0.1732	0.1742	0.1751	0.1760	0.1787	0.1810
12	80	0.1625	0.1639	0.1646	0.1653	0.1660	0.1667	0.1673	0.1694	0.1712
	100	0.1673	0.1688	0.1695	0.1703	0.1710	0.1718	0.1725	0.1748	0.1766
	120	0.1710	0.1726	0.1734	0.1741	0.1749	0.1757	0.1765	0.1789	0.1808
13	80	0.1567	0.1580	0.1587	0.1593	0.1600	0.1606	0.1613	0.1633	0.1649
	100	0.1612	0.1626	0.1633	0.1640	0.1647	0.1654	0.1662	0.1683	0.1701
	120	0.1648	0.1663	0.1670	0.1678	0.1685	0.1693	0.1700	0.1723	0.1741

Table 5.16. Relative damage index at different WBT proportions (Top-down)

Slab thickness (inch)	Tire pressure (psi)	Relative damage index at different WBT proportions								
		0%	4%	6%	8%	10%	12%	14%	20%	25%
6	80	0.1620	0.1627	0.1631	0.1634	0.1638	0.1641	0.1645	0.1656	0.1665
	100	0.1635	0.1642	0.1646	0.1650	0.1653	0.1657	0.1660	0.1671	0.1681
	120	0.1647	0.1654	0.1658	0.1662	0.1665	0.1669	0.1673	0.1684	0.1693
8	80	0.1621	0.1626	0.1629	0.1631	0.1634	0.1637	0.1639	0.1647	0.1654
	100	0.1653	0.1659	0.1661	0.1664	0.1667	0.1670	0.1673	0.1681	0.1688
	120	0.1677	0.1683	0.1686	0.1689	0.1692	0.1695	0.1698	0.1707	0.1714
10	80	0.1610	0.1613	0.1615	0.1617	0.1618	0.1620	0.1621	0.1626	0.1631
	100	0.1634	0.1638	0.1639	0.1641	0.1643	0.1645	0.1646	0.1652	0.1656
	120	0.1653	0.1657	0.1659	0.1660	0.1662	0.1664	0.1666	0.1672	0.1676
12	80	0.1667	0.1669	0.1670	0.1671	0.1672	0.1673	0.1674	0.1677	0.1680
	100	0.1686	0.1688	0.1689	0.1690	0.1692	0.1693	0.1694	0.1697	0.1700
	120	0.1700	0.1702	0.1704	0.1705	0.1706	0.1707	0.1708	0.1712	0.1715
13	80	0.1683	0.1684	0.1685	0.1685	0.1686	0.1687	0.1687	0.1689	0.1691
	100	0.1704	0.1705	0.1706	0.1707	0.1708	0.1708	0.1709	0.1711	0.1713
	120	0.1720	0.1722	0.1722	0.1723	0.1724	0.1725	0.1725	0.1728	0.1730

With the relative damage index in Tables 5.15 - 5.16 and equation (5.3), the CRK (bottom-up and top-down) at different WBT proportions under 95% reliability are calculated, as presented in Tables 5.17 - 5.18.

Table 5.17. CRK (bottom-up) at different WBT proportions

Slab thickness (inch)	Tire pressure (psi)	CRK at different WBT proportions (%)								
		0%	4%	6%	8%	10%	12%	14%	20%	25%
6	80	13.4431	13.6258	13.7176	13.8095	13.9017	13.9941	14.0868	14.3661	14.6004
	100	14.0432	14.2429	14.3431	14.4436	14.5443	14.6454	14.7466	15.0521	15.3084
	120	14.5128	14.7255	14.8323	14.9394	15.0467	15.1544	15.2623	15.5879	15.8611
8	80	13.2649	13.4237	13.5033	13.5831	13.6631	13.7433	13.8236	14.0657	14.2686
	100	13.8020	13.9748	14.0615	14.1484	14.2356	14.3229	14.4104	14.6742	14.8953
	120	14.2164	14.4006	14.4930	14.5857	14.6786	14.7716	14.8650	15.1462	15.3821
10	80	13.6477	13.7855	13.8546	13.9238	13.9931	14.0626	14.1321	14.3417	14.5172
	100	14.1211	14.2710	14.3462	14.4216	14.4971	14.5727	14.6485	14.8768	15.0680
	120	14.4866	14.6461	14.7260	14.8062	14.8865	14.9670	15.0476	15.2905	15.4941
12	80	13.8707	13.9900	14.0498	14.1096	14.1696	14.2296	14.2898	14.4708	14.6224
	100	14.2860	14.4160	14.4812	14.5464	14.6118	14.6773	14.7429	14.9404	15.1058
	120	14.6092	14.7473	14.8166	14.8860	14.9555	15.0251	15.0948	15.3048	15.4806
13	80	13.3751	13.4866	13.5425	13.5985	13.6546	13.7107	13.7669	13.9362	14.0778
	100	13.7591	13.8807	13.9417	14.0028	14.0639	14.1252	14.1866	14.3713	14.5259
	120	14.0691	14.1984	14.2632	14.3281	14.3931	14.4583	14.5235	14.7199	14.8843

Table 5.18. CRK (top-down) at different WBT proportions

Slab thickness (inch)	Tire pressure (psi)	CRK at different WBT proportions (%)								
		0%	4%	6%	8%	10%	12%	14%	20%	25%
6	80	13.8277	13.8890	13.9196	13.9503	13.9810	14.0117	14.0425	14.1349	14.2121
	100	13.9569	14.0197	14.0511	14.0826	14.1141	14.1457	14.1772	14.2721	14.3513
	120	14.0605	14.1242	14.1561	14.1880	14.2199	14.2519	14.2839	14.3800	14.4604
8	80	13.8363	13.8814	13.9039	13.9265	13.9491	13.9717	13.9943	14.0622	14.1189
	100	14.1124	14.1613	14.1857	14.2102	14.2347	14.2592	14.2837	14.3574	14.4189
	120	14.3208	14.3724	14.3982	14.4240	14.4499	14.4757	14.5016	14.5794	14.6443
10	80	13.7419	13.7700	13.7841	13.7982	13.8123	13.8264	13.8405	13.8828	13.9181
	100	13.9482	13.9789	13.9943	14.0097	14.0250	14.0404	14.0558	14.1020	14.1405
	120	14.1124	14.1446	14.1607	14.1769	14.1930	14.2092	14.2253	14.2738	14.3143
12	80	14.2338	14.2515	14.2604	14.2693	14.2781	14.2870	14.2959	14.3225	14.3447
	100	14.3992	14.4188	14.4286	14.4383	14.4481	14.4579	14.4677	14.4971	14.5216
	120	14.5216	14.5422	14.5526	14.5629	14.5732	14.5836	14.5939	14.6250	14.6509
13	80	14.3731	14.3839	14.3893	14.3947	14.4001	14.4055	14.4109	14.4272	14.4407
	100	14.5566	14.5689	14.5750	14.5811	14.5873	14.5934	14.5995	14.6180	14.6333
	120	14.6970	14.7104	14.7171	14.7238	14.7304	14.7371	14.7438	14.7639	14.7806

Compared with the zero WBT load scenario, the CRK (bottom-up and top-down) percent increase for each slab thickness structure at different WBT proportions and tire pressures under 95% reliability is calculated, as presented in Tables 5.19 - 5.20.

Table 5.19. CRK (bottom-up) percent increase at different WBT proportions

Slab thickness (inch)	Tire pressure (psi)	CRK percent increase at different WBT proportions (%)								
		0%	4%	6%	8%	10%	12%	14%	20%	25%
6	80	0.00	1.36	2.04	2.73	3.41	4.10	4.79	6.87	8.61
	100	0.00	1.42	2.14	2.85	3.57	4.29	5.01	7.18	9.01
	120	0.00	1.47	2.20	2.94	3.68	4.42	5.16	7.41	9.29
8	80	0.00	1.20	1.80	2.40	3.00	3.61	4.21	6.04	7.57
	100	0.00	1.25	1.88	2.51	3.14	3.77	4.41	6.32	7.92
	120	0.00	1.30	1.95	2.60	3.25	3.91	4.56	6.54	8.20
10	80	0.00	1.01	1.52	2.02	2.53	3.04	3.55	5.08	6.37
	100	0.00	1.06	1.59	2.13	2.66	3.20	3.74	5.35	6.71
	120	0.00	1.10	1.65	2.21	2.76	3.32	3.87	5.55	6.95
12	80	0.00	0.86	1.29	1.72	2.15	2.59	3.02	4.33	5.42
	100	0.00	0.91	1.37	1.82	2.28	2.74	3.20	4.58	5.74
	120	0.00	0.95	1.42	1.89	2.37	2.85	3.32	4.76	5.96
13	80	0.00	0.83	1.25	1.67	2.09	2.51	2.93	4.19	5.25
	100	0.00	0.88	1.33	1.77	2.22	2.66	3.11	4.45	5.57
	120	0.00	0.92	1.38	1.84	2.30	2.77	3.23	4.63	5.79

Table 5.20. CRK (top-down) percent increase at different WBT proportions

Slab thickness (inch)	Tire pressure (psi)	CRK percent increase at different WBT proportions (%)								
		0%	**4%**	**6%**	**8%**	**10%**	**12%**	**14%**	**20%**	**25%**
6	80	0.00	0.44	0.66	0.89	1.11	1.33	1.55	2.22	2.78
	100	0.00	0.45	0.68	0.90	1.13	1.35	1.58	2.26	2.83
	120	0.00	0.45	0.68	0.91	1.13	1.36	1.59	2.27	2.84
8	80	0.00	0.33	0.49	0.65	0.82	0.98	1.14	1.63	2.04
	100	0.00	0.35	0.52	0.69	0.87	1.04	1.21	1.74	2.17
	120	0.00	0.36	0.54	0.72	0.90	1.08	1.26	1.81	2.26
10	80	0.00	0.20	0.31	0.41	0.51	0.61	0.72	1.03	1.28
	100	0.00	0.22	0.33	0.44	0.55	0.66	0.77	1.10	1.38
	120	0.00	0.23	0.34	0.46	0.57	0.69	0.80	1.14	1.43
12	80	0.00	0.12	0.19	0.25	0.31	0.37	0.44	0.62	0.78
	100	0.00	0.14	0.20	0.27	0.34	0.41	0.48	0.68	0.85
	120	0.00	0.14	0.21	0.28	0.36	0.43	0.50	0.71	0.89
13	80	0.00	0.08	0.11	0.15	0.19	0.23	0.26	0.38	0.47
	100	0.00	0.08	0.13	0.17	0.21	0.25	0.30	0.42	0.53
	120	0.00	0.09	0.14	0.18	0.23	0.27	0.32	0.46	0.57

The research team then used Pavement ME to investigate the contribution of bottom-up and top-down cracking in total transverse cracking. For each of the seven locations in section 5.2, slab thicknesses of 6", 8", 10", 12", and 13" were analyzed, and the proportion of bottom-up and top-down cracking from the output files are presented in Figures 5.18 - 5.22.

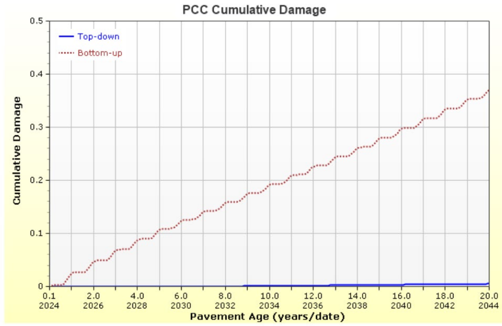

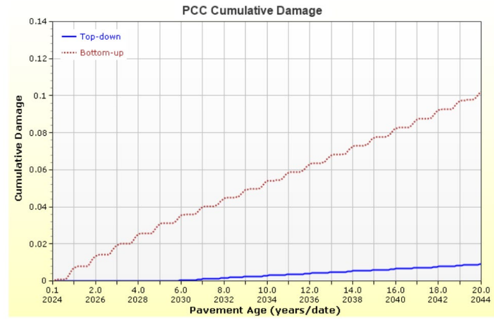

(a) Location 1 (b) Location 2

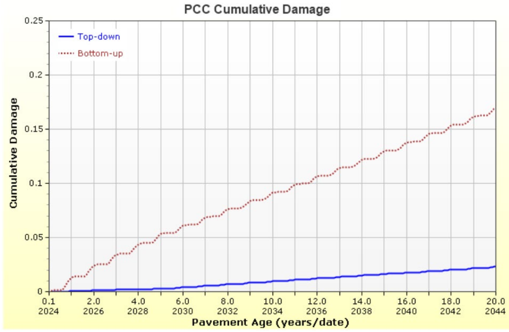

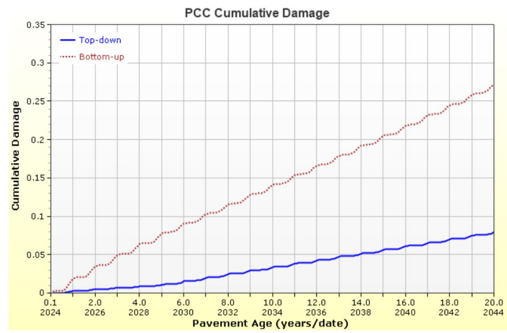

(c) Location 3 (d) Location 4

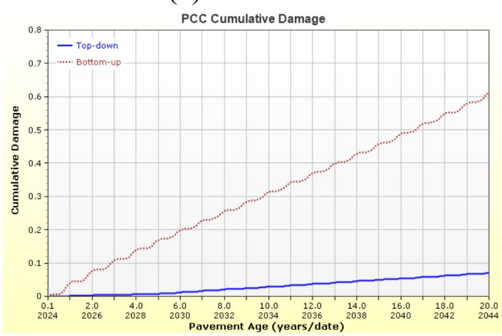

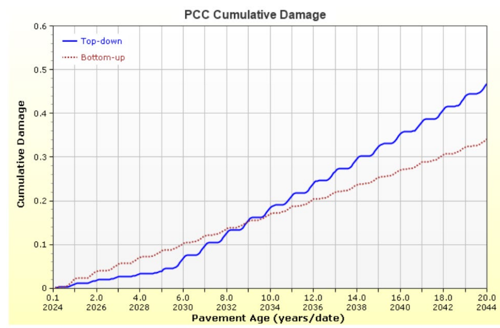

(e) Location 5 (f) Location 6

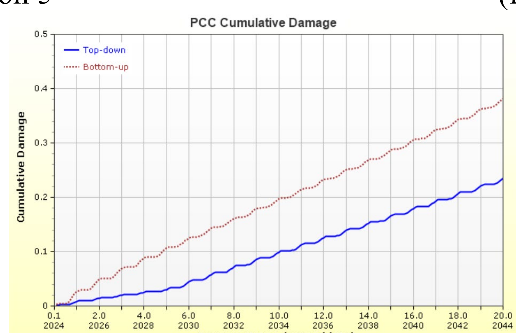

(g) Location 7

Figure 5.18. The proportion of bottom-up and top-down cracking (6" slab thickness)

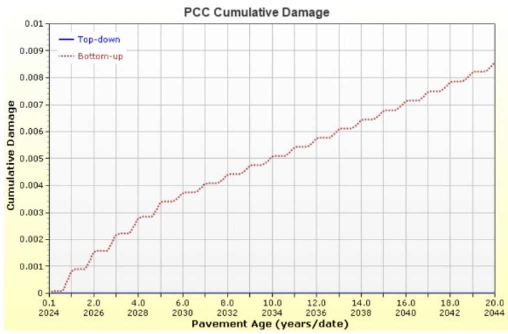

(a) Location 1

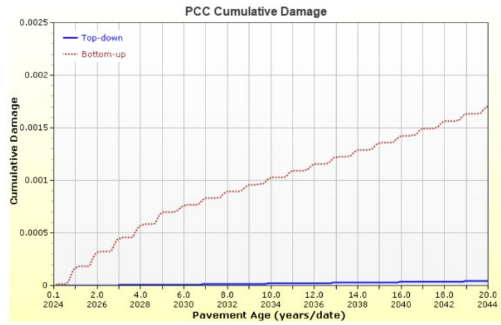

(b) Location 2

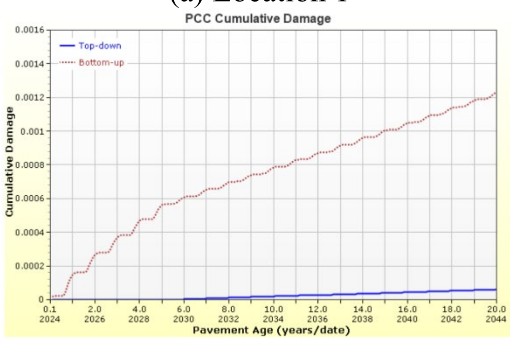

(c) Location 3

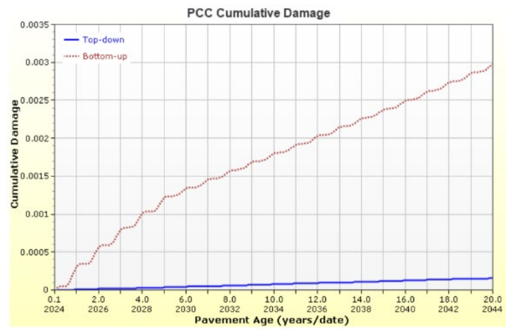

(d) Location 4

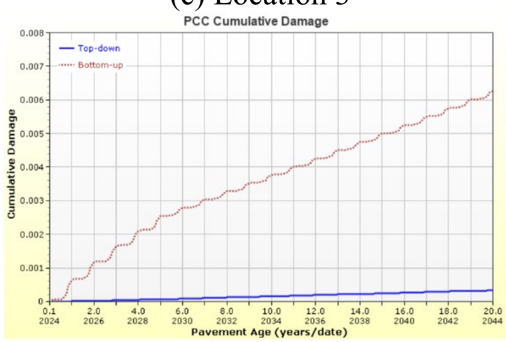

(e) Location 5

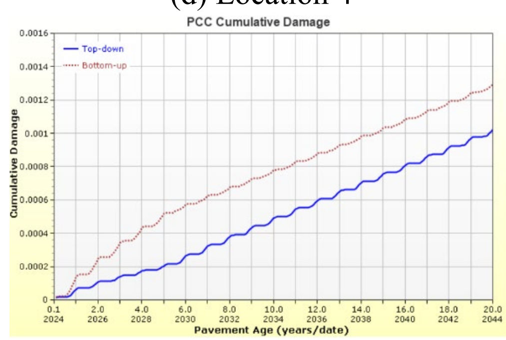

(f) Location 6

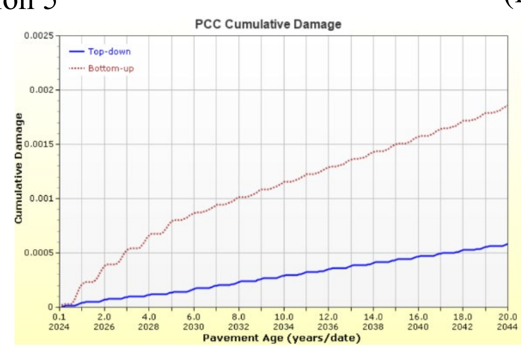

(g) Location 7

Figure 5.19. The proportion of bottom-up and top-down cracking (8" slab thickness)

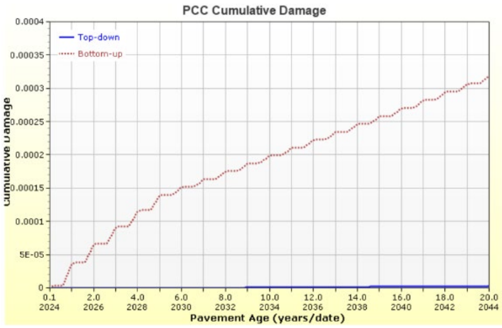

(a) Location 1

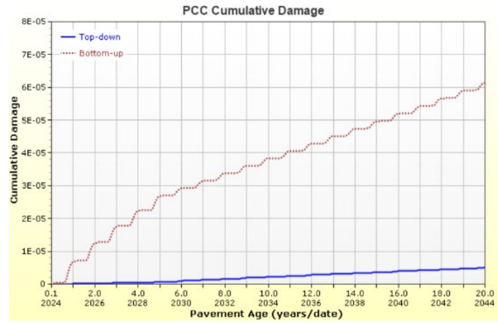

(b) Location 2

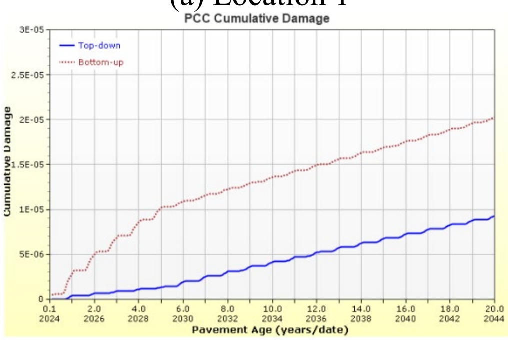

(c) Location 3

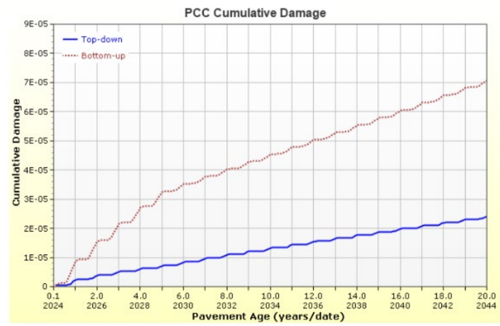

(d) Location 4

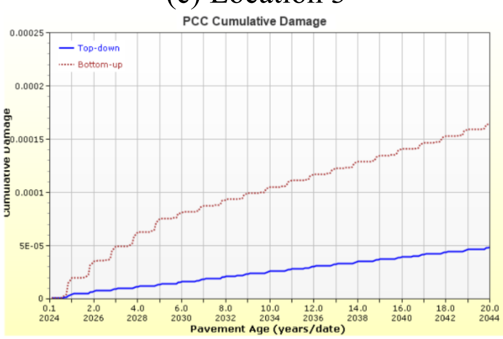

(e) Location 5

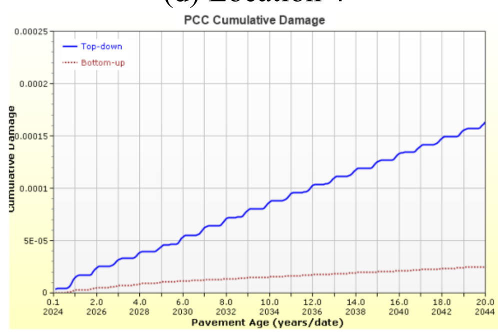

(f) Location 6

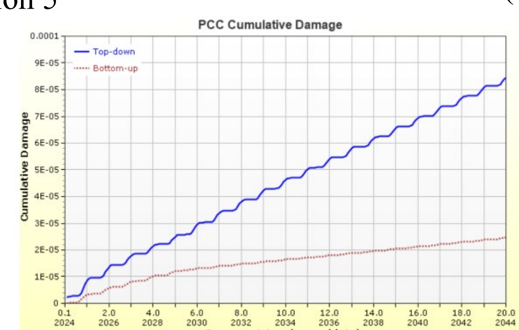

(g) Location 7

Figure 5.20. The proportion of bottom-up and top-down cracking (10" slab thickness)

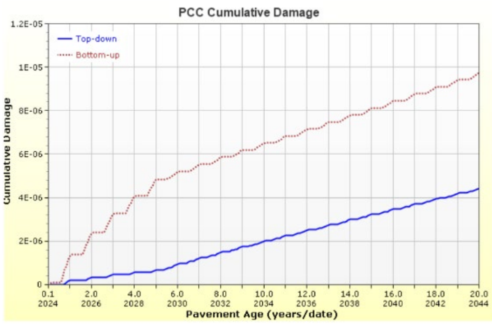

(a) Location 1

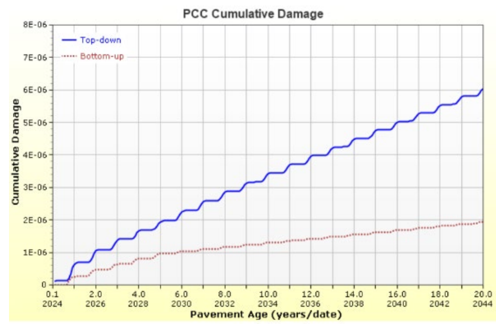

(b) Location 2

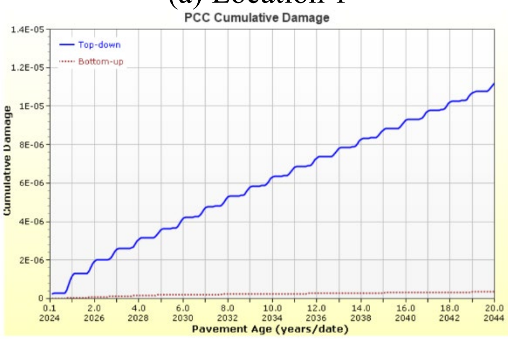

(c) Location 3

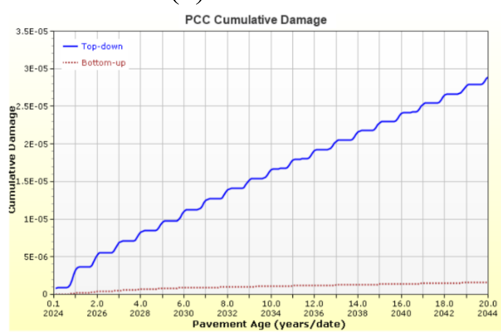

(d) Location 4

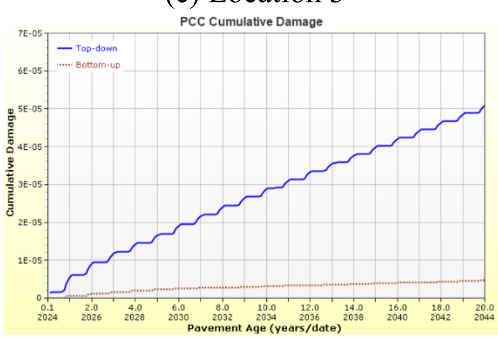

(e) Location 5

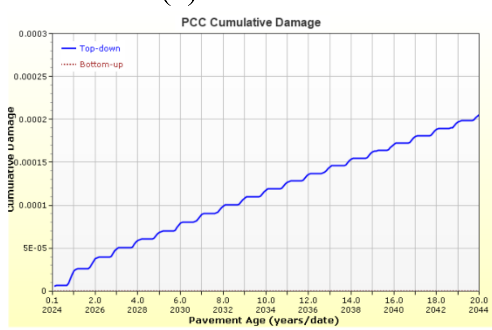

(f) Location 6

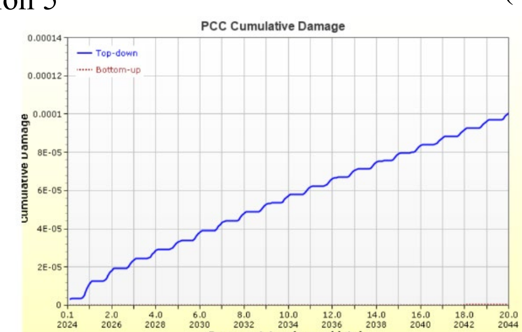

(g) Location 7

Figure 5.21. The proportion of bottom-up and top-down cracking (12" slab thickness)

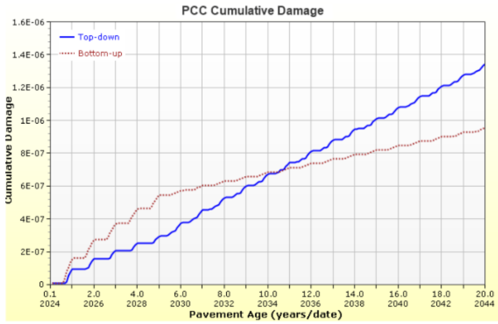

(a) Location 1

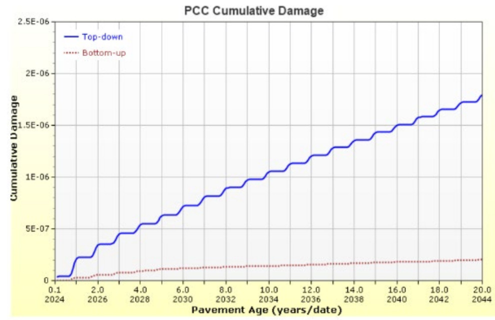

(b) Location 2

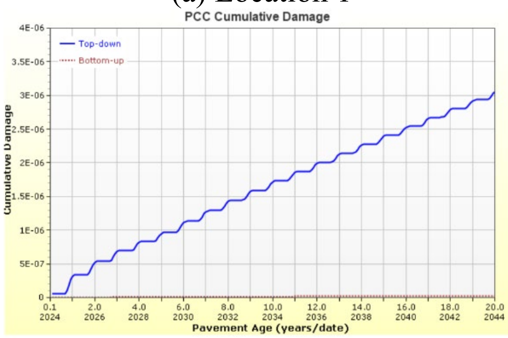

(c) Location 3

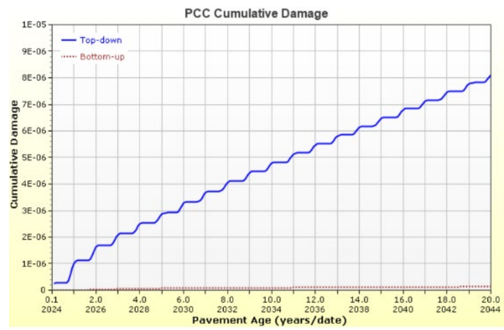

(d) Location 4

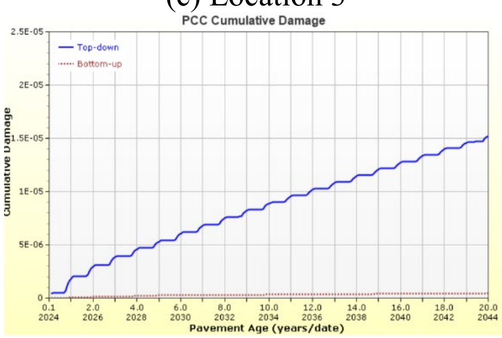

(e) Location 5

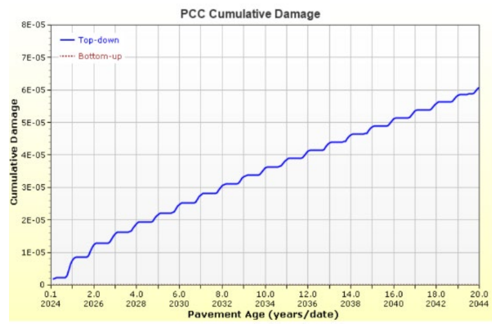

(f) Location 6

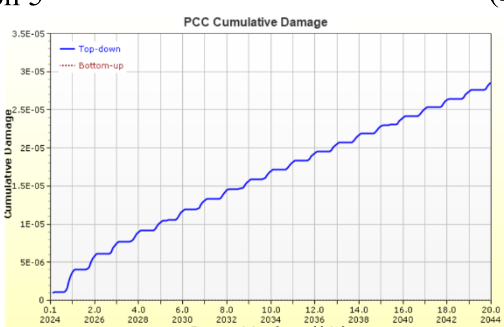

(g) Location 7

Figure 5.22. The proportion of bottom-up and top-down cracking (13" slab thickness)

According to the results in Figures 5.18 - 5.22, thinner slab thicknesses predict more bottom-up cracking, while thicker slab thicknesses have more top-down cracking, which is partially due to different joint spacings. Since the impact of WBTs on bottom-up cracking is much higher, the research team would consider more bottom-up cracking during analysis to avoid pavement performance failure. Table 5.21 presents the determined proportion of bottom-up and top-down cracking used in the following study.

Table 5.21. The determined proportion of bottom-up and top-down cracking

Slab thickness (inch)	**6**	**8**	**10**	**12**	**13**
Proportion of bottom-up cracking (%)	100	90	80	70	60
Proportion of top-down cracking (%)	0	10	20	30	40

With the proportion of bottom-up and top-down cracking in Table 5.21 and CRK (bottom-up; top-down) percent increase results in Tables 5.19 - 5.20, total transverse cracking (TCRACK) percent increase at different WBT proportions is then calculated, as shown in Table 5.22 and Figures 5.23 - 5.24.

Table 5.22. TCRACK percent increase at different WBT proportions

Slab thickness (inch)	**Tire pressure (psi)**	**TCRACK percent increase at different WBT proportions (%)**								
		0%	**4%**	**6%**	**8%**	**10%**	**12%**	**14%**	**20%**	**25%**
6	80	0.00	1.36	2.04	2.73	3.41	4.10	4.79	6.87	8.61
	100	0.00	1.42	2.14	2.85	3.57	4.29	5.01	7.18	9.01
	120	0.00	1.47	2.20	2.94	**3.68**	4.42	5.16	7.41	**9.29**
8	80	0.00	1.11	1.67	2.23	2.78	3.35	3.90	5.60	7.02
	100	0.00	1.16	1.74	2.33	2.91	3.50	4.09	5.86	7.35
	120	0.00	1.21	1.81	2.41	**3.02**	3.63	4.23	6.07	**7.61**
10	80	0.00	0.85	1.28	1.70	2.13	2.55	2.98	4.27	5.35
	100	0.00	0.89	1.34	1.79	2.24	2.69	3.15	4.50	5.64
	120	0.00	0.93	1.39	1.86	**2.32**	2.79	3.26	4.67	**5.85**
12	80	0.00	0.64	0.96	1.28	1.60	1.92	2.25	3.22	4.03
	100	0.00	0.68	1.02	1.36	1.70	2.04	2.38	3.41	4.27
	120	0.00	0.71	1.06	1.41	**1.77**	2.12	2.47	3.55	**4.44**
13	80	0.00	0.53	0.79	1.06	1.33	1.60	1.86	2.67	3.34
	100	0.00	0.56	0.85	1.13	1.42	1.70	1.99	2.84	3.55
	120	0.00	0.59	0.88	1.18	**1.47**	1.77	2.07	2.96	**3.70**

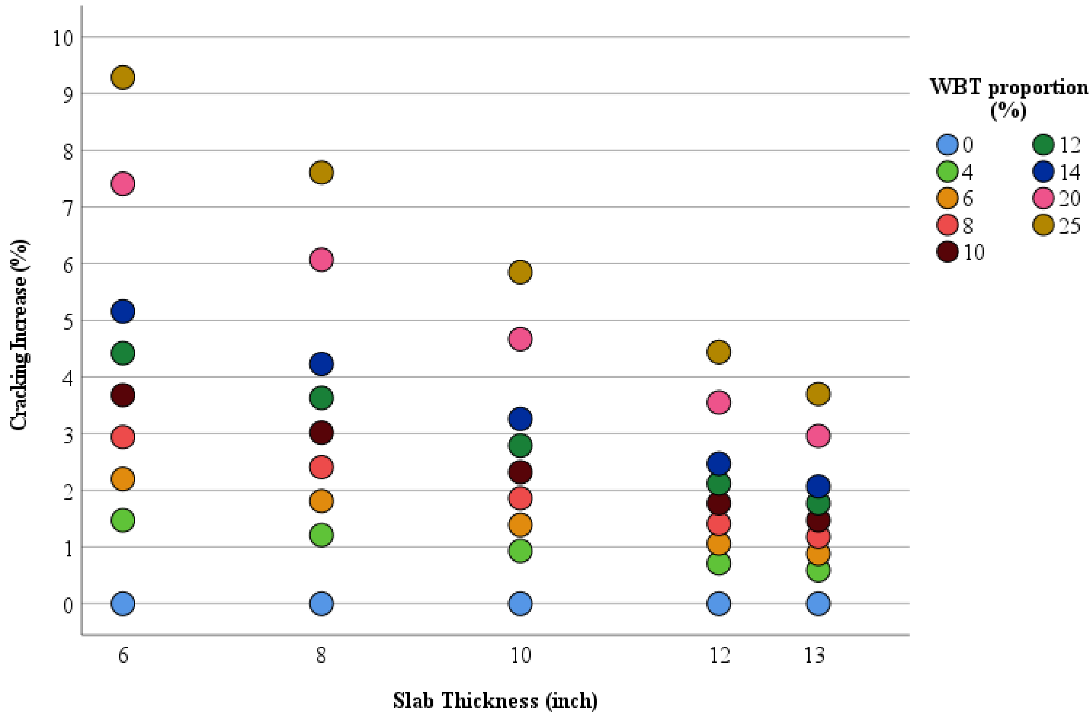

Figure 5.23. Impact of WBT on JPCP transverse cracking at different slab thicknesses

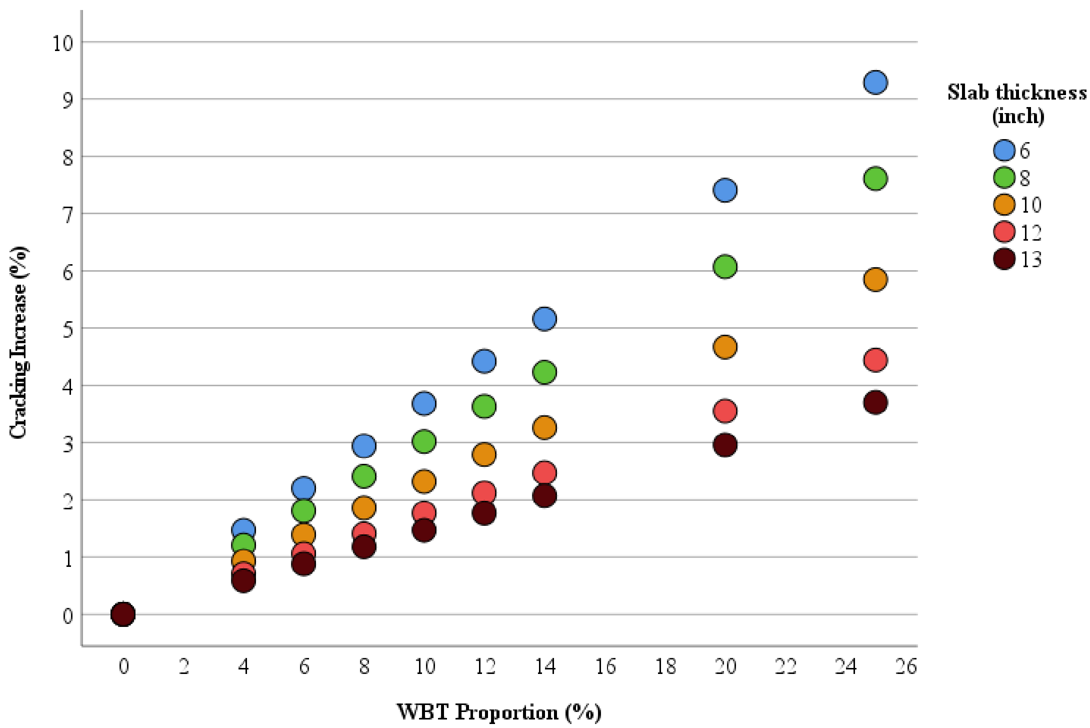

Figure 5.24. Impact of WBT on JPCP transverse cracking at different WBT proportions

According to Table 5.22 under 120 psi tire pressure, the TCRACK with 10% WBT loads ranges from 3.68% (6" slab thickness) to 1.47% (13" slab thickness) larger than that without WBT loads. JPCPs with thicker slabs are less impacted by WBT loads. For a given percentage of WBT loads, higher tire pressure leads to higher cracking increases; however, the difference caused by tire pressure is limited. Based on these research results, the research team predicts that if the proportion of WBT loads in Michigan increased to 25% in the future, the TCRACK would be in the range of 9.29% (6" slab thickness) to 3.70% (13" slab thickness) larger than that without WBT loads. The impact of WBT loads on TCRACK would be significant in the future under these scenarios.

Figures 5.23 – 5.24 prove the impact of WBT loads on JPCP transverse cracking has an apparent relationship with the slab thickness and WBT proportion. With the slab thickness increased, the cracking increase caused by WBT loads decreases approximately linearly.

5.4. Faulting distress analysis

5.4.1. Slab corner deflection analysis with Illislab

When the traffic loads are moved to one edge of the slab, the corner of the slab tends to suffer the most considerable vertical deflection. The deflection difference between the loaded slab and unloaded slab would lead to JPCP faulting distress. Similar to cracking analysis, Illislab software is used to compare the slab corner deflection difference under DT and WBT loads. The variables used in Illislab for faulting analysis are presented in Table 5.23. The slab thickness ranges from 6" to 13", with the dowel diameter and joint spacing corresponding with the slab thickness in section 5.3.1, Figure 5.9.

The transverse load transfer efficiency LTE-y (for joint spacing) ranges from 50% to 90% during the analysis since faulting is extremely sensitive to transverse load transfer capacity. The load edge distance from slab edge ranges from 0 to 18", while the tire pressure for loads is set as 80, 100, and 120 psi in this analysis.

Table 5.23. Variables used in Illislab for faulting analysis

Variables	Values				
Slab thickness (inch)	6	8	10	12	13
Distance from shoulder (inch)	0; 10; 18				
LTE-y (%)	50; 70; 90				
Joint spacing (')	12	12	14	16	16
Tire pressure (psi)	80; 100; 120				

With all parameters set, deflection data at the corner of the slab with different slab thicknesses (6", 8",10",12",13") and load distances are obtained from Illislab, as shown in

Appendix H.

5.4.2. Analysis of WBT impact on faulting

In this section, the research team will process the deflection data in Appendix H to transfer the deflection difference between dual tire loads and WBT loads into faulting difference. According to AASHTO MEPDG 3 [11], the faulting distress is accumulated monthly. The complete process for faulting is quite complex, which should also consider load transfer efficiency change by month. However, for evaluating the impact caused by WBT loads, most material properties and climate conditions variables should be the same except for the deflection difference between under DT load and under WBT load.

Equations (5.4) and (5.5) are introduced in AASHTO MEPDG 3 to calculate the incremental change (monthly) in mean transverse joint faulting.

$$\Delta Fault_i = C_{34} \times (FAULTMAX_{i-1} - Fault_{i-1})^2 \times DE_i \tag{5.4}$$

$$DE_i = \frac{k}{2}(\delta_{loaded}^2 - \delta_{unloaded}^2) \tag{5.5}$$

where:

$\Delta Fault_i$ = Incremental change (monthly) in mean transverse joint faulting in month i, inch

DE = Differential energy, lb/inch

δ_{loaded} = Loaded corner deflection, inch

$\delta_{unloaded}$ = Unloaded corner deflection, inch

As shown in equations (5.4) and (5.5), the $\delta^2{}_{loaded}$ - $\delta^2{}_{loaded}$ value is critical in faulting increment values, so the value of $\delta^2{}_{loaded}$ - $\delta^2{}_{loaded}$ (represented as F_δ) was calculated in this research to assess the difference between DT and WBT loads.

The value of F_δ, as well as the ratio of F_δ between under WBT loads ($F_{\delta\text{-WBT}}$) and DT loads ($F_{\delta\text{-DT}}$) under different LTE-ys, can be calculated considering the distribution of load distance from the edge. The results are shown in Tables 5.24 - 5.26.

Table 5.24. F_δ value in different slab thicknesses (LTE-y = 50%)

Slab thickness (inch)	Tire pressure (psi)	F_δ under DT load	F_δ under WBT load	$F_{\delta\text{-WBT}}$ / $F_{\delta\text{-DT}}$
6	80	2.52E-04	3.58E-04	1.42
	100	2.67E-04	3.86E-04	1.44
	120	2.79E-04	4.07E-04	1.46
8	80	2.02E-04	2.61E-04	1.29
	100	2.12E-04	2.76E-04	1.31
	120	2.19E-04	2.88E-04	1.32
10	80	1.65E-04	1.98E-04	1.20
	100	1.71E-04	2.08E-04	1.21
	120	1.76E-04	2.15E-04	1.22
12	80	1.38E-04	1.58E-04	1.14
	100	1.43E-04	1.65E-04	1.15
	120	1.47E-04	1.70E-04	1.16
13	80	1.28E-04	1.43E-04	1.12
	100	1.32E-04	1.49E-04	1.13
	120	1.35E-04	1.53E-04	1.13

Table 5.25. F_δ value in different slab thicknesses (LTE-y = 70%)

Slab thickness (inch)	Tire pressure (psi)	F_δ under DT load	F_δ under WBT load	$F_{\delta\text{-WBT}}$ / $F_{\delta\text{-DT}}$
6	80	1.02E-04	1.60E-04	1.57
	100	1.09E-04	1.74E-04	1.59
	120	1.15E-04	1.85E-04	1.61
8	80	9.18E-05	1.29E-04	1.40
	100	9.68E-05	1.37E-04	1.42
	120	1.01E-04	1.44E-04	1.43
10	80	7.91E-05	1.03E-04	1.30
	100	8.26E-05	1.08E-04	1.31
	120	8.53E-05	1.13E-04	1.32
12	80	6.82E-05	8.34E-05	1.22
	100	7.07E-05	8.73E-05	1.23
	120	7.27E-05	9.03E-05	1.24
13	80	6.37E-05	7.60E-05	1.19
	100	6.59E-05	7.94E-05	1.20
	120	6.76E-05	8.19E-05	1.21

Table 5.26. F_δ value in different slab thicknesses (LTE-y = 90%)

Slab thickness (inch)	Tire pressure (psi)	F_δ under DT load	F_δ under WBT load	$F_{\delta\text{-WBT}} / F_{\delta\text{-DT}}$
6	80	1.51E-05	3.00E-05	1.98
	100	1.67E-05	3.34E-05	2.00
	120	1.80E-05	3.61E-05	2.01
8	80	1.68E-05	2.85E-05	1.69
	100	1.81E-05	3.09E-05	1.71
	120	1.90E-05	3.29E-05	1.73
10	80	1.71E-05	2.60E-05	1.52
	100	1.81E-05	2.78E-05	1.54
	120	1.88E-05	2.92E-05	1.55
12	80	1.64E-05	2.31E-05	1.41
	100	1.71E-05	2.44E-05	1.43
	120	1.77E-05	2.55E-05	1.44
13	80	1.58E-05	2.17E-05	1.37
	100	1.65E-05	2.29E-05	1.39
	120	1.70E-05	2.38E-05	1.39

As shown in Tables 5.24 - 5.26, LTE-y significantly impacts the F_δ. Pavement ME output files on the JPCP pavement structure show that 90% is the closest value to practice design.

The above analysis did not consider the existence of the temperature gradient of the slab. AASHTO MEPDG 3 introduced that the faulting will be more severe under negative temperature gradient. However, whether the negative temperature gradient has a similar impact extent on WBT and DT loads is still unclear. So, the research team then conducted Illislab with a temperature gradient from -10°F to -30°F to check if the temperature gradient would impact the value of $F_{\delta\text{-WBT}} / F_{\delta\text{-DT}}$.

The deflection at the corner of the slab under various temperature gradients is shown in Tables 5.27 - 5.31.

Table 5.27. Deflection at the corner of the slab at different temperature gradients (6" slab thickness)

Variables		Deflection (inch)			
		Loaded slab		Unloaded slab	
Distance from shoulder joint (inch)	Temperature gradient (°F)	Under DT load	Under WBT tire load (+20% tire pressure)	Under DT load	Under WBT tire load (+20% tire pressure)
0	0	0.027395	0.030357	0.024767	0.026330
	-10	0.019002	0.021959	0.016373	0.017932
	-20	0.007345	0.010511	0.004705	0.006473
	-30	-0.006496	-0.002613	-0.009181	-0.006710
10	0	0.019810	0.022187	0.019314	0.021203
	-10	0.011416	0.013792	0.010919	0.012806
	-20	-0.001136	0.001680	-0.001649	0.000679
	-30	-0.017433	-0.013617	-0.017970	-0.014661
18	0	0.015111	0.017074	0.015193	0.017033
	-10	0.006704	0.008678	0.006783	0.008635
	-20	-0.007120	-0.004390	-0.007057	-0.004454
	-30	-0.025385	-0.021746	-0.025334	-0.021831

Table 5.28. Deflection at the corner of the slab at different temperature gradients (8" slab thickness)

Variables		Deflection (inch)			
		Loaded slab		Unloaded slab	
Distance from shoulder joint (inch)	Temperature gradient (°F)	Under DT load	Under WBT tire load (+20% tire pressure)	Under DT load	Under WBT tire load (+20% tire pressure)
0	0	0.020862	0.022452	0.018450	0.019038
	-10	0.013011	0.014597	0.010598	0.011183
	-20	0.001088	0.002771	-0.001326	-0.000643
	-30	-0.012476	-0.010497	-0.014921	-0.013958
10	0	0.015997	0.017338	0.015209	0.016049
	-10	0.008141	0.009480	0.007352	0.008192
	-20	-0.004313	-0.002777	-0.005110	-0.004075
	-30	-0.019157	-0.017300	-0.019965	-0.018620
18	0	0.012837	0.013974	0.012675	0.013589
	-10	0.004959	0.006106	0.004797	0.005720
	-20	-0.008146	-0.006721	-0.008315	-0.007117
	-30	-0.023947	-0.022220	-0.024121	-0.022626

Table 5.29. Deflection at the corner of the slab at different temperature gradients (10" slab thickness)

Variables		Deflection (inch)			
		Loaded slab		Unloaded slab	
Distance from shoulder joint (inch)	Temperature gradient (°F)	Under DT load	Under WBT tire load (+20% tire pressure)	Under DT load	Under WBT tire load (+20% tire pressure)
0	0	0.017027	0.017971	0.014838	0.015042
	-10	0.009876	0.010819	0.007687	0.007891
	-20	-0.002631	-0.001639	-0.004824	-0.004572
	-30	-0.016703	-0.015610	-0.018916	-0.018573
10	0	0.013586	0.014406	0.012643	0.013017
	-10	0.006426	0.007248	0.005483	0.005859
	-20	-0.006456	-0.005544	-0.007405	-0.006943
	-30	-0.021282	-0.020258	-0.022239	-0.021671
18	0	0.011261	0.011968	0.010901	0.011354
	-10	0.004086	0.004798	0.003726	0.004183
	-20	-0.009193	-0.008363	-0.009558	-0.008985
	-30	-0.024600	-0.023657	-0.024968	-0.024287

Table 5.30. Deflection at the corner of the slab at different temperature gradients (12" slab thickness)

Variables		Deflection (inch)			
		Loaded slab		Unloaded slab	
Distance from shoulder joint (inch)	Temperature gradient (°F)	Under DT load	Under WBT tire load (+20% tire pressure)	Under DT load	Under WBT tire load (+20% tire pressure)
0	0	0.014475	0.015078	0.012496	0.012535
	-10	0.008307	0.008909	0.006328	0.006367
	-20	-0.004522	-0.003890	-0.006507	-0.006441
	-30	-0.018892	-0.018246	-0.020890	-0.020814
10	0	0.011886	0.012422	0.010880	0.011033
	-10	0.005711	0.006249	0.004706	0.004860
	-20	-0.007371	-0.006790	-0.008383	-0.008188
	-30	-0.022202	-0.021594	-0.023218	-0.023001
18	0	0.010083	0.010550	0.009589	0.009805
	-10	0.003900	0.004369	0.003406	0.003624
	-20	-0.009429	-0.008906	-0.009927	-0.009657
	-30	-0.024624	-0.024067	-0.025123	-0.024823

Table 5.31. Deflection at the corner of the slab at different temperature gradients (13" slab thickness)

Variables		Deflection (inch)			
		Loaded slab		Unloaded slab	
Distance from shoulder joint (inch)	Temperature gradient (°F)	Under DT load	Under WBT tire load (+20% tire pressure)	Under DT load	Under WBT tire load (+20% tire pressure)
0	0	0.013510	0.014003	0.011627	0.011623
	-10	0.008235	0.008727	0.006352	0.006348
	-20	-0.004150	-0.003641	-0.006037	-0.006025
	-30	-0.017747	-0.017231	-0.019643	-0.019629
10	0	0.011223	0.011666	0.010208	0.010297
	-10	0.005945	0.006388	0.004930	0.005019
	-20	-0.006619	-0.006149	-0.007636	-0.007523
	-30	-0.020560	-0.020076	-0.021582	-0.021456
18	0	0.009611	0.009998	0.009071	0.009216
	-10	0.004328	0.004716	0.003789	0.003934
	-20	-0.008408	-0.007987	-0.008949	-0.008773
	-30	-0.022627	-0.022185	-0.023169	-0.022974

As shown in Tables 5.27 - 5.31, the slab would curve upward under negative temperature gradients, which would provide incorrect values when calculating F_δ (δ^2_{loaded} - δ^2_{loaded}), as some slab deflection at the corners would be negative. This is because Illislab outputs report overall deflections from a flat slab condition when reporting deflections. In reality, the slab would already show deflections due to curling even without external loading. The deflection required from the F_δ analysis should be relative to the unloaded condition of the slab. In order to eliminate the negative values and make the following analysis possible, the research team then calculated the slab upward deflection values for different temperature gradients and slab thicknesses without loads, as shown in Table 5.32.

Table 5.32. Deflection at the corner of the slab caused by temperature without loads

Variables		Upward slab deflection without loads (inch)
Slab thickness (inch)	**Temperature gradient (°F)**	
6	0	0
	-10	0.012058
	-20	0.038510
	-30	0.069347
8	0	0
	-10	0.009558
	-20	0.029493
	-30	0.052212
10	0	0
	-10	0.008100
	-20	0.026299
	-30	0.047192
12	0	0
	-10	0.006677
	-20	0.023819
	-30	0.043755
13	0	0
	-10	0.005580
	-20	0.021327
	-30	0.039515

The upward slab deflection values in Table 5.32 are added to representative cases in Tables 5.27 - 5.31, and then negative values caused by temperature gradient could be eliminated, while continuing to consider the influence of temperature gradient. The $F_{\delta\text{-WBT}}$ / $F_{\delta\text{-DT}}$ values in different temperature gradients are then calculated as shown in Tables 5.33 - 5.37 and Figures 5.25 - 5.27.

Table 5.33. F_δ value in different temperature gradients (6" slab thickness)

Distance from shoulder joint (inch)	Temperature gradient (°F)	F_δ under DT load	F_δ under WBT load	$F_{\delta\text{-WBT}} / F_{\delta\text{-DT}}$
0	0	1.37E-04	2.28E-04	1.665
	-10	1.56E-04	2.58E-04	1.648
	-20	2.35E-04	3.80E-04	1.614
	-30	3.30E-04	5.30E-04	1.605
10	0	1.94E-05	4.27E-05	2.200
	-10	2.31E-05	5.00E-05	2.166
	-20	3.81E-05	7.95E-05	2.086
	-30	5.55E-05	1.15E-04	2.078
18	0	-2.48E-06	1.40E-06	-0.563
	-10	-2.97E-06	1.78E-06	-0.600
	-20	-3.96E-06	4.36E-06	-1.102
	-30	-4.49E-06	8.08E-06	-1.802

Table 5.34. F_δ value in different temperature gradients (8" slab thickness)

Distance from shoulder joint (inch)	Temperature gradient (°F)	F_δ under DT load	F_δ under WBT load	$F_{\delta\text{-WBT}} / F_{\delta\text{-DT}}$
0	0	9.48E-05	1.42E-04	1.494
	-10	1.03E-04	1.53E-04	1.487
	-20	1.42E-04	2.09E-04	1.471
	-30	1.88E-04	2.77E-04	1.470
10	0	2.46E-05	4.30E-05	1.750
	-10	2.73E-05	4.74E-05	1.735
	-20	3.95E-05	6.77E-05	1.713
	-30	5.28E-05	9.04E-05	1.714
18	0	4.13E-06	1.06E-05	2.568
	-10	4.68E-06	1.19E-05	2.554
	-20	7.19E-06	1.79E-05	2.488
	-30	9.81E-06	2.42E-05	2.467

Table 5.35. F_δ value in different temperature gradients (10" slab thickness)

Distance from shoulder joint (inch)	Temperature gradient (°F)	F_δ under DT load	F_δ under WBT load	$F_{\delta\text{-WBT}} / F_{\delta\text{-DT}}$
0	0	6.98E-05	9.67E-05	1.386
	-10	7.39E-05	1.02E-04	1.383
	-20	9.90E-05	1.36E-04	1.374
	-30	1.30E-04	1.78E-04	1.372
10	0	2.47E-05	3.81E-05	1.540
	-10	2.65E-05	4.07E-05	1.536
	-20	3.68E-05	5.61E-05	1.526
	-30	4.87E-05	7.41E-05	1.523
18	0	7.98E-06	1.43E-05	1.795
	-10	8.64E-06	1.55E-05	1.792
	-20	1.24E-05	2.19E-05	1.775
	-30	1.65E-05	2.93E-05	1.774

Table 5.36. F_δ value in different temperature gradients (12" slab thickness)

Distance from shoulder joint (inch)	Temperature gradient (°F)	F_δ under DT load	F_δ under WBT load	$F_{\delta\text{-WBT}} / F_{\delta\text{-DT}}$
0	0	5.34E-05	7.02E-05	1.316
	-10	5.54E-05	7.28E-05	1.314
	-20	7.27E-05	9.52E-05	1.310
	-30	9.54E-05	1.24E-04	1.305
10	0	2.29E-05	3.26E-05	1.423
	-10	2.39E-05	3.40E-05	1.422
	-20	3.23E-05	4.57E-05	1.415
	-30	4.28E-05	6.04E-05	1.412
18	0	9.72E-06	1.52E-05	1.560
	-10	1.02E-05	1.59E-05	1.558
	-20	1.41E-05	2.18E-05	1.550
	-30	1.88E-05	2.92E-05	1.549

Table 5.37. F_δ value in different temperature gradients (13" slab thickness)

Distance from shoulder joint (inch)	Temperature gradient (°F)	F_δ under DT load	F_δ under WBT load	$F_{\delta\text{-WBT}}$ / $F_{\delta\text{-DT}}$
0	0	4.73E-05	6.10E-05	1.289
	-10	4.85E-05	6.24E-05	1.287
	-20	6.13E-05	7.86E-05	1.284
	-30	7.89E-05	1.01E-04	1.281
10	0	2.18E-05	3.01E-05	1.382
	-10	2.24E-05	3.09E-05	1.381
	-20	2.89E-05	3.98E-05	1.379
	-30	3.77E-05	5.17E-05	1.373
18	0	1.01E-05	1.50E-05	1.489
	-10	1.04E-05	1.55E-05	1.491
	-20	1.37E-05	2.04E-05	1.487
	-30	1.80E-05	2.67E-05	1.484

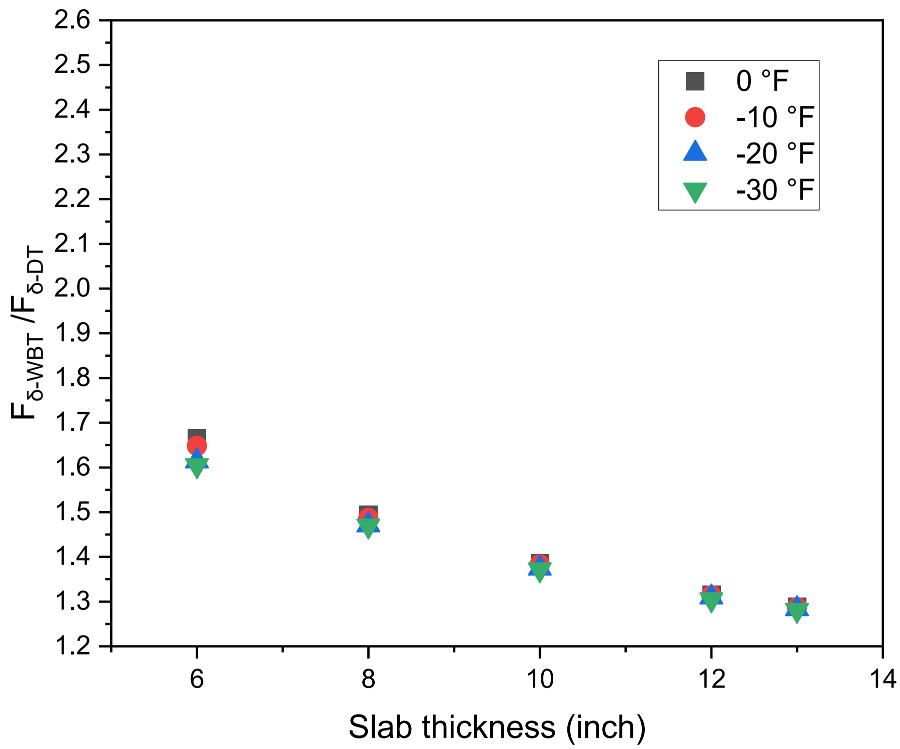

Figure 5.25. $F_{\delta\text{-WBT}}$ / $F_{\delta\text{-DT}}$ values (load edge 0" from shoulder joint)

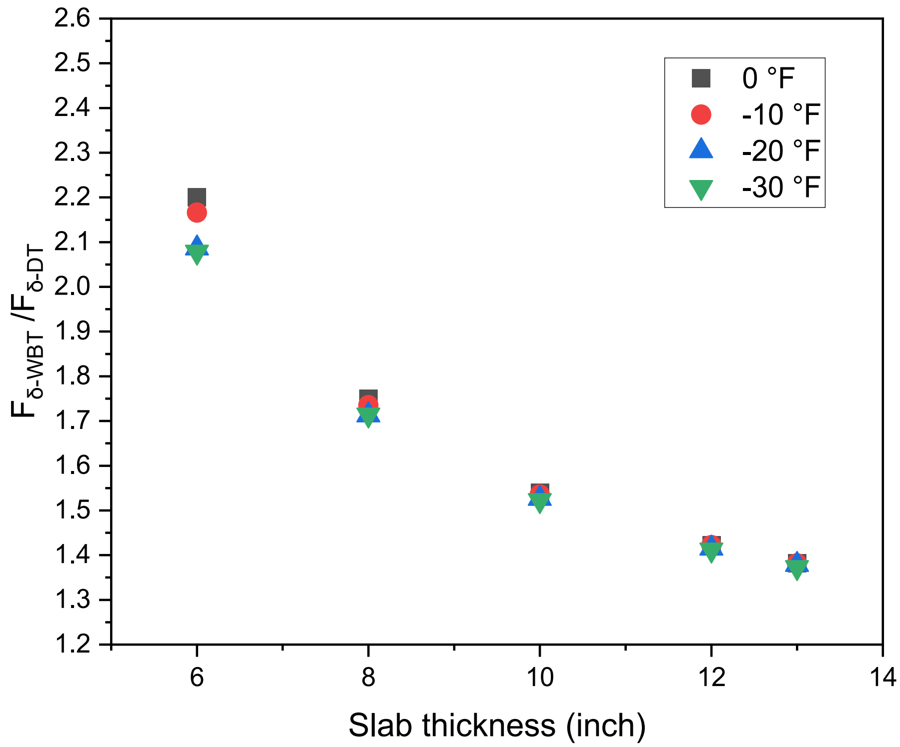

Figure 5.26. $F_{\delta\text{-WBT}}$ / $F_{\delta\text{-DT}}$ values (load edge 10" from shoulder joint)

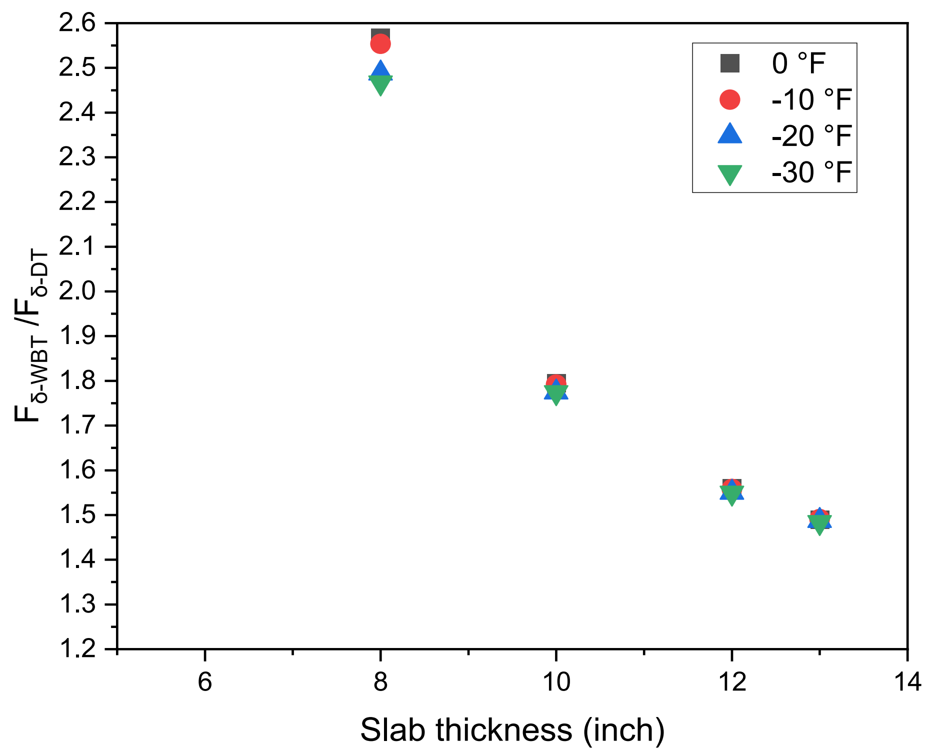

Figure 5.27. $F_{\delta\text{-WBT}}$ / $F_{\delta\text{-DT}}$ (load edge 18" from shoulder joint)

Figures 5.25 - 5.27 prove that in most cases, although both $F_{\delta\text{-WBT}}$ and $F_{\delta\text{-DT}}$ values would be higher in lower temperature gradients, the ratio between them ($F_{\delta\text{-WBT}}$ / $F_{\delta\text{-DT}}$) does not change significantly. This indicates that the existence of the negative temperature gradient will not change the WBT impact extent on faulting. In most cases, when the temperature gradient is 0°F, the value of $F_{\delta\text{-WBT}}$ / $F_{\delta\text{-DT}}$ is the largest. The research team chose F_δ under 0°F, 90% LTE-y as the basis for calculating different WBT proportions, as shown in Table 5.38.

Table 5.38. F_δ value at different WBT proportions

Slab thickness (inch)	Tire pressure (psi)	F_δ at different WBT proportions ($\times 10^{-5}$, %)								
		0%	4%	6%	8%	10%	12%	14%	20%	25%
6	80	1.51	1.57	1.60	1.63	1.66	1.69	1.72	1.81	1.88
	100	1.67	1.74	1.77	1.80	1.84	1.87	1.90	2.00	2.09
	120	1.80	1.87	1.91	1.94	1.98	2.02	2.05	2.16	2.25
8	80	1.68	1.73	1.75	1.77	1.80	1.82	1.84	1.91	1.97
	100	1.81	1.86	1.89	1.91	1.94	1.96	1.99	2.07	2.13
	120	1.90	1.96	1.98	2.01	2.04	2.07	2.09	2.18	2.25
10	80	1.71	1.75	1.76	1.78	1.80	1.82	1.83	1.89	1.93
	100	1.81	1.85	1.87	1.89	1.91	1.93	1.95	2.00	2.05
	120	1.88	1.92	1.94	1.96	1.98	2.00	2.03	2.09	2.14
12	80	1.64	1.67	1.68	1.69	1.71	1.72	1.73	1.77	1.81
	100	1.71	1.74	1.75	1.77	1.78	1.80	1.81	1.86	1.89
	120	1.77	1.80	1.82	1.83	1.85	1.86	1.88	1.93	1.97
13	80	1.58	1.60	1.62	1.63	1.64	1.65	1.66	1.70	1.73
	100	1.65	1.68	1.69	1.70	1.71	1.73	1.74	1.78	1.81
	120	1.70	1.73	1.74	1.75	1.77	1.78	1.80	1.84	1.87

Then, considering the reliability issue, Equation (5.6) can transform JPCP faulting under 50% reliability ($Faulting_{50\%}$) into faulting under 95% reliability ($Faulting_{95\%}$) by using the average rutting, standard error of the prediction (S_e), and Z-value for the 95% confidence level one-tailed test. According to the back calculation of equation (5.6), the $Faulting_{95\%}$ would be close to the Michigan threshold of 0.125” if the mean fatigue cracking parameter $Faulting_{50\%}$ is near 0.068”.

$$Faulting_{95\%} = Faulting_{50\%} + S_e \times Z_{95} \tag{5.6}$$

where:

S_e is the standard error, and $S_e = 0.07162 \times \mathrm{Faulting}_{50\%}{}^{0.368} + 0.00806$; Z_{95} is the Z-value for the 95%-confidence level one-tailed test, which equals 1.65.

The faulting increase caused by WBT loads in 95% reliability would be approximately 0.54 (=0.068”/0.125”) times the faulting increase caused by WBT loads in 50% reliability.

The faulting percent increase with 0°F temperature gradient and 90% LTE-y under 95%

reliability at different WBT proportions is calculated based on Table 5.38, as presented in Table 5.39 and Figures 5.28 - 5.29.

Table 5.39. Faulting percent increase at different WBT proportions

Slab thickness (inch)	Tire pressure (psi)	Faulting percent increase at different WBT proportions (%)								
		0%	4%	6%	8%	10%	12%	14%	20%	25%
6	80	0.00	2.13	3.20	4.26	5.33	6.39	7.46	10.66	13.32
	100	0.00	2.16	3.24	4.32	5.40	6.48	7.56	10.80	13.50
	120	0.00	2.17	3.26	4.34	**5.43**	6.52	7.60	10.86	**13.58**
8	80	0.00	1.51	2.26	3.01	3.76	4.51	5.27	7.52	9.40
	100	0.00	1.53	2.29	3.06	3.82	4.58	5.35	7.64	9.55
	120	0.00	1.58	2.37	3.16	**3.95**	4.74	5.53	7.90	**9.88**
10	80	0.00	1.12	1.68	2.25	2.81	3.38	3.94	5.62	7.03
	100	0.00	1.16	1.74	2.32	2.89	3.47	4.05	5.79	7.24
	120	0.00	1.19	1.79	2.39	**2.99**	3.59	4.18	5.97	**7.47**
12	80	0.00	0.88	1.32	1.77	2.21	2.65	3.09	4.41	5.51
	100	0.00	0.92	1.38	1.85	2.31	2.76	3.23	4.61	5.76
	120	0.00	0.95	1.43	1.91	**2.38**	2.86	3.33	4.76	**5.95**
13	80	0.00	0.80	1.21	1.61	2.01	2.42	2.82	4.03	5.04
	100	0.00	0.84	1.26	1.67	2.10	2.51	2.93	4.19	5.24
	120	0.00	0.86	1.30	1.73	**2.16**	2.59	3.02	4.32	**5.40**

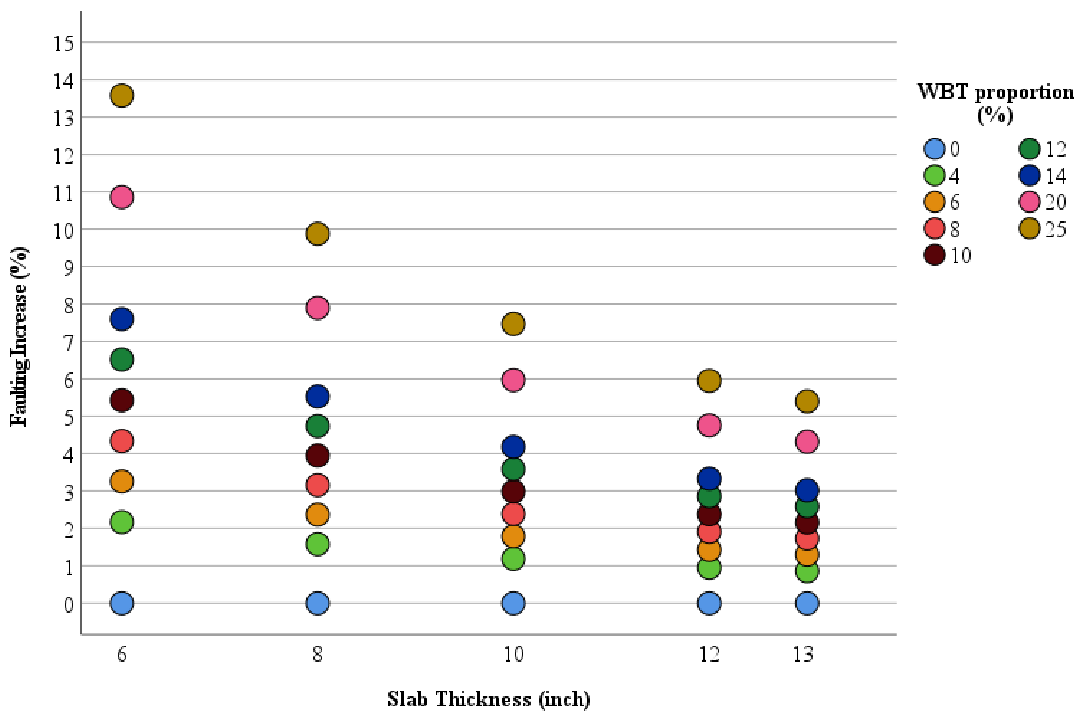

Figure 5.28. Impact of WBT on JPCP faulting at different slab thicknesses

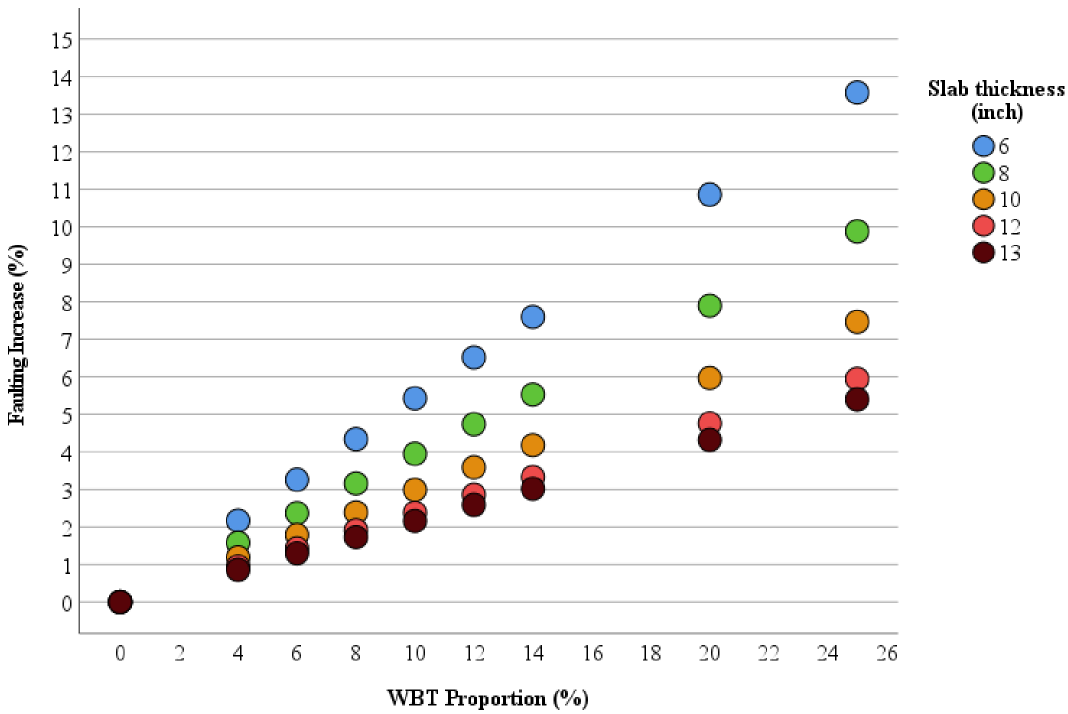

Figure 5.29. Impact of WBT on JPCP faulting at different WBT proportions

According to Table 5.39. the faulting with 10% WBT loads ranges from 5.43% (6" slab thickness) to 2.16% (13" slab thickness) larger than under DT loads using the standard 120 psi tire pressure. Therefore, the impact of WBT loads on JPCP faulting distress is much higher than on transverse cracking distress development.

However, pavements with thicker slab thickness are less impacted by WBT loads. For a given percentage of WBT loads, higher tire pressure leads to higher cracking increases; however, the difference caused by tire pressure is insignificant. The research team predicts that if the proportion of WBT loads in Michigan increases to 25% in the future, the faulting percent increase caused by WBT loads would be in the range of 13.58% (6" slab thickness) to 5.40% (13" slab thickness). Figures 5.28 – 5.29 prove the impact of WBT loads on JPCP faulting has a negative relationship with the slab thickness and a positive relationship with WBT proportion.

5.5. IRI impact analysis

5.5.1. IRI analysis method introduction

The International Roughness Index (IRI), which indicates the smoothness of the pavement, is also a criterion for JPCP pavement design. Using the process developed for the Pavement ME software, the IRI value for JPCPs is predicted with equation (5.7).

$$IRI = IRI_0 + C1 * CRK + C2 * SPALL + C3 * TFAULT + C4 * SF \quad (5.7)$$

where:

IRI = Predicted IRI, in/mile

IRI_0 = Initial smoothness measured as IRI, in/mile

CRK = Percent slabs with transverse cracks

SPALL= Percentage of joints with spalling

TFAULT= Total joint faulting cumulated per mile, inch

C1=0.8203; C2= 0.4417; C3=1.4929; C4=25.24; SF=Site factor

Spalling is related to age and site factor (SF), as introduced in AASHTO MEPDG 3; SF is related to the subgrade's age, climate, and gradation. According to the Guide for ME Design-Part 3 Design analysis[33], the effects of changes in crucial distresses and site variables on JPCP smoothness are shown in Figure 5.30.

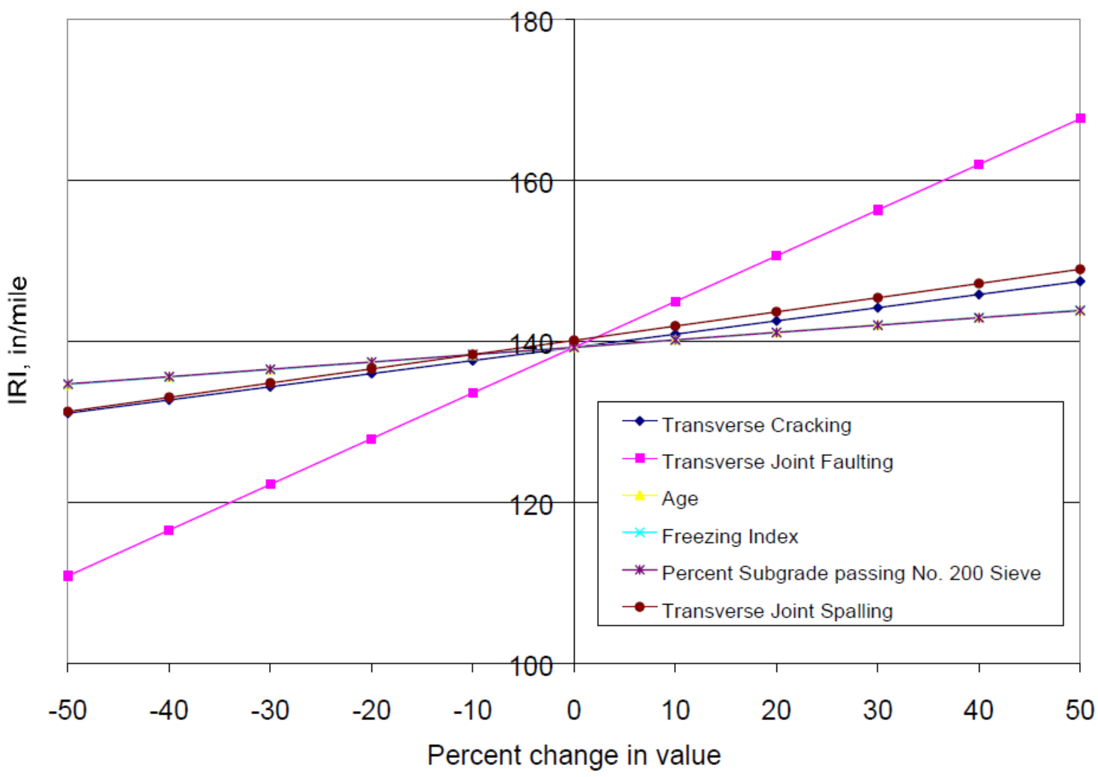

Figure 5.30. The effects of changes in key distresses and site variables on JPCP smoothness [33]

As shown in Figure 5.30, cracking, spalling, and faulting are the most critical factors for IRI; however, spalling is non-load-related distress that would not be included in the WBT loads' impact analysis. The increase of cracking and faulting in Figure 5.30 has a linear relationship with IRI, which indicates that the impact of WBT loads on cracking and faulting could be transformed into the effect on IRI. Similar to flexible pavement, the research team then established the relationship between IRI and other distress from Pavement ME outputs. According to the Pavement ME analysis results in Tables 5.5 - 5.6 from section 5.2.2, the IRI prediction equation (95% reliability) with the format of $IRI = a{\cdot}x + b{\cdot}y + c$ (x is cracking, y is faulting) was established by multiple regression, as shown in Figure 5.31.

Multiple Regression (9/8/2022 20:08:27)

Notes

Input Data

Masked Data - Values Excluded from Computations

Bad Data (missing values) -- Values that are invalid and thus not used in computations

Parameters

		Value	Standard Error	t-Value	Prob>|t|
C	Intercept	110.52848	3.35846	32.91051	3.99344E-32
	A	0.96262	0.15796	6.09404	2.66841E-7
	B	596.83209	32.7426	18.228	7.57344E-22

Standard Error was scaled with square root of reduced Chi-Sqr.

Statistics

	C
Number of Points	46
Degrees of Freedom	43
Residual Sum of Squares	2056.16419
R-Square (COD)	0.88657
Adj. R-Square	0.88129

Summary

	Intercept		A		B		Statistics
	Value	Standard Error	Value	Standard Error	Value	Standard Error	Adj. R-Square
C	110.52848	3.35846	0.96262	0.15796	596.83209	32.7426	0.88129

ANOVA

		DF	Sum of Squares	Mean Square	F Value	Prob>F
C	Model	2	16070.5767	8035.28835	168.03979	0
	Error	43	2056.16419	47.81777		
	Total	45	18126.7409			

At the 0.05 level, the fitting function is significantly better than the function y=constant.

Figure 5.31. IRI multiple regression result

According to Figure 5.31, equation 5.8 could be obtained.

$$IRI = 110.53 + 0.96x + 596.83y \tag{5.8}$$

where:

x is transverse cracking value, %; y is faulting, inch; IRI value is in 95% reliability.

The following equations could be obtained by applying different IRI (IRI_a, IRI_b), cracking (x_a, x_b), and faulting (y_a,y_b) values to equation (5.8).

$$IRI_a = 110.53 + 0.96x_a + 596.83y_a \tag{5.9}$$

$$IRI_b = 110.53 + 0.96x_b + 596.83y_b \quad (5.10)$$

$$\frac{IRI_b - IRI_a}{IRI_a} = \frac{0.96(x_b - x_a)}{IRI_a} + \frac{596.83(y_b - y_a)}{IRI_a} \quad (5.11)$$

Then, the equation with the dependent variable of IRI percent change ($P_{IRI}=\frac{IRI_b-IRI_a}{IRI_a}$) in value and independent variables of percentage change of cracking and faulting in value ($P_{Cracking}=\frac{x_b-x_a}{x_a}$); $P_{Faulting}=\frac{y_b-y_a}{y_a}$) could be established, as shown in equation (5.12).

$$P_{IRI} = 0.96\frac{x_a}{IRI_a}P_{Cracking} + 596.83\frac{y_a}{IRI_a}P_{Faulting} \quad (5.12)$$

Assuming that $m = 0.96\frac{x_a}{IRI_a}$ and $n = 596.83\frac{y_a}{IRI_a}$, m and n values for different pavement ME analysis scenarios could be calculated. Some examples are shown in Table 5.40.

Table 5.40. Factors of IRI percent change equation

NO.	Percent slab cracking (x_a)	Faulting in inches (y_a)	IRI_a (inch/mile)	m	n
1	33.96	0.04	166.47	0.20	0.14
2	12.83	0.04	150.3	0.08	0.16
3	6.13	0.05	148.09	0.04	0.20
4	8.71	0.05	143.24	0.06	0.21
5	4.44	0.05	143.24	0.03	0.21
6	2.79	0.05	143.85	0.02	0.21
7	1.23	0.1	179.72	0.01	0.33
8*	*7.5*	*0.0625*	*155.03*	*0.05*	*0.24*

As shown in NO.1 ~ 7 in Table 5.40, m and n are highly related to the specific distress values (x_a and y_a). The research team decided to use the half design threshold (shown in NO.8 in Table 5.40) to calculate the Factors of the IRI percent change equation, which is presented in equation 5.13.

$$P_{IRI} = 0.05\ P_{Cracking} + 0.24\ P_{Faulting} \quad (5.13)$$

5.5.2. Analysis results of WBT impact on IRI of JPCP pavement

According to the percent increase of cracking (Table 5.22) and faulting (Table 5.39) at different WBT proportions, the $P_{Cracking}$ and $P_{Faulting}$ in equation (5.13) can be obtained. The P_{IRI} (which equals the IRI growth rate) at different WBT proportions can then be calculated, as shown in Table 5.41 and Figures 5.32 - 5.33.

Table 5.41. IRI percent increase at different WBT proportions

Slab thickness (inch)	Tire pressure (psi)	IRI percent increase at different WBT proportions (%)								
		0%	4%	6%	8%	10%	12%	14%	20%	25%
6	80	0.00	0.58	0.87	1.16	1.45	1.74	2.03	2.90	3.63
	100	0.00	0.59	0.88	1.18	1.47	1.77	2.06	2.95	3.69
	120	0.00	0.59	0.89	1.19	**1.49**	1.79	2.08	2.98	**3.72**
8	80	0.00	0.42	0.63	0.83	1.04	1.25	1.46	2.08	2.61
	100	0.00	0.43	0.64	0.85	1.06	1.27	1.49	2.13	2.66
	120	0.00	0.44	0.66	0.88	**1.10**	1.32	1.54	2.20	**2.75**
10	80	0.00	0.31	0.47	0.63	0.78	0.94	1.09	1.56	1.95
	100	0.00	0.32	0.48	0.65	0.81	0.97	1.13	1.61	2.02
	120	0.00	0.33	0.50	0.67	**0.83**	1.00	1.17	1.67	**2.09**
12	80	0.00	0.24	0.36	0.49	0.61	0.73	0.85	1.22	1.52
	100	0.00	0.25	0.38	0.51	0.64	0.76	0.89	1.28	1.60
	120	0.00	0.26	0.40	0.53	**0.66**	0.79	0.92	1.32	**1.65**
13	80	0.00	0.22	0.33	0.44	0.55	0.66	0.77	1.10	1.38
	100	0.00	0.23	0.34	0.46	0.58	0.69	0.80	1.15	1.44
	120	0.00	0.24	0.36	0.47	**0.59**	0.71	0.83	1.18	**1.48**

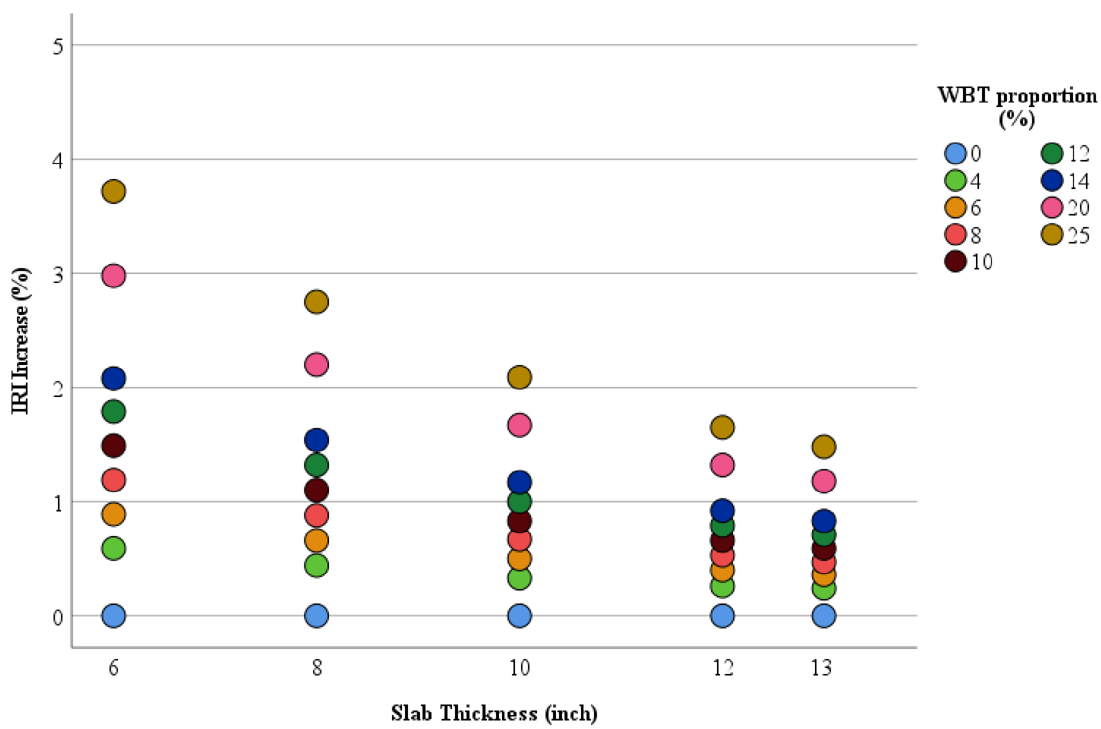

Figure 5.32. Impact of WBT on JPCP IRI at different slab thicknesses

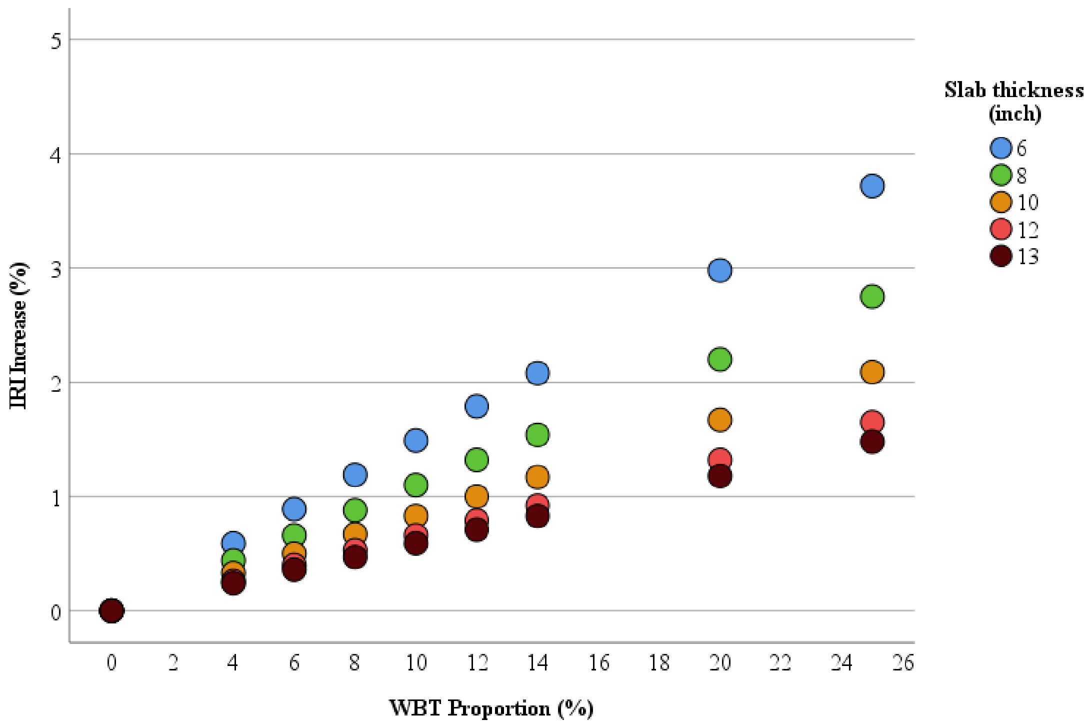

Figure 5.33. Impact of WBT on JPCP IRI at different WBT proportions

According to Table 5.41, the percent increase of IRI with 10% WBT loads ranges from 1.49% (6" slab thickness) to 0.59% (13" slab thickness) under the dual tire standard 120 psi tire pressure. The WBT impact on JPCP IRI is lower than for transverse fatigue and faulting. Similar to cracking and faulting, thicker slab thicknesses are less impacted by WBT loads, and the impact difference between different tire pressures is insignificant in comparison.

The research team predicts that if the proportion of WBT loads in Michigan increased to 25% in the future, the IRI percent increase caused by WBT loads would be in the range of 3.72% (6" slab thickness) to 1.48% (13" slab thickness). According to Figures 5.32 - 5.33, the impact of WBT loads on JPCP IRI is negatively related to the slab thickness, while positively related to the WBT proportion. Higher JPCP slab thickness would decrease the pavement failure risk caused by increasing WBT loads.

5.6. Interpolation of WBT loads' impact on JPCP pavement

According to sections 5.3 - 5.5, the impacts of WBT load on JPCP cracking, faulting, and IRI with slab thicknesses of 6", 8", 10", 12", and 13" have been investigated. Although the analysis has covered many typical thicknesses in Michigan, the effect on some slab thicknesses, such as 7" and 8.5", remains unknown. Assessing the results of WBT loads on the JPCP structure's distresses and IRI, the WBT impact has a nearly linear relationship with the slab thicknesses. Therefore, the linear interpolation method could be adopted to widen the research. The JPCP pavement distress increases at any slab thickness between 6"-13" and WBT proportion between 0-25% can be computed by using linear interpolation. Table 5.42 presents the distress percent increase prediction with integer slab thickness and WBT proportion.

Different colors are used to represent different impact extents. Green represents impact below 2.5%; yellow represents impact above 2.5% but below 5.0%; red represents impact above 5%. As for green scenarios, no action is suggested to be taken, as the WBT load's impact is insignificant. Yellow scenarios mean the revised design method is recommended. Red scenarios mean the revised design process is highly recommended to address the significant WBT impact on pavement.

Table 5.42. Prediction of JPCP pavement distress percent increase

Distress type	Variables		Distress percent increase (%)							
			Slab thickness (inch)							
			6	7	8	9	10	11	12	13
Cracking	WBT proportion (%)	5	1.84	1.67	1.51	1.33	1.16	1.02	0.88	0.74
		10	3.68	3.35	3.02	2.67	2.32	2.04	1.77	1.47
		15	5.54	5.04	4.54	4.01	3.49	3.07	2.65	2.22
		20	7.41	6.74	6.07	5.37	4.67	4.11	3.55	2.96
		25	9.29	8.45	7.61	6.73	5.85	5.14	4.44	3.70
Faulting		5	2.72	2.34	1.98	1.73	1.50	1.34	1.19	1.08
		10	5.43	4.69	3.95	3.47	2.99	2.68	2.38	2.16
		15	8.15	7.04	5.92	5.20	4.48	4.02	3.57	3.24
		20	10.86	9.38	7.90	6.94	5.97	5.37	4.76	4.32
		25	13.58	11.73	9.88	8.67	7.47	6.71	5.95	5.40
IRI		5	0.74	0.65	0.55	0.48	0.42	0.37	0.33	0.30
		10	1.49	1.29	1.10	0.97	0.83	0.75	0.66	0.59
		15	2.23	1.94	1.65	1.45	1.25	1.12	0.99	0.89
		20	2.98	2.59	2.20	1.93	1.67	1.49	1.32	1.18
		25	3.72	3.24	2.75	2.42	2.09	1.87	1.65	1.48

* Green: Low impact, distress percent increase ≤ 2.5%; **no action recommended**.

Yellow: Moderate impact, 2.5% ≤ distress percent increase ≤ 5%; revised design **recommended**.

Red: High impact, 5% ≤ distress percent increase; revised design **highly recommended**.

5.7. Adjustment of JPCP pavement design considering WBT loads

5.7.1. Based on Pavement ME – adjusted distress threshold

Once the JPCP pavement distress percent increase with different slab thicknesses and WBT proportions was obtained, the research team modified the pavement design distress threshold to consider the impact of WBT loads. The general process is similar to that used for flexible pavement as shown in Figure 5.34. The method to compute the adjusted distress threshold is shown in equation (5.14).

$$\text{Adjusted distress threshold} = \text{Initial threshold} / (1 + \text{Increase in percentage}) \qquad (5.14)$$

Figure 5.34. The process of modifying the design considering WBT impact

The adjusted JPCP pavement distress design criteria for transverse cracking, faulting, and IRI are obtained by adopting the above method, as shown in Table 5.43.

Table 5.43. Adjusted JPCP pavement distress threshold

Design criteria	Variables		Adjusted distress threshold (% or inch)							
			Slab thickness (inch)							
			6	7	8	9	10	11	12	13
Cracking (%) (Standard: 15%)	WBT proportion (%)	5	14.73	14.75	14.78	14.80	14.83	14.85	14.87	14.89
		10	14.47	14.51	14.56	14.61	14.66	14.70	14.74	14.78
		15	14.21	14.28	14.35	14.42	14.49	14.55	14.61	14.67
		20	13.97	14.05	14.14	14.24	14.33	14.41	14.49	14.57
		25	13.72	13.83	13.94	14.05	14.17	14.27	14.36	14.46
Faulting (inch) (Standard: 0.125")		5	0.122	0.122	0.123	0.123	0.123	0.123	0.124	0.124
		10	0.119	0.119	0.120	0.121	0.121	0.122	0.122	0.122
		15	0.116	0.117	0.118	0.119	0.120	0.120	0.121	0.121
		20	0.113	0.114	0.116	0.117	0.118	0.119	0.119	0.120
		25	0.110	0.112	0.114	0.115	0.116	0.117	0.118	0.119
IRI (inch/mile) (Standard: 172)		5	170.74	170.89	171.06	171.18	171.28	171.37	171.43	171.49
		10	169.47	169.81	170.13	170.35	170.58	170.72	170.87	170.99
		15	168.25	168.73	169.21	169.54	169.88	170.09	170.31	170.48
		20	167.02	167.66	168.30	168.74	169.17	169.47	169.76	169.99
		25	165.83	166.60	167.40	167.94	168.48	168.84	169.21	169.49

* Green: Low impact, distress percent increase ≤ 2.5%; **no action recommended**.

Yellow: Moderate impact, 2.5% ≤ distress percent increase ≤ 5%; revised design **recommended**.

Red: High impact, 5% ≤ distress percent increase; revised design **highly recommended**.

With the adjusted JPCP pavement distress threshold shown in Table 5.43, the impact of WBT load on JPCP pavement distress can be easily considered in the Pavement ME software by adjusting the distress threshold based on the slab thickness and assumed proportion of WBT loads.

5.7.2. Based on Pavement ME – adjusted CADT

Using a similar method to the flexible pavement CADT adjustment, the research team would adjust the CADT for the ME design of JPCP to include WBT loads' impact. According to results in section 5.7.1, the critical distress for JPCP is faulting in WBTs' impact analysis. So, the value of $F_{\delta\text{-WBT}}$ / $F_{\delta\text{-WBT}}$ for faulting in Table 5.26 would play a similar role to the relative damage index in section 4.7.2 to adjust the CADT for JPCP. In order to simplify the process, the value of $F_{\delta\text{-WBT}}$ / $F_{\delta\text{-WBT}}$ for the 12'' slab JPCP will be the lower limit in adjustment.

The first step is determining the CADT adjustment factor ($F_{CADT\text{-}100}$) when loads were 100% WBT loads. Since the impact of WBT loads on the $F_{\delta\text{-WBT}}$ / $F_{\delta\text{-WBT}}$ values of different slab thicknesses is different, the $F_{CADT\text{-}100}$ is assumed to be a piecewise function with the following control points.

- The relative damage index in the 6" JPCP structure is 2.01, assuming $F_{CADT\text{-}100} = 2.01$ corresponds to CADT < 500;
- The relative damage index in the 8" JPCP structure is 1.73, assuming $F_{CADT\text{-}100} = 1.73$ corresponds to CADT = 1000;
- The relative damage index in the 10" JPCP structure is 1.55, assuming $F_{CADT\text{-}100} = 1.55$ corresponds to CADT = 5000;
- The relative damage index in the 12" JPCP structure is 1.44, assuming $F_{CADT\text{-}100} = 1.44$ corresponds to CADT ≥ 9000;
- Then, the linear interpolation method would be used to determine $F_{CADT\text{-}100}$ in the CADT range of 500 - 1000, 1000 - 5000, and 5000 - 9000.

The piecewise function for the CADT adjustment factor ($F_{CADT\text{-}100}$) when loads were 100% WBT loads are shown in the Figure 5.35 and equation (5.15) as below.

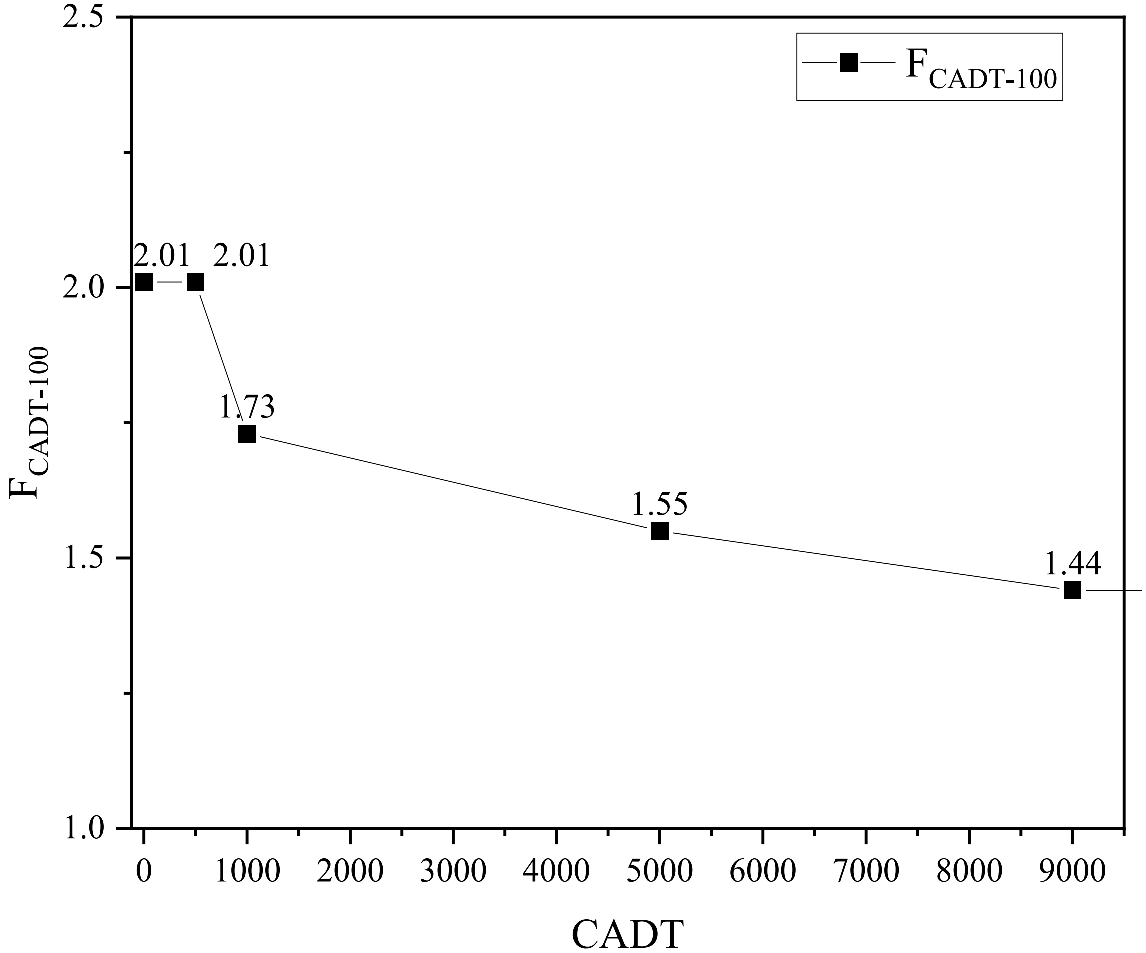

Figure 5.35. The adjustment factor for JPCP under different CADTs

$$F_{CADT-100} = \begin{cases} 2.01 & \text{when CADT} < 500 \\ -0.00056\times CADT + 2.29 & \text{When } 500 \le CADT < 1000 \\ -0.000045\times CADT + 1.775 & \text{When } 1000 \le CADT < 5000 \\ -0.0000275\times CADT + 1.6875 & \text{When } 5000 \le CADT < 9000 \\ 1.44 & \text{When CADT} \ge 9000 \end{cases} \quad (5.15)$$

The second step is determining the CADT adjustment factor (F_{CADT-P}) with the WBT percentage of P. As for DT load, the relative damage index for fatigue is assumed as 1, so the F_{CADT-P} could be calculated with the equation below.

$$F_{CADT-P} = F_{CADT-100} \times P/100 + 1\times(100-P)/100 \quad (5.16)$$

The CADT adjustment factor (F_{CADT-P}) for JPCP with the WBT percentage of P can be computed using the equation (5.16). Below are the examples of F_{CADT-P} with P in 5%, 10%, and 25%.

(1) When $P = 5\%$, the F_{CADT-5} is shown in equation (5.17).

$$F_{CADT-5} = \begin{cases} 1.0505 & \text{When CADT} < 500 \\ -0.000028\times CADT + 1.0645 & \text{When } 500 \le \text{CADT} < 1000 \\ -0.00000225\times CADT + 1.03875 & \text{When } 1000 \le \text{CADT} < 5000 \\ -0.000001375\times CADT + 1.034375 & \text{When } 5000 \le \text{CADT} < 9000 \\ 1.022 & \text{When CADT} \ge 9000 \end{cases} \quad (5.17)$$

(2) When $P = 10\%$, the $F_{CADT-10}$ is shown in equation (5.18).

$$F_{CADT-10} = \begin{cases} 1.101 & \text{When CADT} < 500 \\ -0.000056\times CADT + 1.129 & \text{When } 500 \le \text{CADT} < 1000 \\ -0.0000045\times CADT + 1.0775 & \text{When } 1000 \le \text{CADT} < 5000 \\ -0.00000275\times CADT + 1.06875 & \text{When } 5000 \le \text{CADT} < 9000 \\ 1.044 & \text{When CADT} \ge 9000 \end{cases} \quad (5.18)$$

(3) When $P = 25\%$, the $F_{CADT-25}$ is shown in equation (5.19).

$$F_{CADT-25} = \begin{cases} 1.2525 & \text{When CADT} < 500 \\ -0.00014\times CADT + 1.3225 & \text{When } 500 \le \text{CADT} < 1000 \\ -0.00001125\times CADT + 1.19375 & \text{When } 1000 \le \text{CADT} < 5000 \\ -0.000006875\times CADT + 1.171875 & \text{When } 5000 \le \text{CADT} < 9000 \\ 1.11 & \text{When CADT} \ge 9000 \end{cases} \quad (5.19)$$

5.7.3. Based on AASHTO 93 – adjusted slab thickness

Slab thickness is the critical parameter used in AASHTO 93 for JPCP pavement design. The design slab thickness (D) is related to traffic, subgrade resilient modulus, change in serviceability, reliability, etc., as presented in equation (5.20).

$$\log_{10}(W_{18}) = Z_R S_0 + 7.35 \log_{10}(D+1) - 0.06 + \frac{\log_{10}\left(\frac{\Delta PSI}{4.5-1.5}\right)}{1 + \frac{1.64\times 10^7}{(D+1)^{8.46}}} + (4.22 - 0.32\,p_t)\log_{10}\left[\frac{S_c\,C_d\,(D^{0.75} - 1.132)}{215.63\,J\left(D^{0.75} - \frac{18.42}{(E_c/k)^{0.25}}\right)}\right] \quad (5.20)$$

where:

W_{18} = Equivalent single axle loads (ESALs);

Z_R = Z-value for the 95% (MDOT) confidence level one-tailed test;

S_0 = Standard deviation, typically 0.39 for MDOT;

ΔPSI = Change in present serviceability index, typically 2.0 for MDOT;

Pt = Terminal serviceability;

S_C = Modulus of rupture;

Cd = Drainage coefficient;

J = Load transfer coefficient;

Ec = Modulus of elasticity;

k = Effective modulus of subgrade reaction.

The research team would use the most significantly impacted distress, *faulting,* as the basis to adjust the AASHTO 93 design method; the WBT impact on pavement serviceability (AASHTO 93 process) is assumed to be the same as the impact on faulting (ME process).

As WBT loads lead to more distress, the pavement's ΔPSI should be lower than the default design value for MDOT (which = 4.5-2.5 = 2). Through this process, the designed pavement structure would be stronger to offset the impact of WBT loads. Enlarging the terminal PSI is a feasible way to lower the ΔPSI. For example, if the WBT loads caused 10% more distress, the ΔPSI should be 10% less, meaning the terminal PSI would be 2.7 (or 2.5+2*10%).

The relationship between fatigue cracking percent increase and the terminal PSI is shown in equation (5.21).

$$Terminal_{PSI} = 2.5 + 0.02 \times P_{faulting} \tag{5.21}$$

where:

$Terminal_{PSI}$ = Adjusted terminal PSI considering WBT impact;

$P_{faulting}$ = Percent change in faulting caused by WBT loads, %;

Table 5.44. Adjusted terminal PSI considering WBT impact

Slab thickness (inch)	Adjusted terminal PSI considering WBT impact								
	0%	4%	6%	8%	10%	12%	14%	20%	25%
6	2.50	2.54	2.57	2.59	**2.61**	2.63	2.65	2.72	**2.77**
8	2.50	2.53	2.55	2.56	**2.58**	2.59	2.61	2.66	**2.70**
10	2.50	2.52	2.54	2.55	**2.56**	2.57	2.58	2.62	**2.65**
12	2.50	2.52	2.53	2.54	**2.55**	2.56	2.57	2.60	**2.62**
13	2.50	2.52	2.53	2.53	**2.54**	2.55	2.56	2.59	**2.61**

The process of adjusting AASHTO 93 rigid pavement design considering WBT impact would be as follows:

(1) Calculate the design slab thickness (D) of rigid pavement as usual;

(2) Use the D from process (1) and Table 5.44 with linear interpolation to get the properly adjusted terminal PSI and reconduct step (1).

The research team also conducted a sensitivity check of different terminal PSI numbers on D. The input parameters are shown in Figure 5.36. The sensitivity analysis results are shown in Figures 5.37 - 5.38.

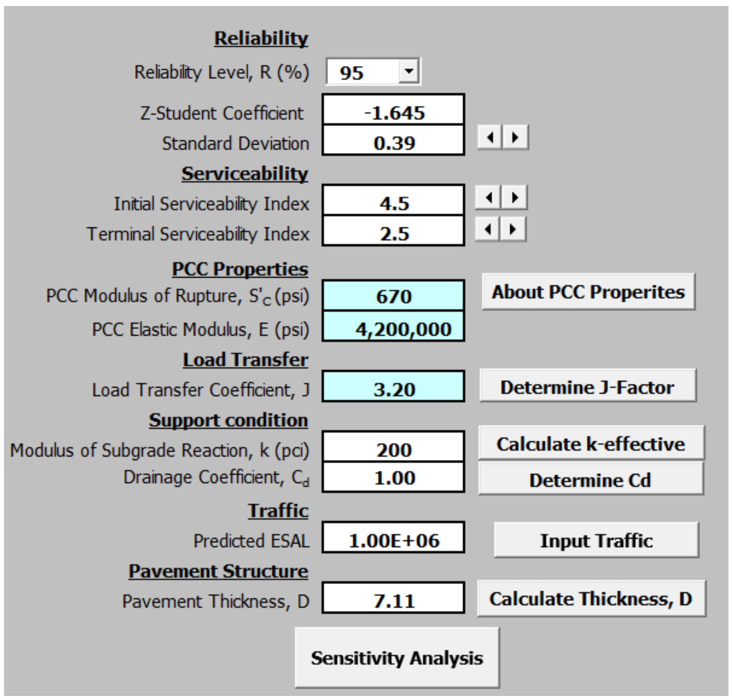

Figure 5.36. The AASHTO 93 analysis process for JPCP

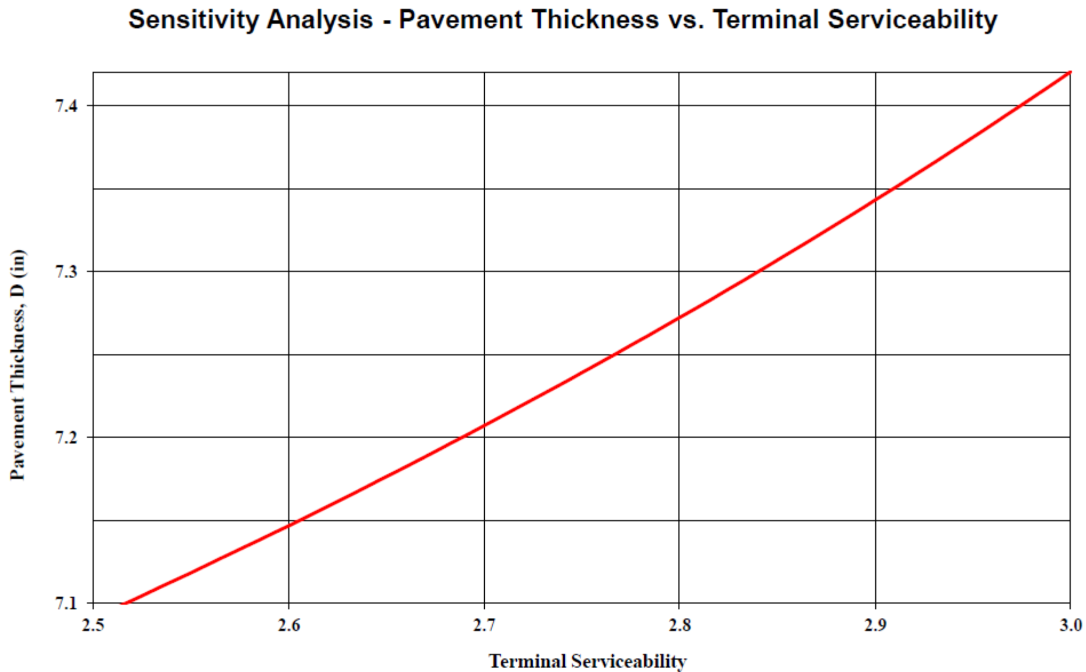

Figure 5.37. Sensitivity analysis of terminal PSI (ESALs: 1E6)

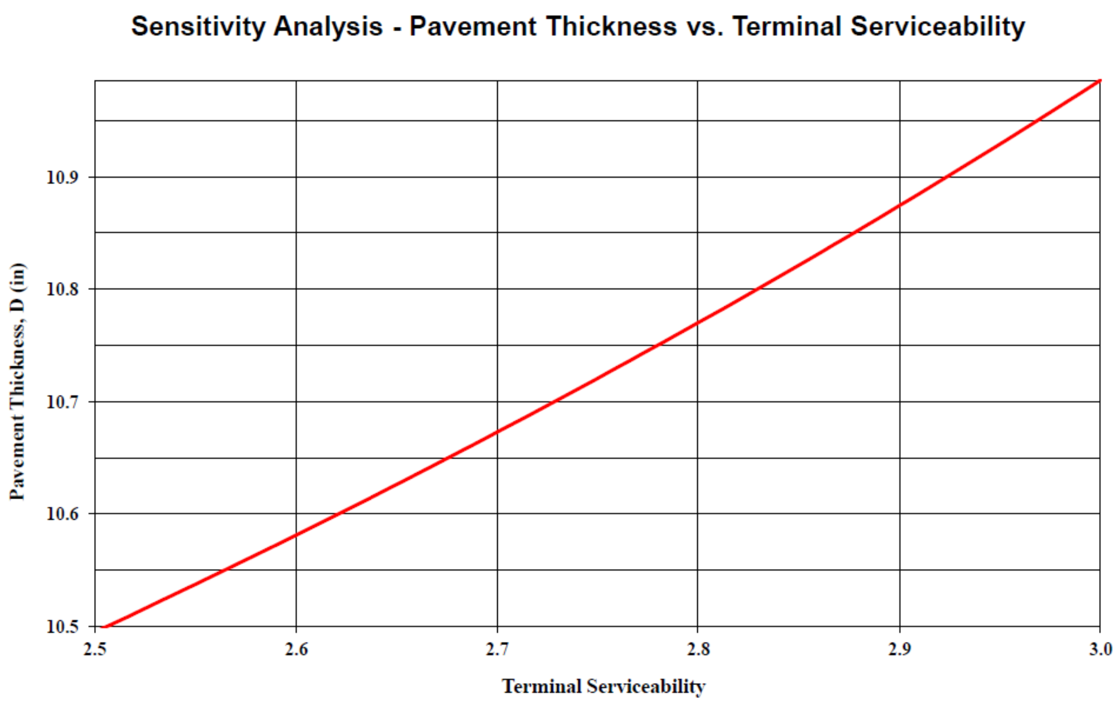

Figure 5.38. Sensitivity analysis of terminal PSI (ESALs: 1E7)

5.7.4. Based on AASHTO 93 – adjusted ESAL

A similar adjustment process in section 5.7.2 will be used to adjust ESAL in this section's AASHTO 93 pavement design process. The Michigan freeway average vehicle class distribution and freeway axle load spectrum (average of 12 month) [32], and other traffic parameters same to Table 4.67 in section 4.7.4 would be used for calculation. The CADT to ESAL transformation for JPCP result is then obtained and presented Table 5.45.

Table 5.45. CADT to ESAL transformation for JPCP

CADT	Estimated ESAL
500	1.7×10^6
1000	3.2×10^6
5000	11×10^6
9000	18.5×10^6

The first step is determining the ESAL adjustment factor ($F_{ESAL-100}$) if all loads were WBT loads (100% WBT) with the following control points.

- The relative damage index in the 6" JPCP structure is 2.01, assuming $F_{ESAL-100} = 2.01$ corresponds to ESAL $< 1.7\times10^6$;
- The relative damage index in the 8" JPCP structure is 1.73, assuming $F_{ESAL-100} = 1.73$ corresponds to ESAL $= 3.2\times10^6$;
- The relative damage index in the 10" JPCP structure is 1.55, assuming $F_{ESAL-100} = 1.55$ corresponds to ESAL $= 11\times10^6$;
- The relative damage index in the 12" JPCP structure is 1.44, assuming $F_{ESAL-100} = 1.44$ corresponds to ESAL $\geq 18.5\times10^6$;
- Then, the linear interpolation method was used to determine $F_{ESAL-100}$ in the ESAL range of 1.7×10^6- 3.2×10^6, 3.2×10^6- 11×10^6, and 11×10^6- 18.5×10^6.

The piecewise function for the ESAL adjustment factor ($F_{ESAL-100}$) when loads were 100% WBT loads are shown in the Figure 5.39 and equation (5.22) as below.

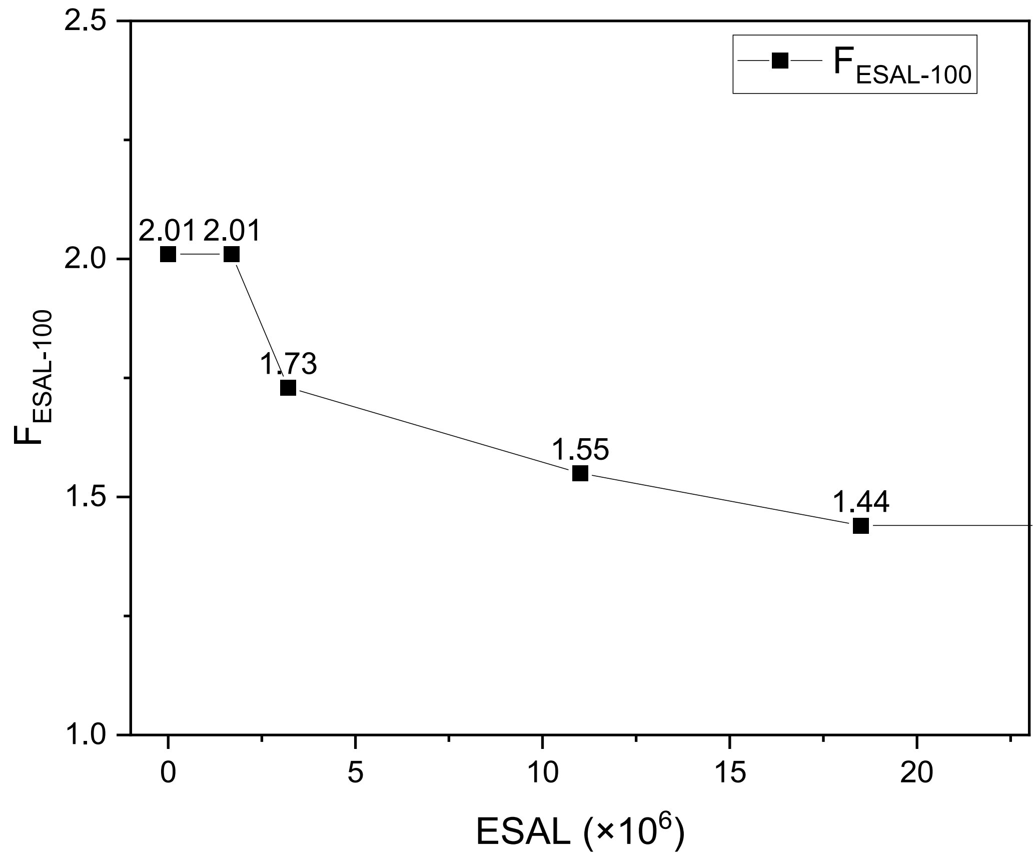

Figure 5.39. Adjust factor for JPCP under different ESALs

$F_{ESAL-100}$ = 2.01 when ESAL < 1.7×10^6

$-0.187\times10^{-6}\times$ESAL + 2.327 When $1.7\times10^6 \le$ ESAL < 3.2×10^6

$-0.023\times10^{-6}\times$ESAL + 1.804 When $3.2\times10^6 \le$ ESAL < 11×10^6

$-0.015\times10^{-6}\times$ESAL + 1.711 When $11\times10^6 \le$ ESAL < 18.5×10^6

1.44 When ESAL $\ge 18.5\times10^6$ (5.22)

The second step is determining the ESAL adjustment factor (F_{ESAL-P}) with the WBT percentage of P. As for DT load, the relative damage index for fatigue is assumed as 1, so the F_{ESAL-P} could be calculated with the equation below.

$$F_{ESAL-P} = F_{ESAL-100} \times P/100 + 1\times(100-P)/100 \quad (5.23)$$

The ESAL adjustment factor (F_{ESAL-P}) with the WBT percentage of P can be computed using equation (5.23). Below are the examples of F_{ESAL-P} with P in 5%, 10%, and 25%.

(1) When $P = 5\%$, the $F_{ESAL\text{-}5}$ is shown in equation (5.24).

$$F_{ESAL\text{-}5} = \begin{cases} 1.0505 & \text{When } ESAL < 1.7\times10^{6} \\ -0.00935\times10^{-6}\times ESAL + 1.06635 & \text{When } 1.7\times10^{6} \le ESAL < 3.2\times10^{6} \\ -0.00115\times10^{-6}\times ESAL + 1.0402 & \text{When } 3.2\times10^{6} \le ESAL < 11\times10^{6} \\ -0.00075\times10^{-6}\times ESAL + 1.03555 & \text{When } 11\times10^{6} \le ESAL < 18.5\times10^{6} \\ 1.022 & \text{When } ESAL \ge 18.5\times10^{6} \end{cases} \quad (5.24)$$

(2) When $P = 10\%$, the $F_{ESAL\text{-}10}$ is shown in equation (5.25).

$$F_{ESAL\text{-}10} = \begin{cases} 1.101 & \text{When } ESAL < 1.7\times10^{6} \\ -0.0187\times10^{-6}\times ESAL + 1.1327 & \text{When } 1.7\times10^{6} \le ESAL < 3.2\times10^{6} \\ -0.0023\times10^{-6}\times ESAL + 1.0804 & \text{When } 3.2\times10^{6} \le ESAL < 11\times10^{6} \\ -0.0015\times10^{-6}\times ESAL + 1.0711 & \text{When } 11\times10^{6} \le ESAL < 18.5\times10^{6} \\ 1.044 & \text{When } ESAL \ge 18.5\times10^{6} \end{cases} \quad (5.25)$$

(3) When $P = 25\%$, the $F_{ESAL\text{-}25}$ is shown in equation (5.26).

$$F_{ESAL\text{-}25} = \begin{cases} 1.2525 & \text{When } ESAL < 1.7\times10^{6} \\ -0.04675\times10^{-6}\times ESAL + 1.33175 & \text{When } 1.7\times10^{6} \le ESAL < 3.2\times10^{6} \\ -0.00575\times10^{-6}\times ESAL + 1.201 & \text{When } 3.2\times10^{6} \le ESAL < 11\times10^{6} \\ -0.00375\times10^{-6}\times ESAL + 1.17775 & \text{When } 11\times10^{6} \le ESAL < 18.5\times10^{6} \\ 1.11 & \text{When } ESAL \ge 18.5\times10^{6} \end{cases} \quad (5.26)$$

5.8. Chapter summary

Based on the above JPCP pavement distress analysis, the research team summarized WBT loads' impact on the distress of different JPCP slab thickness structures under tire pressures of 120 psi. According to field WBT load survey results section 3, Michigan's current WBT load proportion is approximately 10% for design purposes in the Lower Peninsula and 5% for the Upper Peninsula. The distresses' percent increase under 10% WBT loads were plotted, corresponding with Michigan's current WBT loads proportion, and the results are presented in Figure 5.40.

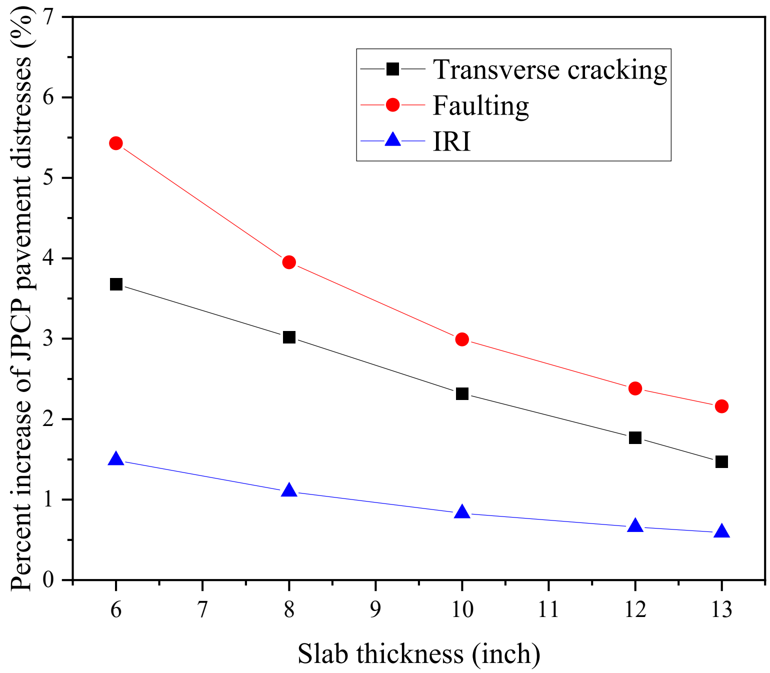

Figure 5.40. Distress increase under 10% WBT load for different slab thickness structures

Considering WBT loads' increase in the future, the research team compared the increase of distress under 25% WBT loads, as shown in Figure 5.41.

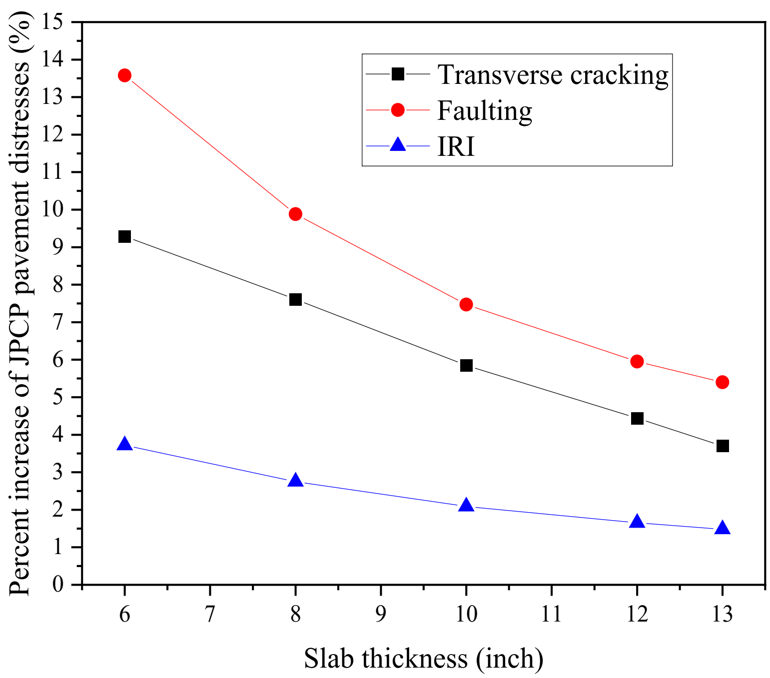

Figure 5.41. Distress increase under 25% WBT load for different slab thickness structures

Figures 5.40 and 5.41 show that faulting of JPCP pavement is the most easily impacted distress by WBT loads. The impact extent of transverse cracking, faulting, and IRI are all negatively related to the slab thickness, which is different from that of flexible pavement. It is also worth noting that the impact of WBT loads on JPCP pavement's IRI is more significant than that on flexible pavement's IRI, especially under higher WBT proportions.

Under the roughly 10% WBT load proportion as measured in several Michigan truckline locations from this study, JPCP pavement's distress increases are relatively minor. However, suppose the WBT load proportion in Michigan were to increase to 25% in the future. In that case, the WBT impact on JPCP distresses, especially faulting, should receive more attention, and the adjusted design threshold (or adjusted terminal PSI in the AASHTO 93 method) should be adopted if needed.

6. CHAPTER 6: WIM TECHNOLOGY INVESTIGATION

6.1. Conventional WIM technologies

Weigh-in-motion (WIM) devices are meant to detect and record axle weights and gross vehicle weights as vehicles pass through a measuring location. WIM systems, unlike static scales, can measure vehicles operating at reduced or normal traffic speeds and do not require the vehicle to come to a complete stop. WIM technology speeds up the weighing process and, in the case of commercial vehicles, permits trucks under the weight limit to avoid static scales and inspection.

The research team conducted a literature review on the Weigh-in-Motion (WIM) system to identify the accuracy of load weight results in motion with the intention to assess the impacts WBTs may have in measurement. WIM estimates a vehicle's static gross weight and weight allocation by measuring and analyzing dynamic tire forces transmitted by each wheel and axle/axle group [34]. WIM systems primarily consist of sensors and a data collection and analysis controller. For this data collection process, the weight sensors can utilize load cells, bending plates, piezoelectric systems, in-line strain gauges, and capacitive and optical fiber sensors [35, 36]. The process of the WIM system operation with different sensors is presented in Table 6.1. The typical layouts of different WIM technologies are shown in Figures 6.1 - 6.3.

Table 6.1. The process of the WIM system operation [37]

Sensor types	**Operation Process**
Piezoelectric sensors	Force → Proportional voltage in piezoelectric sensor generated→ Record → Calculate dynamic load → Estimate static load
Bending Plate	Force → Strain gauges under metal plates record strain → Calculate dynamic load → Estimate static load
Load cell	Force → wire under the strain gauge compressed and modified → Resistance difference to the current in the wire → Calculate the weight of two in-line scales → Estimate static load

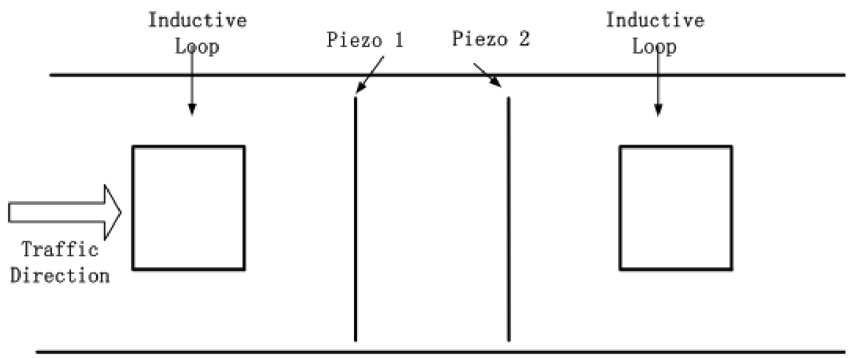

Figure 6.1. Piezoelectric sensors layout example [37]

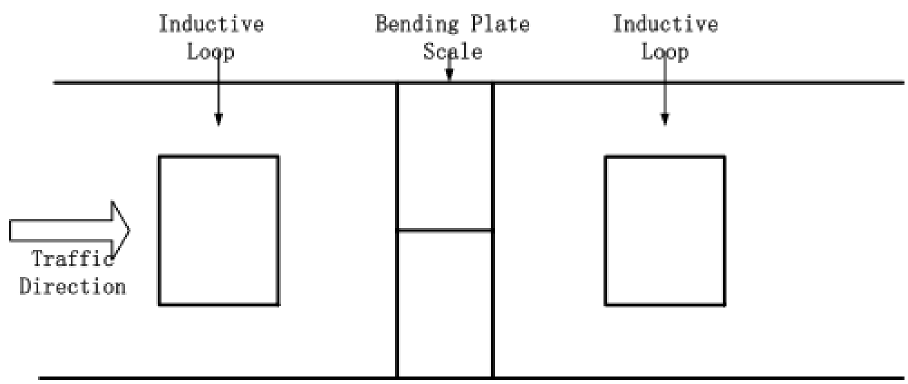

Figure 6.2. Bending plate layout example [37]

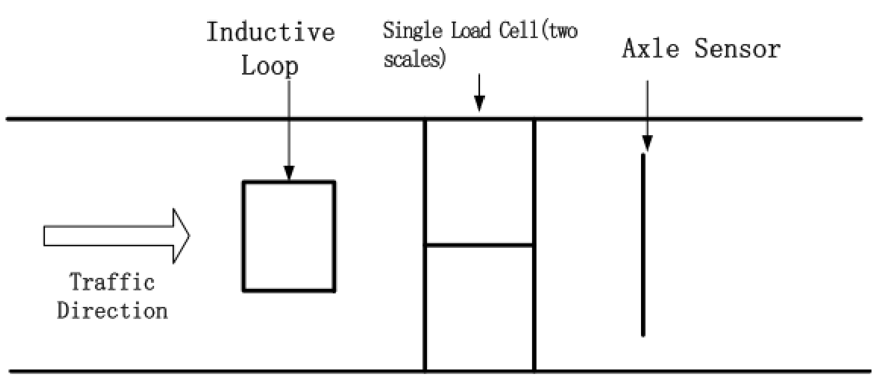

Figure 6.3. Load cell layout example [37]

If the WIM system is well equipped, other multi-sensors, cameras, and laser scanners make it possible to collect more parameters like vehicle class, length, direction, registration number, number of axles, and distance [38]. For example, inductive loop or axle detectors can be placed before and after weight sensors to measure vehicles' speed and spacing [37]. The WIM station may be equipped with an automatic vehicle classification system to obtain vehicle classification data

[39].

Factors affecting WIM systems and causing errors are complex, including WIM site, characteristics of the vehicles, and environmental conditions, as shown in Table 6.2 [34, 40, 41]. Sujon et al. noted that the wheel's friction might lead to higher or lower weight depending on the direction of the axle movement while crossing the WIM sensor [42].

Table 6.2. Factors affecting the WIM systems [34, 40, 41]

Factors	Specification
WIM site conditions	Road geometry, slopes, and surface condition
Characteristics of vehicles	Speed, oscillation, axle configurations
Environmental conditions	Temperature
Calibration	Procedure and frequency

WIM generally has more significant errors than static weight measurement due to the speed of the vehicles evaluated. Methods based on reliability characteristics and tolerance interval boundaries have been used for error analysis [43]. Load cell sensors can reach an accuracy of 2% during static measurements but may deteriorate to 10% in WIM systems [38]. Ji et al. investigated the relative error between the static weight and WIM (using a polyvinylidene fluoride piezoelectric sensor) of vehicles at different speeds, as shown in Figure 6.4 [44]. The error did not present a significant correlation with speed in this research.

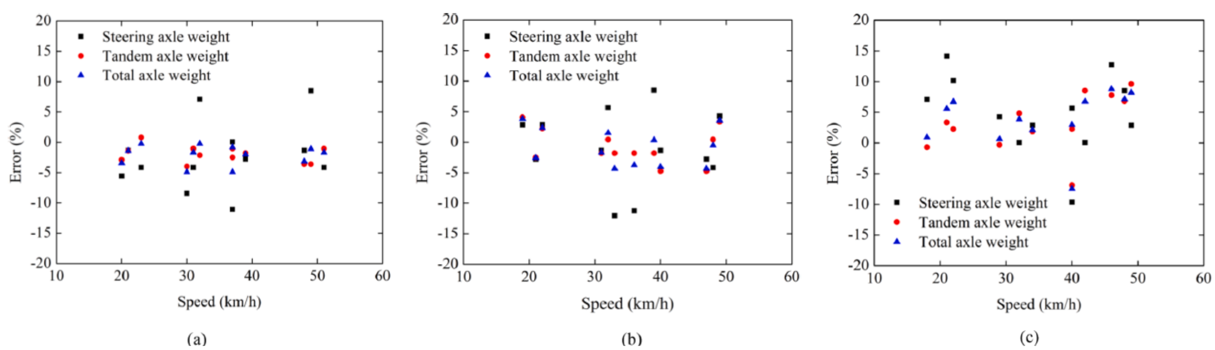

(a) no-load **(b) half-load** **(c) full-load**

Figure 6.4. Relative error of axle load at different vehicle speeds

The percentages of error of WIM systems with different sensors in current research are summarized in Table 6.3. The Error column, if without a specific note, refers to gross vehicle weight error between WIM and estimating static load.

Table 6.3. The error of WIM systems with different sensors

Author	Sensor types	Error, %
Pham et al. [34]	Load cells	*GVW: ±6
Al-Qadi et al. [39]	Bending Plate Single Load cell Piezoelectric Sensor- Quartz Piezoelectric Sensor-Other	GVW: ±10 GVW: ±6 GVW: ±10 GVW: ±15
Cheng et al. [45]	Capacitive flexible weighing sensor	GVW: ±10
Haidar et al. [46]	Quartz piezo Bending plate load cells Piezo polymer	GVW: ±9.8 GVW: ±9.0 GVW: ±5.0 GVW: ±9.8
Bermejo et al. [47]	/	GVW: ±6.35
Zhang et al. [48]	Single sensor Three Sensors array	GVW: ±6 GVW: ±4

* GVW: Gross Vehicle Weight

As for the cost of WIM technologies, Dontu et al. estimated the average cost per lane and 12-year lifespan for five types of WIM technologies, as shown in Table 6.4 [49].

Table 6.4. Estimated average cost per lane and 12-year lifespan

WIM technologies	Estimated annual average cost/lane ($)
Piezo polymer	4,224 – 5,917
Piezo quartz	7,500
Bending plate	4,990 – 6,750
Double bending plate	7,709
Single load cell	6,200 – 8,750

6.2. Advanced WIM technologies in identifying tire types

Newer advanced WIM technologies have been developed that may help agencies such as MDOT identify standard WIM data as well as automate the process for identifying other key parameters affecting pavement response, such as tire type (DT or WBT), axle width, and tire pressure. While a 120 psi tire pressure is assumed in the Pavement ME analysis, this is generally higher than most in-service truck tires even under "hot" conditions. These technologies would help MDOT understand the distribution of tire pressure and tire types to develop a more robust, on-going database to monitor changes in the loads experienced on the MDOT trunkline system.

(1) Technology from Kistler

Kistler's technology could help detect single and dual tires and identify flat tires, as shown in Figure 6.5. The Automated Tire Screening (ATS) system from Kistler offers a reliable solution to monitor tire pressures. The ATS system will promote the accuracy of the quartz sensors and deliver vital data to identify missing or under-inflated tires. The system can easily be integrated into existing WIM screening sites. More details on this technology can be found at the following link: https://www.kistler.com/en/.

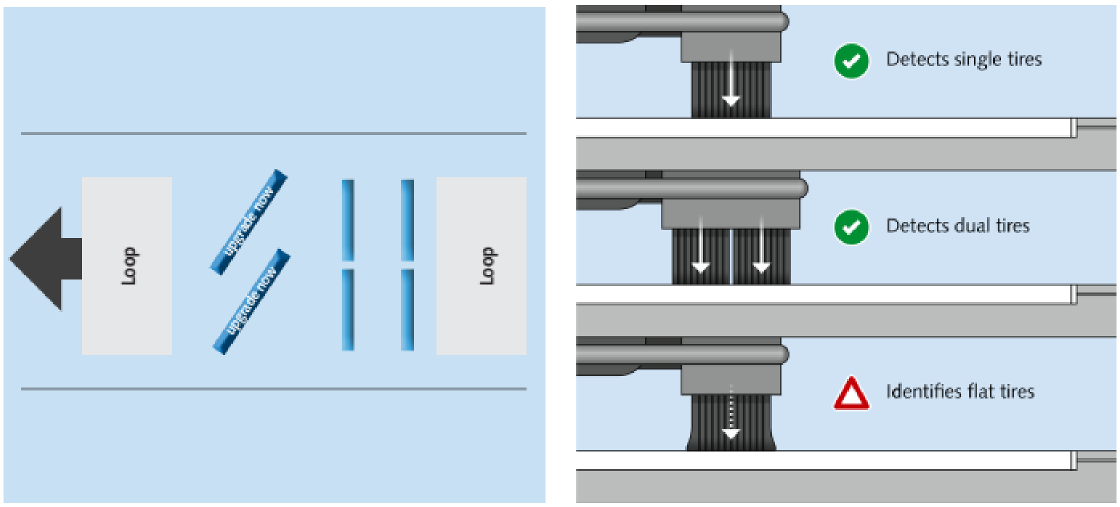

Upgrade your existing WIM site by adding 2 tilted WIM sensors.

Detects single/double, flat and missing tires.

Figure 6.5. Demonstration of WIM technology from Kistler

(2) Technology from OptiWIM

The OptiWIM® sensor offers multiple valuable features, and the sensor can directly measure the vehicle's axle width. It is also able to detect the use of double-wheel assemblies or the presence of underinflated tires, even in dual-assembly, separately. It has demonstrated a 10-year lifespan. It provides weight assessment in the sensor's whole length, which means that the recorded value is the same in any part of the road, no matter where the vehicle passes. A demonstration of WIM technology from OptiWIM is shown in Figure 6.6. More details can be found on their website: https://www.optiwim.com/.

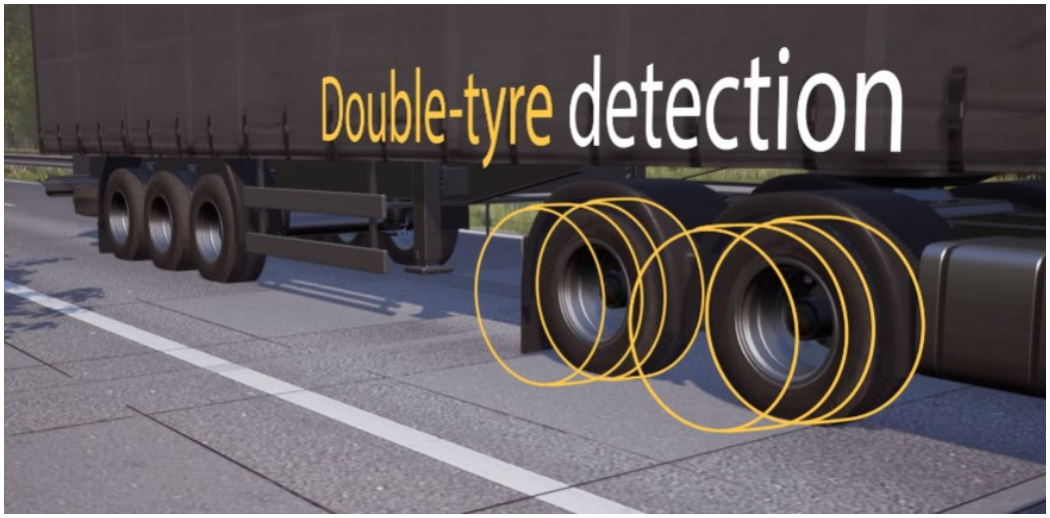

Figure 6.6. Demonstration of WIM technology from OptiWIM

(3) Technology from Fiscal Tech America

A demonstration of WIM technology from Fiscal Tech America is shown in Figure 6.7. It complies with several standards, such as ASTM E1318-09 Type I, Type II, Type III and COST 323 A(5), B+(7), or B(10). It is a complete system, including OIML-certified strain gauge strip sensors, electronics, and a friendly web-based user interface. It is highly effective for weight overload control, enhancing road safety, and reduced maintenance costs. Its advanced weighing-in-motion technology allows traffic to remain flowing, while pre-selected vehicles are routed to the weighing station. It can also be applied to industrial truck weighing. The following can be highlighted: (1) High-speed WIM up to 80 mph, (2) Width, length, and height measurement (3D Laser Scanner), and (3) Single/Dual tire detection and Vehicle classification. More details can be found on their website: https://ft-america.com/.

Figure 6.7. Demonstration of WIM technology from Fiscal Tech America

7. CHAPTER 7: SUMMARY AND CONCLUSIONS

This research analyzed WBT loads' impact on the distress of flexible and rigid pavements under Michigan's climate and construction practices. The following conclusions could be drawn from the research.

(1) Field investigation at weigh stations in the Lower Peninsula shows that the percentage of trucks with any WBTs is 11% on average, contributed to mainly by Class 9 trucks. The percentage of load axles with WBTs in all load axles in the Lower Peninsula is 7.32%, from the limited data set in this study. The percentage of trucks using any WBTs is 5.8% on average in the Upper Peninsula, and it is estimated that less than 5% of load axles would contain WBTs. Based on field investigation, 10% would be recommended as the current proportion of WBTs in the quantitative impact analysis to account for near-term growth during the pavement design life and conservativeness in design, while 25% would be recommended as the future WBT proportion considering WBT growth.

(2) The impact of WBT loads on pavement distress (Flexible: fatigue cracking, rutting, IRI; Rigid: transverse cracking, faulting, IRI) are all positively related to the proportion of WBTs; more WBTs would cause more risk of pavement failure. However, the extent of the WBT loads' impact on different pavement distress varies. Fatigue cracking of flexible pavement and faulting of JPCP are critical distresses, which should be given attention considering WBT loads.

(3) Thickness is another parameter affecting WBT loads' impact. Thicker AC is beneficial in reducing WBT loads' impact on fatigue cracking but does not work to reduce total rutting. 10% of trucks utilizing WBT axle loads would cause 6.59% more bottom-up fatigue cracking on a 5" AC structure and 1.76% more on an 11.5" AC structure than a standard Pavement ME DT analysis, indicating thinner AC structures are more likely to fail in fatigue when under the same WBT loads. For flexible pavements' rutting, 10% WBT axles loads would cause only 0.31% more distress on a 5" AC structure and 1.43% more on an 11.5" AC structure, which is much less than fatigue cracking.

(4) Thicker slabs help reduce WBT loads' impact on both transverse cracking and faulting for JPCP. 10% of axles utilizing WBTs caused 3.68% more transverse cracking and 5.43% more faulting on the 6" slab structure, while for the 13" slab structure under the same WBT axle load percentage, the increase of the two distresses was limited to 1.47% and 2.16%, respectively.

(5) The impact of WBT loads on the IRI of different pavement structures was obtained by

establishing the relationship between IRI and other distress. Results show that WBT load will not affect flexible pavement's IRI significantly (approximately 0.4% more terminal IRI under 10% WBT and 0.9% more terminal IRI under 25% WBT). For JPCP, IRI is more impacted by WBT loads compared with flexible pavement, but the impact is still less than transverse cracking and faulting of JPCP (less than 1.5% more terminal IRI under 10% WBT axles and less than 4% more terminal IRI under 25% WBT).

(6) Using the distress change results under the scattered AC or slab thicknesses and scattered WBT proportions, the WBT loads' impact on structures with 5-12" AC layer, 6-13" PCC slab, and under WBT proportion within 25% could be estimated using quadratic equations or the linear interpolation method. The design threshold in Pavement ME can then be adjusted considering different WBT load impacts. An impact of less than 2.5% is considered minor in this approach, and no action is recommended in the design process. However, if the impact exceeds 5% for a given distress prediction, the adjusted Pavement ME design threshold is recommended as noted in red in Table 4.63 for AC pavements and Table 5.43 for JPCPs. In addition, the traffic parameter for Pavement ME design - CADT, was also adjusted considering different percentages of WBTs.

(7) Considering that the AASHTO 93 pavement design method is still adopted by MDOT, an adjusted AASHTO 93 pavement design was also proposed, by artificially adjusting the terminal PSI (from 2.5) to indirectly account for additional loss in serviceability due to WBT loads (see Tables 4.66 and 5.44). WBT loads' impact on fatigue cracking of flexible pavement and faulting of JPCP is used to determine the adjustment of terminal PSI, as these two distresses are critical according to analysis results. In addition, the traffic parameter for AASHTO 93 design - ESAL, was adjusted considering different percentages of WBTs.

(8) Conventional WIM technologies with different sensors were reviewed with regard to the operation process while noting its limitation with respect to WBT identification. Factors affecting conventional WIM systems come from the site, vehicles, environment, and calibration process. WIM systems with load cell sensors have corrected minor errors but at a relatively higher cost. Some advanced WIM technologies from Kistler, OptiWIM, and Fiscal Tech America show potential in identifying WBTs in addition to other factors such as wheel spacing and tire pressure to help DOTs better identify critical factors that affect pavement response and distress development.

REFERENCES

1. Al-Qadi, I.L. and M.A. Elseifi, *New generation of wide-base tires: impact on trucking operations, environment, and pavements.* Transportation research record, 2007. **2008**(1): p. 100-109.

2. Kang, S., et al., *Environmental and economic impact of using new-generation wide-base tires.* The International Journal of Life Cycle Assessment, 2019. **24**(4): p. 753-766.

3. Said, I., et al., *Impact of New Generation Wide-Base Tires on Fuel Consumption.* Journal of Transportation Engineering, Part B: Pavements, 2021. **147**(2): p. 04021011.

4. Zhao, J. and H. Wang, *Dynamic pavement response analysis under wide-base tyre considering vehicle-tyre–pavement interaction.* Road Materials and Pavement Design, 2022. **23**(7): p. 1650-1666.

5. Al-Qadi, I.L., et al., *Impact of wide-base tires on pavements: a national study.* Transportation research record, 2018. **2672**(40): p. 186-196.

6. Al-Qadi, I.L. and H. Wang, *Evaluation of pavement damage due to new tire designs*. 2009, Illinois Center for Transportation (ICT).

7. Al-Qadi, I.L. and H. Wang, *Impact of wide-base tires on pavements: Results from instrumentation measurements and modeling analysis.* Transportation research record, 2012. **2304**(1): p. 169-176.

8. Hernandez, J.A., I. Al-Qadi, and M. De Beer, *Impact of tire loading and tire pressure on measured 3D contact stresses.* 2013.

9. Gungor, O.E., et al., *Quantitative assessment of the effect of wide-base tires on pavement response by finite element analysis.* Transportation Research Record, 2016. **2590**(1): p. 37-43.

10. Gagan. *Tyre upsize guide. risks, rules to know before upsize else your car handling will be impacted*. 2020 [cited 2022 0919]; Available from: https://www.mycarhelpline.com/index.php?option=com_easyblog&view=entry&id=527&Itemid=91.

11. AASHTO, *Mechanistic-Empirical Pavement Design Guide — A Manual of Practice (Third Edition)*. 2020.

12. Priest, A.L. and D.H. Timm, *Mechanistic Comparison of Wide-Base Single versus Standard Dual Tire Configurations.* Transportation Research Record, 2006. **1949**(1): p. 155-163.

13. Greene, J., et al., *Impact of wide-base single tires on pavement damage.* Transportation research record, 2010. **2155**(1): p. 82-90.

14. Wang, H. and I.L. Al-Qadi, *Impact quantification of wide-base tire loading on secondary road flexible pavements.* Journal of Transportation Engineering, 2011. **137**(9): p. 630-639.

15. Said, I.M., et al., *Structural and environmental impact of new-generation wide-base tires in New Brunswick, Canada.* Road Materials and Pavement Design, 2020. **21**(7): p. 1968-1984.

16. Molavi Nojumi, M., et al., *Investigation of the Impact of Tire Configurations on Different Pavement Structures Using Finite Element Analysis.* International Journal of Pavement Research and Technology, 2021.

17. Elseifi, M.A., et al., *Quantification of pavement damage caused by dual and wide-base tires.* Transportation research record, 2005. **1940**(1): p. 125-135.

18. Fedujwar, R.R. and U.C. Sahoo, *Pavement responses under wide base tyres subjected to moving loads.* International Journal of Transportation Science and Technology, 2022.

19. Elhamrawy, S., M. Moharram, and U. Heneash, *The Effects of Truck Axle Loads and Tire Pressure on the Responses of Flexible Pavement.* ERJ. Engineering Research Journal, 2022. **45**(3): p. 439-446.

20. Fahad, M. and R. Nagy, *Fatigue damage analysis of pavements under autonomous truck tire passes.* Pollack Periodica, 2022.

21. Transportation, M.D.o., *Michigan DOT User Guide for Mechanistic-Empirical Pavement Design*. 2021.

22. Muniandy, R., et al., *Characterization of Effective Tire Contact Area for Various Tread Patterns.* Instrumentation Science & Technology, 2013. **42**(1): p. 15-26.

23. Greene, J., et al., *Impact of Wide-Base Single Tires on Pavement Damage.* Transportation Research Record: Journal of the Transportation Research Board, 2010. **2155**(1): p. 82-90.

24. Brawner, S. *Fleets weigh benefits, drawbacks of wide-base tires versus duals*. 2020 [cited 2022 13 October].

25. Mei, Q.P. and M. Gul, *A cost effective solution for pavement crack inspection using cameras and deep neural networks.* Construction and Building Materials, 2020. **256**.

26. Meegoda, J.N., et al., *Pavement texture from high-speed laser for pavement management system.* International Journal of Pavement Engineering, 2013. **14**(8): p. 697-705.

27. Minge, E., S. Petersen, and J. Kotzenmacher, *Evaluation of Nonintrusive Technologies for Traffic Detection, Phase 3.* Transportation Research Record, 2011(2256): p. 95-103.

28. Bai, J., et al., *Robust Target Detection and Tracking Algorithm Based on Roadside Radar and Camera.* Sensors, 2021. **21**(4).

29. Yu, X., P.D. Prevedouros, and G. Sulijoadikusumo, *Evaluation of Autoscope, SmartSensor HD, and Infra-Red Traffic Logger for Vehicle Classification.* Transportation Research Record, 2010(2160): p. 77-86.

30. Liu, C.Q., et al., *Three-dimensional texture measurement using deep learning and multi-view pavement images.* Measurement, 2021. **172**.

31. Yang, G.W., et al., *Automatic Pavement Type Recognition for Image-Based Pavement Condition Survey Using Convolutional Neural Network.* Journal of Computing in Civil Engineering, 2021. **35**(1).

32. *Mechanistic-Empirical (ME) Pavement Design - MDOT Traffic Data for Mechanistic Empirical Pavement Design*. [cited 2022 1207]; Available from: https://www.michigan.gov/mdot/business/construction/pavement-operations/me-pavement-design.

33. *Guide for Mechanistic-Empirical Design of new and rehabilitated pavement structures. Part 3: Design analysis. Chapter 4: Design for new and reconstructed rigid pavements*. March 2004, NCHRP: Champaign, Illinois.

34. Pham, X.T., et al., *An estimation method for pavement weigh-in-motion system with preliminary experiment.* Mechanical Engineering Journal, 2020. **7**(6): p. 14.

35. Zhang, Z., *An integrated system for road condition and weigh-in-motion measurements using in-pavement strain sensors*. 2016, North Dakota State University.

36. Xiang, T., et al., *Detection of Moving Load on Pavement Using Piezoelectric Sensors.* Sensors, 2020. **20**(8): p. 12.

37. Zhang, L., C. Haas, and S.L. Tighe. *Evaluating weigh-in-motion sensing technology for traffic data collection*. in *Annual Conference of the Transportation Association of Canada*. 2007.

38. Nieoczym, A., K. Drozd, and A. Wojcik, *GEOMETRIC OPTIMIZATION OF A BEAM DETECTOR FOR A WIM SYSTEM.* Advances in Science and Technology-Research Journal, 2018. **12**(3): p. 233-241.

39. Al-Qadi, I., et al., *LTBP Program's Literature Review on Weigh-in-Motion Systems.* 2016.

40. Scheuter, F. *Evaluation of factors affecting WIM system accuracy*. in *Proceedings of the Second European Conference on COST*. 1998.

41. Qin, T.H., et al., *Effects of Sensor Location on Dynamic Load Estimation in Weigh-in-Motion System.* Sensors, 2018. **18**(9): p. 17.

42. Sujon, M. and F. Dai, *Application of weigh-in-motion technologies for pavement and bridge response monitoring: State-of-the-art review.* Automation in Construction, 2021. **130**: p. 16.

43. Burnos, P., J. Gajda, and R. Sroka, *ACCURACY CRITERIA FOR EVALUATION OF WEIGH-IN-MOTION SYSTEMS.* Metrology and Measurement Systems, 2018. **25**(4): p. 743-754.

44. Ji, S.B., et al., *Improvement of vehicle axle load test method based on portable WIM.* Measurement, 2021. **173**: p. 10.

45. Cheng, L., H.J. Zhang, and Q. Li, *Design of a capacitive flexible weighing sensor for vehicle WIM system.* Sensors, 2007. **7**(8): p. 1530-1544.

46. Haider, S.W., et al., *Assessment of Factors Affecting Measurement Accuracy for High-Quality Weigh-in-Motion Sites in the Long-Term Pavement Performance Database.* Transportation Research Record, 2020. **2674**(10): p. 269-284.

47. Bermejo, J.L. and J.M.P. Mayora, *Application of WIM to pavement design. Effect of WIM accuracy.* Informes De La Construccion, 2017. **69**(545): p. 10.

48. Zhang, W.B., C.G. Suo, and Q. Wang, *A Novel Sensor System for Measuring Wheel Loads of Vehicles on Highways.* Sensors, 2008. **8**(12): p. 7671-7689.

49. Dontu, A., et al. *Weigh-in-motion sensors and traffic monitoring systems-Sate of the art and development trends*. in *IOP Conference Series: Materials Science and Engineering*. 2020. IOP Publishing.

A. APPENDIX A: USER'S SURVEY AND MANUFACTURER'S SURVEY

User's survey results:

Question 1: What is your company's name?

- Company name redacted.

Question 2: How many trucks are in your fleet (using either dual or wide-base tire configurations)?

- 107 Trucks / 600 Trailers
- 3050
- 26
- 2750
- 850
- 200
- 250
- 1000
- 56
- 25

Question 3: What percentage of trucks in your fleet utilize wide-base tires?

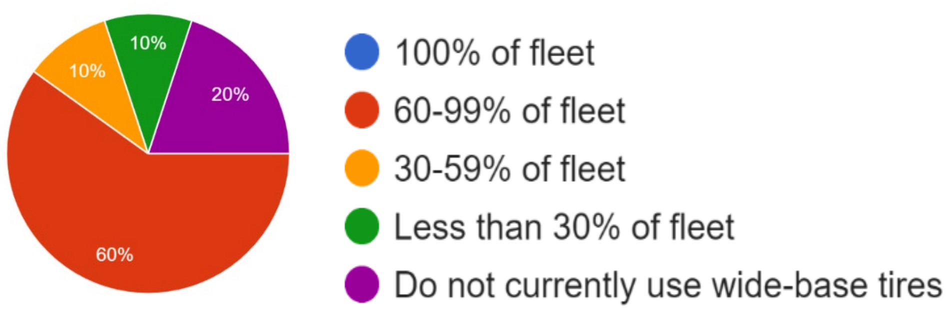

Figure A.1. Percentage of trucks from user's survey

Question 4: What types of wide-base tires are being used in your fleet?

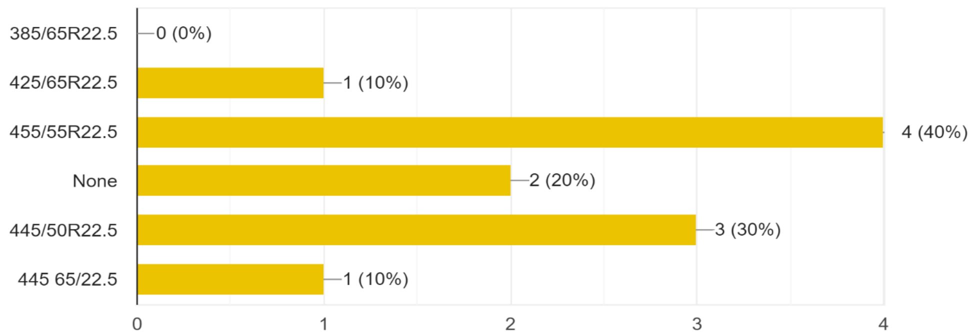

Figure A.2. Types of WBT used from user's survey

Question 5: If wide-base tires are utilized, what tire pressure do you typically operate these tires (in psi)?

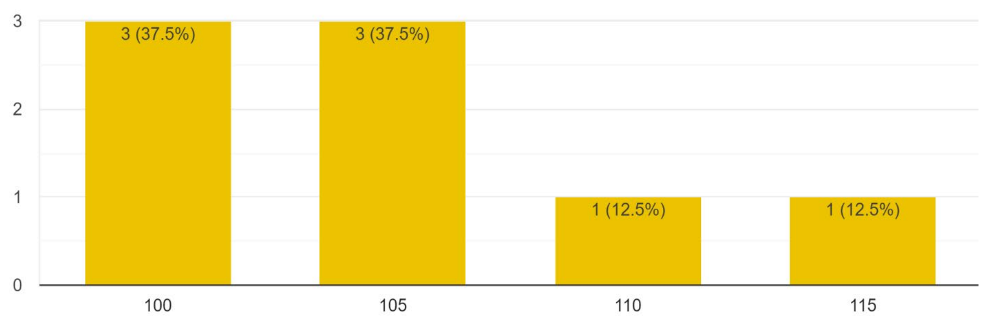

Figure A.3. Tire pressure used in WBT from user's survey

Question 6: What axle(s) does your company utilize wide-base tires on?

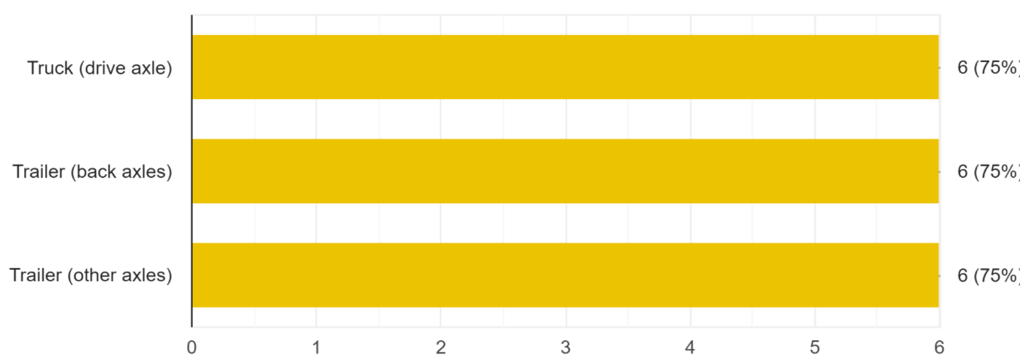

Figure A.4. Axle type used in WBT from user's survey

Question 7: What routes are primarily used by trucks using wide-base tires in the state of Michigan?

- various
- Interstate and truck routes
- I79, I69, I75
- None
- I75, US23
- Highway and regional transport, to store and back to highway.
- I94, I75

Question 8: What is the average distance of the routes taken?

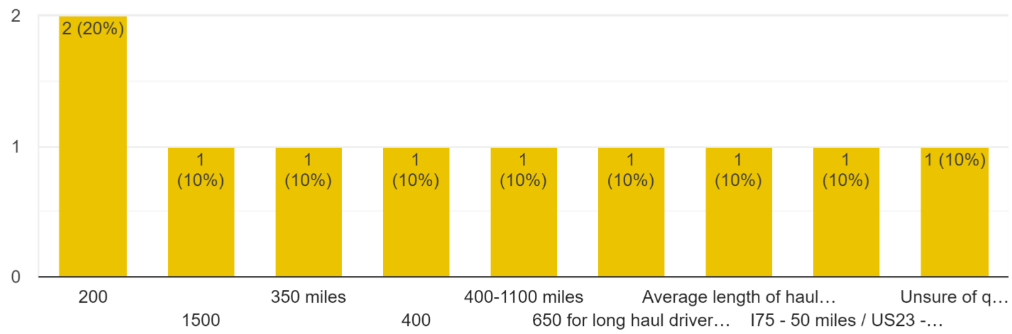

Figure A.5. Average distance of routes from user's survey

Question 9: Why do you use wide-base tires in your fleet?

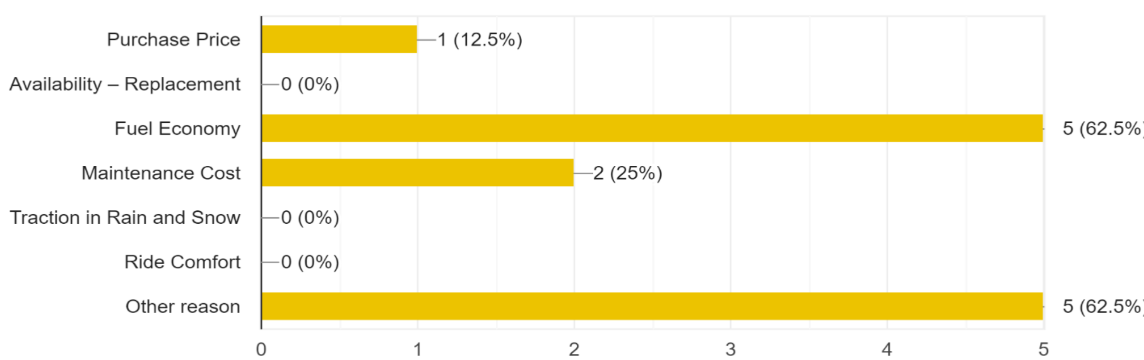

Figure A.6. Reasons for using WBTs from user's survey

Question 10: In the near future, does your company plan on utilizing wide-based tires _____ than previous years?

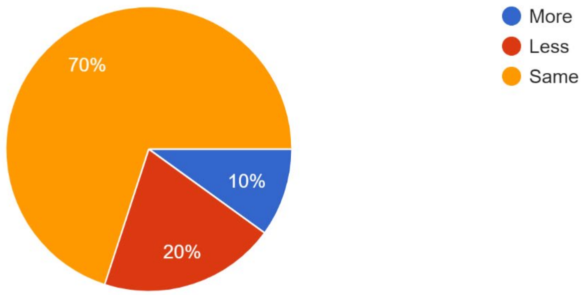

Figure A.7. Attitude toward using WBTs from user's survey

Manufacturer's survey results:

Question 1: Please provide your company name and a contact person(name and email)

- No response

Question 2: Based on total truck tire sales, what percentage of these sales are for wide-base tires?

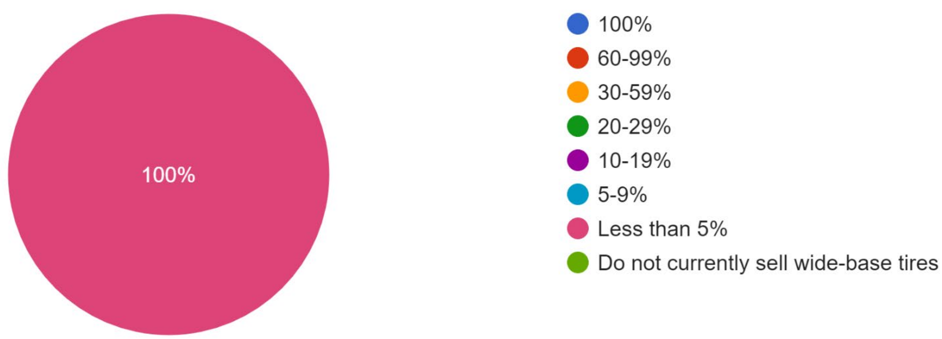

Figure A.8. Percentage of WBTs sold from manufacturer's survey

Question 3: What types of wide-base tires does your company sell?

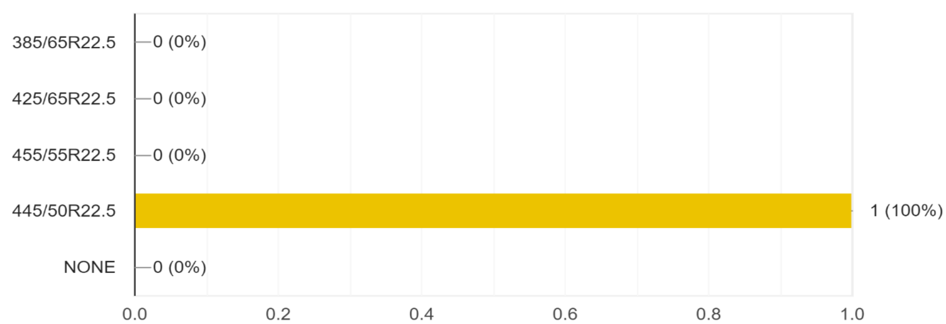

Figure A.9. Types of WBTs sold from manufacturer's survey

Question 4: What are the primary reasons for purchases of wide-base tires from your company?

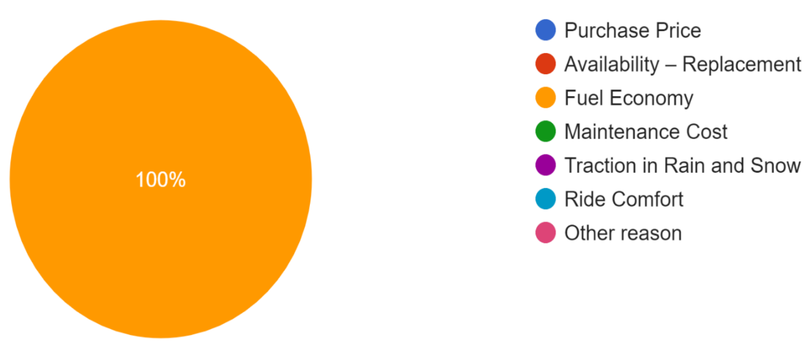

Figure A.10. Reasons for purchasing WBTs from manufacturer's survey

Question 5: In the near future, what does your company foresee in terms of sales projections of wide-base tires?

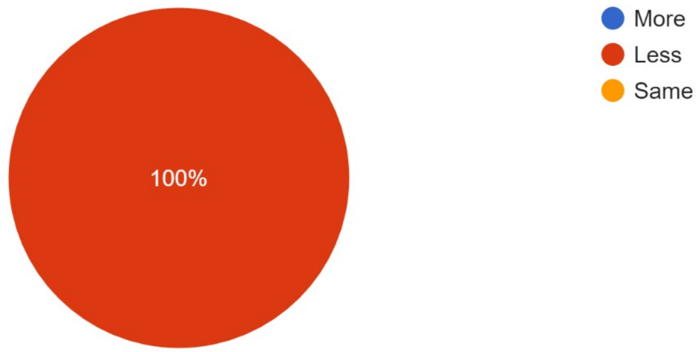

Figure A.11. Projections of WBT sales from manufacturer's survey

Question 6: Do you have any other comments regarding the sale or manufacturing of wide-base tires by your company?

- No response

Question 7: What companies/organizations/industries are purchasers of your wide-base tires?

- Regional over the road fleets. Grocery distribution

B. APPENDIX B: APPROVAL OF PERMITTED ACTIVITIES FILES FOR WBT PROPORTION ROAD INVESTIGATION

MDOT
Michigan Department of Transportation

ADVANCE NOTICE AND APPROVAL OF PERMITTED ACTIVITIES

Issued To:
Michigan technological university, Dr. You from Civil and engineering
Dillman 301A, Dillman 301A
Houghton MI 49931

Permit Number: 98000-077309-21-050521
Permit Type: Annual Application
Advance Notice Number: 79161

Contact:
dongzhao Jin
906-370-6531(O)
dongj@mtu.edu

Purpose:

We will take a few videos with the truck tires at the weigh station for the MDOT project "Quantify the Impact of Super Single (Wide-Base) Tires on Pavement Performance in Michigan
MDOT OR# 21-008", Contact person from MDOT: Justin P. Schenkel, P.E. IN FREE ACCESS STATE TRUNKLINE RIGHT-OF-WAY

MDOT Job Number:

Date Work To Begin:	**Proposed Completion Date:**	**Number of Days:**
6/7/21	6/25/21	18
Work Time From:	9.00 AM	**To:** 5.00 PM

Lane Closure Proposed: No

Work Located on restricted route: No

Work performed outside of time restrictions: No

STATE ROUTE: I-94 **CITY OF:** New Buffalo **County: Berrien County**

NEAREST INTERSECTION:	**SIDE OF ROAD:**	**DISTANCE TO NEAREST INTERSECTION:** (in feet)	**DIRECTION TO NEAREST INTERECTION:**
I80	East,North	0.00	East

Comments:
Approved

Attachments/ Plans included:
1 CrystalViewer.pdf

James Hendrix	**6/4/21**
Approved By	**Approved Date**

Figure B.1. Advance notice and approval of permitted activities at New Buffalo weigh station

MDOT
Michigan Department of Transportation

ADVANCE NOTICE AND APPROVAL OF PERMITTED ACTIVITIES

Issued To:
Michigan technological university, Dr. You from Civil and engineering
Dillman 301A, Dillman 301A
Houghton MI 49931

Permit Number: 98000-077309-21-050521
Permit Type: Annual Application
Advance Notice Number: 79162

Contact:
dongzhao Jin
906-370-6531(O)
dongj@mtu.edu

Purpose:

We will take a few videos with the truck tires at the weigh station for the MDOT project "Quantify the Impact of Super Single (Wide-Base) Tires on Pavement Performance in Michigan
MDOT OR# 21-008", Contact person from MDOT: Justin P. Schenkel, P.E. IN FREE ACCESS STATE TRUNKLINE RIGHT-OF-WAY

MDOT Job Number:

Date Work To Begin:	**Proposed Completion Date:**	**Number of Days:**
6/7/21	6/25/21	18

Work Time From: 9.00 AM **To:** 5.00 PM

Lane Closure Proposed: No

Work Located on restricted route: No

Work performed outside of time restrictions: No

STATE ROUTE: I-75 **CITY OF:** Luna Pier **County: Monroe County**

NEAREST INTERSECTION:	**SIDE OF ROAD:**	**DISTANCE TO NEAREST INTERSECTION: (in miles)**	**DIRECTION TO NEAREST INTERECTION:**
I275	East,North	50.00	East

Comments:
Work approved as submitted.

Attachments/ Plans included:
1 CrystalViewer.pdf

Pascal Bui	6/7/21
Approved By	**Approved Date**

Figure B.2. Advance notice and approval of permitted activities at Luna Pier weigh station

MDOT
Michigan Department of Transportation

ADVANCE NOTICE AND APPROVAL OF PERMITTED ACTIVITIES

Issued To:
Michigan technological university, Dr. You from Civil and engineering
Dillman 301A, Dillman 301A
Houghton MI 49931

Permit Number: 98000-077309-21-050521
Permit Type: Annual Application
Advance Notice Number: 79163

Contact:
dongzhao Jin
906-370-6531(O)
dongj@mtu.edu

Purpose:
We will take a few videos with the truck tires at the weigh station for the MDOT project "Quantify the Impact of Super Single (Wide-Base) Tires on Pavement Performance in Michigan
MDOT OR# 21-008", Contact person from MDOT: Justin P. Schenkel, P.E. IN FREE ACCESS STATE TRUNKLINE RIGHT-OF-WAY

MDOT Job Number:

Date Work To Begin:	**Proposed Completion Date:**	**Number of Days:**
6/7/21	6/25/21	18

Work Time From: 9.00 AM **To:** 5.00 PM

Lane Closure Proposed: No

Work Located on restricted route: No

Work performed outside of time restrictions: No

STATE ROUTE: I-94 **VILLAGE OF:** Grass Lake **County: Jackson County**

NEAREST INTERSECTION:	**SIDE OF ROAD:**	**DISTANCE TO (in miles) NEAREST INTERSECTION:**	**DIRECTION TO NEAREST INTERECTION:**
I96	East,North	50.00	North

Comments:
Approved

Attachments/ Plans included:
1 CrystalViewer.pdf

Jared Boll 6/4/21
Approved By **Approved Date**

Figure B.3. Advance notice and approval of permitted activities at Grass Lake weigh station

Michigan Department of Transportation

ADVANCE NOTICE AND APPROVAL OF PERMITTED ACTIVITIES

Issued To:
Michigan technological university, Dr. You from Civil and engineering
Dillman 301A, Dillman 301A
Houghton MI 49931

Permit Number: 98000-077309-21-050521
Permit Type: Annual Application
Advance Notice Number: 79164

Contact:
dongzhao Jin
906-370-6531(O)
dongj@mtu.edu

Purpose:

We will take a few videos with the truck tires at the weigh station for the MDOT project "Quantify the Impact of Super Single (Wide-Base) Tires on Pavement Performance in Michigan
MDOT OR# 21-008", Contact person from MDOT: Justin P. Schenkel, P.E. IN FREE ACCESS STATE TRUNKLINE RIGHT-OF-WAY

MDOT Job Number:

Date Work To Begin:	**Proposed Completion Date:**	**Number of Days:**
6/7/21	6/25/21	18

Work Time From: 9.00 AM **To:** 5.00 PM

Lane Closure Proposed: No

Work Located on restricted route: No

Work performed outside of time restrictions: No

STATE ROUTE: I-69 **CITY OF:** Coldwater **County: Branch County**

NEAREST INTERSECTION:	**SIDE OF ROAD:**	**DISTANCE TO NEAREST INTERSECTION:** (in miles)	**DIRECTION TO NEAREST INTERECTION:**
I94	East,West	50.00	West

Comments:

Must coordinate with Michigan State Police at the weigh station. No impact to mainline I-69 traffic allowed.

Attachments/ Plans included:
1 CrystalViewer.pdf

Bob Coy	**6/4/21**
Approved By	**Approved Date**

Figure B.4. Advance notice and approval of permitted activities at Coldwater weigh station

MDOT
Michigan Department of Transportation

ADVANCE NOTICE AND APPROVAL OF PERMITTED ACTIVITIES

Issued To:
Michigan technological university, Dr. You from Civil and engineering
Dillman 301A, Dillman 301A
Houghgton MI 49931

Permit Number: **98000-077309-21-050521**
Permit Type: **Annual Application**
Advance Notice Number: 79165

Contact:
dongzhao Jin
906-370-6531(O)
dongj@mtu.edu

Purpose:

We will take a few videos with the truck tires at the weigh station for the MDOT project "Quantify the Impact of Super Single (Wide-Base) Tires on Pavement Performance in Michigan
MDOT OR# 21-008", Contact person from MDOT: Justin P. Schenkel, P.E. IN FREE ACCESS STATE TRUNKLINE RIGHT-OF-WAY

MDOT Job Number:

Date Work To Begin:	**Proposed Completion Date:**	**Number of Days:**
6/7/21	6/25/21	18
Work Time From:	9.00 AM	**To:** 5.00 PM

Lane Closure Proposed: No

Work Located on restricted route: No

Work performed outside of time restrictions: No

STATE ROUTE: I-96 **CITY OF:** Portland **County: Ionia County**

NEAREST INTERSECTION:	**SIDE OF ROAD:**	**DISTANCE TO (in miles) NEAREST INTERSECTION:**	**DIRECTION TO NEAREST INTERECTION:**
I69	East,North	50.00	East

Comments:

Please coordinate activities with the weigh station operators.

Attachments/ Plans included:
1 CrystalViewer.pdf

Kerwin Keen	6/4/21
Approved By	**Approved Date**

Figure B.5. Advance notice and approval of permitted activities at Ionia weigh station

ADVANCE NOTICE AND APPROVAL OF PERMITTED ACTIVITIES

Issued To:
Michigan technological university, Dr. You from Civil and engineering
Dillman 301A, Dillman 301A
Houghton MI 49931

Permit Number: 98000-077309-21-050521
Permit Type: Annual Application
Advance Notice Number: 79166

Contact:
dongzhao Jin
906-370-6531(O)
dongj@mtu.edu

Purpose:

We will take a few videos with the truck tires at the weigh station for the MDOT project "Quantify the Impact of Super Single (Wide-Base) Tires on Pavement Performance in Michigan
MDOT OR# 21-008", Contact person from MDOT: Justin P. Schenkel, P.E. IN FREE ACCESS STATE TRUNKLINE RIGHT-OF-WAY

MDOT Job Number:

Date Work To Begin:	**Proposed Completion Date:**	**Number of Days:**
6/8/21	6/25/21	17

Work Time From: 9.00 AM **To:** 5.00 PM

Lane Closure Proposed: No

Work Located on restricted route: No

Work performed outside of time restrictions: No

STATE ROUTE: I-96 **VILLAGE OF:** Fowlerville **County: Livingston County**

NEAREST INTERSECTION:	**SIDE OF ROAD:**	**DISTANCE TO NEAREST INTERSECTION:** (in miles)	**DIRECTION TO NEAREST INTERECTION:**
I69	East,North	50.00	South

Comments:

Work approved as submitted.

Attachments/ Plans included:

1 CrystalViewer.pdf
2 CrystalViewer.pdf

Pascal Bui 6/7/21

Approved By **Approved Date**

Figure B.6. Advance notice and approval of permitted activities at Fowlerville weigh station

MDOT
Michigan Department of Transportation

ANNUAL CONSTRUCTION PERMIT

For Operations within State Highway Right-of-Way

Issued To:	**Permit Number:**	**98000-077309-21-050521**
Michigan technological university, Dr. You from Civil and engineering	**Permit Type:**	**Annual Application**
Dillman 301A, Dillman 301A	**Permit Fee:**	**$45.00**
Houghton MI 49931	**Effective Date:**	**May 05, 2021 to Dec 31, 2021**
	Bond Numbers:	

Contact:
dongzhao Jin
906-370-6531(O)
dongj@mtu.edu

THIS PERMIT IS VALID ONLY FOR THE FOLLOWING PROPOSED OPERATIONS IN THE TYPE OF RIGHT OF WAY AS NOTED:

12-Other:We will take a few videos with the truck tires at the weigh station for the MDOT project "Quantify the Impact of Super Single (Wide-Base) Tires on Pavement Performance in Michigan
MDOT OR# 21-008", Contact person from MDOT: Justin P. Schenkel, P.E. IN FREE ACCESS STATE TRUNKLINE RIGHT-OF-WAY

This permit is incomplete without "General Conditions and Supplemental Specifications"

I certify that I accept the following:

1. I am the legal owner of this property or facility, the owner's authorized representative, or have statutory authority to work within state highway Right-of-Way.
2. Commencement of work set forth in the permit application constitutes acceptance of the permit as issued.
3. Failure to object, ***within ten (10) days*** to the permit as issued constitutes acceptance of the permit as issued.
4. If this permit is accepted by either of the above methods, I will comply with the provisions of the permit.
5. I agree that Advance Notice for Permitted Activities for shall be submitted **5 days prior** to the commencement of the proposed work.

   I agree that Advance Notice for Permitted Utility Tree Trimming and Tree Removal Activities shall be submitted **15 days prior** to the commencement of the proposed work for an annual permit.

CAUTION

Work shall NOT begin until the Advance Notice has been approved.

Failure to submit the advance notice may result in a Stop Work Order.

Michigan technological university, Dr. You from Civil and engineering	**Lauri Olsen** **MDOT**	**May 05, 2021** **Approved Date**
TSC Contact Info	**Central Office**	**(517) 373-2090**

THE STANDARD ATTACHMENTS, ATTACHMENTS AND SPECIAL CONDITIONS MARKED BELOW ARE A PART OF THIS PERMIT.

Figure B.7. Annual construction permit for operations within the state highway right-of-way

C. APPENDIX C: CNN APP INTRODUCTION

Two examples of the CNN operation windows developed by the research team are shown in Figures C.1 and C.2 below.

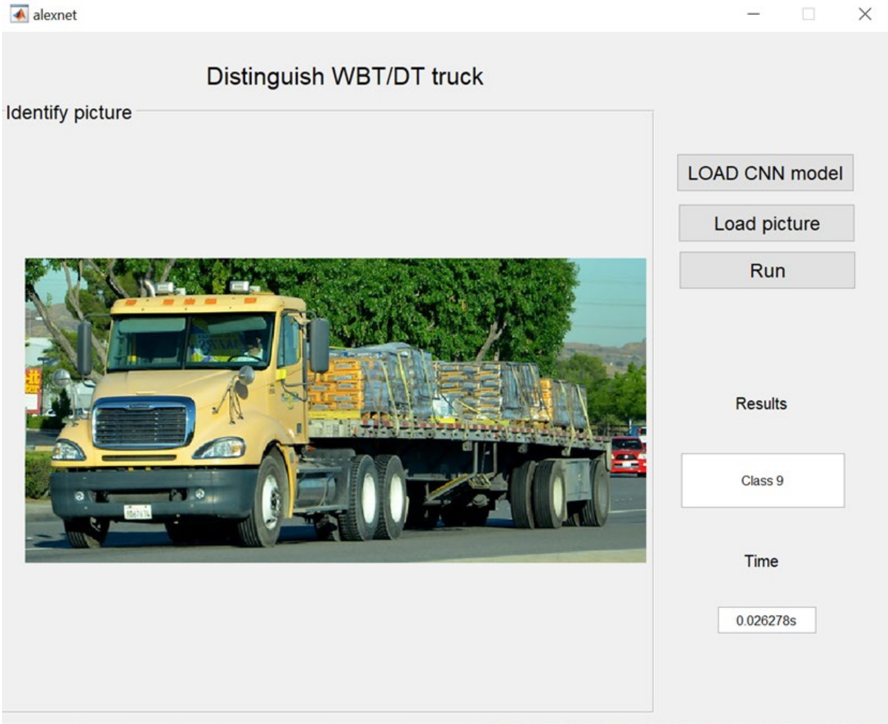

Figure C.1. CNN App interface showing DT truck

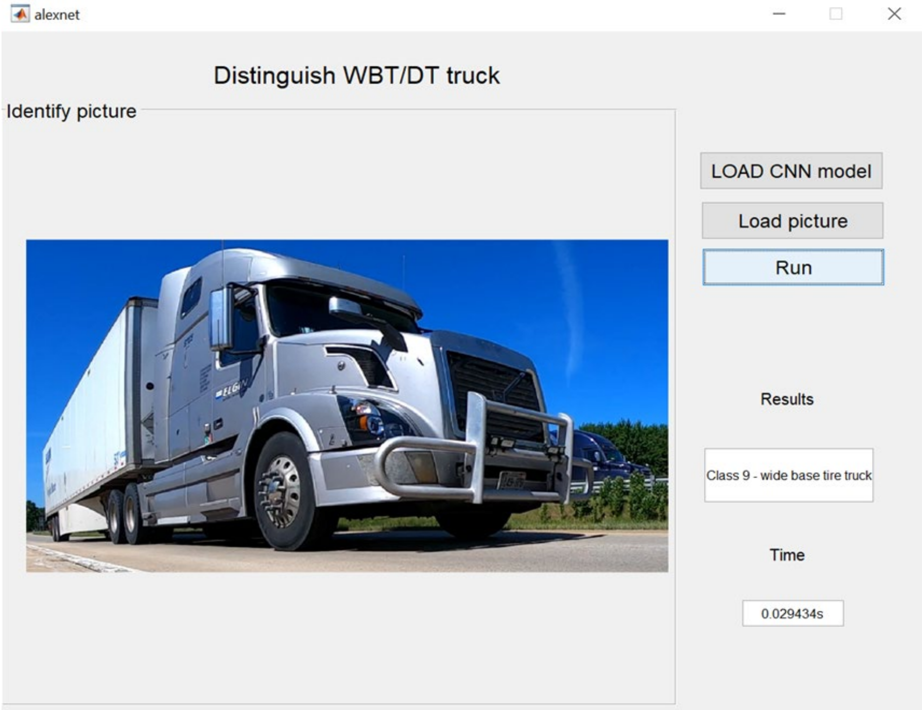

Figure C.2. CNN App interface showing WBT truck

The MATLAB code used to transfer the video to a picture that could be used for CNN training is shown below. The picture database is shown in Figure C.3.

MATLAB CODE:

```
%%%%%Video cut into image sequence
fileName = 'F:\Google drive\Jin-DongZhao\1Project\Wide-base Tire\20000221_041851.MOV';
%image_path=
obj = VideoReader(fileName);
numFrames = obj.NumberOfFrames;% Read the number of frames of the video CurrentTime
for i = 1 : numFrames
frame = read(obj,i);% Read every frame
imshow(frame);%Show every frame
namestyle=sprintf('%06d',i);
imwrite(frame,strcat(namestyle,'.png'),'png');% Save every frame
%imwrite(frame,strcat(num2str(i),'.png'),'png');% Save every frame
End
```

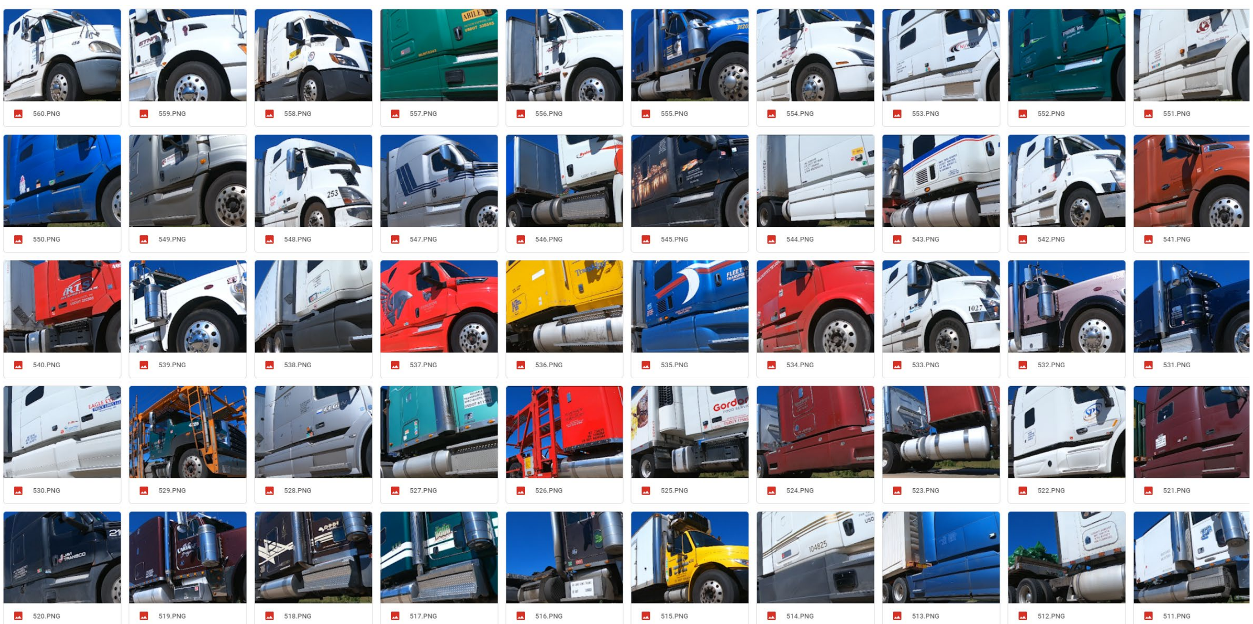

Figure C.3. CNN Training pictures that show WBT trucks

The MATLAB code used to train the picture based on the CNN method is shown below.

MATLAB CODE:

```
clear
clc
imds = imageDatastore('F:\Google drive\2016-Asphalt-Group\Jin-DongZhao\1Project\Wide-base
Tire\CNN\train', ...
   'IncludeSubfolders',true, ...
   'LabelSource','foldernames');
numTrainImages = numel(imds.Labels);
```

```
for i = 1:numTrainImages
    s = string(imds.Files(i));
    I = imread(s);
    I = imresize(I,[227,227]);
    imwrite(I,s);
    s
end

[imdsTrain,imdsValidation] = splitEachLabel(imds,0.76,'randomized');

net = alexnet;

inputSize = net.Layers(1).InputSize

layersTransfer = net.Layers(1:end-7);

numClasses = numel(categories(imdsTrain.Labels));

layers = [
    layersTransfer
    fullyConnectedLayer(numClasses,'WeightLearnRateFactor',20,'BiasLearnRateFactor',20)
    softmaxLayer
    classificationLayer];

augimdsValidation = augmentedImageDatastore(inputSize(1:2),imdsValidation);
augimdsTrain = augmentedImageDatastore(inputSize(1:2),imdsValidation);

options = trainingOptions('sgdm', ...
    'MiniBatchSize',8, ...
    'MaxEpochs',8, ...
    'InitialLearnRate',1e-4, ...
    'Shuffle','every-epoch', ...
    'ValidationData',augimdsValidation, ...
    'ValidationFrequency',4, ...
    'Verbose',false, ...
    'Plots','training-progress');

netTransfer = trainNetwork(augimdsTrain,layers,options);
```

The results of the CNN training process for distinguishing wide-base tire trucks are shown in Figure C.4. After training, the accuracy reached up to 96%.

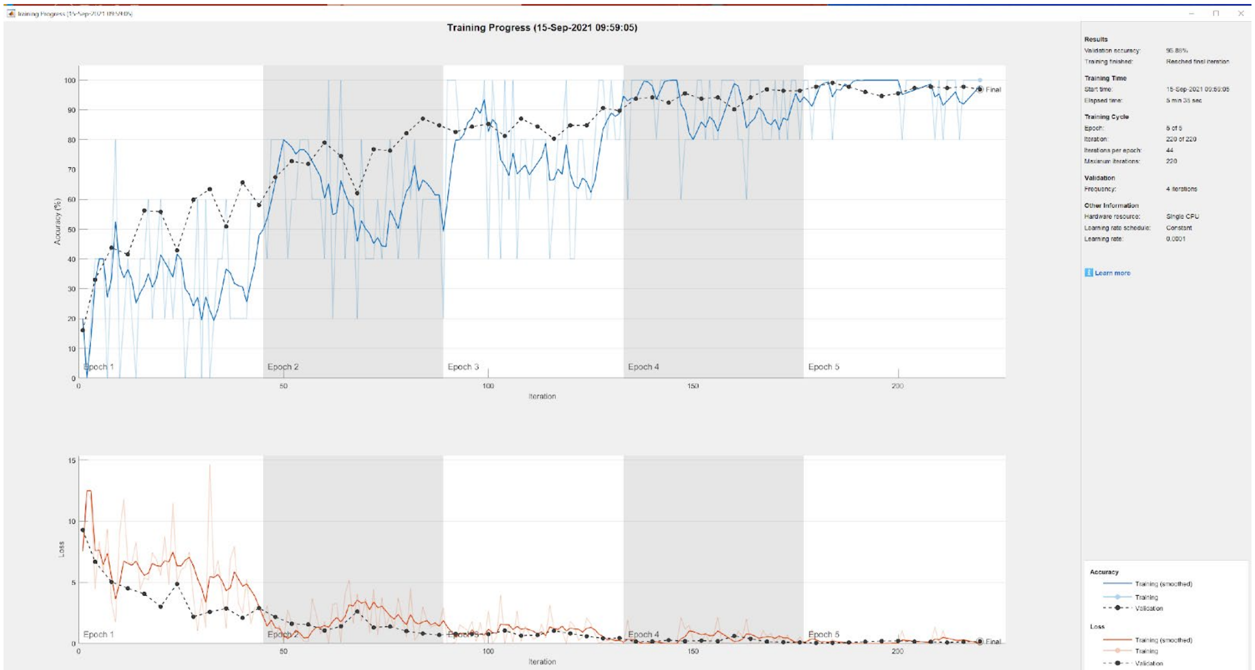

Figure C.4. CNN training process for wide-base tire trucks

The MATLAB code for the interface is shown below. After uploading the trained CNN model database and selecting pictures of trucks with WBT or not, the class level and whether the truck had WBTs would show in the results.

MATLAB CODE:

```
function varargout = alexnet(varargin)

gui_Singleton = 1;
gui_State = struct('gui_Name',       mfilename, ...
                   'gui_Singleton',  gui_Singleton, ...
                   'gui_OpeningFcn', @alexnet_OpeningFcn, ...
                   'gui_OutputFcn',  @alexnet_OutputFcn, ...
                   'gui_LayoutFcn',  [] , ...
                   'gui_Callback',   []);
if nargin && ischar(varargin{1})
   gui_State.gui_Callback = str2func(varargin{1});
end

if nargout
   [varargout{1:nargout}] = gui_mainfcn(gui_State, varargin{:} );
else
   gui_mainfcn(gui_State, varargin{:});
```

```
end

% --- Executes just before alexnet is made visible.
function alexnet_OpeningFcn(hObject, eventdata, handles, varargin)

handles.output = hObject;

% Update handles structure
guidata(hObject, handles);


% --- Outputs from this function are returned to the command line.
function varargout = alexnet_OutputFcn(hObject, eventdata, handles)

varargout [1]= handles.output;


% --- Executes on button press in pushbutton1.
function pushbutton1_Callback(hObject, eventdata, handles)
clear;
global netTransfer;
load('wbt.mat');

% --- Executes on button press in pushbutton2.
function pushbutton2_Callback(hObject, eventdata, handles)
global pic;
[filename filepath]=uigetfile('*.*','ÇëÑ¡ÔñÎÄ¼þ');
picpath = [filepath filename];
pic = imread(picpath);
axes(handles.axes1);
imshow(pic);


% --- Executes on button press in pushbutton3.
function pushbutton3_Callback(hObject, eventdata, handles)
global netTransfer;
global pic;
Pic = imresize(pic,[227,227]);
tic;
Tr = classify(netTransfer,Pic);
Tt = toc;
str_show1 = string(Tr);
str_show2 = [num2str(Tt) 's'];
set(handles.edit1,'string',str_show1);
set(handles.edit2,'string',str_show2);
function edit1_Callback(hObject, eventdata, handles)
```

```
% --- Executes during object creation, after setting all properties.
function edit1_CreateFcn(hObject, eventdata, handles)

if ispc && isequal(get(hObject,'BackgroundColor'), get(0,'defaultUicontrolBackgroundColor'))
    set(hObject,'BackgroundColor','white');
end


function edit2_Callback(hObject, eventdata, handles)


% --- Executes during object creation, after setting all properties.
function edit2_CreateFcn(hObject, eventdata, handles)

if ispc && isequal(get(hObject,'BackgroundColor'), get(0,'defaultUicontrolBackgroundColor'))
    set(hObject,'BackgroundColor','white');
end

% --- Executes during object creation, after setting all properties.
function axes1_CreateFcn(hObject, eventdata, handles)
```

D. APPENDIX D: FLEXIBLE PAVEMENT ME OUTPUT

Location 1. (5" AC) Global calibration; Asphalt and mixture: Level 3

Distress Prediction Summary

Distress Type	Distress @ Specified Reliability		Reliability (%)		Criterion Satisfied?
	Target	Predicted	Target	Achieved	
Terminal IRI (in/mile)	172.00	166.73	95.00	96.50	Pass
Permanent deformation - total pavement (in)	0.75	0.58	95.00	99.99	Pass
AC bottom-up fatigue cracking (% lane area)	20.00	1.86	95.00	100.00	Pass
AC thermal cracking (ft/mile)	1000.00	277.34	95.00	100.00	Pass
AC top-down fatigue cracking (% lane area)	20.00	9.57	95.00	100.00	Pass
Permanent deformation - AC only (in)	0.25	0.09	95.00	100.00	Pass

Location 1. (5" AC) Michigan calibration; Asphalt and mixture: Level 3

Distress Prediction Summary

Distress Type	Distress @ Specified Reliability		Reliability (%)		Criterion Satisfied?
	Target	Predicted	Target	Achieved	
Terminal IRI (in/mile)	172.00	138.84	95.00	99.78	Pass
Permanent deformation - total pavement (in)	0.50	0.36	95.00	99.93	Pass
AC bottom-up fatigue cracking (% lane area)	20.00	28.55	95.00	79.10	Fail
AC thermal cracking (ft/mile)	1000.00	1025.61	95.00	94.56	Fail
AC top-down fatigue cracking (% lane area)	20.00	9.57	95.00	100.00	Pass
Permanent deformation - AC only (in)	0.50	0.31	95.00	100.00	Pass

Location 1. (5" AC) Global calibration; Asphalt and mixture: Level 1

Distress Prediction Summary

Distress Type	Distress @ Specified Reliability		Reliability (%)		Criterion Satisfied?
	Target	Predicted	Target	Achieved	
Terminal IRI (in/mile)	172.00	166.92	95.00	96.45	Pass
Permanent deformation - total pavement (in)	0.75	0.57	95.00	100.00	Pass
AC bottom-up fatigue cracking (% lane area)	20.00	1.86	95.00	100.00	Pass
AC thermal cracking (ft/mile)	1000.00	277.34	95.00	100.00	Pass
AC top-down fatigue cracking (% lane area)	20.00	11.32	95.00	99.97	Pass
Permanent deformation - AC only (in)	0.25	0.09	95.00	100.00	Pass

Location 1. (5" AC) Michigan calibration; Asphalt and mixture: Level 1

Distress Prediction Summary

Distress Type	Distress @ Specified Reliability		Reliability (%)		Criterion Satisfied?
	Target	Predicted	Target	Achieved	
Terminal IRI (in/mile)	172.00	137.36	95.00	99.83	Pass
Permanent deformation - total pavement (in)	0.50	0.36	95.00	99.93	Pass
AC bottom-up fatigue cracking (% lane area)	20.00	26.27	95.00	84.52	Fail
AC thermal cracking (ft/mile)	1000.00	346.55	95.00	100.00	Pass
AC top-down fatigue cracking (% lane area)	20.00	11.32	95.00	99.97	Pass
Permanent deformation - AC only (in)	0.50	0.31	95.00	100.00	Pass

Figure D.1. Flexible Pavement ME output in location 1

Location 2. (5" AC) Global calibration; Asphalt and mixture: Level 3

Distress Prediction Summary

Distress Type	Distress @ Specified Reliability		Reliability (%)		Criterion Satisfied?
	Target	Predicted	Target	Achieved	
Terminal IRI (in/mile)	172.00	167.76	95.00	96.24	Pass
Permanent deformation - total pavement (in)	0.75	0.58	95.00	99.99	Pass
AC bottom-up fatigue cracking (% lane area)	20.00	1.86	95.00	100.00	Pass
AC thermal cracking (ft/mile)	1000.00	277.34	95.00	100.00	Pass
AC top-down fatigue cracking (% lane area)	20.00	10.13	95.00	99.99	Pass
Permanent deformation - AC only (in)	0.25	0.10	95.00	100.00	Pass

Location 2. (5" AC) Michigan calibration; Asphalt and mixture: Level 3

Distress Prediction Summary

Distress Type	Distress @ Specified Reliability		Reliability (%)		Criterion Satisfied?
	Target	Predicted	Target	Achieved	
Terminal IRI (in/mile)	172.00	141.09	95.00	99.71	Pass
Permanent deformation - total pavement (in)	0.50	0.39	95.00	99.79	Pass
AC bottom-up fatigue cracking (% lane area)	20.00	28.80	95.00	78.48	Fail
AC thermal cracking (ft/mile)	1000.00	1025.64	95.00	94.56	Fail
AC top-down fatigue cracking (% lane area)	20.00	10.13	95.00	99.99	Pass
Permanent deformation - AC only (in)	0.50	0.34	95.00	99.99	Pass

Location 2. (5" AC) Global calibration; Asphalt and mixture: Level 1

Distress Prediction Summary

Distress Type	Distress @ Specified Reliability		Reliability (%)		Criterion Satisfied?
	Target	Predicted	Target	Achieved	
Terminal IRI (in/mile)	172.00	168.52	95.00	96.03	Pass
Permanent deformation - total pavement (in)	0.75	0.57	95.00	100.00	Pass
AC bottom-up fatigue cracking (% lane area)	20.00	1.86	95.00	100.00	Pass
AC thermal cracking (ft/mile)	1000.00	277.34	95.00	100.00	Pass
AC top-down fatigue cracking (% lane area)	20.00	13.27	95.00	99.82	Pass
Permanent deformation - AC only (in)	0.25	0.10	95.00	100.00	Pass

Location 2. (5" AC) Michigan calibration; Asphalt and mixture: Level 1

Distress Prediction Summary

Distress Type	Distress @ Specified Reliability		Reliability (%)		Criterion Satisfied?
	Target	Predicted	Target	Achieved	
Terminal IRI (in/mile)	172.00	140.10	95.00	99.75	Pass
Permanent deformation - total pavement (in)	0.50	0.40	95.00	99.71	Pass
AC bottom-up fatigue cracking (% lane area)	20.00	26.44	95.00	84.16	Fail
AC thermal cracking (ft/mile)	1000.00	346.55	95.00	100.00	Pass
AC top-down fatigue cracking (% lane area)	20.00	13.27	95.00	99.82	Pass
Permanent deformation - AC only (in)	0.50	0.35	95.00	99.98	Pass

Figure D.2. Flexible Pavement ME output in location 2

Location 3. (6.5" AC) Global calibration; Asphalt and mixture: Level 3

Distress Prediction Summary

Distress Type	Distress @ Specified Reliability		Reliability (%)		Criterion Satisfied?
	Target	Predicted	Target	Achieved	
Terminal IRI (in/mile)	172.00	174.65	95.00	94.11	Fail
Permanent deformation - total pavement (in)	0.75	0.67	95.00	99.46	Pass
AC bottom-up fatigue cracking (% lane area)	20.00	1.89	95.00	100.00	Pass
AC thermal cracking (ft/mile)	1000.00	277.34	95.00	100.00	Pass
AC top-down fatigue cracking (% lane area)	20.00	17.08	95.00	98.29	Pass
Permanent deformation - AC only (in)	0.25	0.19	95.00	99.82	Pass

Location 3. (6.5" AC) Michigan calibration; Asphalt and mixture: Level 3

Distress Prediction Summary

Distress Type	Distress @ Specified Reliability		Reliability (%)		Criterion Satisfied?
	Target	Predicted	Target	Achieved	
Terminal IRI (in/mile)	172.00	160.40	95.00	97.84	Pass
Permanent deformation - total pavement (in)	0.50	0.69	95.00	43.15	Fail
AC bottom-up fatigue cracking (% lane area)	20.00	29.19	95.00	77.17	Fail
AC thermal cracking (ft/mile)	1000.00	1042.09	95.00	94.27	Fail
AC top-down fatigue cracking (% lane area)	20.00	17.08	95.00	98.29	Pass
Permanent deformation - AC only (in)	0.50	0.64	95.00	55.94	Fail

Location 3. (6.5" AC) Global calibration; Asphalt and mixture: Level 1

Distress Prediction Summary

Distress Type	Distress @ Specified Reliability		Reliability (%)		Criterion Satisfied?
	Target	Predicted	Target	Achieved	
Terminal IRI (in/mile)	172.00	178.14	95.00	92.79	Fail
Permanent deformation - total pavement (in)	0.75	0.73	95.00	97.06	Pass
AC bottom-up fatigue cracking (% lane area)	20.00	1.88	95.00	100.00	Pass
AC thermal cracking (ft/mile)	1000.00	304.00	95.00	100.00	Pass
AC top-down fatigue cracking (% lane area)	20.00	19.82	95.00	95.27	Pass
Permanent deformation - AC only (in)	0.25	0.27	95.00	91.36	Fail

Location 3. (6.5" AC) Michigan calibration; Asphalt and mixture: Level 1

Distress Prediction Summary

Distress Type	Distress @ Specified Reliability		Reliability (%)		Criterion Satisfied?
	Target	Predicted	Target	Achieved	
Terminal IRI (in/mile)	172.00	172.96	95.00	94.69	Fail
Permanent deformation - total pavement (in)	0.50	0.91	95.00	2.43	Fail
AC bottom-up fatigue cracking (% lane area)	20.00	28.09	95.00	80.04	Fail
AC thermal cracking (ft/mile)	1000.00	346.61	95.00	100.00	Pass
AC top-down fatigue cracking (% lane area)	20.00	19.82	95.00	95.27	Pass
Permanent deformation - AC only (in)	0.50	0.86	95.00	3.21	Fail

Figure D.3. Flexible Pavement ME output in location 3

Location 4. (9.5" AC) Global calibration; Asphalt and mixture: Level 3

Distress Prediction Summary

Distress Type	Distress @ Specified Reliability		Reliability (%)		Criterion Satisfied?
	Target	Predicted	Target	Achieved	
Terminal IRI (in/mile)	172.00	166.56	95.00	96.54	Pass
Permanent deformation - total pavement (in)	0.75	0.51	95.00	100.00	Pass
AC bottom-up fatigue cracking (% lane area)	20.00	1.86	95.00	100.00	Pass
AC thermal cracking (ft/mile)	1000.00	277.34	95.00	100.00	Pass
AC top-down fatigue cracking (% lane area)	20.00	16.25	95.00	98.84	Pass
Permanent deformation - AC only (in)	0.25	0.09	95.00	100.00	Pass

Location 4. (9.5" AC) Michigan calibration; Asphalt and mixture: Level 3

Distress Prediction Summary

Distress Type	Distress @ Specified Reliability		Reliability (%)		Criterion Satisfied?
	Target	Predicted	Target	Achieved	
Terminal IRI (in/mile)	172.00	142.42	95.00	99.64	Pass
Permanent deformation - total pavement (in)	0.50	0.39	95.00	99.83	Pass
AC bottom-up fatigue cracking (% lane area)	20.00	18.90	95.00	96.19	Pass
AC thermal cracking (ft/mile)	1000.00	2044.57	95.00	71.50	Fail
AC top-down fatigue cracking (% lane area)	20.00	16.25	95.00	98.84	Pass
Permanent deformation - AC only (in)	0.50	0.35	95.00	99.98	Pass

Location 4. (9.5" AC) Global calibration; Asphalt and mixture: Level 1

Distress Prediction Summary

Distress Type	Distress @ Specified Reliability		Reliability (%)		Criterion Satisfied?
	Target	Predicted	Target	Achieved	
Terminal IRI (in/mile)	172.00	187.98	95.00	88.24	Fail
Permanent deformation - total pavement (in)	0.75	0.49	95.00	100.00	Pass
AC bottom-up fatigue cracking (% lane area)	20.00	1.86	95.00	100.00	Pass
AC thermal cracking (ft/mile)	1000.00	2874.69	95.00	0.82	Fail
AC top-down fatigue cracking (% lane area)	20.00	15.50	95.00	99.22	Pass
Permanent deformation - AC only (in)	0.25	0.08	95.00	100.00	Pass

Structure 4. (9.5" AC) Michigan calibration; Asphalt and mixture: Level 1

Distress Prediction Summary

Distress Type	Distress @ Specified Reliability		Reliability (%)		Criterion Satisfied?
	Target	Predicted	Target	Achieved	
Terminal IRI (in/mile)	172.00	147.40	95.00	99.37	Pass
Permanent deformation - total pavement (in)	0.50	0.34	95.00	99.98	Pass
AC bottom-up fatigue cracking (% lane area)	20.00	17.47	95.00	97.44	Pass
AC thermal cracking (ft/mile)	1000.00	2625.96	95.00	33.12	Fail
AC top-down fatigue cracking (% lane area)	20.00	15.50	95.00	99.22	Pass
Permanent deformation - AC only (in)	0.50	0.30	95.00	100.00	Pass

Figure D.4. Flexible Pavement ME output in location 4

Location 5. (9.5" AC) Global calibration; Asphalt and mixture: Level 3 (Default)

Distress Prediction Summary

Distress Type	Distress @ Specified Reliability		Reliability (%)		Criterion Satisfied?
	Target	Predicted	Target	Achieved	
Terminal IRI (in/mile)	172.00	168.22	95.00	96.11	Pass
Permanent deformation - total pavement (in)	0.75	0.56	95.00	100.00	Pass
AC bottom-up fatigue cracking (% lane area)	20.00	1.89	95.00	100.00	Pass
AC thermal cracking (ft/mile)	1000.00	277.34	95.00	100.00	Pass
AC top-down fatigue cracking (% lane area)	20.00	16.33	95.00	98.80	Pass
Permanent deformation - AC only (in)	0.25	0.11	95.00	100.00	Pass

Location 5. (9.5" AC) Michigan calibration; Asphalt and mixture: Level 3 (Default)

Distress Prediction Summary

Distress Type	Distress @ Specified Reliability		Reliability (%)		Criterion Satisfied?
	Target	Predicted	Target	Achieved	
Terminal IRI (in/mile)	172.00	140.44	95.00	99.73	Pass
Permanent deformation - total pavement (in)	0.50	0.43	95.00	99.16	Pass
AC bottom-up fatigue cracking (% lane area)	20.00	21.87	95.00	92.51	Fail
AC thermal cracking (ft/mile)	1000.00	1076.93	95.00	93.63	Fail
AC top-down fatigue cracking (% lane area)	20.00	16.33	95.00	98.80	Pass
Permanent deformation - AC only (in)	0.50	0.39	95.00	99.88	Pass

Location 5. (9.5" AC) Global calibration; Asphalt and mixture: Level 1

Distress Prediction Summary

Distress Type	Distress @ Specified Reliability		Reliability (%)		Criterion Satisfied?
	Target	Predicted	Target	Achieved	
Terminal IRI (in/mile)	172.00	189.50	95.00	87.42	Fail
Permanent deformation - total pavement (in)	0.75	0.53	95.00	100.00	Pass
AC bottom-up fatigue cracking (% lane area)	20.00	1.87	95.00	100.00	Pass
AC thermal cracking (ft/mile)	1000.00	2874.69	95.00	0.82	Fail
AC top-down fatigue cracking (% lane area)	20.00	15.88	95.00	99.04	Pass
Permanent deformation - AC only (in)	0.25	0.09	95.00	100.00	Pass

Location 5. (9.5" AC) Michigan calibration; Asphalt and mixture: Level 1

Distress Prediction Summary

Distress Type	Distress @ Specified Reliability		Reliability (%)		Criterion Satisfied?
	Target	Predicted	Target	Achieved	
Terminal IRI (in/mile)	172.00	136.15	95.00	99.86	Pass
Permanent deformation - total pavement (in)	0.50	0.38	95.00	99.88	Pass
AC bottom-up fatigue cracking (% lane area)	20.00	20.07	95.00	94.91	Fail
AC thermal cracking (ft/mile)	1000.00	372.30	95.00	100.00	Pass
AC top-down fatigue cracking (% lane area)	20.00	15.88	95.00	99.04	Pass
Permanent deformation - AC only (in)	0.50	0.33	95.00	99.99	Pass

Figure D.5. Flexible Pavement ME output in location 5

Location 6. (11.5" AC) Global calibration; Asphalt and mixture: Level 3 (Default)

Distress Prediction Summary

Distress Type	Distress @ Specified Reliability		Reliability (%)		Criterion Satisfied?
	Target	Predicted	Target	Achieved	
Terminal IRI (in/mile)	172.00	161.33	95.00	97.68	Pass
Permanent deformation - total pavement (in)	0.75	0.44	95.00	100.00	Pass
AC bottom-up fatigue cracking (% lane area)	20.00	1.93	95.00	100.00	Pass
AC thermal cracking (ft/mile)	1000.00	277.34	95.00	100.00	Pass
AC top-down fatigue cracking (% lane area)	20.00	16.41	95.00	98.75	Pass
Permanent deformation - AC only (in)	0.25	0.09	95.00	100.00	Pass

Location 6. (11.5" AC) Michigan calibration; Asphalt and mixture: Level 3 (Default)

Distress Prediction Summary

Distress Type	Distress @ Specified Reliability		Reliability (%)		Criterion Satisfied?
	Target	Predicted	Target	Achieved	
Terminal IRI (in/mile)	172.00	137.01	95.00	99.84	Pass
Permanent deformation - total pavement (in)	0.50	0.39	95.00	99.83	Pass
AC bottom-up fatigue cracking (% lane area)	20.00	19.95	95.00	95.06	Pass
AC thermal cracking (ft/mile)	1000.00	1025.61	95.00	94.56	Fail
AC top-down fatigue cracking (% lane area)	20.00	16.41	95.00	98.75	Pass
Permanent deformation - AC only (in)	0.50	0.36	95.00	99.97	Pass

Location 6. (11.5" AC) Global calibration; Asphalt and mixture: Level 1

Distress Prediction Summary

Distress Type	Distress @ Specified Reliability		Reliability (%)		Criterion Satisfied?
	Target	Predicted	Target	Achieved	
Terminal IRI (in/mile)	172.00	161.14	95.00	97.72	Pass
Permanent deformation - total pavement (in)	0.75	0.44	95.00	100.00	Pass
AC bottom-up fatigue cracking (% lane area)	20.00	1.87	95.00	100.00	Pass
AC thermal cracking (ft/mile)	1000.00	277.34	95.00	100.00	Pass
AC top-down fatigue cracking (% lane area)	20.00	16.38	95.00	98.77	Pass
Permanent deformation - AC only (in)	0.25	0.11	95.00	100.00	Pass

Location 6. (11.5" AC) Michigan calibration; Asphalt and mixture: Level 1

Distress Prediction Summary

Distress Type	Distress @ Specified Reliability		Reliability (%)		Criterion Satisfied?
	Target	Predicted	Target	Achieved	
Terminal IRI (in/mile)	172.00	138.95	95.00	99.79	Pass
Permanent deformation - total pavement (in)	0.50	0.43	95.00	99.30	Pass
AC bottom-up fatigue cracking (% lane area)	20.00	18.16	95.00	96.88	Pass
AC thermal cracking (ft/mile)	1000.00	346.55	95.00	100.00	Pass
AC top-down fatigue cracking (% lane area)	20.00	16.38	95.00	98.77	Pass
Permanent deformation - AC only (in)	0.50	0.40	95.00	99.79	Pass

Figure D.6. Flexible Pavement ME output in location 6

Location 7. (11.5" AC) Global calibration; Asphalt and mixture: Level 3 (Default)

Distress Prediction Summary

Distress Type	Distress @ Specified Reliability		Reliability (%)		Criterion Satisfied?
	Target	Predicted	Target	Achieved	
Terminal IRI (in/mile)	172.00	164.87	95.00	96.95	Pass
Permanent deformation - total pavement (in)	0.75	0.47	95.00	100.00	Pass
AC bottom-up fatigue cracking (% lane area)	20.00	1.89	95.00	100.00	Pass
AC thermal cracking (ft/mile)	1000.00	277.34	95.00	100.00	Pass
AC top-down fatigue cracking (% lane area)	20.00	16.42	95.00	98.74	Pass
Permanent deformation - AC only (in)	0.25	0.10	95.00	100.00	Pass

Location 7. (11.5" AC) Michigan calibration; Asphalt and mixture: Level 3 (Default)

Distress Prediction Summary

Distress Type	Distress @ Specified Reliability		Reliability (%)		Criterion Satisfied?
	Target	Predicted	Target	Achieved	
Terminal IRI (in/mile)	172.00	138.85	95.00	99.79	Pass
Permanent deformation - total pavement (in)	0.50	0.40	95.00	99.69	Pass
AC bottom-up fatigue cracking (% lane area)	20.00	18.93	95.00	96.16	Pass
AC thermal cracking (ft/mile)	1000.00	1049.34	95.00	94.14	Fail
AC top-down fatigue cracking (% lane area)	20.00	16.42	95.00	98.74	Pass
Permanent deformation - AC only (in)	0.50	0.37	95.00	99.95	Pass

Location 7. (11.5" AC) Global calibration; Asphalt and mixture: Level 1

Distress Prediction Summary

Distress Type	Distress @ Specified Reliability		Reliability (%)		Criterion Satisfied?
	Target	Predicted	Target	Achieved	
Terminal IRI (in/mile)	172.00	180.92	95.00	91.64	Fail
Permanent deformation - total pavement (in)	0.75	0.47	95.00	100.00	Pass
AC bottom-up fatigue cracking (% lane area)	20.00	1.86	95.00	100.00	Pass
AC thermal cracking (ft/mile)	1000.00	2095.18	95.00	10.10	Fail
AC top-down fatigue cracking (% lane area)	20.00	16.41	95.00	98.75	Pass
Permanent deformation - AC only (in)	0.25	0.12	95.00	100.00	Pass

Location 7. (11.5" AC) Michigan calibration; Asphalt and mixture: Level 1

Distress Prediction Summary

Distress Type	Distress @ Specified Reliability		Reliability (%)		Criterion Satisfied?
	Target	Predicted	Target	Achieved	
Terminal IRI (in/mile)	172.00	141.79	95.00	99.69	Pass
Permanent deformation - total pavement (in)	0.50	0.46	95.00	98.18	Pass
AC bottom-up fatigue cracking (% lane area)	20.00	17.27	95.00	97.60	Pass
AC thermal cracking (ft/mile)	1000.00	346.57	95.00	100.00	Pass
AC top-down fatigue cracking (% lane area)	20.00	16.41	95.00	98.75	Pass
Permanent deformation - AC only (in)	0.50	0.43	95.00	99.39	Pass

Figure D.7. Flexible Pavement ME output in location 7

E. APPENDIX E: RIGID PAVEMENT ME OUTPUT

Open graded:

Location 1. 6" slab ; 1" dowel diameter; 12" joint spacing;

Distress Prediction Summary

Distress Type	Distress @ Specified Reliability		Reliability (%)		Criterion Satisfied?
	Target	Predicted	Target	Achieved	
Terminal IRI (in/mile)	172.00	166.47	95.00	96.40	Pass
Mean joint faulting (in)	0.13	0.04	95.00	100.00	Pass
JPCP transverse cracking (percent slabs)	15.00	33.96	95.00	41.15	Fail

Location 1. 6.5" slab ; 1" dowel diameter; 12" joint spacing;

Distress Prediction Summary

Distress Type	Distress @ Specified Reliability		Reliability (%)		Criterion Satisfied?
	Target	Predicted	Target	Achieved	
Terminal IRI (in/mile)	172.00	150.30	95.00	98.95	Pass
Mean joint faulting (in)	0.13	0.04	95.00	100.00	Pass
JPCP transverse cracking (percent slabs)	15.00	12.83	95.00	97.77	Pass

Location 1. 7" slab ; 1" dowel diameter; 12" joint spacing;

Distress Prediction Summary

Distress Type	Distress @ Specified Reliability		Reliability (%)		Criterion Satisfied?
	Target	Predicted	Target	Achieved	
Terminal IRI (in/mile)	172.00	148.09	95.00	99.15	Pass
Mean joint faulting (in)	0.13	0.05	95.00	100.00	Pass
JPCP transverse cracking (percent slabs)	15.00	6.13	95.00	100.00	Pass

Figure E.1. Rigid Pavement ME output in location 1 (Open graded)

Location 2. 6" slab ; 1" dowel diameter; 12" joint spacing;

Distress Prediction Summary

Distress Type	Distress @ Specified Reliability		Reliability (%)		Criterion Satisfied?
	Target	Predicted	Target	Achieved	
Terminal IRI (in/mile)	172.00	143.24	95.00	99.48	Pass
Mean joint faulting (in)	0.13	0.05	95.00	100.00	Pass
JPCP transverse cracking (percent slabs)	15.00	8.71	95.00	99.88	Pass

Location 2. 6.5" slab ; 1" dowel diameter; 12" joint spacing;

Distress Prediction Summary

Distress Type	Distress @ Specified Reliability		Reliability (%)		Criterion Satisfied?
	Target	Predicted	Target	Achieved	
Terminal IRI (in/mile)	172.00	143.24	95.00	99.48	Pass
Mean joint faulting (in)	0.13	0.05	95.00	100.00	Pass
JPCP transverse cracking (percent slabs)	15.00	4.44	95.00	100.00	Pass

Location 2. 7" slab ; 1" dowel diameter; 12" joint spacing;

Distress Prediction Summary

Distress Type	Distress @ Specified Reliability		Reliability (%)		Criterion Satisfied?
	Target	Predicted	Target	Achieved	
Terminal IRI (in/mile)	172.00	143.85	95.00	99.44	Pass
Mean joint faulting (in)	0.13	0.05	95.00	100.00	Pass
JPCP transverse cracking (percent slabs)	15.00	2.79	95.00	100.00	Pass

Figure E.2. Rigid Pavement ME output in location 2 (Open graded)

Location 3. 7.5" slab ; 1" dowel diameter; 12" joint spacing;

Distress Prediction Summary

Distress Type	Distress @ Specified Reliability		Reliability (%)		Criterion Satisfied?
	Target	Predicted	Target	Achieved	
Terminal IRI (in/mile)	172.00	179.72	95.00	92.65	Fail
Mean joint faulting (in)	0.13	0.10	95.00	99.36	Pass
JPCP transverse cracking (percent slabs)	15.00	1.23	95.00	100.00	Pass

Location 3. 8" slab ; 1.25" dowel diameter; 12" joint spacing;

Distress Prediction Summary

Distress Type	Distress @ Specified Reliability		Reliability (%)		Criterion Satisfied?
	Target	Predicted	Target	Achieved	
Terminal IRI (in/mile)	172.00	143.59	95.00	99.46	Pass
Mean joint faulting (in)	0.13	0.05	95.00	100.00	Pass
JPCP transverse cracking (percent slabs)	15.00	1.23	95.00	100.00	Pass

Location 3. 8.5" slab ; 1.25" dowel diameter; 12" joint spacing;

Distress Prediction Summary

Distress Type	Distress @ Specified Reliability		Reliability (%)		Criterion Satisfied?
	Target	Predicted	Target	Achieved	
Terminal IRI (in/mile)	172.00	142.25	95.00	99.54	Pass
Mean joint faulting (in)	0.13	0.05	95.00	100.00	Pass
JPCP transverse cracking (percent slabs)	15.00	1.23	95.00	100.00	Pass

Figure E.3. Rigid Pavement ME output in location 3 (Open graded)

Location 4. 7.5" slab ; 1" dowel diameter; 12" joint spacing;

Distress Prediction Summary

Distress Type	Distress @ Specified Reliability		Reliability (%)		Criterion Satisfied?
	Target	Predicted	Target	Achieved	
Terminal IRI (in/mile)	172.00	223.90	95.00	71.38	Fail
Mean joint faulting (in)	0.13	0.16	95.00	76.09	Fail
JPCP transverse cracking (percent slabs)	15.00	2.46	95.00	100.00	Pass

Location 4. 8" slab ; 1.25" dowel diameter; 12" joint spacing;

Distress Prediction Summary

Distress Type	Distress @ Specified Reliability		Reliability (%)		Criterion Satisfied?
	Target	Predicted	Target	Achieved	
Terminal IRI (in/mile)	172.00	156.57	95.00	98.02	Pass
Mean joint faulting (in)	0.13	0.07	95.00	99.99	Pass
JPCP transverse cracking (percent slabs)	15.00	1.23	95.00	100.00	Pass

Location 4. 8.5" slab ; 1.25" dowel diameter; 12" joint spacing;

Distress Prediction Summary

Distress Type	Distress @ Specified Reliability		Reliability (%)		Criterion Satisfied?
	Target	Predicted	Target	Achieved	
Terminal IRI (in/mile)	172.00	154.64	95.00	98.42	Pass
Mean joint faulting (in)	0.13	0.07	95.00	99.99	Pass
JPCP transverse cracking (percent slabs)	15.00	1.23	95.00	100.00	Pass

Figure E.4. Rigid Pavement ME output in location 4 (Open graded)

Location 5. 8" slab ; 1.25" dowel diameter; 12" joint spacing;

Distress Prediction Summary

Distress Type	Distress @ Specified Reliability		Reliability (%)		Criterion Satisfied?
	Target	Predicted	Target	Achieved	
Terminal IRI (in/mile)	172.00	172.75	95.00	94.80	Fail
Mean joint faulting (in)	0.13	0.10	95.00	99.47	Pass
JPCP transverse cracking (percent slabs)	15.00	1.23	95.00	100.00	Pass

Location 5. 8" slab ; 1.5" dowel diameter; 12" joint spacing;

Distress Prediction Summary

Distress Type	Distress @ Specified Reliability		Reliability (%)		Criterion Satisfied?
	Target	Predicted	Target	Achieved	
Terminal IRI (in/mile)	172.00	154.22	95.00	98.47	Pass
Mean joint faulting (in)	0.13	0.07	95.00	99.98	Pass
JPCP transverse cracking (percent slabs)	15.00	1.23	95.00	100.00	Pass

Location 5. 8.5" slab ; 1.25" dowel diameter; 12" joint spacing;

Distress Prediction Summary

Distress Type	Distress @ Specified Reliability		Reliability (%)		Criterion Satisfied?
	Target	Predicted	Target	Achieved	
Terminal IRI (in/mile)	172.00	170.42	95.00	95.41	Pass
Mean joint faulting (in)	0.13	0.09	95.00	99.60	Pass
JPCP transverse cracking (percent slabs)	15.00	1.23	95.00	100.00	Pass

Location 5. 9" slab ; 1.25" dowel diameter; 14" joint spacing;

Distress Prediction Summary

Distress Type	Distress @ Specified Reliability		Reliability (%)		Criterion Satisfied?
	Target	Predicted	Target	Achieved	
Terminal IRI (in/mile)	172.00	175.19	95.00	94.08	Fail
Mean joint faulting (in)	0.13	0.11	95.00	97.66	Pass
JPCP transverse cracking (percent slabs)	15.00	1.23	95.00	100.00	Pass

Figure E.5. Rigid Pavement ME output in location 5 (Open graded)

Location 6. 12" slab ; 1.5" dowel diameter; 16" joint spacing;

Distress Prediction Summary

Distress Type	Distress @ Specified Reliability		Reliability (%)		Criterion Satisfied?
	Target	Predicted	Target	Achieved	
Terminal IRI (in/mile)	172.00	176.24	95.00	93.74	Fail
Mean joint faulting (in)	0.13	0.13	95.00	93.96	Fail
JPCP transverse cracking (percent slabs)	15.00	1.23	95.00	100.00	Pass

Location 6. 12" slab ; 1.5" dowel diameter; 14" joint spacing;

Distress Prediction Summary

Distress Type	Distress @ Specified Reliability		Reliability (%)		Criterion Satisfied?
	Target	Predicted	Target	Achieved	
Terminal IRI (in/mile)	172.00	169.07	95.00	95.76	Pass
Mean joint faulting (in)	0.13	0.10	95.00	98.87	Pass
JPCP transverse cracking (percent slabs)	15.00	1.23	95.00	100.00	Pass

Location 6. 12.5" slab ; 1.5" dowel diameter; 16" joint spacing;

Distress Prediction Summary

Distress Type	Distress @ Specified Reliability		Reliability (%)		Criterion Satisfied?
	Target	Predicted	Target	Achieved	
Terminal IRI (in/mile)	172.00	173.53	95.00	94.56	Fail
Mean joint faulting (in)	0.13	0.12	95.00	95.34	Pass
JPCP transverse cracking (percent slabs)	15.00	1.23	95.00	100.00	Pass

Location 6. 13" slab ; 1.5" dowel diameter; 16" joint spacing;

Distress Prediction Summary

Distress Type	Distress @ Specified Reliability		Reliability (%)		Criterion Satisfied?
	Target	Predicted	Target	Achieved	
Terminal IRI (in/mile)	172.00	172.65	95.00	94.82	Fail
Mean joint faulting (in)	0.13	0.12	95.00	95.72	Pass
JPCP transverse cracking (percent slabs)	15.00	1.23	95.00	100.00	Pass

Figure E.6. Rigid Pavement ME output in location 6 (Open graded)

Location 7. 10" slab ; 1.25" dowel diameter; 14" joint spacing;

Distress Prediction Summary

Distress Type	Distress @ Specified Reliability		Reliability (%)		Criterion Satisfied?
	Target	Predicted	Target	Achieved	
Terminal IRI (in/mile)	172.00	197.57	95.00	85.17	Fail
Mean joint faulting (in)	0.13	0.14	95.00	86.91	Fail
JPCP transverse cracking (percent slabs)	15.00	1.23	95.00	100.00	Pass

Location 7. 10.5" slab ; 1.5" dowel diameter; 14" joint spacing;

Distress Prediction Summary

Distress Type	Distress @ Specified Reliability		Reliability (%)		Criterion Satisfied?
	Target	Predicted	Target	Achieved	
Terminal IRI (in/mile)	172.00	164.00	95.00	96.91	Pass
Mean joint faulting (in)	0.13	0.09	95.00	99.60	Pass
JPCP transverse cracking (percent slabs)	15.00	1.23	95.00	100.00	Pass

Location 7. 11" slab ; 1.5" dowel diameter; 14" joint spacing;

Distress Prediction Summary

Distress Type	Distress @ Specified Reliability		Reliability (%)		Criterion Satisfied?
	Target	Predicted	Target	Achieved	
Terminal IRI (in/mile)	172.00	161.85	95.00	97.33	Pass
Mean joint faulting (in)	0.13	0.09	95.00	99.72	Pass
JPCP transverse cracking (percent slabs)	15.00	1.23	95.00	100.00	Pass

Figure E.7. Rigid Pavement ME output in location 7 (Open graded)

Dense graded:

Location 1. 6" slab ; 1" dowel diameter; 12" joint spacing;

Distress Prediction Summary

Distress Type	Distress @ Specified Reliability		Reliability (%)		Criterion Satisfied?
	Target	Predicted	Target	Achieved	
Terminal IRI (in/mile)	172.00	173.03	95.00	94.71	Fail
Mean joint faulting (in)	0.13	0.05	95.00	100.00	Pass
JPCP transverse cracking (percent slabs)	15.00	35.33	95.00	37.41	Fail

Location 1. 6.5" slab ; 1" dowel diameter; 12" joint spacing;

Distress Prediction Summary

Distress Type	Distress @ Specified Reliability		Reliability (%)		Criterion Satisfied?
	Target	Predicted	Target	Achieved	
Terminal IRI (in/mile)	172.00	156.60	95.00	98.19	Pass
Mean joint faulting (in)	0.13	0.05	95.00	100.00	Pass
JPCP transverse cracking (percent slabs)	15.00	13.24	95.00	97.35	Pass

Location 1. 7" slab ; 1" dowel diameter; 12" joint spacing;

Distress Prediction Summary

Distress Type	Distress @ Specified Reliability		Reliability (%)		Criterion Satisfied?
	Target	Predicted	Target	Achieved	
Terminal IRI (in/mile)	172.00	154.38	95.00	98.49	Pass
Mean joint faulting (in)	0.13	0.06	95.00	100.00	Pass
JPCP transverse cracking (percent slabs)	15.00	6.26	95.00	100.00	Pass

Figure E.8. Rigid Pavement ME output in location 1 (Dense graded)

Location 2. 6" slab ; 1" dowel diameter; 12" joint spacing;

Distress Prediction Summary

Distress Type	Distress @ Specified Reliability		Reliability (%)		Criterion Satisfied?
	Target	Predicted	Target	Achieved	
Terminal IRI (in/mile)	172.00	146.77	95.00	99.23	Pass
Mean joint faulting (in)	0.13	0.05	95.00	100.00	Pass
JPCP transverse cracking (percent slabs)	15.00	9.08	95.00	99.82	Pass

Location 2. 6.5" slab ; 1" dowel diameter; 12" joint spacing;

Distress Prediction Summary

Distress Type	Distress @ Specified Reliability		Reliability (%)		Criterion Satisfied?
	Target	Predicted	Target	Achieved	
Terminal IRI (in/mile)	172.00	146.80	95.00	99.23	Pass
Mean joint faulting (in)	0.13	0.06	95.00	100.00	Pass
JPCP transverse cracking (percent slabs)	15.00	4.52	95.00	100.00	Pass

Location 2. 7" slab ; 1" dowel diameter; 12" joint spacing;

Distress Prediction Summary

Distress Type	Distress @ Specified Reliability		Reliability (%)		Criterion Satisfied?
	Target	Predicted	Target	Achieved	
Terminal IRI (in/mile)	172.00	147.26	95.00	99.19	Pass
Mean joint faulting (in)	0.13	0.06	95.00	100.00	Pass
JPCP transverse cracking (percent slabs)	15.00	2.79	95.00	100.00	Pass

Figure E.9. Rigid Pavement ME output in location 2 (Dense graded)

Location 3. 7.5" slab ; 1" dowel diameter; 12" joint spacing;

Distress Prediction Summary

Distress Type	Distress @ Specified Reliability		Reliability (%)		Criterion Satisfied?
	Target	Predicted	Target	Achieved	
Terminal IRI (in/mile)	172.00	188.94	95.00	89.21	Fail
Mean joint faulting (in)	0.13	0.11	95.00	98.12	Pass
JPCP transverse cracking (percent slabs)	15.00	1.23	95.00	100.00	Pass

Location 3. 8" slab ; 1.25" dowel diameter; 12" joint spacing;

Distress Prediction Summary

Distress Type	Distress @ Specified Reliability		Reliability (%)		Criterion Satisfied?
	Target	Predicted	Target	Achieved	
Terminal IRI (in/mile)	172.00	146.69	95.00	99.25	Pass
Mean joint faulting (in)	0.13	0.05	95.00	100.00	Pass
JPCP transverse cracking (percent slabs)	15.00	1.23	95.00	100.00	Pass

Location 3. 8.5" slab ; 1.25" dowel diameter; 12" joint spacing;

Distress Prediction Summary

Distress Type	Distress @ Specified Reliability		Reliability (%)		Criterion Satisfied?
	Target	Predicted	Target	Achieved	
Terminal IRI (in/mile)	172.00	145.04	95.00	99.37	Pass
Mean joint faulting (in)	0.13	0.05	95.00	100.00	Pass
JPCP transverse cracking (percent slabs)	15.00	1.23	95.00	100.00	Pass

Figure E.10. Rigid Pavement ME output in location 3 (Dense graded)

Location 4. 7.5" slab ; 1" dowel diameter; 12" joint spacing;

Distress Prediction Summary

Distress Type	Distress @ Specified Reliability		Reliability (%)		Criterion Satisfied?
	Target	Predicted	Target	Achieved	
Terminal IRI (in/mile)	172.00	233.61	95.00	65.67	Fail
Mean joint faulting (in)	0.13	0.17	95.00	66.12	Fail
JPCP transverse cracking (percent slabs)	15.00	2.46	95.00	100.00	Pass

Location 4. 8" slab ; 1.25" dowel diameter; 12" joint spacing;

Distress Prediction Summary

Distress Type	Distress @ Specified Reliability		Reliability (%)		Criterion Satisfied?
	Target	Predicted	Target	Achieved	
Terminal IRI (in/mile)	172.00	161.21	95.00	97.41	Pass
Mean joint faulting (in)	0.13	0.08	95.00	99.94	Pass
JPCP transverse cracking (percent slabs)	15.00	1.23	95.00	100.00	Pass

Location 4. 8.5" slab ; 1.25" dowel diameter; 12" joint spacing;

Distress Prediction Summary

Distress Type	Distress @ Specified Reliability		Reliability (%)		Criterion Satisfied?
	Target	Predicted	Target	Achieved	
Terminal IRI (in/mile)	172.00	158.68	95.00	97.84	Pass
Mean joint faulting (in)	0.13	0.08	95.00	99.96	Pass
JPCP transverse cracking (percent slabs)	15.00	1.23	95.00	100.00	Pass

Figure E.11. Rigid Pavement ME output in location 4 (Dense graded)

Location 5. 8" slab ; 1.25" dowel diameter; 12" joint spacing;

Distress Prediction Summary

Distress Type	Distress @ Specified Reliability		Reliability (%)		Criterion Satisfied?
	Target	Predicted	Target	Achieved	
Terminal IRI (in/mile)	172.00	178.73	95.00	93.00	Fail
Mean joint faulting (in)	0.13	0.10	95.00	98.87	Pass
JPCP transverse cracking (percent slabs)	15.00	1.23	95.00	100.00	Pass

Location 5. 8" slab ; 1.5" dowel diameter; 12" joint spacing;

Distress Prediction Summary

Distress Type	Distress @ Specified Reliability		Reliability (%)		Criterion Satisfied?
	Target	Predicted	Target	Achieved	
Terminal IRI (in/mile)	172.00	158.47	95.00	97.87	Pass
Mean joint faulting (in)	0.13	0.08	95.00	99.95	Pass
JPCP transverse cracking (percent slabs)	15.00	1.23	95.00	100.00	Pass

Location 5. 8.5" slab ; 1.25" dowel diameter; 12" joint spacing;

Distress Prediction Summary

Distress Type	Distress @ Specified Reliability		Reliability (%)		Criterion Satisfied?
	Target	Predicted	Target	Achieved	
Terminal IRI (in/mile)	172.00	176.04	95.00	93.84	Fail
Mean joint faulting (in)	0.13	0.10	95.00	99.16	Pass
JPCP transverse cracking (percent slabs)	15.00	1.23	95.00	100.00	Pass

Location 5. 9" slab ; 1.25" dowel diameter; 14" joint spacing;

Distress Prediction Summary

Distress Type	Distress @ Specified Reliability		Reliability (%)		Criterion Satisfied?
	Target	Predicted	Target	Achieved	
Terminal IRI (in/mile)	172.00	180.38	95.00	92.39	Fail
Mean joint faulting (in)	0.13	0.12	95.00	96.01	Pass
JPCP transverse cracking (percent slabs)	15.00	1.23	95.00	100.00	Pass

Figure E.12. Rigid Pavement ME output in location 5 (Dense graded)

Location 6. 12" slab ; 1.5" dowel diameter; 16" joint spacing;

Distress Prediction Summary

Distress Type	Distress @ Specified Reliability		Reliability (%)		Criterion Satisfied?
	Target	Predicted	Target	Achieved	
Terminal IRI (in/mile)	172.00	178.71	95.00	92.93	Fail
Mean joint faulting (in)	0.13	0.13	95.00	92.44	Fail
JPCP transverse cracking (percent slabs)	15.00	1.23	95.00	100.00	Pass

Location 6. 12" slab ; 1.5" dowel diameter; 14" joint spacing;

Distress Prediction Summary

Distress Type	Distress @ Specified Reliability		Reliability (%)		Criterion Satisfied?
	Target	Predicted	Target	Achieved	
Terminal IRI (in/mile)	172.00	171.46	95.00	95.15	Pass
Mean joint faulting (in)	0.13	0.11	95.00	98.47	Pass
JPCP transverse cracking (percent slabs)	15.00	1.23	95.00	100.00	Pass

Location 6. 12.5" slab ; 1.5" dowel diameter; 16" joint spacing;

Distress Prediction Summary

Distress Type	Distress @ Specified Reliability		Reliability (%)		Criterion Satisfied?
	Target	Predicted	Target	Achieved	
Terminal IRI (in/mile)	172.00	175.72	95.00	93.90	Fail
Mean joint faulting (in)	0.13	0.13	95.00	94.21	Fail
JPCP transverse cracking (percent slabs)	15.00	1.23	95.00	100.00	Pass

Location 6. 13" slab ; 1.5" dowel diameter; 16" joint spacing;

Distress Prediction Summary

Distress Type	Distress @ Specified Reliability		Reliability (%)		Criterion Satisfied?
	Target	Predicted	Target	Achieved	
Terminal IRI (in/mile)	172.00	172.79	95.00	94.78	Fail
Mean joint faulting (in)	0.13	0.12	95.00	95.65	Pass
JPCP transverse cracking (percent slabs)	15.00	1.23	95.00	100.00	Pass

Figure E.13. Rigid Pavement ME output in location 6 (Dense graded)

Location 7. 10" slab ; 1.25" dowel diameter; 14" joint spacing;

Distress Prediction Summary

Distress Type	Distress @ Specified Reliability		Reliability (%)		Criterion Satisfied?
	Target	Predicted	Target	Achieved	
Terminal IRI (in/mile)	172.00	204.75	95.00	81.53	Fail
Mean joint faulting (in)	0.13	0.16	95.00	80.29	Fail
JPCP transverse cracking (percent slabs)	15.00	1.23	95.00	100.00	Pass

Location 7. 10.5" slab ; 1.5" dowel diameter; 14" joint spacing;

Distress Prediction Summary

Distress Type	Distress @ Specified Reliability		Reliability (%)		Criterion Satisfied?
	Target	Predicted	Target	Achieved	
Terminal IRI (in/mile)	172.00	168.58	95.00	95.88	Pass
Mean joint faulting (in)	0.13	0.10	95.00	99.19	Pass
JPCP transverse cracking (percent slabs)	15.00	1.23	95.00	100.00	Pass

Location 7. 11" slab ; 1.5" dowel diameter; 14" joint spacing;

Distress Prediction Summary

Distress Type	Distress @ Specified Reliability		Reliability (%)		Criterion Satisfied?
	Target	Predicted	Target	Achieved	
Terminal IRI (in/mile)	172.00	164.99	95.00	96.70	Pass
Mean joint faulting (in)	0.13	0.10	95.00	99.52	Pass
JPCP transverse cracking (percent slabs)	15.00	1.23	95.00	100.00	Pass

Figure E.14. Rigid Pavement ME output in location 7 (Dense graded)

F. APPENDIX F: STRESS AT BOTTOM OF SLAB WITH DIFFERENT SLAB THICKNESSES

Table F.1. Stress at the bottom of the slab (0" from shoulder joint; 6" slab thickness)

Variables		Stress (psi)		
ΔT (°F)	**Tire pressure (psi)**	**Under DT load**	**Under WBT tire load (+20% tire pressure)**	**Percent increase (%)**
-30	**80**	-343.610	-439.375	27.87
	100	-366.492	-476.387	29.99
	120	-385.569	-507.438	31.61
-20	**80**	-340.530	-436.685	28.24
	100	-363.501	-473.805	30.34
	120	-382.646	-504.941	31.96
-10	**80**	-358.970	-456.044	27.04
	100	-382.048	-493.284	29.12
	120	-401.276	-524.512	30.71
0	**80**	-421.649	-519.376	23.18
	100	-444.774	-556.660	25.16
	120	-464.036	-587.922	26.70
10	**80**	-496.120	-593.832	19.70
	100	-519.244	-631.114	21.54
	120	-538.505	-662.374	23.00
20	**80**	-564.443	-662.488	17.37
	100	-587.596	-699.806	19.10
	120	-606.880	-731.092	20.47
30	**80**	-628.688	-725.675	15.43
	100	-651.876	-763.029	17.05
	120	-671.187	-794.345	18.35

Table F.2. Stress at the bottom of the slab (10" from shoulder joint; 6" slab thickness)

Variables		Stress (psi)		
ΔT (°F)	Tire pressure (psi)	Under DT load	Under WBT tire load (+20% tire pressure)	Percent increase (%)
-30	80	-127.059	-172.290	35.60
	100	-132.323	-181.253	36.98
	120	-136.354	-188.174	38.00
-20	80	-122.249	-167.343	36.89
	100	-127.516	-176.402	38.34
	120	-131.550	-183.394	39.41
-10	80	-137.431	-183.639	33.62
	100	-142.821	-192.841	35.02
	120	-146.948	-199.944	36.06
0	80	-198.600	-245.664	23.70
	100	-204.044	-254.927	24.94
	120	-208.213	-262.075	25.87
10	80	-273.076	-320.141	17.24
	100	-278.521	-329.404	18.27
	120	-282.690	-336.552	19.05
20	80	-340.647	-388.075	13.92
	100	-346.123	-397.374	14.81
	120	-350.315	-404.549	15.48
30	80	-404.115	-450.555	11.49
	100	-409.617	-459.892	12.27
	120	-413.830	-467.097	12.87

Table F.3. Stress at the bottom of the slab (18" from shoulder joint; 6" slab thickness)

Variables		Stress (psi)		
ΔT (°F)	Tire pressure (psi)	Under DT load	Under WBT tire load (+20% tire pressure)	Percent increase (%)
-30	**80**	-54.882	-82.495	50.31
	100	-57.704	-87.133	51.00
	120	-59.850	-90.653	51.47
-20	**80**	-51.081	-77.115	50.97
	100	-53.815	-81.678	51.78
	120	-55.897	-85.171	52.37
-10	**80**	-63.668	-90.799	42.61
	100	-66.508	-95.504	43.60
	120	-68.673	-99.106	44.32
0	**80**	-123.470	-151.568	22.76
	100	-126.374	-156.345	23.72
	120	-128.586	-160.000	24.43
10	**80**	-197.929	-226.035	14.20
	100	-200.834	-230.813	14.93
	120	-203.047	-234.469	15.48
20	**80**	-264.908	-293.358	10.74
	100	-267.843	-298.173	11.32
	120	-270.078	-301.857	11.77
30	**80**	-327.814	-355.443	8.43
	100	-330.774	-360.289	8.92
	120	-333.030	-363.997	9.30

Table F.4. Stress at the bottom of the slab (0" from shoulder joint; 8" slab thickness)

Variables		Stress (psi)		
ΔT (°F)	Tire pressure (psi)	Under DT load	Under WBT tire load (+20% tire pressure)	Percent increase (%)
-30	80	-223.607	-281.529	25.90
	100	-236.974	-303.052	27.88
	120	-248.080	-321.053	29.42
-20	80	-225.608	-283.525	25.67
	100	-239.016	-305.098	27.65
	120	-250.154	-323.138	29.18
-10	80	-242.629	-300.748	23.95
	100	-256.092	-322.388	25.89
	120	-267.274	-340.478	27.39
0	80	-286.818	-345.179	20.35
	100	-300.308	-366.848	22.16
	120	-311.510	-384.961	23.58
10	80	-335.598	-393.959	17.39
	100	-349.088	-415.628	19.06
	120	-360.290	-433.740	20.39
20	80	-382.256	-440.777	15.31
	100	-395.761	-462.464	16.85
	120	-406.974	-480.589	18.09
30	80	-423.153	-480.474	13.55
	100	-436.657	-502.171	15.00
	120	-447.872	-520.306	16.17

Table F.5. Stress at the bottom of the slab (10" from shoulder joint; 8" slab thickness)

Variables		Stress (psi)		
ΔT (°F)	**Tire pressure (psi)**	**Under DT load**	**Under WBT tire load (+20% tire pressure)**	**Percent increase (%)**
-30	**80**	-91.564	-120.291	31.37
	100	-94.899	-125.870	32.64
	120	-97.451	-130.169	33.57
-20	**80**	-92.666	-121.232	30.83
	100	-96.007	-126.853	32.13
	120	-98.563	-131.185	33.10
-10	**80**	-108.063	-136.892	26.68
	100	-111.463	-142.588	27.92
	120	-114.065	-146.977	28.85
0	**80**	-151.439	-180.587	19.25
	100	-154.871	-186.319	20.31
	120	-157.496	-190.735	21.10
10	**80**	-200.214	-229.366	14.56
	100	-203.646	-235.099	15.44
	120	-206.272	-239.515	16.12
20	**80**	-246.535	-275.850	11.89
	100	-249.980	-281.599	12.65
	120	-252.616	-286.028	13.23
30	**80**	-287.421	-315.406	9.74
	100	-290.874	-321.172	10.42
	120	-293.519	-325.615	10.93

Table F.6. Stress at the bottom of the slab (18" from shoulder joint; 8" slab thickness)

Variables		Stress (psi)		
ΔT (°F)	**Tire pressure (psi)**	**Under DT load**	**Under WBT tire load (+20% tire pressure)**	**Percent increase (%)**
-30	**80**	-44.905	-62.911	40.10
	100	-46.786	-65.907	40.87
	120	-48.218	-68.195	41.43
-20	**80**	-46.053	-63.498	37.88
	100	-47.898	-66.496	38.83
	120	-49.304	-68.787	39.52
-10	**80**	-60.121	-77.844	29.48
	100	-62.026	-80.920	30.46
	120	-63.477	-83.269	31.18
0	**80**	-102.783	-120.866	17.59
	100	-104.722	-123.981	18.39
	120	-106.199	-126.361	18.99
10	**80**	-151.549	-169.638	11.94
	100	-153.488	-172.754	12.55
	120	-154.966	-175.135	13.02
20	**80**	-197.612	-215.866	9.24
	100	-199.563	-218.998	9.74
	120	-201.050	-221.391	10.12
30	**80**	-238.333	-255.237	7.09
	100	-240.299	-258.388	7.53
	120	-241.799	-260.797	7.86

Table F.7. Stress at the bottom of the slab (0" from shoulder joint; 10" slab thickness)

Variables		Stress (psi)		
ΔT (°F)	Tire pressure (psi)	Under DT load	Under WBT tire load (+20% tire pressure)	Percent increase (%)
-30	80	-130.836	-169.464	29.52
	100	-139.604	-183.535	31.47
	120	-146.876	-195.280	32.96
-20	80	-139.595	-178.189	27.65
	100	-148.389	-192.291	29.59
	120	-155.680	-204.060	31.08
-10	80	-163.252	-201.874	23.66
	100	-172.076	-216.013	25.53
	120	-179.390	-227.811	26.99
0	80	-208.554	-247.257	18.56
	100	-217.390	-261.410	20.25
	120	-224.714	-273.218	21.58
10	80	-256.600	-295.300	15.08
	100	-265.436	-309.452	16.58
	120	-272.760	-321.260	17.78
20	80	-303.342	-342.108	12.78
	100	-312.185	-356.270	14.12
	120	-319.515	-368.086	15.20
30	80	-342.436	-380.439	11.10
	100	-351.280	-394.609	12.33
	120	-358.613	-406.432	13.33

Table F.8. Stress at the bottom of the slab (10" from shoulder joint; 10" slab thickness)

Variables		Stress (psi)		
ΔT (°F)	**Tire pressure (psi)**	**Under DT load**	**Under WBT tire load (+20% tire pressure)**	**Percent increase (%)**
-30	**80**	-41.755	-61.389	47.02
	100	-44.042	-65.195	48.03
	120	-45.791	-68.124	48.77
-20	**80**	-49.821	-69.423	39.34
	100	-52.134	-73.261	40.52
	120	-53.904	-76.215	41.39
-10	**80**	-72.599	-92.261	27.08
	100	-74.945	-96.141	28.28
	120	-76.740	-99.127	29.17
0	**80**	-117.542	-137.306	16.81
	100	-119.903	-141.203	17.76
	120	-121.708	-144.201	18.48
10	**80**	-165.594	-185.355	11.93
	100	-167.953	-189.251	12.68
	120	-169.759	-192.250	13.25
20	**80**	-212.140	-231.969	9.35
	100	-214.508	-235.875	9.96
	120	-216.319	-238.881	10.43
30	**80**	-251.187	-270.163	7.55
	100	-253.563	-274.083	8.09
	120	-255.382	-277.102	8.50

Table F.9. Stress at the bottom of the slab (18" from shoulder joint; 10" slab thickness)

Variables		Stress (psi)		
ΔT (°F)	Tire pressure (psi)	Under DT load	Under WBT tire load (+20% tire pressure)	Percent increase (%)
-30	80	-9.237	-21.652	134.41
	100	-10.550	-23.748	125.10
	120	-11.550	-25.348	119.46
-20	80	-16.807	-29.154	73.46
	100	-18.137	-31.279	72.46
	120	-19.152	-32.901	71.79
-10	80	-38.834	-51.252	31.98
	100	-40.200	-53.421	32.89
	120	-41.241	-55.077	33.55
0	80	-83.460	-95.990	15.01
	100	-84.841	-98.178	15.72
	120	-85.894	-99.848	16.25
10	80	-131.513	-144.042	9.53
	100	-132.894	-146.230	10.04
	120	-133.947	-147.900	10.42
20	80	-177.908	-190.505	7.08
	100	-179.297	-192.703	7.48
	120	-180.355	-194.381	7.78
30	80	-216.788	-228.503	5.40
	100	-218.190	-230.719	5.74
	120	-219.260	-232.413	6.00

Table F.10. Stress at the bottom of the slab (0" from shoulder joint; 12" slab thickness)

Variables		Stress (psi)		
ΔT (°F)	Tire pressure (psi)	Under DT load	Under WBT tire load (+20% tire pressure)	Percent increase (%)
-30	80	-71.256	-98.763	38.60
	100	-77.455	-108.684	40.32
	120	-82.589	-116.955	41.61
-20	80	-84.751	-112.233	32.43
	100	-90.967	-122.175	34.31
	120	-96.114	-130.461	35.74
-10	80	-113.501	-140.965	24.20
	100	-119.734	-150.928	26.05
	120	-124.895	-159.231	27.49
0	80	-160.179	-187.668	17.16
	100	-166.417	-197.637	18.76
	120	-171.582	-205.944	20.03
10	80	-208.364	-235.851	13.19
	100	-214.603	-245.821	14.55
	120	-219.767	-254.128	15.64
20	80	-255.738	-283.259	10.76
	100	-261.981	-293.233	11.93
	120	-267.149	-301.545	12.88
30	80	-295.331	-322.399	9.17
	100	-301.575	-332.380	10.21
	120	-306.747	-340.698	11.07

Table F.11. Stress at the bottom of the slab (10" from shoulder joint; 12" slab thickness)

Variables		Stress (psi)		
ΔT (°F)	Tire pressure (psi)	Under DT load	Under WBT tire load (+20% tire pressure)	Percent increase (%)
-30	80	-6.900	-21.136	206.32
	100	-8.582	-23.906	178.56
	120	-9.869	-26.036	163.82
-20	80	-19.942	-34.160	71.30
	100	-21.641	-36.951	70.75
	120	-22.942	-39.099	70.43
-10	80	-48.179	-62.390	29.50
	100	-49.898	-65.206	30.68
	120	-51.213	-67.372	31.55
0	80	-94.699	-108.941	15.04
	100	-96.424	-111.765	15.91
	120	-97.744	-113.937	16.57
10	80	-142.887	-157.129	9.97
	100	-144.612	-159.952	10.61
	120	-145.932	-162.124	11.10
20	80	-190.151	-204.428	7.51
	100	-191.880	-207.257	8.01
	120	-193.204	-209.433	8.40
30	80	-229.666	-243.432	5.99
	100	-231.402	-246.273	6.43
	120	-232.733	-248.460	6.76

Table F.12. Stress at the bottom of the slab (18" from shoulder joint; 12" slab thickness)

Variables		Stress (psi)		
ΔT (°F)	**Tire pressure (psi)**	**Under DT load**	**Under WBT tire load (+20% tire pressure)**	**Percent increase (%)**
-30	**80**	17.375	8.234	-52.61
	100	16.386	6.670	-59.29
	120	15.632	5.476	-64.97
-20	**80**	4.711	-4.412	-193.65
	100	3.705	-5.998	-261.89
	120	2.937	-7.209	-345.45
-10	**80**	-23.076	-32.198	39.53
	100	-24.104	-33.812	40.28
	120	-24.888	-35.044	40.81
0	**80**	-69.449	-78.608	13.19
	100	-70.485	-80.230	13.83
	120	-71.274	-81.469	14.30
10	**80**	-117.639	-126.796	7.78
	100	-118.674	-128.419	8.21
	120	-119.463	-129.658	8.53
20	**80**	-164.818	-174.012	5.58
	100	-165.858	-175.640	5.90
	120	-166.650	-176.882	6.14
30	**80**	-204.169	-212.824	4.24
	100	-205.221	-214.469	4.51
	120	-206.024	-215.726	4.71

Table F.13. Stress at the bottom of the slab (0" from shoulder joint; 13" slab thickness)

Variables		Stress (psi)		
ΔT (°F)	**Tire pressure (psi)**	**Under DT load**	**Under WBT tire load (+20% tire pressure)**	**Percent increase (%)**
-30	**80**	-62.534	-86.180	37.81
	100	-67.856	-94.687	39.54
	120	-72.261	-101.774	40.84
-20	**80**	-75.790	-99.406	31.16
	100	-81.124	-107.929	33.04
	120	-85.540	-115.029	34.47
-10	**80**	-102.730	-126.329	22.97
	100	-108.079	-134.869	24.79
	120	-112.505	-141.983	26.20
0	**80**	-143.385	-166.996	16.47
	100	-148.736	-175.540	18.02
	120	-153.165	-182.657	19.26
10	**80**	-184.822	-208.433	12.77
	100	-190.174	-216.977	14.09
	120	-194.602	-224.093	15.15
20	**80**	-225.941	-249.572	10.46
	100	-231.296	-258.120	11.60
	120	-235.726	-265.238	12.52
30	**80**	-261.098	-284.411	8.93
	100	-266.454	-292.964	9.95
	120	-270.887	-300.088	10.78

Table F.14. Stress at the bottom of the slab (10" from shoulder joint; 13" slab thickness)

Variables		Stress (psi)		
ΔT (°F)	**Tire pressure (psi)**	**Under DT load**	**Under WBT tire load (+20% tire pressure)**	**Percent increase (%)**
-30	**80**	-6.802	-19.117	181.05
	100	-8.270	-21.523	160.25
	120	-9.393	-23.374	148.84
-20	**80**	-19.710	-31.999	62.35
	100	-21.190	-34.422	62.44
	120	-22.324	-36.285	62.54
-10	**80**	-46.234	-58.513	26.56
	100	-47.730	-60.955	27.71
	120	-48.876	-62.835	28.56
0	**80**	-86.796	-99.093	14.17
	100	-88.297	-101.540	15.00
	120	-89.445	-103.423	15.63
10	**80**	-128.236	-140.532	9.59
	100	-129.736	-142.979	10.21
	120	-130.885	-144.862	10.68
20	**80**	-169.286	-181.602	7.28
	100	-170.789	-184.053	7.77
	120	-171.939	-185.938	8.14
30	**80**	-204.383	-216.324	5.84
	100	-205.891	-218.785	6.26
	120	-207.048	-220.679	6.58

Table F.15. Stress at the bottom of the slab (18" from shoulder joint; 13" slab thickness)

Variables		Stress (psi)		
ΔT (°F)	**Tire pressure (psi)**	**Under DT load**	**Under WBT tire load (+20% tire pressure)**	**Percent increase (%)**
-30	**80**	14.512	6.554	-54.84
	100	13.639	5.180	-62.02
	120	12.973	4.132	-68.15
-20	**80**	1.908	-6.024	-415.72
	100	1.021	-7.416	-826.35
	120	0.344	-8.478	-2564.53
-10	**80**	-24.252	-32.180	32.69
	100	-25.156	-33.594	33.54
	120	-25.847	-34.673	34.15
0	**80**	-64.727	-72.674	12.28
	100	-65.636	-74.094	12.89
	120	-66.330	-75.177	13.34
10	**80**	-106.168	-114.115	7.49
	100	-107.077	-115.534	7.90
	120	-107.770	-116.617	8.21
20	**80**	-147.163	-155.132	5.42
	100	-148.075	-156.555	5.73
	120	-148.771	-157.641	5.96
30	**80**	-182.132	-189.708	4.16
	100	-183.053	-191.143	4.42
	120	-183.757	-192.240	4.62

G. APPENDIX G: STRESS AT TOP OF SLAB WITH DIFFERENT SLAB THICKNESSES

Table G.1. Stress at the top of the slab (0" from shoulder joint; 6" slab thickness)

Variables		Stress (psi)		
ΔT (°F)	**Tire pressure (psi)**	**Under DT load**	**Under WBT tire load (+20% tire pressure)**	**Percent increase (%)**
-30	**80**	-330.505	-345.249	4.46
	100	-331.910	-346.809	4.49
	120	-332.974	-347.951	4.50
-20	**80**	-268.378	-282.092	5.11
	100	-269.251	-283.041	5.12
	120	-269.911	-283.741	5.12
-10	**80**	-195.314	-209.138	7.08
	100	-195.898	-209.843	7.12
	120	-196.345	-210.367	7.14
0	**80**	-120.503	-134.350	11.49
	100	-121.089	-135.059	11.54
	120	-121.539	-135.586	11.56
10	**80**	-47.411	-61.499	29.71
	100	-48.184	-62.470	29.65
	120	-48.787	-63.212	29.57
20	**80**	6.183	-7.547	-222.06
	100	4.805	-9.193	-291.32
	120	3.759	-10.451	-378.03
30	**80**	45.269	32.665	-27.84
	100	43.397	30.447	-29.84
	120	41.988	28.752	-31.52

Table G.2. Stress at the top of the slab (10" from shoulder joint; 6" slab thickness)

Variables		Stress (psi)		
ΔT (°F)	Tire pressure (psi)	Under DT load	Under WBT tire load (+20% tire pressure)	Percent increase (%)
-30	80	-293.164	-307.122	4.76
	100	-294.891	-309.221	4.86
	120	-296.175	-310.749	4.92
-20	80	-238.505	-250.019	4.83
	100	-239.573	-251.277	4.89
	120	-240.376	-252.206	4.92
-10	80	-167.591	-178.913	6.76
	100	-168.266	-179.683	6.79
	120	-168.777	-180.245	6.79
0	80	-92.392	-104.071	12.64
	100	-93.006	-104.843	12.73
	120	-93.468	-105.407	12.77
10	80	-18.928	-30.741	62.41
	100	-19.670	-31.692	61.12
	120	-20.240	-32.410	60.13
20	80	34.813	23.480	-32.55
	100	33.467	21.819	-34.80
	120	32.447	20.571	-36.60
30	80	73.057	62.801	-14.04
	100	71.221	60.539	-15.00
	120	69.836	58.858	-15.72

Table G.3. Stress at the top of the slab (18" from shoulder joint; 6" slab thickness)

Variables		Stress (psi)		
ΔT (°F)	Tire pressure (psi)	Under DT load	Under WBT tire load (+20% tire pressure)	Percent increase (%)
-30	80	-265.195	-277.450	4.62
	100	-267.016	-279.757	4.77
	120	-268.379	-281.456	4.87
-20	80	-216.135	-226.639	4.86
	100	-217.399	-228.139	4.94
	120	-218.346	-229.255	5.00
-10	80	-149.264	-158.214	6.00
	100	-150.009	-159.082	6.05
	120	-150.573	-159.734	6.08
0	80	-73.393	-83.101	13.23
	100	-74.023	-83.923	13.37
	120	-74.495	-84.522	13.46
10	80	0.195	-9.590	-5017.95
	100	-0.536	-10.550	1868.28
	120	-1.094	-11.269	930.07
20	80	53.678	44.516	-17.07
	100	52.351	42.844	-18.16
	120	51.340	41.599	-18.97
30	80	91.057	82.963	-8.89
	100	89.225	80.702	-9.55
	120	87.835	79.017	-10.04

Table G.4. Stress at the top of the slab (0" from shoulder joint; 8" slab thickness)

Variables		Stress (psi)		
ΔT (°F)	**Tire pressure (psi)**	**Under DT load**	**Under WBT tire load (+20% tire pressure)**	**Percent increase (%)**
-30	**80**	-257.913	-266.344	3.27
	100	-259.942	-268.892	3.44
	120	-261.468	-270.775	3.56
-20	**80**	-222.489	-230.359	3.54
	100	-224.139	-232.437	3.70
	120	-225.382	-233.980	3.81
-10	**80**	-176.539	-183.954	4.20
	100	-178.059	-185.871	4.39
	120	-179.204	-187.298	4.52
0	**80**	-127.551	-134.975	5.82
	100	-129.071	-136.893	6.06
	120	-130.216	-138.321	6.22
10	**80**	-78.814	-86.231	9.41
	100	-80.335	-88.150	9.73
	120	-81.481	-89.578	9.94
20	**80**	-38.998	-46.631	19.57
	100	-40.791	-48.900	19.88
	120	-42.145	-50.594	20.05
30	**80**	-10.860	-18.276	68.29
	100	-12.910	-20.851	61.51
	120	-14.446	-22.769	57.61

Table G.5. Stress at the top of the slab (10" from shoulder joint; 8" slab thickness)

Variables		Stress (psi)		
ΔT (°F)	**Tire pressure (psi)**	**Under DT load**	**Under WBT tire load (+20% tire pressure)**	**Percent increase (%)**
-30	**80**	-228.412	-235.793	3.23
	100	-230.439	-238.386	3.45
	120	-231.960	-240.310	3.60
-20	**80**	-196.706	-203.829	3.62
	100	-198.371	-205.930	3.81
	120	-199.619	-207.482	3.94
-10	**80**	-152.690	-159.218	4.28
	100	-154.144	-161.084	4.50
	120	-155.236	-162.468	4.66
0	**80**	-103.690	-110.201	6.28
	100	-105.137	-112.063	6.59
	120	-106.224	-113.445	6.80
10	**80**	-54.975	-61.477	11.83
	100	-56.422	-63.340	12.26
	120	-57.510	-64.722	12.54
20	**80**	-14.953	-21.653	44.81
	100	-16.647	-23.833	43.17
	120	-17.922	-25.459	42.05
30	**80**	12.856	6.335	-50.72
	100	10.901	3.863	-64.56
	120	9.435	2.022	-78.57

Table G.6. Stress at the top of the slab (18" from shoulder joint; 8" slab thickness)

Variables		Stress (psi)		
ΔT (°F)	Tire pressure (psi)	Under DT load	Under WBT tire load (+20% tire pressure)	Percent increase (%)
-30	80	-207.041	-213.388	3.07
	100	-209.019	-215.965	3.32
	120	-210.499	-217.874	3.50
-20	80	-177.576	-183.821	3.52
	100	-179.248	-185.958	3.74
	120	-180.500	-187.549	3.91
-10	80	-135.799	-141.401	4.13
	100	-137.185	-143.209	4.39
	120	-138.225	-144.551	4.58
0	80	-86.940	-92.464	6.35
	100	-88.311	-94.257	6.73
	120	-89.339	-95.588	6.99
10	80	-38.243	-43.758	14.42
	100	-39.614	-45.552	14.99
	120	-40.643	-46.883	15.35
20	80	1.659	-4.035	-343.22
	100	0.053	-6.129	-11664.15
	120	-1.151	-7.683	567.51
30	80	28.926	23.487	-18.80
	100	27.069	21.092	-22.08
	120	25.681	19.312	-24.80

Table G.7. Stress at the top of the slab (0" from shoulder joint; 10" slab thickness)

Variables		Stress (psi)		
ΔT (°F)	**Tire pressure (psi)**	**Under DT load**	**Under WBT tire load (+20% tire pressure)**	**Percent increase (%)**
-30	**80**	-221.339	-225.433	1.85
	100	-222.689	-227.149	2.00
	120	-223.708	-228.423	2.11
-20	**80**	-188.155	-192.034	2.06
	100	-189.267	-193.435	2.20
	120	-190.107	-194.479	2.30
-10	**80**	-143.851	-147.567	2.58
	100	-144.883	-148.873	2.75
	120	-145.664	-149.847	2.87
0	**80**	-95.849	-99.564	3.88
	100	-96.881	-100.869	4.12
	120	-97.661	-101.844	4.28
10	**80**	-47.737	-51.450	7.78
	100	-48.768	-52.755	8.18
	120	-49.548	-53.729	8.44
20	**80**	-6.633	-10.407	56.90
	100	-7.835	-11.926	52.21
	120	-8.742	-13.061	49.41
30	**80**	22.434	18.873	-15.87
	100	21.070	17.157	-18.57
	120	20.045	15.879	-20.78

Table G.8. Stress at the top of the slab (10" from shoulder joint; 10" slab thickness)

Variables		Stress (psi)		
ΔT (°F)	Tire pressure (psi)	Under DT load	Under WBT tire load (+20% tire pressure)	Percent increase (%)
-30	80	-202.384	-206.274	1.92
	100	-203.710	-207.974	2.09
	120	-204.710	-209.239	2.21
-20	80	-171.788	-175.665	2.26
	100	-172.899	-177.074	2.41
	120	-173.734	-178.122	2.53
-10	80	-128.832	-132.313	2.70
	100	-129.816	-133.570	2.89
	120	-130.557	-134.507	3.03
0	80	-80.837	-84.304	4.29
	100	-81.817	-85.558	4.57
	120	-82.556	-86.492	4.77
10	80	-32.734	-36.200	10.59
	100	-33.713	-37.453	11.09
	120	-34.451	-38.386	11.42
20	80	8.454	4.903	-42.00
	100	7.317	3.451	-52.84
	120	6.462	2.370	-63.32
30	80	37.109	33.763	-9.02
	100	35.818	32.120	-10.32
	120	34.848	30.897	-11.34

Table G.9. Stress at the top of the slab (18" from shoulder joint; 10" slab thickness)

Variables		Stress (psi)		
ΔT (°F)	**Tire pressure (psi)**	**Under DT load**	**Under WBT tire load (+20% tire pressure)**	**Percent increase (%)**
-30	**80**	-188.464	-192.059	1.91
	100	-189.753	-193.733	2.10
	120	-190.721	-194.978	2.23
-20	**80**	-159.394	-163.026	2.28
	100	-160.490	-164.433	2.46
	120	-161.313	-165.476	2.58
-10	**80**	-118.022	-121.169	2.67
	100	-118.961	-122.381	2.87
	120	-119.667	-123.283	3.02
0	**80**	-70.090	-73.208	4.45
	100	-71.021	-74.413	4.78
	120	-71.723	-75.310	5.00
10	**80**	-21.993	-25.110	14.17
	100	-22.924	-26.314	14.79
	120	-23.625	-27.211	15.18
20	**80**	19.066	15.862	-16.80
	100	17.983	14.468	-19.55
	120	17.170	13.428	-21.79
30	**80**	47.257	44.263	-6.34
	100	46.020	42.678	-7.26
	120	45.093	41.499	-7.97

Table G.10. Stress at the top of the slab (0" from shoulder joint; 12" slab thickness)

Variables		Stress (psi)		
ΔT (°F)	**Tire pressure (psi)**	**Under DT load**	**Under WBT tire load (+20% tire pressure)**	**Percent increase (%)**
-30	**80**	-200.846	-202.895	1.02
	100	-201.783	-204.094	1.15
	120	-202.494	-204.989	1.23
-20	**80**	-167.598	-169.672	1.24
	100	-168.380	-170.663	1.36
	120	-168.971	-171.400	1.44
-10	**80**	-123.302	-125.294	1.62
	100	-124.026	-126.214	1.76
	120	-124.576	-126.902	1.87
0	**80**	-75.195	-77.187	2.65
	100	-75.919	-78.107	2.88
	120	-76.468	-78.796	3.04
10	**80**	-26.962	-28.955	7.39
	100	-27.686	-29.875	7.91
	120	-28.235	-30.562	8.24
20	**80**	16.413	14.433	-12.06
	100	15.585	13.383	-14.13
	120	14.960	12.597	-15.80
30	**80**	47.476	45.700	-3.74
	100	46.534	44.510	-4.35
	120	45.824	43.621	-4.81

Table G.11. Stress at the top of the slab (10" from shoulder joint; 12" slab thickness)

Variables		Stress (psi)		
ΔT (°F)	**Tire pressure (psi)**	**Under DT load**	**Under WBT tire load (+20% tire pressure)**	**Percent increase (%)**
-30	**80**	-188.124	-190.262	1.14
	100	-189.038	-191.443	1.27
	120	-189.729	-192.322	1.37
-20	**80**	-156.712	-158.844	1.36
	100	-157.482	-159.827	1.49
	120	-158.064	-160.560	1.58
-10	**80**	-113.189	-115.152	1.73
	100	-113.880	-116.035	1.89
	120	-114.403	-116.694	2.00
0	**80**	-65.083	-67.042	3.01
	100	-65.772	-67.923	3.27
	120	-66.294	-68.581	3.45
10	**80**	-16.853	-18.813	11.63
	100	-17.542	-19.694	12.27
	120	-18.063	-20.352	12.67
20	**80**	26.543	24.578	-7.40
	100	25.758	23.575	-8.48
	120	25.165	22.825	-9.30
30	**80**	57.231	55.452	-3.11
	100	56.335	54.313	-3.59
	120	55.661	53.464	-3.95

Table G.12. Stress at the top of the slab (18" from shoulder joint; 12" slab thickness)

Variables		Stress (psi)		
ΔT (°F)	**Tire pressure (psi)**	**Under DT load**	**Under WBT tire load (+20% tire pressure)**	**Percent increase (%)**
-30	**80**	-178.585	-180.625	1.14
	100	-179.478	-181.782	1.28
	120	-180.153	-182.643	1.38
-20	**80**	-148.466	-150.550	1.40
	100	-149.219	-151.520	1.54
	120	-149.788	-152.241	1.64
-10	**80**	-105.846	-107.696	1.75
	100	-106.507	-108.547	1.92
	120	-107.006	-109.182	2.03
0	**80**	-57.760	-59.602	3.19
	100	-58.418	-60.450	3.48
	120	-58.916	-61.083	3.68
10	**80**	-9.532	-11.376	19.35
	100	-10.191	-12.223	19.94
	120	-10.688	-12.856	20.28
20	**80**	33.761	31.908	-5.49
	100	33.009	30.942	-6.26
	120	32.442	30.221	-6.85
30	**80**	64.058	62.385	-2.61
	100	63.199	61.288	-3.02
	120	62.553	60.471	-3.33

Table G.13. Stress at the top of the slab (0" from shoulder joint; 13" slab thickness)

Variables		Stress (psi)		
ΔT (°F)	Tire pressure (psi)	Under DT load	Under WBT tire load (+20% tire pressure)	Percent increase (%)
-30	80	-183.346	-184.794	0.79
	100	-184.275	-185.982	0.93
	120	-184.979	-186.870	1.02
-20	80	-153.939	-155.438	0.97
	100	-154.746	-156.463	1.11
	120	-155.357	-157.226	1.20
-10	80	-115.219	-116.675	1.26
	100	-115.987	-117.652	1.44
	120	-116.569	-118.383	1.56
0	80	-73.809	-75.268	1.98
	100	-74.578	-76.245	2.24
	120	-75.160	-76.975	2.41
10	80	-32.330	-33.789	4.51
	100	-33.098	-34.766	5.04
	120	-33.680	-35.496	5.39
20	80	6.635	5.181	-21.91
	100	5.802	4.123	-28.94
	120	5.172	3.331	-35.60
30	80	35.236	33.910	-3.76
	100	34.310	32.736	-4.59
	120	33.611	31.859	-5.21

Table G.14. Stress at the top of the slab (10" from shoulder joint; 13" slab thickness)

Variables		Stress (psi)		
ΔT (°F)	**Tire pressure (psi)**	**Under DT load**	**Under WBT tire load (+20% tire pressure)**	**Percent increase (%)**
-30	**80**	-172.190	-173.754	0.91
	100	-173.092	-174.915	1.05
	120	-173.774	-175.782	1.16
-20	**80**	-144.164	-145.745	1.10
	100	-144.952	-146.753	1.24
	120	-145.548	-147.503	1.34
-10	**80**	-105.923	-107.408	1.40
	100	-106.655	-108.344	1.58
	120	-107.208	-109.043	1.71
0	**80**	-64.508	-65.993	2.30
	100	-65.239	-66.928	2.59
	120	-65.791	-67.627	2.79
10	**80**	-23.031	-24.517	6.45
	100	-23.762	-25.452	7.11
	120	-24.314	-26.150	7.55
20	**80**	15.967	14.475	-9.34
	100	15.176	13.463	-11.29
	120	14.579	12.708	-12.83
30	**80**	44.295	42.917	-3.11
	100	43.414	41.793	-3.73
	120	42.751	40.956	-4.20

Table G.15. Stress at the top of the slab (18" from shoulder joint; 13" slab thickness)

Variables		Stress (psi)		
ΔT (°F)	Tire pressure (psi)	Under DT load	Under WBT tire load (+20% tire pressure)	Percent increase (%)
-30	**80**	-163.743	-165.300	0.95
	100	-164.621	-166.436	1.10
	120	-165.283	-167.283	1.21
-20	**80**	-136.793	-138.353	1.14
	100	-137.560	-139.340	1.29
	120	-138.138	-140.076	1.40
-10	**80**	-99.151	-100.577	1.44
	100	-99.851	-101.478	1.63
	120	-100.378	-102.150	1.77
0	**80**	-57.742	-59.166	2.47
	100	-58.440	-60.065	2.78
	120	-58.967	-60.736	3.00
10	**80**	-16.267	-17.691	8.75
	100	-16.964	-18.590	9.59
	120	-17.491	-19.261	10.12
20	**80**	22.679	21.244	-6.33
	100	21.924	20.272	-7.54
	120	21.354	19.546	-8.47
30	**80**	50.704	49.373	-2.63
	100	49.860	48.294	-3.14
	120	49.225	47.489	-3.53

H. APPENDIX H: DEFLECTION AT CORNER OF SLAB WITH DIFFERENT SLAB THICKNESSES

Table H.1. Deflection at the corner of the slab (6" slab thickness)

Variables			Deflection (inch)			
			Loaded slab		Unloaded slab	
Distance from shoulder joint (inch)	**LTE-y (%)**	**Tire pressure (psi)**	**Under DT load**	**Under WBT tire load (+20% tire pressure)**	**Under DT load**	**Under WBT tire load (+20% tire pressure)**
0	**50**	**80**	0.032854	0.036480	0.017335	0.017511
		100	0.033667	0.037629	0.017644	0.017896
		120	0.034285	0.038502	0.017878	0.018185
	70	**80**	0.029251	0.032433	0.020938	0.021558
		100	0.029976	0.033464	0.021335	0.022061
		120	0.030527	0.034248	0.021635	0.022439
	90	**80**	0.026292	0.028795	0.023897	0.025195
		100	0.026919	0.029681	0.024393	0.025843
		120	0.027395	0.030357	0.024767	0.026330
10	**50**	**80**	0.023060	0.026147	0.014514	0.015086
		100	0.023657	0.027008	0.014798	0.015454
		120	0.024111	0.027661	0.015013	0.015730
	70	**80**	0.020542	0.023143	0.017032	0.018090
		100	0.021066	0.023898	0.017390	0.018564
		120	0.021464	0.024471	0.017660	0.018920
	90	**80**	0.019003	0.021047	0.018570	0.020186
		100	0.019462	0.021695	0.018994	0.020766
		120	0.019810	0.022187	0.019314	0.021203
18	**50**	**80**	0.016863	0.019381	0.012186	0.012960
		100	0.017320	0.020045	0.012443	0.013301
		120	0.017667	0.020549	0.012637	0.013558
	70	**80**	0.015165	0.017241	0.013883	0.015099
		100	0.015565	0.017819	0.014197	0.015527
		120	0.015869	0.018257	0.014435	0.015850
	90	**80**	0.014475	0.016175	0.014573	0.016165
		100	0.014837	0.016687	0.014926	0.016659
		120	0.015111	0.017074	0.015193	0.017033

Table H.2. Deflection at the corner of the slab (8" slab thickness)

Variables			Deflection (inch)			
			Loaded slab		Unloaded slab	
Distance from shoulder joint (inch)	LTE-y (%)	Tire pressure (psi)	Under DT load	Under WBT tire load (+20% tire pressure)	Under DT load	Under WBT tire load (+20% tire pressure)
0	50	80	0.025466	0.027394	0.012650	0.012496
		100	0.025968	0.028085	0.012830	0.012720
		120	0.026349	0.028607	0.012966	0.012887
	70	80	0.022628	0.024354	0.015486	0.015533
		100	0.023077	0.024976	0.015719	0.015825
		120	0.023418	0.025447	0.015895	0.016043
	90	80	0.020179	0.021506	0.017934	0.018380
		100	0.020567	0.022044	0.018228	0.018756
		120	0.020862	0.022452	0.018450	0.019038
10	50	80	0.019244	0.021025	0.010975	0.011025
		100	0.019639	0.021576	0.011143	0.011238
		120	0.019938	0.021993	0.011270	0.011397
	70	80	0.017049	0.018573	0.013167	0.013474
		100	0.017397	0.019060	0.013383	0.013751
		120	0.017661	0.019429	0.013545	0.013959
	90	80	0.015470	0.016607	0.014747	0.015440
		100	0.015770	0.017023	0.015010	0.015788
		120	0.015997	0.017338	0.015209	0.016049
18	50	80	0.015067	0.016632	0.009606	0.009787
		100	0.015389	0.017084	0.009763	0.009989
		120	0.015632	0.017425	0.009881	0.010141
	70	80	0.013378	0.014673	0.011293	0.011744
		100	0.013659	0.015068	0.011491	0.012003
		120	0.013872	0.015367	0.011640	0.012198
	90	80	0.012404	0.013377	0.012268	0.013040
		100	0.012650	0.013717	0.012500	0.013354
		120	0.012837	0.013974	0.012675	0.013589

Table H.3. Deflection at the corner of the slab (10" slab thickness)

Variables			Deflection (inch)			
			Loaded slab		Unloaded slab	
Distance from shoulder joint (inch)	LTE-y (%)	Tire pressure (psi)	Under DT load	Under WBT tire load (+20% tire pressure)	Under DT load	Under WBT tire load (+20% tire pressure)
0	50	80	0.021054	0.022150	0.009996	0.009784
		100	0.021401	0.022619	0.010115	0.009933
		120	0.021664	0.022973	0.010205	0.010044
	70	80	0.018627	0.019643	0.012420	0.012288
		100	0.018936	0.020065	0.012576	0.012484
		120	0.019171	0.020384	0.012695	0.012630
	90	80	0.016555	0.017327	0.014491	0.014604
		100	0.016823	0.017693	0.014689	0.014854
		120	0.017027	0.017971	0.014838	0.015042
10	50	80	0.016656	0.017724	0.008875	0.008769
		100	0.016944	0.018114	0.008990	0.008911
		120	0.017158	0.018408	0.009074	0.009018
	70	80	0.014691	0.015634	0.010839	0.010857
		100	0.014944	0.015979	0.010987	0.011044
		120	0.015133	0.016240	0.011096	0.011183
	90	80	0.013205	0.013887	0.012324	0.012603
		100	0.013424	0.014183	0.012507	0.012840
		120	0.013586	0.014406	0.012643	0.013017
18	50	80	0.013593	0.014573	0.007959	0.007928
		100	0.013836	0.014906	0.008067	0.008065
		120	0.014017	0.015157	0.008147	0.008168
	70	80	0.011990	0.012825	0.009559	0.009675
		100	0.012203	0.013116	0.009698	0.009853
		120	0.012362	0.013336	0.009801	0.009986
	90	80	0.010939	0.011530	0.010610	0.010970
		100	0.011124	0.011780	0.010777	0.011189
		120	0.011261	0.011968	0.010901	0.011354

Table H.4. Deflection at the corner of the slab (12" slab thickness)

Variables			Deflection (inch)			
			Loaded slab		Unloaded slab	
Distance from shoulder joint (inch)	LTE-y (%)	Tire pressure (psi)	Under DT load	Under WBT tire load (+20% tire pressure)	Under DT load	Under WBT tire load (+20% tire pressure)
0	50	80	0.018129	0.018779	0.008244	0.008049
		100	0.018387	0.019123	0.008329	0.008155
		120	0.018583	0.019383	0.008393	0.008235
	70	80	0.015951	0.016581	0.010419	0.010243
		100	0.016180	0.016889	0.010533	0.010386
		120	0.016354	0.017122	0.010619	0.010493
	90	80	0.014126	0.014606	0.012243	0.012216
		100	0.014325	0.014875	0.012387	0.012399
		120	0.014475	0.015078	0.012496	0.012535
10	50	80	0.014796	0.015453	0.007446	0.007308
		100	0.015015	0.015749	0.007528	0.007411
		120	0.015181	0.015971	0.007589	0.007488
	70	80	0.012981	0.013588	0.009258	0.009171
		100	0.013174	0.013849	0.009366	0.009307
		120	0.013320	0.014046	0.009448	0.009410
	90	80	0.011595	0.012028	0.010644	0.010729
		100	0.011760	0.012253	0.010778	0.010903
		120	0.011886	0.012422	0.010880	0.011033
18	50	80	0.012410	0.013032	0.006791	0.006697
		100	0.012602	0.013292	0.006869	0.006797
		120	0.012746	0.013487	0.006928	0.006871
	70	80	0.010884	0.011436	0.008315	0.008291
		100	0.011051	0.011663	0.008418	0.008423
		120	0.011177	0.011834	0.008496	0.008521
	90	80	0.009831	0.010209	0.009368	0.009517
		100	0.009974	0.010404	0.009494	0.009682
		120	0.010083	0.010550	0.009589	0.009805

Table H.5. Deflection at the corner of the slab (13" slab thickness)

Variables			Deflection (inch)			
			Loaded slab		Unloaded slab	
Distance from shoulder joint (inch)	LTE-y (%)	Tire pressure (psi)	Under DT load	Under WBT tire load (+20% tire pressure)	Under DT load	Under WBT tire load (+20% tire pressure)
0	50	80	0.017027	0.017532	0.007591	0.007411
		100	0.017253	0.017834	0.007664	0.007504
		120	0.017426	0.018062	0.007719	0.007573
	70	80	0.014940	0.015443	0.009672	0.009495
		100	0.015141	0.015712	0.009770	0.009619
		120	0.015293	0.015915	0.009845	0.009712
	90	80	0.013204	0.013591	0.011406	0.011344
		100	0.013378	0.013825	0.011531	0.011504
		120	0.013510	0.014003	0.011627	0.011623
10	50	80	0.014066	0.014586	0.006905	0.006768
		100	0.014261	0.014848	0.006975	0.006858
		120	0.014409	0.015046	0.007029	0.006925
	70	80	0.012309	0.012801	0.008657	0.008549
		100	0.012480	0.013032	0.008751	0.008669
		120	0.012610	0.013206	0.008823	0.008758
	90	80	0.010964	0.011317	0.010000	0.010031
		100	0.011111	0.011516	0.010118	0.010183
		120	0.011223	0.011666	0.010208	0.010297
18	50	80	0.011924	0.012422	0.006340	0.006238
		100	0.012097	0.012655	0.006408	0.006325
		120	0.012227	0.012830	0.006460	0.006390
	70	80	0.010429	0.010882	0.007831	0.007774
		100	0.010579	0.011086	0.007922	0.007890
		120	0.010693	0.011239	0.007990	0.007977
	90	80	0.009384	0.009693	0.008875	0.008962
		100	0.009513	0.009867	0.008987	0.009107
		120	0.009611	0.009998	0.009071	0.009216